

UC 94c
LBL-18335
c.1



Lawrence Berkeley Laboratory

UNIVERSITY OF CALIFORNIA

RECEIVED
LAWRENCE
BERKELEY LABORATORY

Materials & Molecular Research Division

MAR 15 1985

LIBRARY AND
DOCUMENTS SECTION

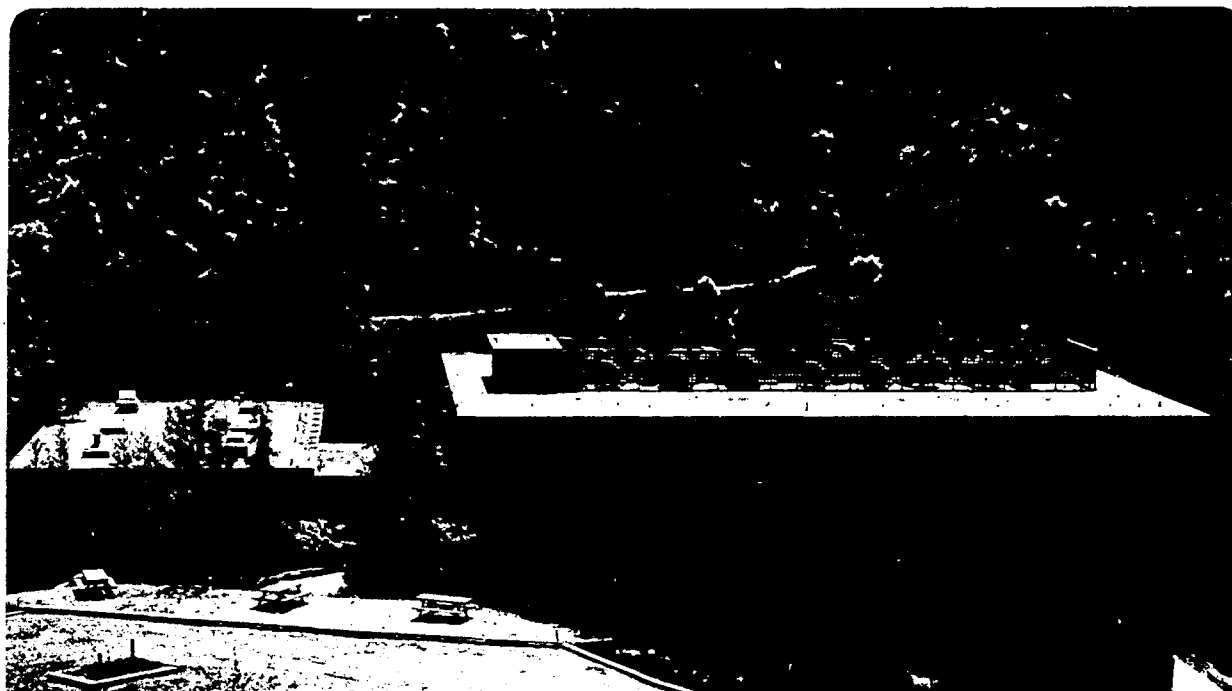
ON THE ELECTROCHEMISTRY OF HALOGEN ELECTRODES
IN PROPYLENE CARBONATE

K.J. Hanson
(Ph.D. Thesis)

December 1984

For Reference

Not to be taken from this room



LBL-18335
c.1

DISCLAIMER

This document was prepared as an account of work sponsored by the United States Government. While this document is believed to contain correct information, neither the United States Government nor any agency thereof, nor the Regents of the University of California, nor any of their employees, makes any warranty, express or implied, or assumes any legal responsibility for the accuracy, completeness, or usefulness of any information, apparatus, product, or process disclosed, or represents that its use would not infringe privately owned rights. Reference herein to any specific commercial product, process, or service by its trade name, trademark, manufacturer, or otherwise, does not necessarily constitute or imply its endorsement, recommendation, or favoring by the United States Government or any agency thereof, or the Regents of the University of California. The views and opinions of authors expressed herein do not necessarily state or reflect those of the United States Government or any agency thereof or the Regents of the University of California.

ON THE ELECTROCHEMISTRY OF HALOGEN ELECTRODES
IN
PROPYLENE CARBONATE

Karrie Jo Hanson

Materials and Molecular Research Division
Lawrence Berkeley Laboratory

and

Department of Chemical Engineering
University of California
Berkeley, California 94720

This work was supported by the U.S. Department of Energy
under Contract No. DE-AC03-76SF00098

CONTENTS

Abstract	iii
Acknowledgments	v
Nomenclature	vii
Abbreviations	ix
I. Introduction	1
II. Characterization of Propylene Carbonate	
2.1 Introduction	4
2.2 Analysis of Propylene Carbonate	5
2.3 Purification of Propylene Carbonate	5
2.4 Infrared Spectroscopy	7
2.5 Conclusions	16
III. Stability of Propylene Carbonate in the Presence of Halogens	
3.1 Introduction	19
3.2 Chlorine	19
3.3 Bromine and Iodine	38
3.4 Discussion	54
3.5 Conclusions	55
IV. Halide Double Salts in Propylene Carbonate	
4.1 Introduction	57
4.2 Experimental	58

4.3 Results	60
4.4 Discussion	62
4.5 Conclusions	63
V. Conductivity of Halide Salts in Propylene Carbonate	
5.1 Introduction	65
5.2 Conductivity of Alkali Halides	66
5.3 Conductivity of Mixtures of Halides and Halogens	75
5.4 Conclusions	82
VI. Electrochemical Oxidation of Iodide in Propylene Carbonate: Cyclic Voltammetry	
6.1 Introduction	84
6.2 Literature	88
6.3 Theoretical Model	104
6.4 Cyclic Voltammetry Experiments	119
6.5 Parameters for Model	152
6.6 Comparison of Model and Experiment	159
6.7 Spectral Electrochemical Experiments	166
6.8 Discussion	187
6.9 Conclusions	189
VII. Conclusions	194
Appendix 1 Distillation Manual	195
Appendix 2 Computer Programs for HP9825	206

On Halogen Electrochemistry in

Propylene Carbonate

Karrie Jo Hanson

Materials and Molecular Research Division, Lawrence Berkeley Laboratory,

and

Department of Chemical Engineering, University of California,

Berkeley, California 94720

ABSTRACT

Propylene carbonate is one of the more promising solvents for use in galvanic cells and in electrolysis processes involving alkali metal negatives. In this study, the electrochemical behavior of halogen/halide electrodes has been investigated. Included in this work are a study of the stability of propylene carbonate with respect to elemental chlorine, bromine, and iodine; an investigation of the solubility and conductivity of halogens and halide salts; and the determination of thermodynamic and kinetic characteristics of the iodide/triiodide/iodine couple.

Uv-visible spectroscopy experiments of iodine and bromine solutions have demonstrated that the stable form of the halogen in PC is the trihalide. In the case of iodine, the equilibrium constant of the disproportionation reaction at 25°C was determined to be 0.85. Gas chromatography analysis showed that chlorine attacks even dried, distilled PC (less than 7 ppm water), and that the extent of the reaction increases with increasing water content of the solvent. However, solutions of iodine in PC are stable for several months.

Conductivity experiments were performed to determine the extent of ion-pair formation of KI and KBr in PC. In addition, the conductivity of these solutions was measured as a function of the concentration of the corresponding halogen. Increased conductivity was noted for each solution, and a maximum was observed for equimolar iodide and iodine concentrations.

Cyclic voltammograms of KI in supported (KAsF_6) propylene carbonate show two anodic peaks. To characterize the voltammograms, the following sequence of reactions is proposed:



The validity of this mechanism was tested in an optically transparent thin layer cell by performing simultaneous cyclic voltammetry and UV-visible spectroscopy at a narrow mesh gold working electrode. The sequence of formation and disappearance of triiodide and iodine according to (i) and (ii) was confirmed by the spectral scans repeated at 30 second intervals.

A transport model for the simulation of the voltammograms was developed which takes into account the presence of two electron transfer steps; the fact that these steps have a complex (i.e. not 1:1) stoichiometry; the effect of mass transfer of the three species; and the kinetics of the charge transfer reactions. The results indicate that reaction (i) is kinetically inhibited while reaction (ii) is reversible.

ACKNOWLEDGMENTS

It has been my privilege to work with Charles Tobias throughout my stay at Berkeley. The creative and cooperative spirit that exists in the group is a tribute to him. I will miss him enormously.

I wish to acknowledge the fine undergraduate students who worked with me on the study of the stability of PC/halogen mixtures: Fred Watanabe (chlorine), Tim Brummer (iodine), and Cynthia Zee (iodine and bromine).

It has been a pleasure to work with Larry Galovich, a talented and conscientious technician, who cheerfully used his off-hours to repair our cars, bikes, etc. I appreciated the help of Ms. Susan Gangwer during the preparation of the final document.

I am grateful to Professors Elton Cairns and Leo Brewer for their thoughtful review of this manuscript.

I would particularly like to thank Mike Matlosz for his patience, persistence and friendship throughout our collaboration. My talented colleague, Paul Johnson, deserves much appreciation for his many contributions to this work. I am also grateful to Morgan Conrad for his help with the FTIR experiments and to Carol Balfe for teaching me spectral electrochemical techniques at the worst possible time for her.

There is a group of people who have made my stay at Berkeley very rich. I feel lucky to have been associated with the eclectic and high-spirited collection of individuals who comprise the Tobias, Muller, and Newman research groups. I have been fortunate to have made wonderful friends for science, camping or hijinks. They include Jeff Prentice, Paul Sides, Felix Schwager, Philippe Cettou, Gina Whitney, Roger Carr, Leslie Dixon and especially Susan Blew. Finally, I offer my warmest appreciation to Rob Moore, partly for his extremely helpful review of this manuscript, but mostly for his continuous support and love.

This work was supported by the Assistant Secretary of Conservation and Renewable Energy, Office of Energy Systems Research, Energy Storage Division of the U.S. Department of Energy, under Contract DE-AC03-76SF00098.

NOMENCLATURE

<i>A</i>	Electrode area, cm^2
<i>b</i>	Potential sweep rate, mV/sec
C_R	Concentration of reduced species, R, $moles/cm^3$
C_O	Concentration of oxidized species, O, $moles/cm^3$
C_R^0	Initial concentration of reduced species, R, $moles/cm^3$
C_O^0	Initial concentration of oxidized species, O, $moles/cm^3$
$[C_i]$	Concentration of species <i>i</i> , $moles/l$
D_O	Diffusion coefficient of species O, cm^2/sec
D_R	Diffusion coefficient of species R, cm^2/sec
<i>E</i>	Electrode potential relative to a given reference, <i>V</i>
E^0	Standard electrode potential, <i>V</i>
$E_{\lambda}, E_{\lambda'}$	Switching potentials for cyclic voltammetry, <i>V</i>
<i>F</i>	Faraday constant, 96485 <i>C/equiv.</i>
<i>i</i>	Current density, A/cm^2
$i_{0,ref}$	Exchange current density at a given reference state, A/cm^2
K_A	Association constant
k_f^I	Rate constant for Case I, $cm^3/mol-sec$
k_b^I	Rate constant for Case I, sec^{-1}
k_f^{II}	Rate constant for case II, $cm^4/mol-sec$
k_b^{II}	Rate constant for case II, cm/sec
<i>n</i>	number of electrons

O	Oxidized form in standard reaction, $R \rightarrow O + ne^-$
R	Reduced form in standard reaction, $R \rightarrow O + ne^-$
m, q	Stoichiometric coefficients
t	Time, <i>sec</i>
T	Temperature, °K
x	Distance from the electrode surface, <i>cm</i>
ν	Frequency, cm^{-1}
$\lambda^+ \cdot \lambda^-$	Single ionic mobilities, $cm^2/\Omega\text{-mol}$
Λ	Molar conductance, $cm^2/\Omega\text{-mol}$
λ	Switching time during a cyclic voltammetry sweep, <i>sec</i>
ρ	Density, kg/cm^3
ρ_0	Solvent density, kg/cm^3
β	Symmetry factor
γ	Activity coefficient

NONAQUEOUS SOLVENT ABBREVIATIONS

AN	Acetonitrile
DMA	Dimethylacetamide
DMF	Dimethyl formamide
DMSO	Dimethyl sulfoxide
EC	Ethylene carbonate
FA	Formamide
HMPTA	Hexamethylphosphotriamide
NMF	N-Methyl formamide
PC	Propylene Carbonate
THF	Tetrahydrofuran

Chapter I/ Introduction

The behavior of highly electropositive metals such as the alkali and alkaline earth metals is an area of active research for applications such as in high energy density batteries, liquid metal heat transfer fluids, or light-weight alloy materials. The electrodeposition of these metals at room temperature requires the use of non-aqueous solvents that are both stable under potential differences in excess of 5 volts and capable of dissolving metal salts to form conducting solutions. Previous work in this laboratory has established the feasibility of propylene carbonate as an ionizing solvent which also meets the criteria of stability with respect to alkali metals[1]. The electrodeposition of alkali metals in this solvent has been demonstrated[2], but the choice of a compatible anodic reaction remains an open question. This work presents an experimental evaluation of the feasibility of the electrochemical evolution of the halogens, chlorine, bromine, and iodine, in propylene carbonate.

To date industrial applications of halogen solutions in PC have been few. In 1980, a U.S. patent was issued to Tataria and Schneider[3] for an electrochemical cell which utilized a PC-based electrolyte to detect small quantities of chlorine. In 1974, Weiniger and Secor published the results of their study of a nonaqueous lithium-bromine secondary galvanic cell[4]. An ultra-fine polyethylene separator was used to contain the halogen within the negative electrode compartment. The electrolyte was lithium perchlorate and lithium bromide in PC. Tested in continuous ninety minute cycles, the cell performed for 1785 cycles, a surprisingly good result for the first test cell. No problems with solvent stability were noted in either of these cases.

Of principal interest in this evaluation are solvent stability, the solubility and conductivity of halide salts in PC, and the characteristics of the electrochemical reaction. An investigation was undertaken to determine the limits of

gas chromatography and FTIR spectroscopy to detect water and other impurities. The stability of the solvent in the presence of chlorine, bromine, and iodine was investigated using gas chromatography and UV-visible spectroscopy. To establish the characteristics of the electrochemical reaction of the halides in PC, iodide and iodine solutions were studied using cyclic voltammetry. The results of these experiments were analysed with the aid of a mathematical model that was developed in collaboration with M. Matlosz to simulate the voltammograms based on a proposed reaction mechanism. Spectral electrochemical experiments were conducted to independently verify this reaction mechanism.

- [1] J. Jorne, *Electrochemical Behavior of the Alkali Metals in Propylene Carbonate*, Ph.D Thesis, University of California, Dept. of Chem. Eng., (1972).
- [2] H. H. Law, *Studies on the Electrochemical Behavior of Potassium in Propylene Carbonate* Ph. D Thesis, Univ. of California, Dept. of Chem. Eng., LBL Report 9207, (1979).
- [3] H. Tataria and A. Schneider *U.S. Patent 973,204*, 26, Dec., (1978).
- [4] J. L. Weinagar and F. W. Secor *J. Electrochem. Soc.*, 121, 3, 315, (1974).
- [5] M. Matlosz *Experimental and Software Tools for the Study of Electrochemical Systems*, Ph. D Thesis, University of California, Dept. of Chem. Eng., (1985).

Chapter II/ Characterization of Propylene Carbonate

2.1. INTRODUCTION

Much has been written about the purification and characterization of propylene carbonate. The literature is not in complete agreement on certain points. The solvent has been described as "not hygroscopic to any great extent"[1], [2] yet it has been recommended as a drying agent for natural gas[3] and CO₂[4]. We noticed that dry PC will absorb water from the atmosphere so quickly that even brief exposure affects the precision of most electrochemical experiments. This observation is in accord with the bulk of the electrochemistry literature [5] [6]. Rigorous exclusion of water is necessary because impurities having labile protons, such as water, are extremely active in PC and often play a large role in electrochemical processes. For example, Jansta et al. report that current-potential curves for potassium deposition are smooth only in highly dried electrolyte. Water present in tens of ppm was sufficient to slow and eventually stop the deposition process[7]. These results were confirmed by Law[8]. Trace water can strongly influence the determination of properties of dilute electrolyte solutions. A solution of 10 ppm water, about 6×10^{-4} M, is enough to bind 10% of the cations in a 6 mM alkali metal solution[9].

In this chapter the techniques we used to purify and characterize propylene carbonate are presented and discussed. In addition, the use of Fourier transform infrared spectroscopy to detect water in propylene carbonate is evaluated. The results of a preliminary IR investigation to monitor the water content in salt solutions in PC are also presented¹.

¹ The Fourier transform spectrometer was generously loaned to us for use in off-peak hours by Dr. Herb Strauss of the Department of Chemistry. This investigation was therefore intended only to test the feasibility of the technique.

2.2. Analysis of Propylene Carbonate

Gas chromatography was the primary technique used to evaluate the solvent. Two types of detectors were used: flame ionization (FID) to detect organic impurities and thermal conductivity (TC) to detect water. The details of the instrument, the column and the injection procedure are described in section 3.2.1.

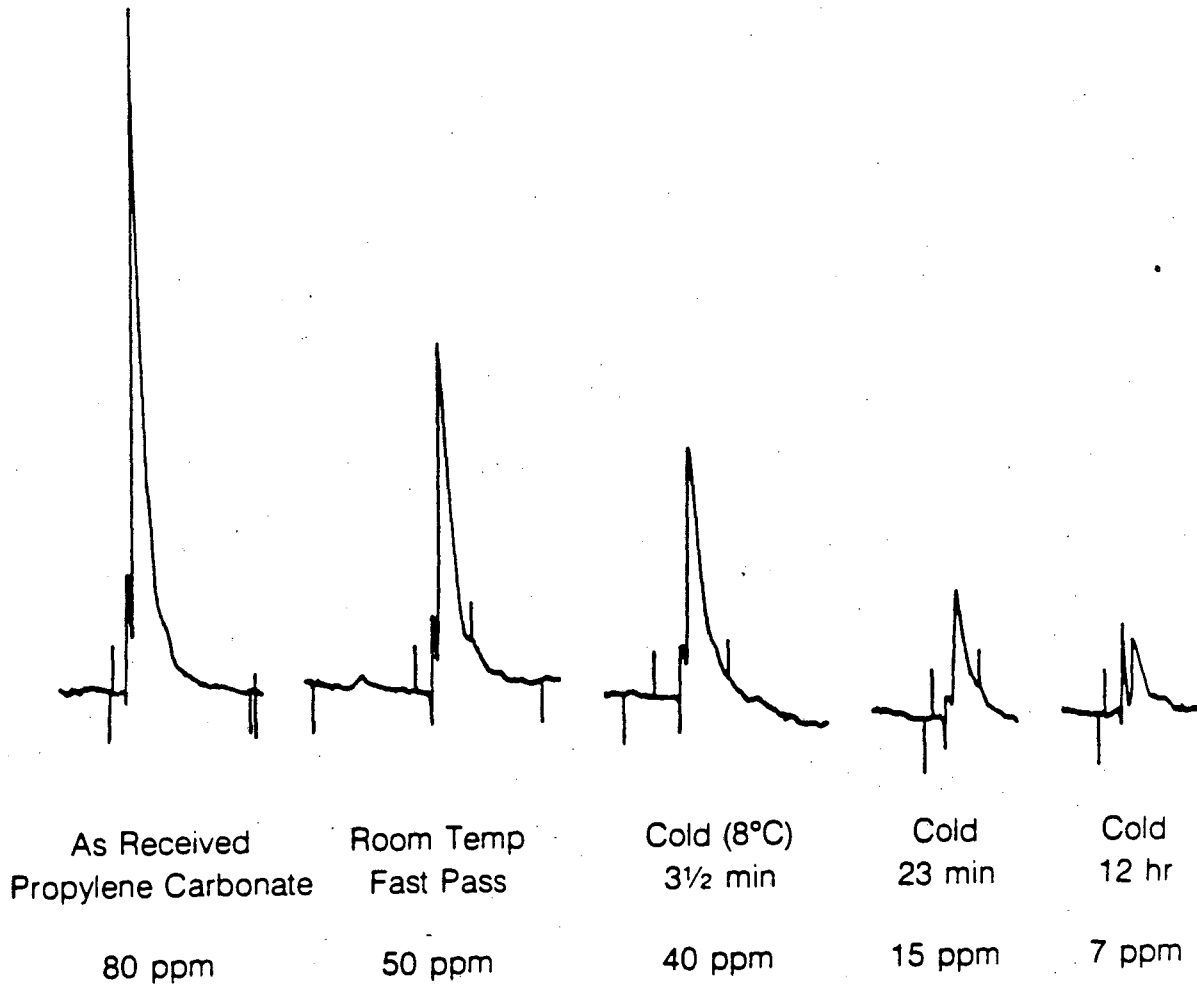
2.3. Purification of Propylene Carbonate

The purification procedures followed in this work were based upon work by Jasinski and Kirkland[10] and the subsequent extension by Law[11]. The starting material was either purified (Burdick and Jackson) or commercial grade (Jefferson Chemical) PC. The method consists of three steps: (i) pretreatment with dried molecular sieves and alumina, (ii) stripping the low boiling impurities by bubbling dry helium through the solvent overnight, and (iii) vacuum distillation. This purification scheme is described in detail in Appendix I.

Two changes from the process used by Law were made. First, because the heat of adsorption of water onto molecular sieves is large, the solvent becomes very hot when it is poured into a fixed bed of sieves. Therefore, to avoid decomposition at this step the solvent is chilled first to 0 °C before pretreatment. In addition, about 400 cc of sieves are added to the PC before it is poured through the sieve bed. In this way most of the heat of adsorption is dissipated into the solvent.

Secondly, our studies of water removal by molecular sieves indicate that the process is relatively slow. The effectiveness of water removal was evaluated by duplicating the pretreatment steps in the glovebox and analyzing the water content at each stage. Figure 2.3.1 demonstrates the effect of retention time and solution temperature on the performance of the molecular sieves. The water level of "as received" (Burdick and Jackson) solvent was reduced from 80 ppm to

Effect of Temperature and Retention Time on Molecular Sieve Performance



XBL 8410-10905

Figure 2.3.1 Effect of temperature and retention time on molecular sieve performance. The GC-TC water peak is shown. The water of "as received" PC is reduced from 80 to 50 ppm by a single pass through a bed of sieves. The water level in chilled (18°C) PC is reduced to 7 ppm after 12 hours.

40 ppm by immersing about 20 ml of dry sieves in about 100 ml of cold PC (8°C) for four minutes. The water content was further reduced to 7 ppm after 12 hours. As a result of these experiments, the retention time of the PC over the sieves was increased to two hours. PC purified in this way contained less than 5 ppm water and undetectable levels of glycols (less than 20 ppm) and formaldehyde (less than 1 ppm) as measured by GC.

2.4. Infrared Spectroscopy

Detection of impurities in propylene carbonate by the use of gas chromatography *only* has inherent limitations. First, the experiments are not easily reproduced. This is partially due to the ease with which PC will absorb atmospheric humidity. Inconsistent sample injection techniques and the decomposition of PC in the GC column at temperatures greater than 150 °C also contribute to this problem. (These difficulties are described in detail in section 3.2.) In addition, the water content of salt solutions cannot be analyzed by GC because the salt apparently catalyzes the breakdown of PC in the injection port. Thus alternative methods were sought which would operate at or near room temperature. One such alternative is infrared spectroscopy.

Infrared spectroscopy is a technique to measure the vibrational modes of a molecule. Water and PC have sufficiently different vibrational spectra to distinguish between the two molecules. Water is an asymmetric molecule with three vibrational modes which are active in the IR region. In the gas phase, the symmetric stretch ν_1 , the symmetric bend ν_2 , and the asymmetric stretch ν_3 are seen at 3657, 1595, and 3756 cm^{-1} , respectively[12]. In PC the carbonyl absorption in the IR is very strong and obscures the fundamental water absorption, ν_1 , at 3635 cm^{-1} for small concentrations of water. However, the $\nu_2 + \nu_3$ combination band at 5250 cm^{-1} in PC (5275 cm^{-1} in the gas phase) can be observed with little interference from PC. Conrad[13] has shown that the frequencies and bandwidths of the combination band correlate without exception to the those of

the fundamental ν_3 band in several solvents. The absorption of water in solvents is shifted to lower frequencies than in the gas phase. This shift can be correlated with the degree of interaction between the solvent and water, as shown in Figure 2.4.1. On the far right, the small frequency shift observed for water in carbon tetrachloride ($\sim 30 \text{ cm}^{-1}$ from water in the gas phase) indicates that water is only very weakly coordinated to the solvent. On the other hand, water is strongly bound to tetrahydrofuran (a shift of 195 cm^{-1}). Water in propylene carbonate shows intermediate behavior. Cogley et al.[14] have reported that, based on IR and NMR studies, the interaction of water in PC is best described by a continuum model in which water molecules form hydrogen bonds to PC solvent molecules. Water retains a C_{2v} symmetry. In PC, the self-association of water is reported as limited to two distinct solvated species: a monomer and a dimer.

IR has been used as an analytical tool to detect water in a variety of organic and inorganic solvents[15], [16]. A preliminary test of the method in PC solutions by Jasinski and Carroll[17] has shown detection of less than 100 ppm water in salt solutions in PC. However, the addition of lithium perchlorate to the solution complicated the analysis. With increasing concentrations of the salt (equal water concentration), a shift in the peak maximum and a decrease in the intensity from pure solvent values was observed. The authors conclude that, in these solutions, water exists as hydrated lithium ions. In addition, the extinction coefficient decreases with increasing LiClO_4 concentration, even though at these concentrations (0.5 to 1.0 M), there is a large excess of lithium ions over water molecules. This preliminary work showed promise and it was hoped that the use of a Fourier transform spectrometer, such as the one available for this study, would improve the sensitivity to the water signal to equal or exceed the results obtained by GC.

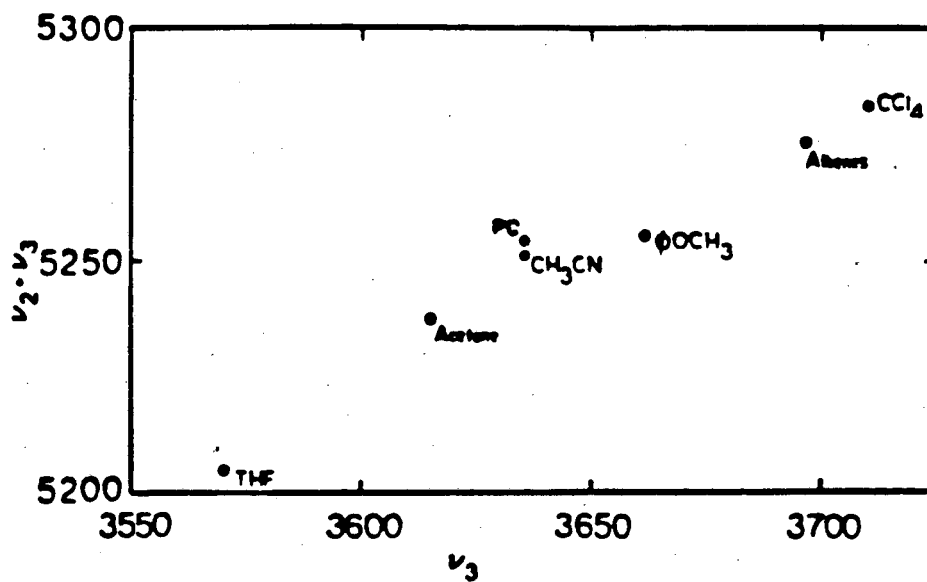


Figure 2.4.1 Correlation between the $U_2 + U_3$ combination band frequency (in wavenumbers) of water and its U_3 frequency as a function of solvent. Taken from M. Conrad [13] with permission.

2.4.1. Experimental

Because the water stretching region in PC occurs near solvent bands, it was necessary to obtain an accurate spectrum of dry solvent as a reference for subtraction. In this study, the reference sample was dried, distilled PC, as described in section 2.3. Occasionally a small amount of potassium was added to the cell to make sure that the sample remained dry while the spectrum was taken.

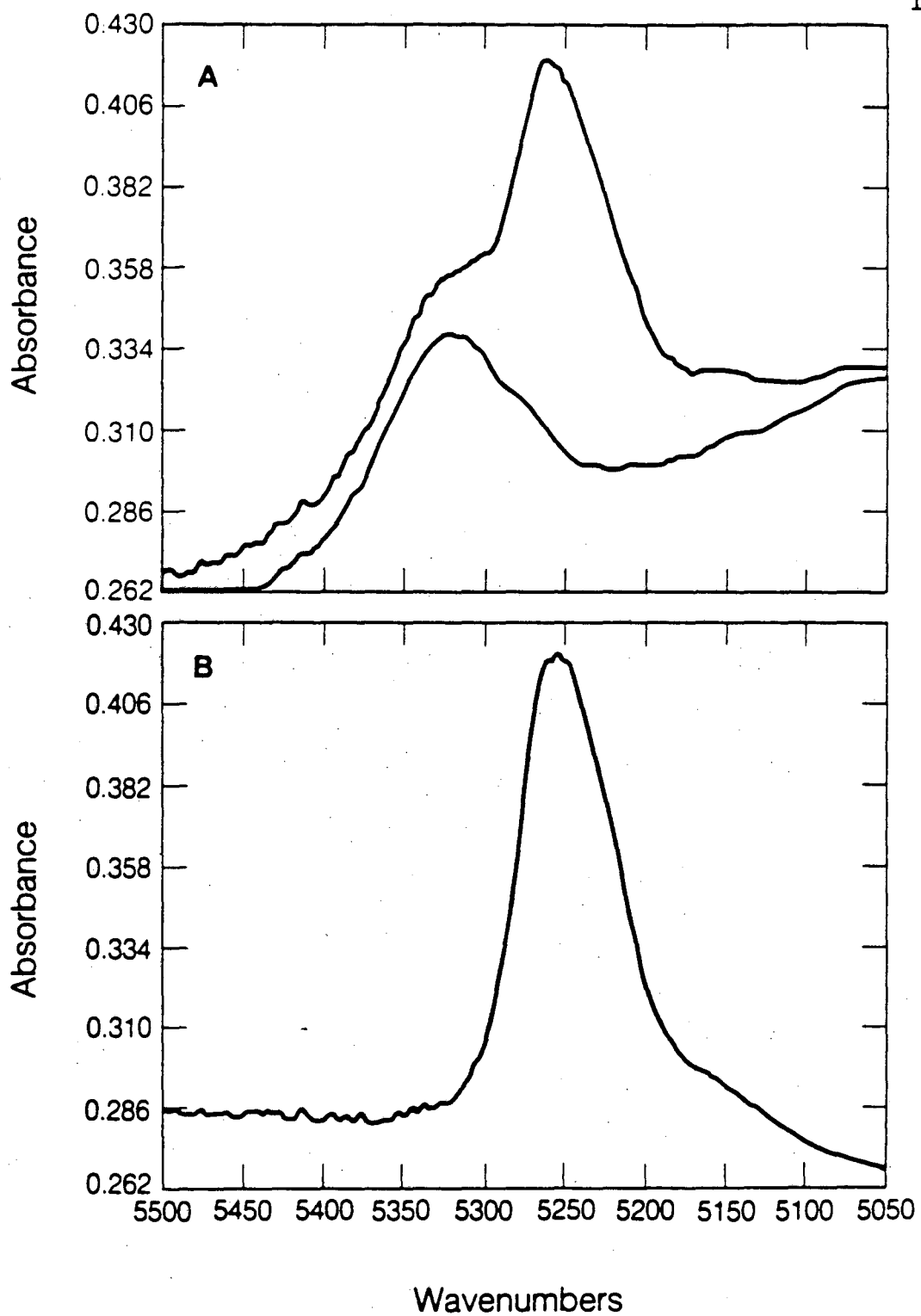
Water in the low ppm range can only be observed with an instrument with extremely high ratio of signal to noise. We² used a Nicolet model 8000 vacuum Fourier transform infrared (FTIR) spectrometer with the entire optical path length except a small tub (about two liter capacity) evacuated to less than 1 mm. The tub, which contained the sample, was purged with house nitrogen passing through a 4-ft drying tube filled with calcium sulfate. The cell (Harrick liquid cell) used 2-mm teflon spacers between 1" diameter windows, and was sealed with Viton o-rings and teflon plugs. The cell windows were CaF₂ because KBr windows were too hygroscopic. All spectra were run at a nominal 2-cm⁻¹ resolution; several thousand scans were obtained in two hours.

2.4.2. Results

Water in Propylene Carbonate

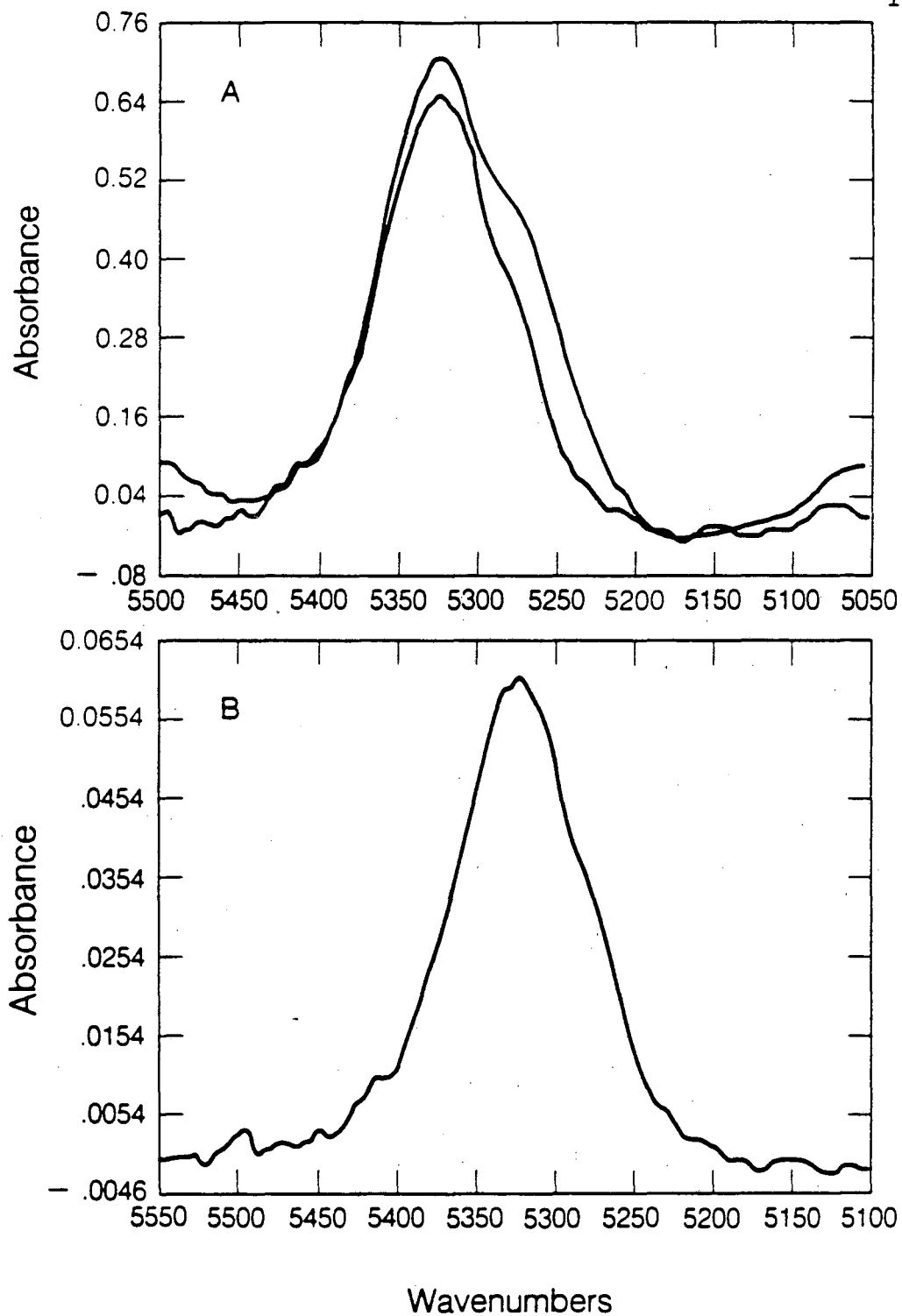
Figure 2.4.2 illustrates the difference between a sample of wet (1.3 %) and dried, distilled PC. The water peak appears very clearly at 5250 cm⁻¹. The difference spectrum (Figure 2.4.2B) shows a relatively narrow peak for water. However, detection is more difficult at lower water concentrations. The IR spectrum of a solution containing 80 ppm water compared to dried, distilled solvent is given in Figure 2.4.3. The water absorption appears as a shoulder to the PC

² All experiments were done with Morgan Conrad, a graduate student of Dr. H. Strauss, using their group's instrument.



XBL 849-10869

Figure 2.4.2 FTIR spectra of water in PC. (A) Upper curve: 1.3% water in PC. Lower curve: dried, distilled PC. (B) Difference spectrum.



XBL 849-10867

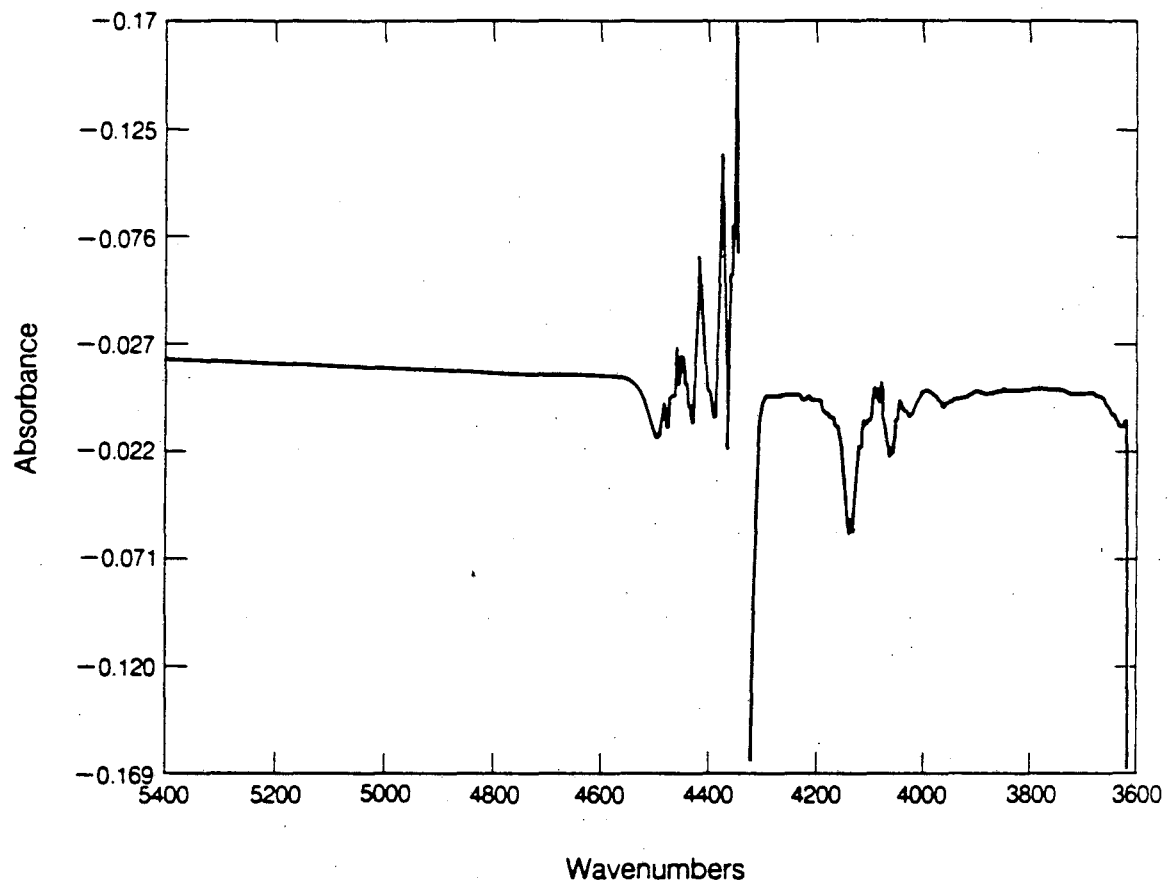
Figure 2.4.3 FTIR spectra of water in PC. (A) Upper curve: 80 ppm water in PC. Lower curve: dried, distilled PC. (B) Difference spectrum.

band at 5380 cm^{-1} , and the peak seen in the difference spectrum (Figure 2.4.3 B) is much smaller. From several trials at lower concentrations, it appears that about 10 ppm is the limit of detection for water. Although this is better than that reported by Jasinski (100 ppm), it is approximately the same sensitivity as can be obtained by GC analysis.

Detection of Water in the Presence of Electrolytic Salts

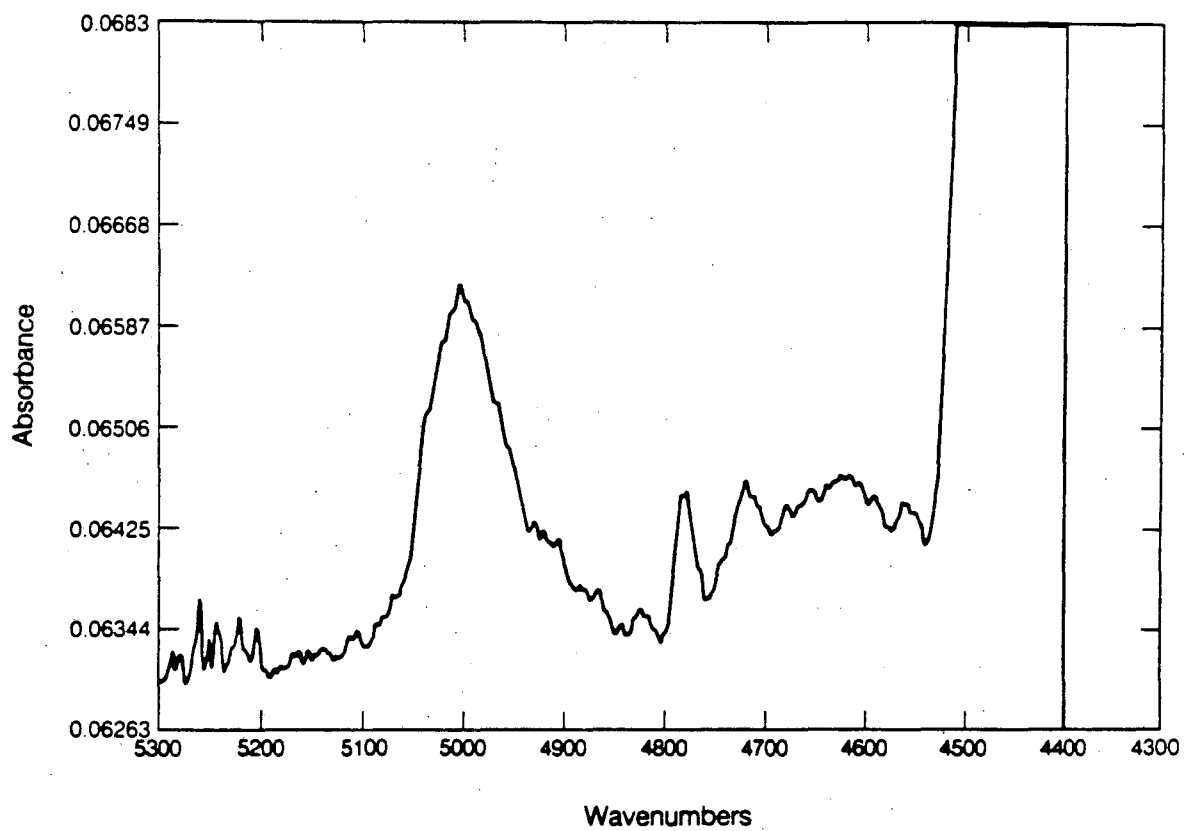
Additional preliminary FTIR experiments were carried out with solutions of KOH and KBr. Concentration measurements of water in salt solutions are of interest because the salt interferes with GC analysis. The results outlined here are intended only to demonstrate the type of information that can be obtained. KOH was studied to evaluate the use of metallic potassium as a drying agent. Potassium reacts with trace water in the solvent to produce KOH which remains in the bottoms when PC is distilled. It was decided to try to use FTIR to monitor the water removal and see if evidence of KOH could be found. To approximate this procedure, a small lump of potassium was scraped under a helium atmosphere and placed in 2 ml of PC containing about 25 - 30 ppm water. The difference spectrum (untreated PC subtracted from PC dried with potassium) is shown in Figure 2.4.4. Differences are small, however several small peaks are seen. The spectrum shows evidence of an undifferentiated band at $\sim 4359\text{ cm}^{-1}$ (peak A) and a negative peak at 4150 cm^{-1} (peak B). No change in the water peak is observed at 5250 cm^{-1} to indicate a change in the water concentration.

To interpret this spectrum, a solution of KOH in PC was analyzed. The difference spectrum (PC/KOH solution minus PC) is given in Figure 2.4.5. Three peaks are observed at 5006 cm^{-1} , 4781 cm^{-1} , and 4400 cm^{-1} . Tentatively the peaks are assigned to the free OH stretch (5006 cm^{-1}), and OH^- coordinated to PC ($\sim 4400\text{ cm}^{-1}$). The small peak at 4781 cm^{-1} is not assigned. From these results the difference spectrum of PC dried with potassium indicates that the PC carbonyl peak at $\sim 4400\text{ cm}^{-1}$ is slightly shifted, possibly as a result of the OH^-



XBL 849-10868

Figure 2.4.4 FTIR difference spectrum of PC that has been dried with potassium minus PC.



XBL 849-10870

Figure 2.4.5 FTIR difference spectrum of 0.2 M KOH in PC minus pure PC.

coordination of PC. No peaks appear at 5006 cm^{-1} (from free hydroxide) or at 5250 cm^{-1} (from the disappearance of water). Thus, these early results seem to indicate that little water is removed. Several explanations are possible. Either an undetectable amount of water was removed, or the potassium is quickly covered with a protective oxide and thus ceases to be effective, or potassium reacts with PC instead of water. Clearly, further study is needed to elucidate this process.

The effect of KBr on the IR spectrum of PC solutions was also examined. The effects of a saturated solution ($6 \times 10^{-3}\text{ M}$) were small. The only change we observed was a shift of about 30 cm^{-1} for the λ_{max} of water at 5250 cm^{-1} . This change is approximately the same magnitude as that observed by Jasinski for perchlorate solutions in PC.

2.5. CONCLUSIONS

FTIR spectroscopy has been evaluated as an analytical technique to detect water at levels below 100 ppm in PC. We find that the limit of detection is about 10 ppm. Water content can also be monitored in salt solutions. However, the peaks are somewhat attenuated and shifted by about 30 wavenumbers. The preliminary results are encouraging. But to obtain reliable data for salt solutions, careful calibration would be required. Because few other methods are available for this type of measurement, this technique merits further study.

REFERENCES

- [1] R. F. Nelson and R. N. Adams, *J. Electroanal. Chem.*, **13**, 184 (1967).
- [2] T. Fujinaga and K. Izutsu in "Recommended Methods for Purification of Solvents", J. F. Coetzee, Ed., IUPAC, Pergamon Press, (1982).
- [3] P.D. Kravets, et al., USSR Patent, 1983, Chem. Abstracts Reference, 83: P 150166m.
- [4] G.L. Smith et al., U.S. Patent Application No. 863,355, Dec. 22, 1977.
- [5] R. Jasinski and S. Kirkland, *Anal. Chem.*, **39**, 1663, (1968).
- [6] F. P. Dousek, J. Riha, *J. Electroanal. Chem.*, **39**, 217, (1972).
- [7] J. Jansta, F. P. Dousek and J. Riha, *Electroanal. Chem. and Interfacial Electrochem.*, **44**, 263 (1973).
- [8] H. Law, *Studies on the Electrochemical Behavior of Potassium in Propylene Carbonate*, Ph.D Dissertation, Department of Chemical Engineering, Univ. of California, Berkeley, May, 1979.
- [9] R. Jasinski, in "Advances in Electrochemistry and Electrochemical Engineering", P. Delahay and C.W. Tobias, Ed., Vol. 8, Wiley-Interscience, (1971).
- [10] R. Jasinski and S. Kirkland, *op cit.*
- [11] H. Law, *op cit.*
- [12] J.R. Scherer, *The Vibrational Spectroscopy of Water*, Vol. 5, Chap. 5 in "Advances in Infrared and Raman Spectroscopy", Heyden Press, 1978.
- [13] M. Conrad "Infrared Studies of Low Interaction Binary Systems", Ph. D. Dissertation, Chemistry Department, University of California, Berkeley, California (1984).
- [14] D. R. Cogley, M. Falk, J. N. Butler, and E. Grunwald, *J. Phys. Chem.*, **76**, 6, (1972).
- [15] H. Cordes and C. W. Tait, *Anal. Chem.*, **29**, 4, 485 (1957).

[16] R. Meeker, F. Critchfield, and E. Bishop, *ibid.*, 29, 1511 (1962).

[17] R. Jasinski and S. Carroll, *Anal. Chem.* 40, 12, 1908 (1968).

Chapter III / Stability of Propylene Carbonate in the Presence of Halogens

3.1. INTRODUCTION

Propylene carbonate must be stable in the presence of halogens for halide/halogen electrodes to be considered viable candidates for large scale electrochemical applications. In this chapter, we address the question of the durability of the solvent in the presence of chlorine, bromine, and iodine.

Two different experimental techniques were used in this work. Because iodine and bromine solutions in PC are highly colored, UV-Visible spectroscopy can be used to determine the concentration of these species. The advantage of this technique is that measurements can be carried out at room temperature, thereby avoiding the decomposition of PC. Solutions of chlorine in PC were analyzed by gas chromatography. This technique is more problematic because it is sometimes difficult to distinguish decomposition products in the solution from those resulting from solvent breakdown in the GC column, or from trace water introduced during sample injection.

From the the UV-Visible-experiments, we found that iodine disproportionates in PC to form triiodide and probably a positively charged iodine species. Similar behavior was noted in bromine solutions. Conductivity experiments confirmed the formation of charged species. This type of reaction has been reported in pyridine, but has not been reported in PC. Although halogen disproportionation in PC and solvent stability may be completely separate phenomena, it is more likely that they are related. Both subjects are covered in this chapter.

3.2. CHLORINE

From the point of view of the economics of alkali metal deposition, the evolution of chlorine would be the anodic reaction of choice. It has been

demonstrated that the salt, $KAlCl_4$, is soluble in PC in excess of one molar, and that it can be easily synthesized by fusing KCl and $AlCl_3$ at about $500^\circ C$ [1]. But from the point of view of feasibility, chlorine is the strongest oxidizing agent of the three halogens we have considered and is the most likely to attack PC. In this section, the results of experiments designed to test the compatibility of PC with chlorine are presented. In particular, we have tried to evaluate the influence of impurities in PC on the decomposition reactions in the presence of chlorine.

To date, only one study has addressed the question of the compatibility of PC and chlorine. In 1979, Yu, Ross, and Tobias published a short report which demonstrated extensive degradation of PC in the presence of chlorine [2]. Chlorine was found to degrade even the most carefully purified propylene carbonate. In experiments in which chlorine was bubbled at a rate of about 1 ml per minute through approximately 15 ml of PC, color changes were observed and rapid degradation was detected by GC analysis. After 30 seconds of bubbling, the propylene glycol and propylene oxide levels rose from 5 ppm to about 200 ppm. After two hours, these levels were measured in excess of 1×10^4 ppm. In experiments in which chlorine was electrochemically generated from a potassium chloro-aluminate solution in PC, degradation was again observed in the anolyte chamber. At a current density of $80 \mu A/cm^2$ (one cm^2 electrode area), the amounts of propylene glycol and propylene oxide reached the same level found in the chlorine bubbling experiments after two hours. In addition, it was reported that water plays an important role in the degradation process. Addition of as little as 10 ppm water caused the extent of degradation to increase as much as tenfold. Unfortunately, Yu did not dry the chlorine gas (from standard cylinders) used in his experiments. Wet chlorine could drastically influence the results.

The discovery that even small amounts of water can apparently enhance the breakdown of PC in the presence of chlorine cast doubt on "inherent" instability

of PC. If water levels could be reduced to below 1 ppm (say), could the breakdown of PC be avoided? In this section, the study by Yu is extended to try to answer this question as well as to try to elucidate the mechanism of degradation.

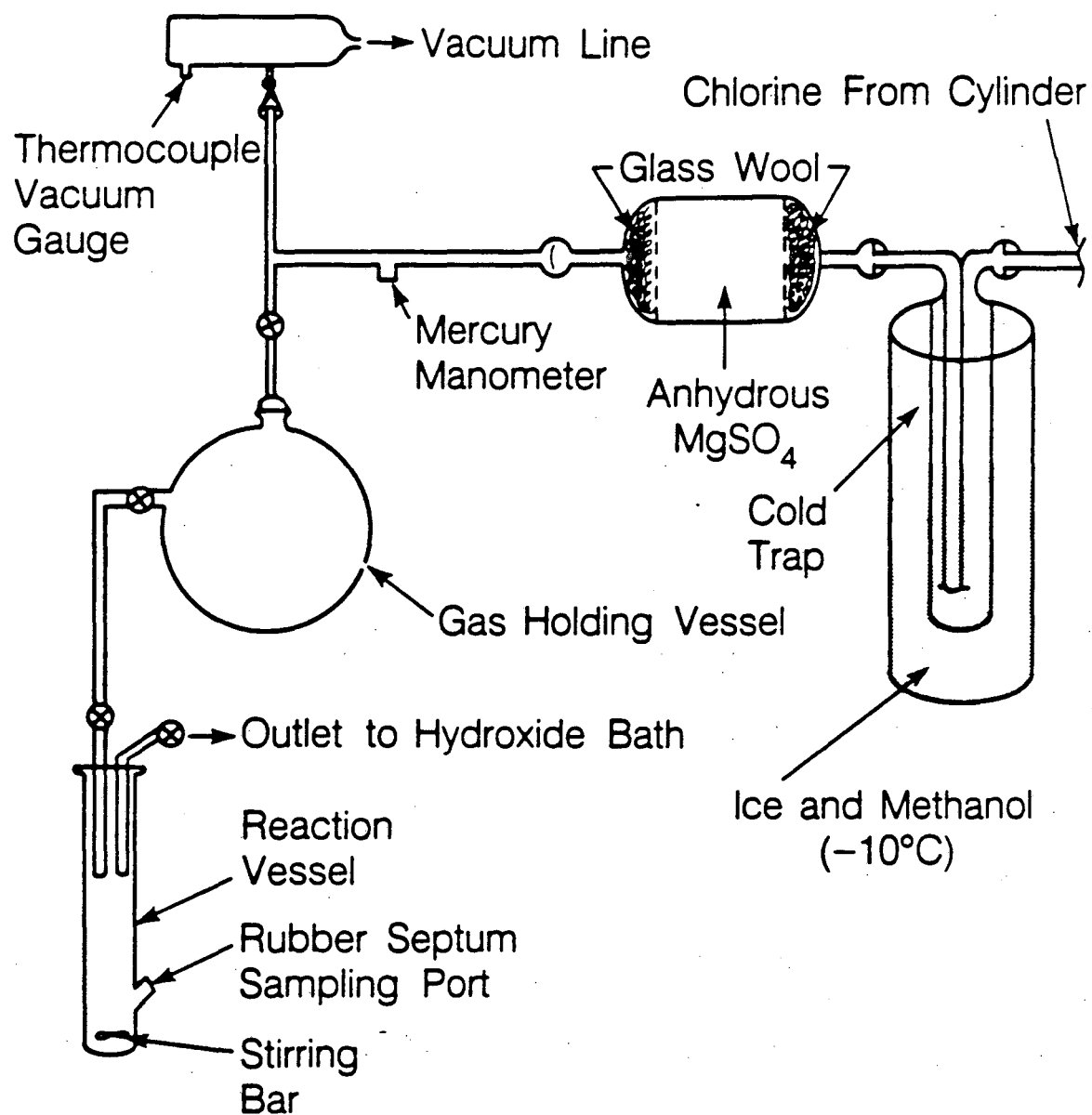
3.2.1. Experimental

Exposure Vessel and Pressure/Vacuum Manifold

The general approach to this study was to expose well-characterized PC to elemental chlorine and water in varying combinations. The PC was characterized before and after exposure by gas chromatography to determine the degradation products and to monitor the extent of degradation.

The equipment designed for this experiment is shown in Figure 3.2.1. Five ml of PC containing a known amount of water is transferred to this vessel inside the glovebox under a helium atmosphere. The vessel is connected to the pressure/vacuum manifold (which is already under helium) and evacuated to $100 \mu\text{m Hg}$. Chlorine (Matheson, Research Grade, 99.97%) is added using a mercury manometer to monitor the pressure¹. Before contacting the PC, the chlorine is passed through two cold traps containing a methanol/ice mixture (-10°C) and a filter containing anhydrous magnesium sulfate. This system was designed to remove water from the chlorine before it contacted the PC. The PC is agitated vigorously by a stirring bar for the duration of the exposure. At the end of the run, samples were taken through a rubber septum with a microsyringe for GC analysis. Chlorine was purged then from the system by bubbling helium throughout the manifold and the exposure vessel. The helium was finally bubbled through a concentrated (6 N) hydroxide solution to strip the chlorine before the apparatus was disassembled. This procedure was repeated for various combinations of exposure time, chlorine pressure, and water content of PC.

¹ A thin film of mercuric chloride was formed at the mercury interface in the manometer. This film did not hinder the measurement.



XBL 849-10819

Figure 3.2.1 Reaction vessel and pressure-vacuum manifold for controlled exposure of PC to dry chlorine gas.

Gas Chromatography

The PC was analyzed with a Varian model 3700 gas chromatograph equipped with both a thermal conductivity (TC) detector for water analysis and a flame ionization (FID) detector for organics. The column packing material was "Poropak Q" (Waters Scientific, 100 mesh) contained in 1/4 in OD, 24 in stainless steel columns. Because the decomposition products had differing sensitivities to the GC packing and appeared in varying amounts, the temperature of the column was programmed in a systematic fashion for each sample injection. Under this regime, PC appeared after about 70 minutes so each run lasted about 2 hours. In addition, each run was recorded simultaneously at three different GC sensitivities using a three-pen recorder. Table 3.2.1 lists the operating conditions used for the GC for this series of experiments.

Table 3.2.1 Gas Chromatograph Operating Conditions		
	TC Conditions	FID Conditions
Injection Size	2 μ l	2 μ l
Injector Temp.	130 °C	130 °C
Column Temp.	100 °C	$T_1 = 100\text{ }^\circ\text{C}$ (30 min) $\Delta T = 5\text{ }^\circ\text{C}/\text{min}$ $T_2 = 160\text{ }^\circ\text{C}$
Detector Temp.	200 °C	200 °C
Attenuation	1	1
Detector Current	205–207 mA	
Filament Temp.	270 °C	
Helium Flow	60 ml/min	120 ml/min
Air Flow		300 ml/min
Hydrogen Flow		60 ml/min
Range	10 ⁻¹²	0.05

The reaction products were identified by comparing the unknown GC trace to GC traces of known compounds dissolved in pure PC. This process was guided by the results of GC analysis of PC reported by Jasinski and Kirkland [3]. The results we obtained are in agreement with this work. A calibration curve was established for each of the major impurities, including formaldehyde, propylene oxide, acetone, allyl alcohol, and the propylene glycols (1,2 and 1,3). This was done using the same temperature programming schedule used for the sample analysis. The analysis of PC by gas chromatography is complicated by the fact that PC will decompose in the column near the temperature required to elute high-boiling components from the column. Although precautions were taken to assure reproducibility, the results often varied by as much as 25%. To obtain reliable data, the calibration curves were often repeated and several sample injections were made for one measurement².

The Varian GC showed a large variation in sensitivity for different components. Formaldehyde, acetone and allyl alcohol can easily be detected below 10 ppm at the most sensitive setting of the GC and recorder (1 mV full scale). To detect 1,2 and 1,3 propylene glycol, the chart recorder was set to 50 mV full scale. At this setting, the detection limit for these compounds is about 50 ppm. These curves were recorded simultaneously using a multiple pen chart recorder.

The water content of the PC was analyzed using the thermal conductivity detector. This is a difficult analysis because sufficient water can be absorbed by PC from the air during injection to give spurious results. For this reason our reported water contents are probably slightly high.

Gas Chromatography with Mass Spectroscopy Detection

We were not able to identify all components in the samples of reacted PC. To obtain a better understanding of the identity of the reaction products, some

² Reproducibility could be greatly enhanced if a sample loop were to be installed in the glovebox. In this way samples could be directly injected into the GC without handling them in air.

samples were evaluated by the Mass Spectroscopy Laboratory of the Department of Chemistry using a Finnegan Model 400 GC equipped with a mass spectrophotometer³. This approach proved to be helpful for components present in large amounts (greater than at least 100 ppm) but we found that in general this instrument was about one hundred times less sensitive than the Varian 3700. Also, because the instrument is used for many different types of analysis, it was extremely difficult to obtain reproducible results.

Solubility of Chlorine in PC

The solubility of chlorine in PC was estimated by analyzing a sample of PC exposed to 155 mm Hg chlorine for 60 hours. Total chlorine was determined to be 0.5 weight percent. These experiments were performed at 25 °C.

3.2.2. Results

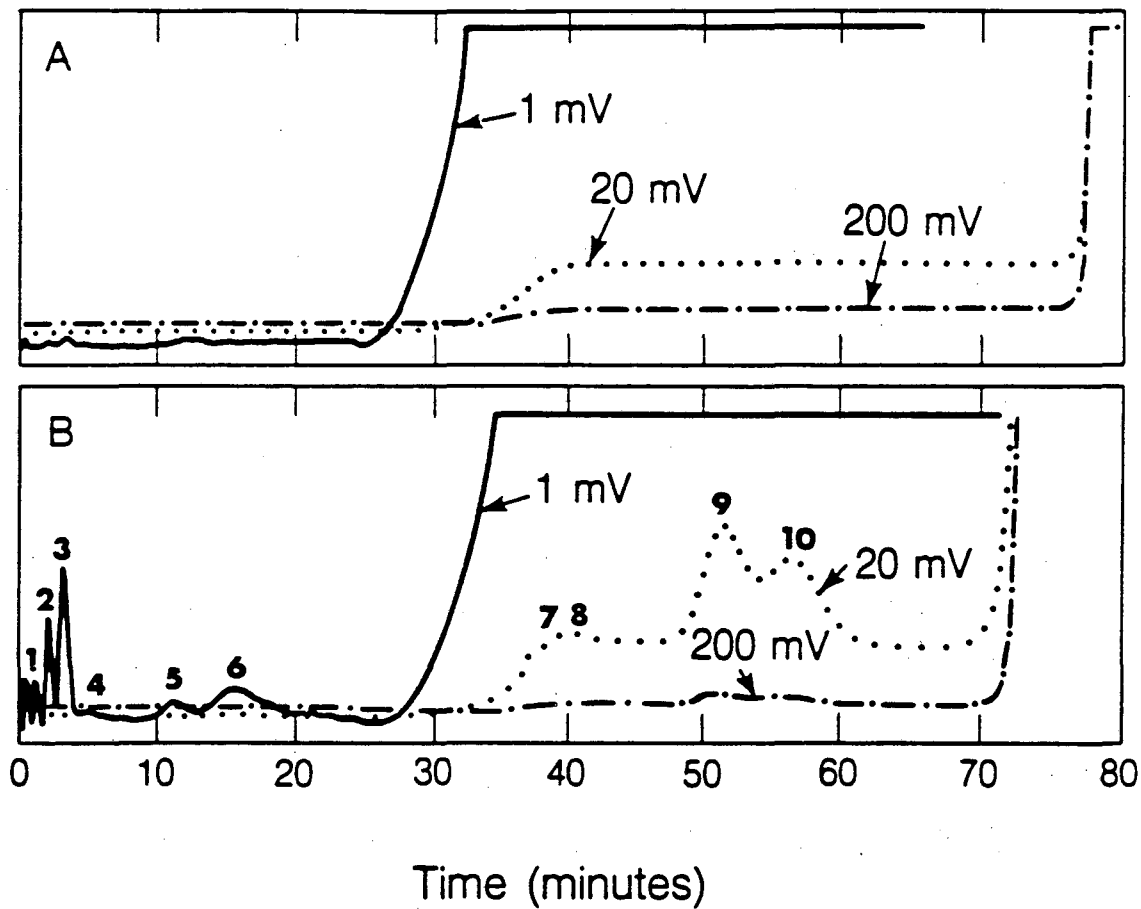
PC Analysis

Different batches of PC containing varying amounts of water were evaluated in these experiments. Preliminary runs to test the equipment and provide "worst case" results were done with PC containing approximately 800 ppm water. The final runs, designed to test the driest PC, were performed with the solvent containing less than 10 ppm water. (In this range, water is undetectable by GC analysis.) Figure 3.2.2A shows the chromatogram of PC containing less than 7 ppm water. A small peak for acetone and propylene oxide/propionaldehyde appears (less than 3 ppm), but in general the trace is featureless until the PC emerges. The step at 35 minutes is a baseline shift caused by the temperature program.

³ A DB-5 capillary column (32 mm ID x 50 m) was used for these measurements. The temperature program was 30°C for 10 minutes, then 5 °C/min to 240 °C.

Reaction Products

Figure 3.2.2B shows an example of the complete chromatogram for a sample of wet (140 ppm) PC exposed to approximately 50 mm Hg chlorine for 1 hour. The temperature of the column was programmed as described above, and all of the major product peaks can be seen. A summary of the reaction products detected and their retention times is given in Table 3.2.2. Peak 5 is marked "propylene oxide/propionaldehyde" because these two components are not separated in the column. The peaks having retention times of 1.1 minutes, 2.4 minutes, 5.7 minutes, and 40.5 minutes remain unidentified because known compounds having the same retention time were not found.



XBL 849-10821

Figure 3.2.2 (A) GC-FID chromatogram of pure PC containing less than 7 ppm water. (B) GC-FID chromatogram of wet (140 ppm) PC exposed to 50 mm Hg chlorine for 12 hours. Three recorder sensitivities, 1, 20, and 200 mV full scale, are shown. Numbers at each peak correspond to components listed in Table 3.2.2.

Component	Retention Time (minutes)
1)	1.1
2)	2.4
3) Formaldehyde	3.6
4)	5.7
5) Propylene Oxide/ Propionaldehyde	12.7
6) Acetone	18.2
7) Allyl Alcohol	37.5
8)	40.5
9) 1,2 Propylene Glycol	52.4
10) 1,3 Propylene Glycol	58.4

Summary of Experiments

A summary of the relevant experiments is given in Table 3.2.3. The results are characterized in terms of the product concentrations of formaldehyde, propylene oxide, acetone, allyl alcohol, propylene diol, and propylene oxide as a function of the amount of water in the PC and the exposure of chlorine. All experiments were carried out at room temperature.

Table 3.2.3 Summary of Experiments: Reaction Products					
	Experimental Conditions				
Water (ppm) Cl ₂ (mm Hg) Time (Hours)	33 0 0	33 50 1	33 150 1	133 50 1	7 155 60
COMPOUND (ppm)					
Formaldehyde	<1	23	42	45	70
Propylene Oxide/ Propionaldehyde	<1	7	22	17	10
Acetone	<1	<1	20	15	15
Allyl Alcohol	<1	<50	500	200	2000
1, 2 Propylene Glycol	<1	<50	5 × 10 ³	10 ³	10 ⁴
1, 3 Propylene Glycol	<1	<50	5 × 10 ³	10 ³	10 ⁴

Effect of Chlorine Exposure Pressure

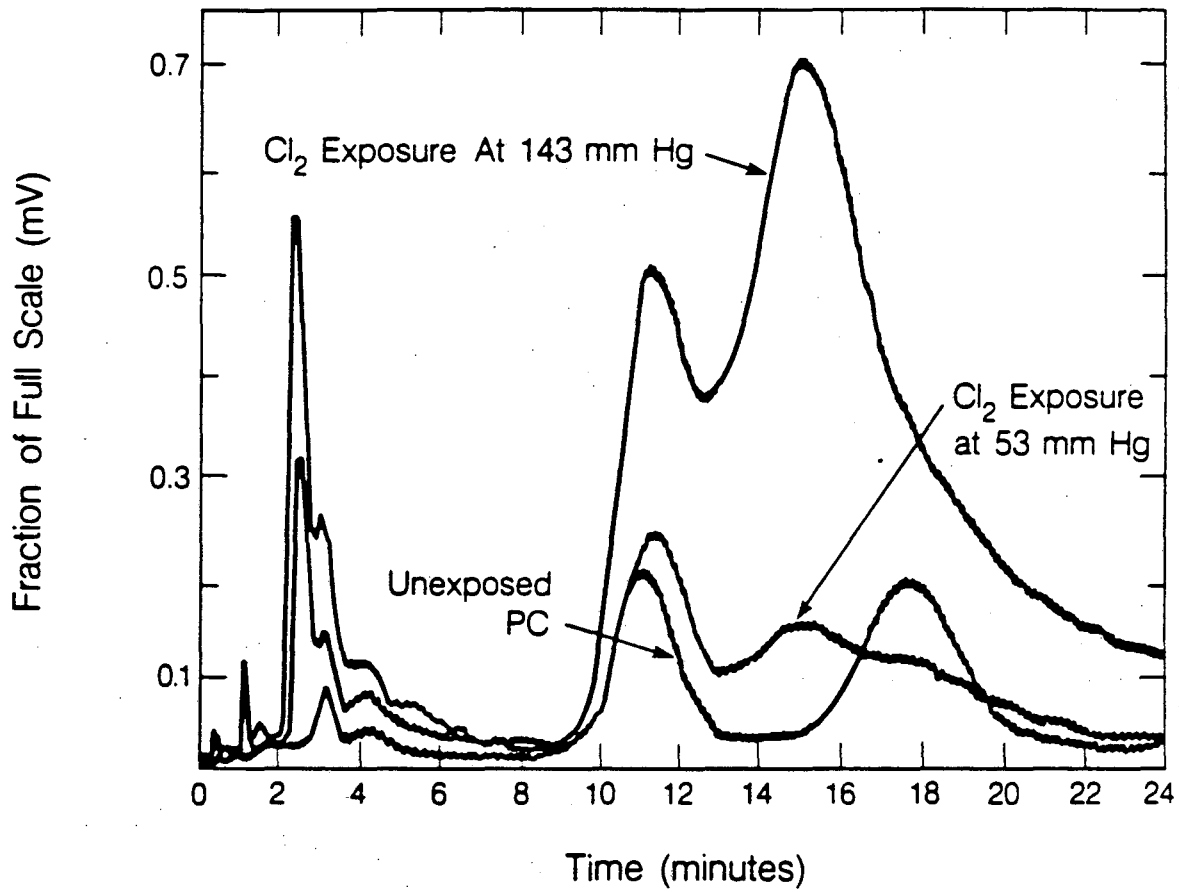
The concentration of decomposition products increases as the pressure of chlorine in the exposure vessel is increased. Figure 3.2.3 illustrates the effect of chlorine pressure on the chromatogram of wet (800 ppm) PC for an exposure time of one hour. As the chlorine partial pressure is increased from zero to 143 mm Hg, the concentration of the major impurities shows a threefold increase.

The concentration of products depends upon the amount of water in the PC. Figure 3.2.4 illustrates the same series for PC containing 33 ppm water. In this case, the chromatogram for PC exposed to 50 mm Hg chlorine for one hour (C) shows little change from unexposed PC (A). However, if the pressure is raised to 150 mm Hg (also for one hour), an increase in the amount of all impurities is seen (B). In particular, the concentration of the diol compounds rises from an undetectable level (less than 30 ppm) to over 300 ppm.

Effect of Chlorine Exposure Time

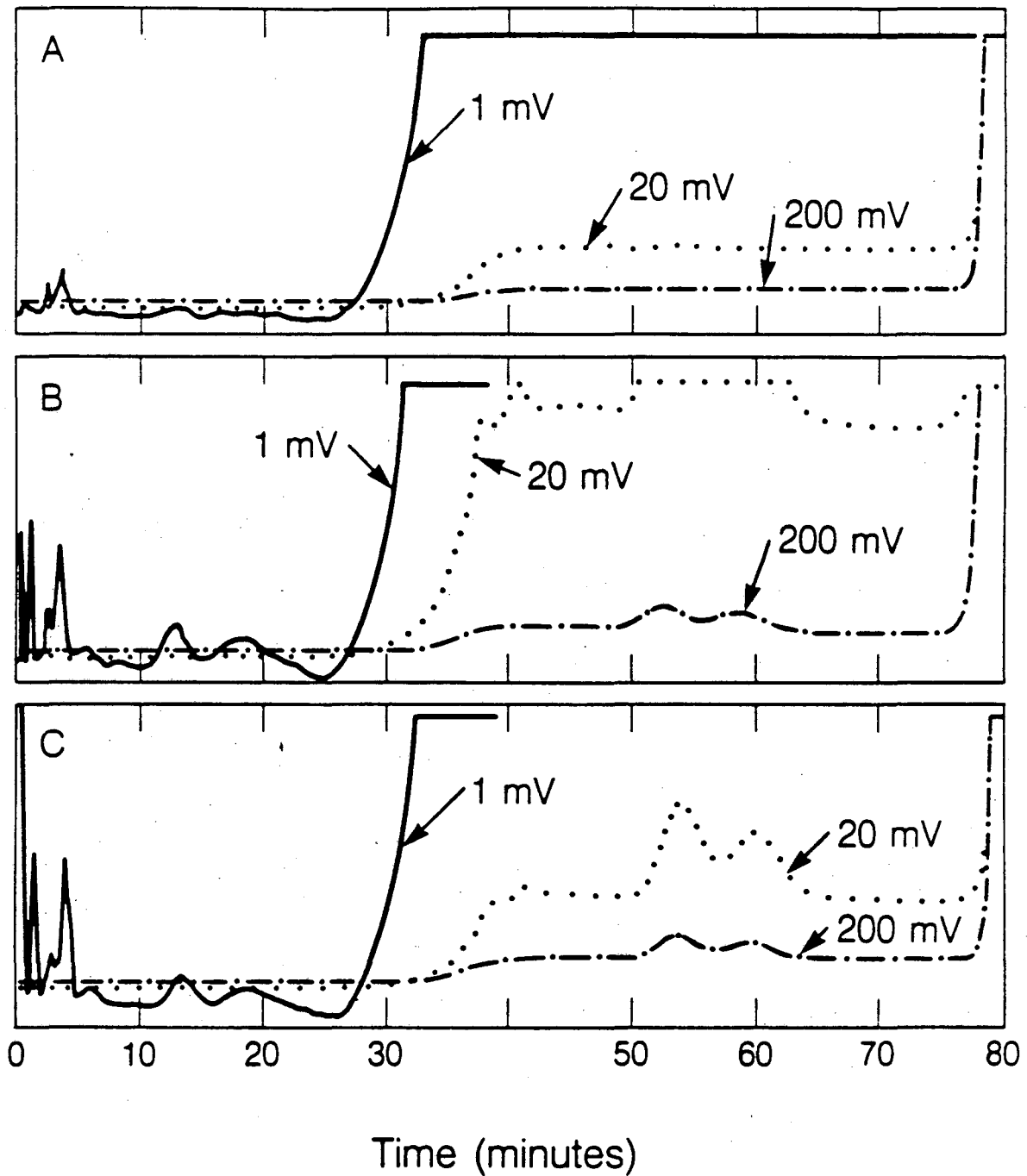
Changing the amount of time that the PC sample is exposed to a chlorine atmosphere has qualitatively the same effect as increasing the chlorine pressure. Again, the amount of water in the sample is important. Figure 3.2.5 illustrates the difference in the gas chromatogram for exposure times of 1 and 12 hours. The PC sample in this case contained 33 ppm water and the chlorine pressure was 50 mm Hg. Unfortunately, the glycol concentration for these runs was not carefully monitored.

Several runs were made at a chlorine pressure of 50 mm Hg and monitored by GC-MS. The duration of these runs varied from one hour to eight days and the water content of the PC was 15-20 ppm. No impurities except CO₂ were detected by GC-MS. This is a reflection of the lack of sensitivity of the instrument; unfortunately the samples were not also evaluated by the GC-FID.



XBL 849-10813

Figure 3.2.3 Effect of chlorine on wet PC. All PC samples contained 800 ppm water.



XBL 849-10831

Figure 3.2.4 Effect of chlorine pressure on PC containing trace water. All samples contained 33 ppm water. (A) Unexposed PC. (B) Chlorine pressure: 150 mm Hg, one hour exposure. (C) Chlorine pressure: 50 mm Hg, one hour exposure time.

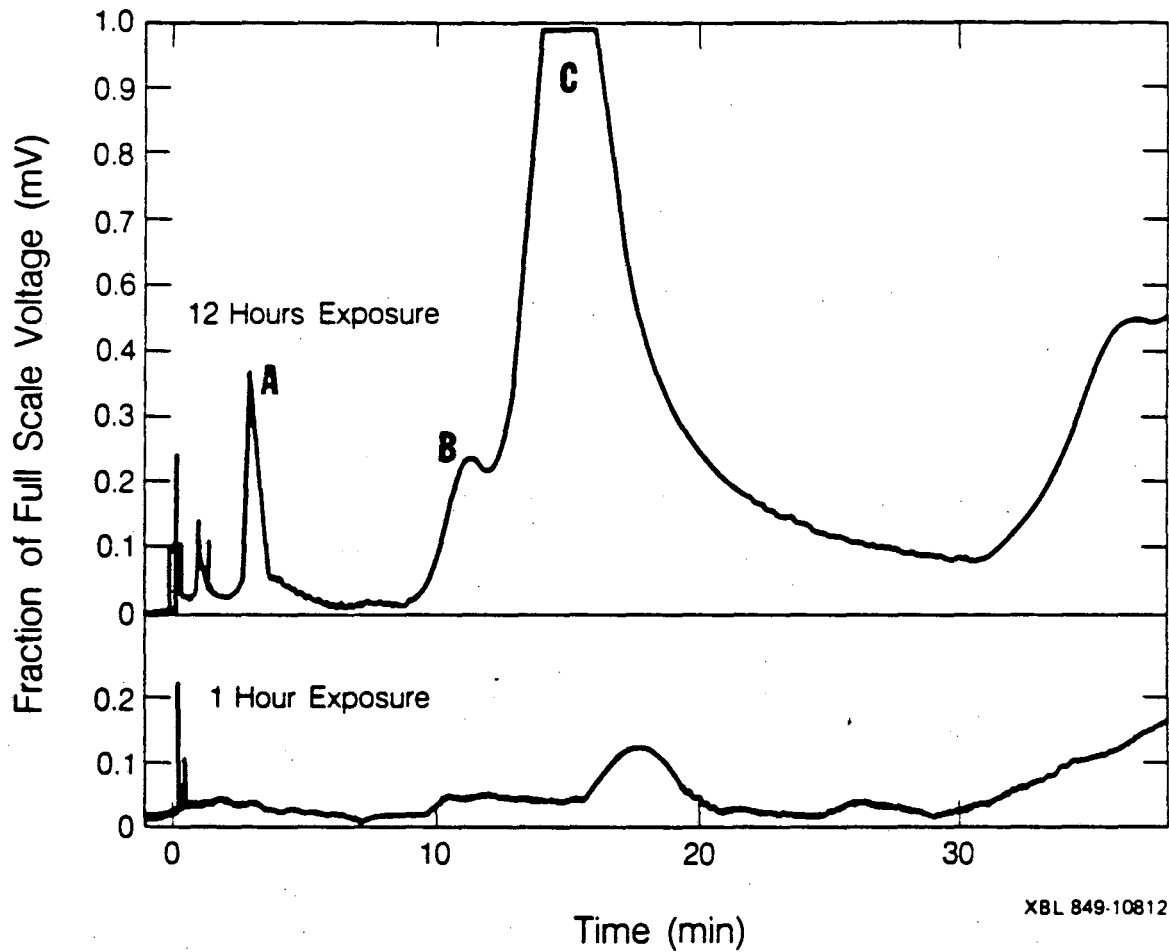


Figure 3.2.5 Effect of chlorine exposure time. Both samples were exposed to 50 mm Hg of chlorine and contained 33 ppm water. The formaldehyde (A), propionaldehyde (B), and acetone (C), peaks increase from less than one ppm to 35, 15, and 30, respectively.

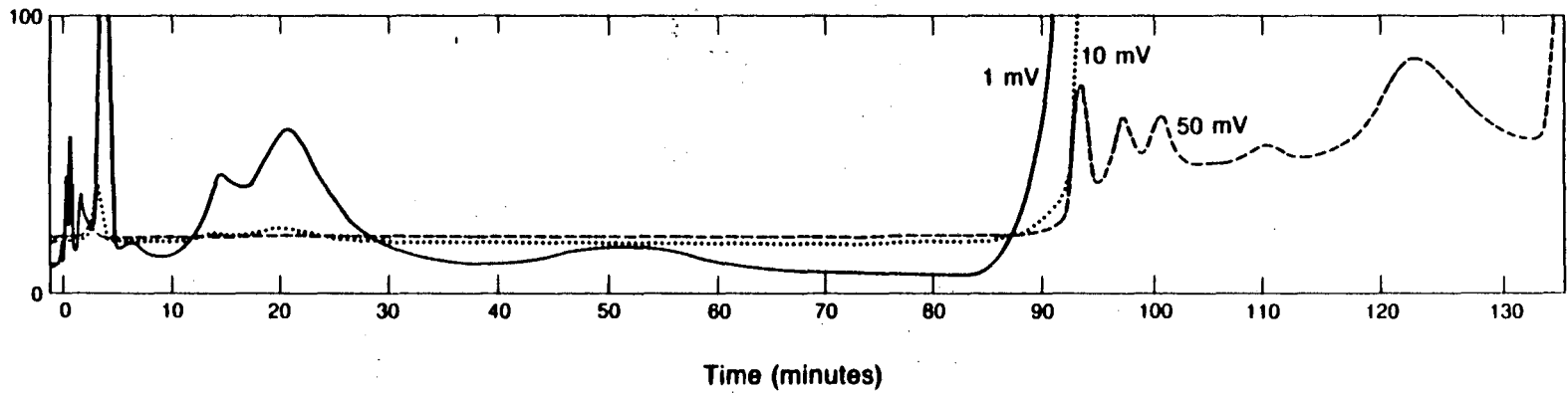
Long Time Chlorine Exposure to Anhydrous PC

To try to exclude the possibility of PC decomposition by catalysis of water, an experiment was designed to expose the driest PC to 155 mm Hg chlorine for several days. A five ml sample of PC containing less than 7 ppm water was exposed to a chlorine atmosphere at 150 mm Hg pressure for 60 hours. The GC-FID trace of this run is given in in Figure 3.2.6. Again, acetone and proprionaldehyde peaks are seen (10-15 ppm). Also formaldehyde (70 ppm) and the propylene glycols (about 500 -1000 ppm) are found.

The GC-MS trace for this run is given in Figure 3.2.7. Except PC, the two major peaks were CO₂ and HCl (peaks A and B, respectively). These compounds were both present in excess of one percent, as estimated by the operator[4]. The glycol peaks, (marked "E") merge together with the PC peak (F) and cannot be identified with the mass spectrometer. There is some evidence to indicate that the peaks after PC are chlorinated. The peak marked "I" shows fragments which correspond to -CH₂Cl and give the correct isotope ratio for chlorine. Because the peaks are very sharp, it is unlikely that the reaction of PC occurs in the column. Water, propene, propyne, acetone, propylene oxide, and formaldehyde were not detected.

3.2.3. Summary

Chlorine appears to react with PC even if the water level in the PC is lower than 7 ppm. The reaction is accelerated by the presence of water in the solvent. The reaction produces several decomposition products including 1,2 and 1,3 propylene glycol, formaldehyde, acetone, propylene oxide, and CO₂. The degree of degradation is increased with increasing chlorine concentration in the PC.



XBL 849 10830

Figure 3.2.6 GC-FID chromatogram for the 60-hour chlorine exposure test. Chlorine pressure: 150 mm Hg, water content of PC: less than 7 ppm. The temperature program in the GC was initiated at 80 minutes.

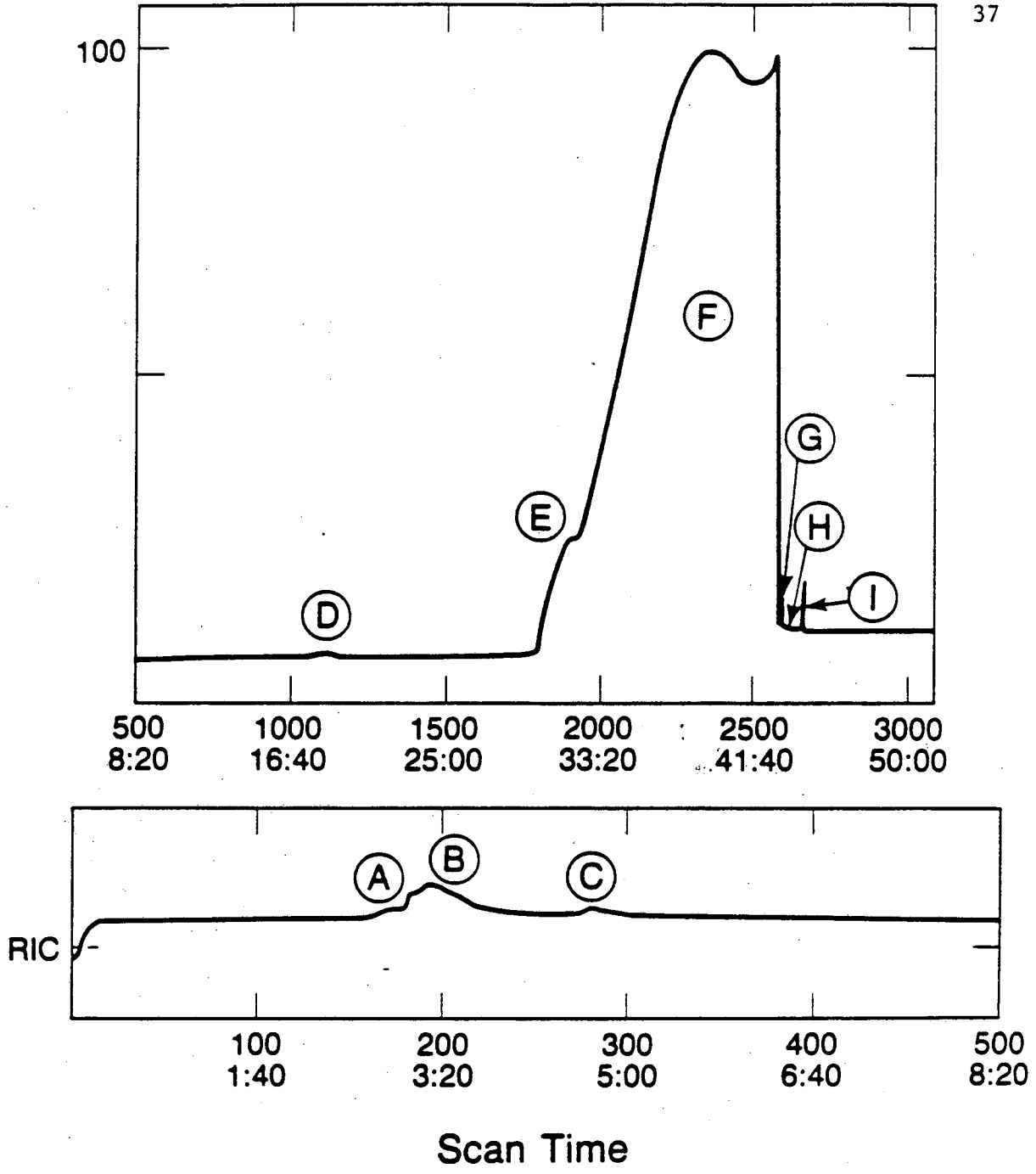


Figure 3.2.7 GC-MS trace for 60-hour chlorine exposure test. Peaks are identified in the text.

3.3. BROMINE AND IODINE

The experimental program to determine the stability of PC in the presence of bromine and iodine employed UV-Visible absorption measurements designed to directly follow the halogen concentration in PC as a function of time. If a reaction with PC occurs, we expect to see a decline in the halogen concentration. The result of this series of experiments was the discovery that iodine and bromine disproportionate in PC. The reaction was investigated in detail for iodine.

3.3.1. Experimental

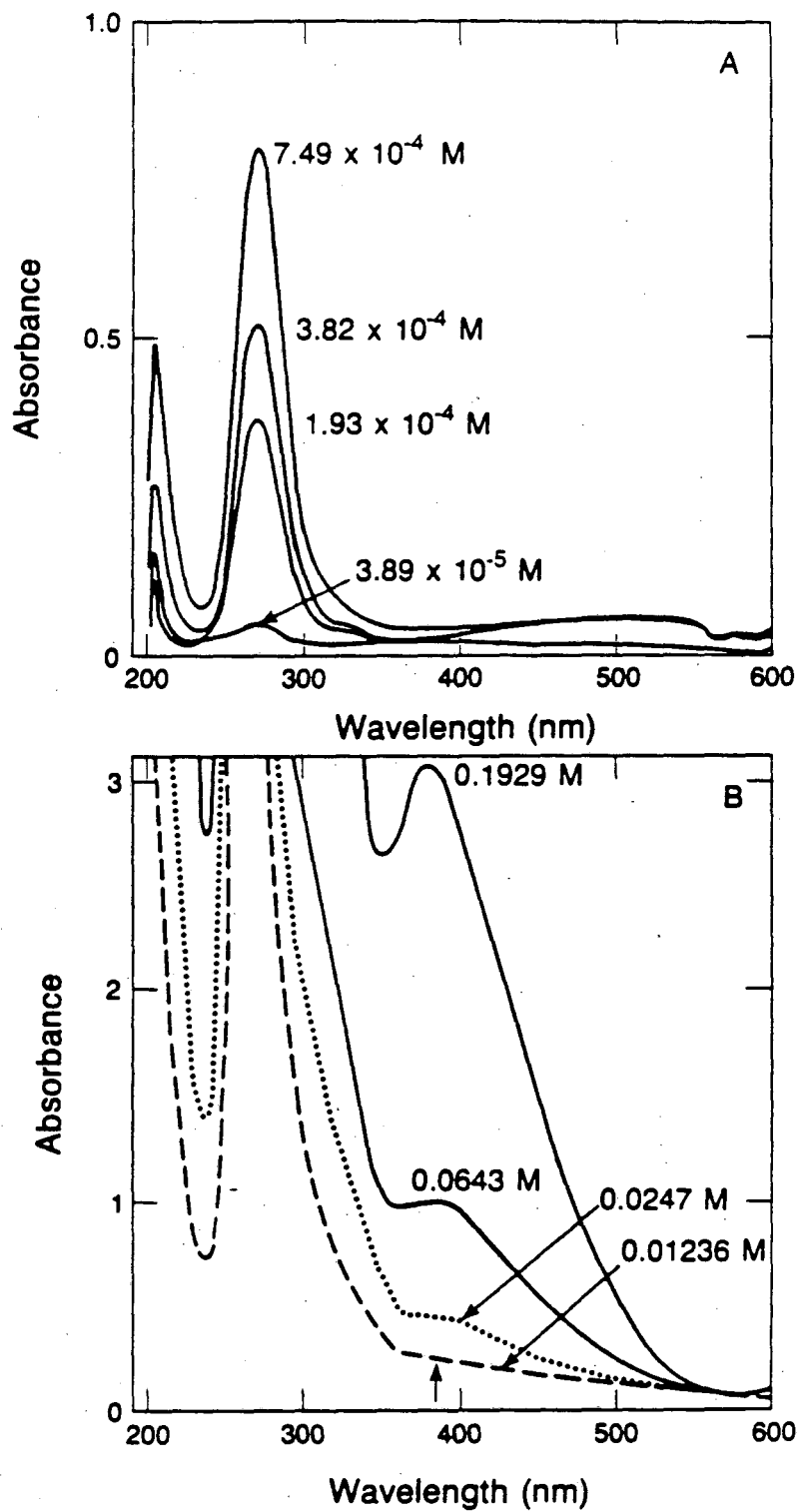
Experiments were performed with a Perkin-Elmer Model 555 UV-Vis double beam spectrophotometer. Samples were thermostated at 25 °C. The instrument was calibrated by comparing the measured benzene spectrum to literature values[5].

Early runs were carried out using PC supplied by Burdick and Jackson (50 to 75 ppm water). These results were checked by repeating experiments using PC distilled in-house (less than 10 ppm water). Bromine (Mallinckrodt, Analytical Reagent Grade) was redistilled under dry nitrogen before use. Iodine (Mallinckrodt, Analytical Reagent Grade) was resublimed in a helium atmosphere. Absorption spectra measurements were carried out in "Quarasil" cuvettes (NSG Precision cells, 0.1 and 1.0 cm).

3.3.2. Bromine and Iodine Spectra in PC

Pure Halogen in PC

Figure 3.3.1 shows the spectrum of bromine in PC at several concentrations. These spectra were taken immediately after mixing. At high concentrations (greater than 0.02 F), the bromine peak at 386 nm is evident. At lower



XBL 849-10815

Figure 3.3.1 Spectra of bromine in PC at several bromine concentrations. At high concentration, the bromine peak at 386 nm can be seen. At low concentration only the tribromide peak at 271 nm is visible.

concentrations only the absorption at 271 nm due to tribromide is visible. The same behavior is observed with iodine solutions in PC. The spectrum of a solution of iodine (9×10^{-4} F) in PC is given in Figure 3.3.2. Peaks corresponding to triiodide (at 291 and 363 nm) are observed, as well as the characteristic absorption of iodine at 462 nm. These peak assignments are consistent with published spectra of bromine and iodine in several solvents[6]. The changes in the absorption spectrum of iodine in PC with time is shown in Figure 3.3.3. In two days, peaks due to triiodide increase in size and the iodine absorption diminishes. Bromine solutions show analogous behavior. Both bromine and iodine solutions obey Beer's Law at the wavelengths we examined.

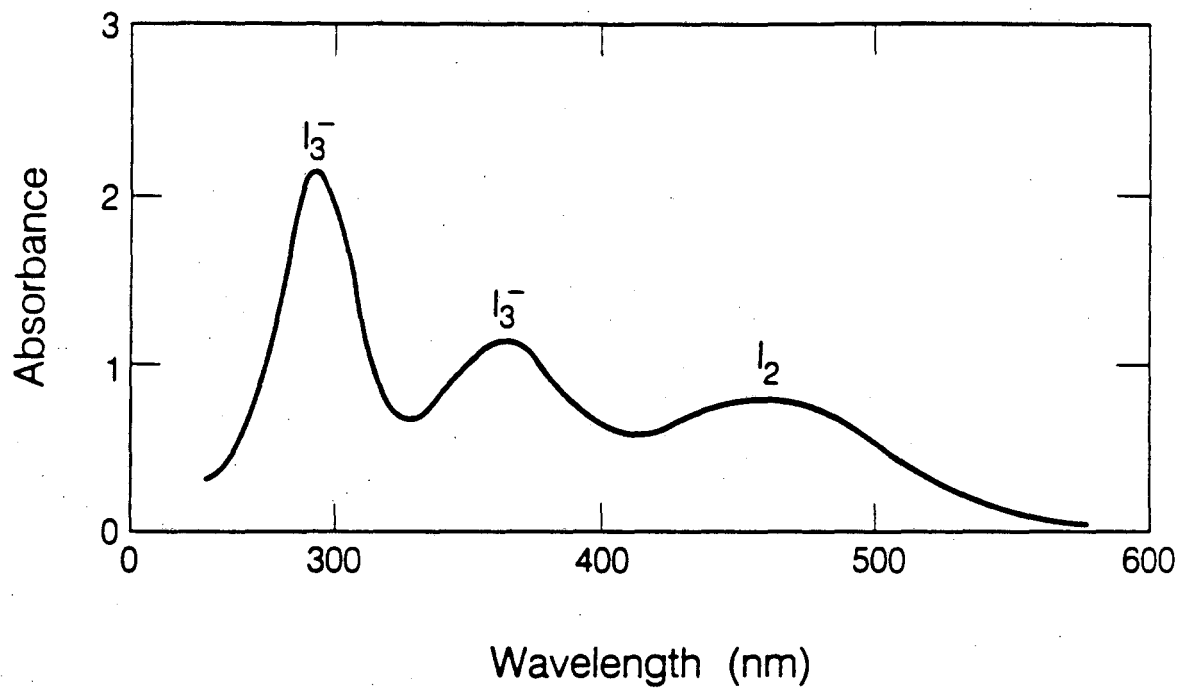
Trihalides

Addition of excess LiBr to bromine solutions in PC⁴ or excess KI to iodine solutions shifts the halogen species to the trihalide form. This is illustrated in Figure 3.3.4 for bromine. The addition of bromine to a 0.88 M solution of LiBr increases the concentration of tribromide. The same effect is observed for iodine solutions. These spectra were used to determine the trihalide extinction coefficients at the λ_{\max} for the halogen. In this way the individual contribution of the halide or halogen could be determined.

Effect of Water

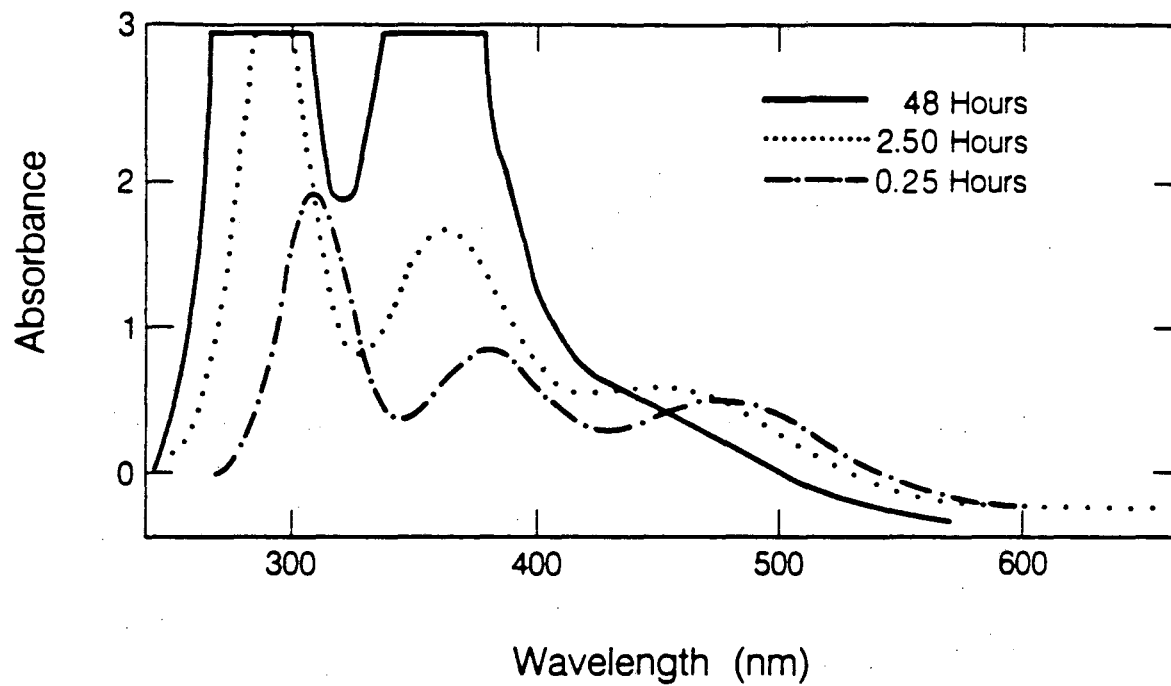
The deliberate addition of water to solutions of iodine in PC does not change the appearance of the spectra. Figure 3.3.5 shows a comparison of the spectra of a solution of 1.03×10^{-3} F iodine in pure PC and 95% PC/5% water. These spectra are indistinguishable. However, the addition of PC to a solution of iodine and water does change the spectrum to reflect an increase in triiodide

⁴ LiBr was used instead of KBr because it is far more soluble in PC. (Solubilities: LiBr: 2.43 m; KBr: 6×10^{-3} m [7])



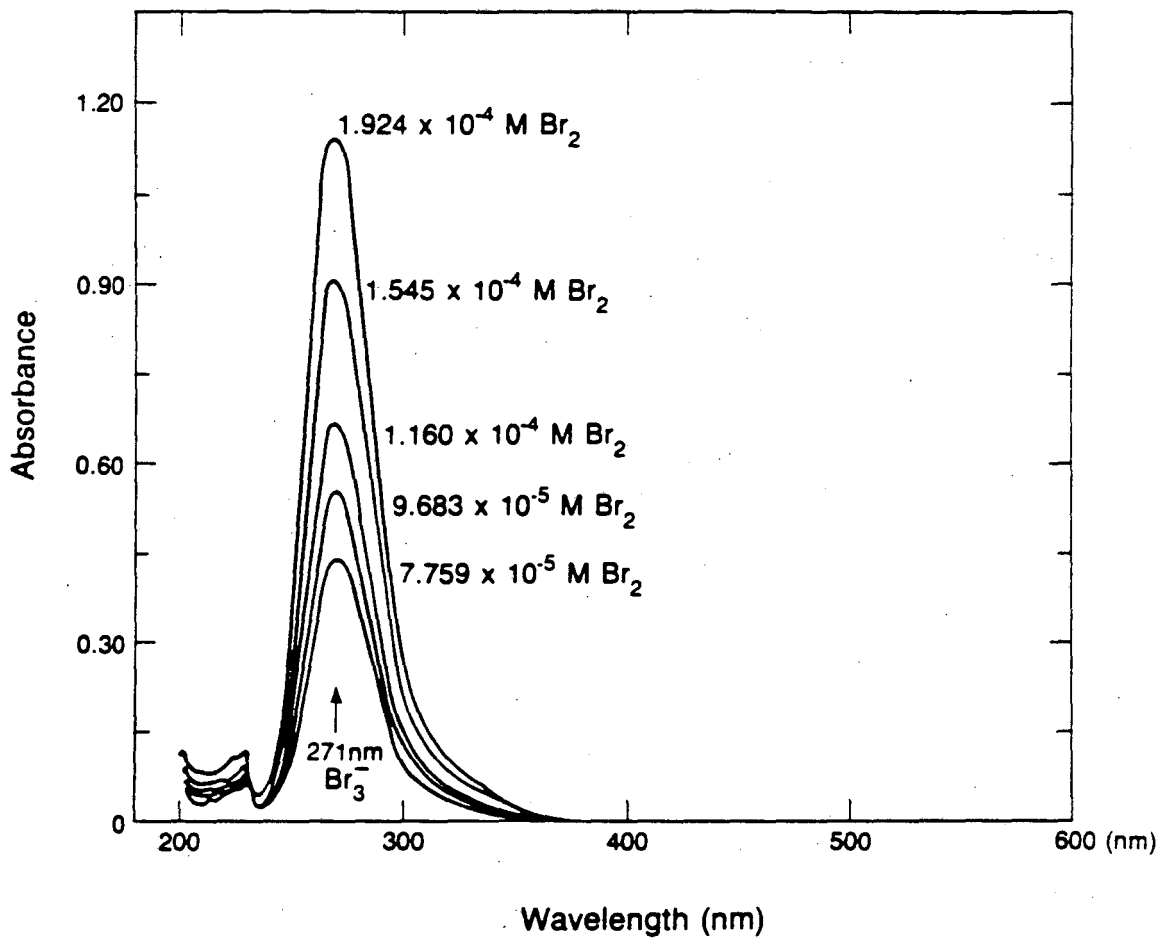
XBL 849-10808

Figure 3.3.2 UV-Visible absorption spectrum of iodine (9×10^{-4} F) in PC. Temperature: 25°C.



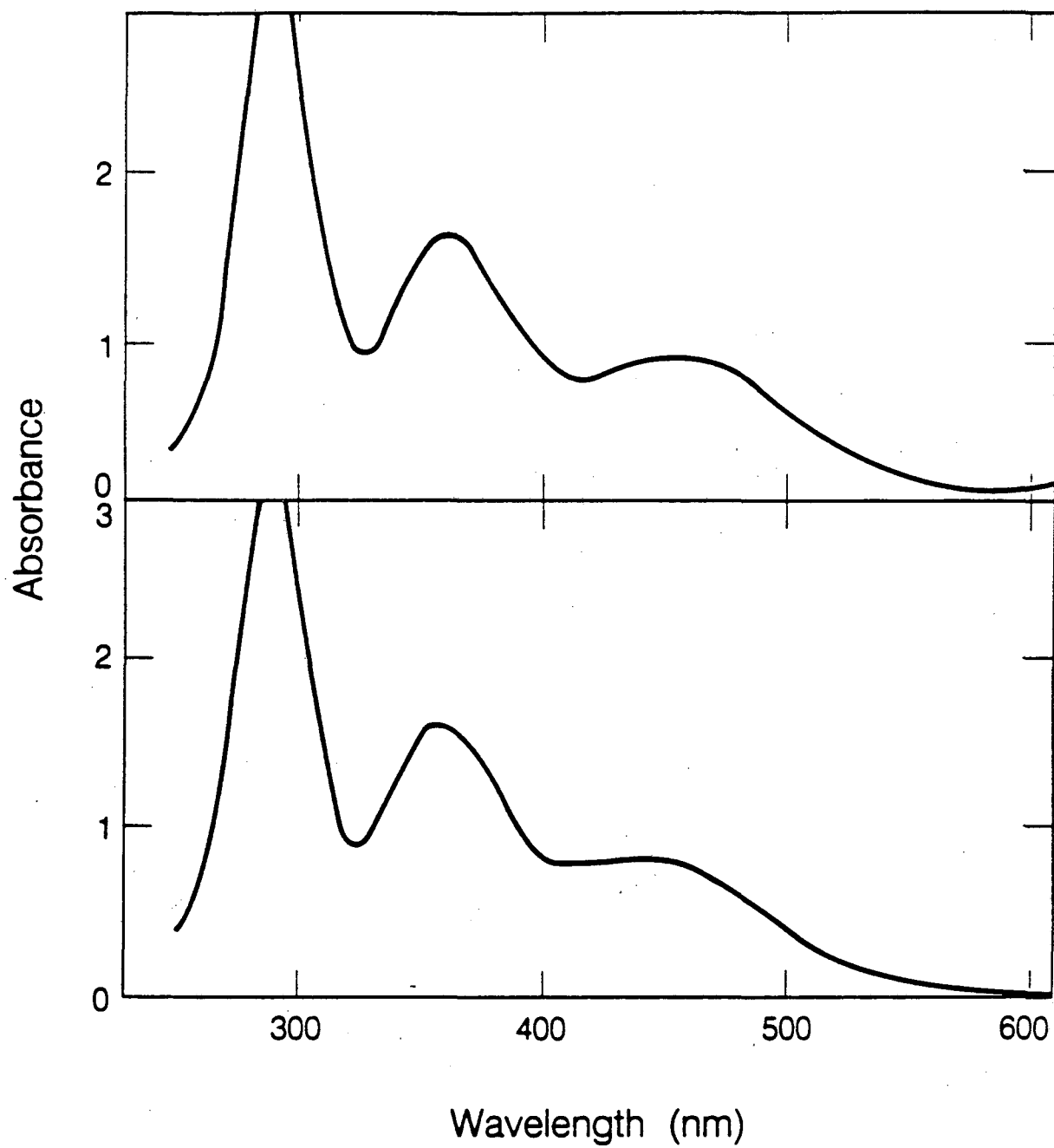
XBL 849-10818

Figure 3.3.3 Change in absorption spectrum of iodine in PC with time. Iodine concentration: 9×10^{-4} F. Temperature: 25°C .



XBL B49-10809

Figure 3.3.4 Addition of bromine to bromide solutions (LiBr concentration: 0.88 F) increases the concentration of tribromide. Temperature: 25°C.



XBL 849-10820

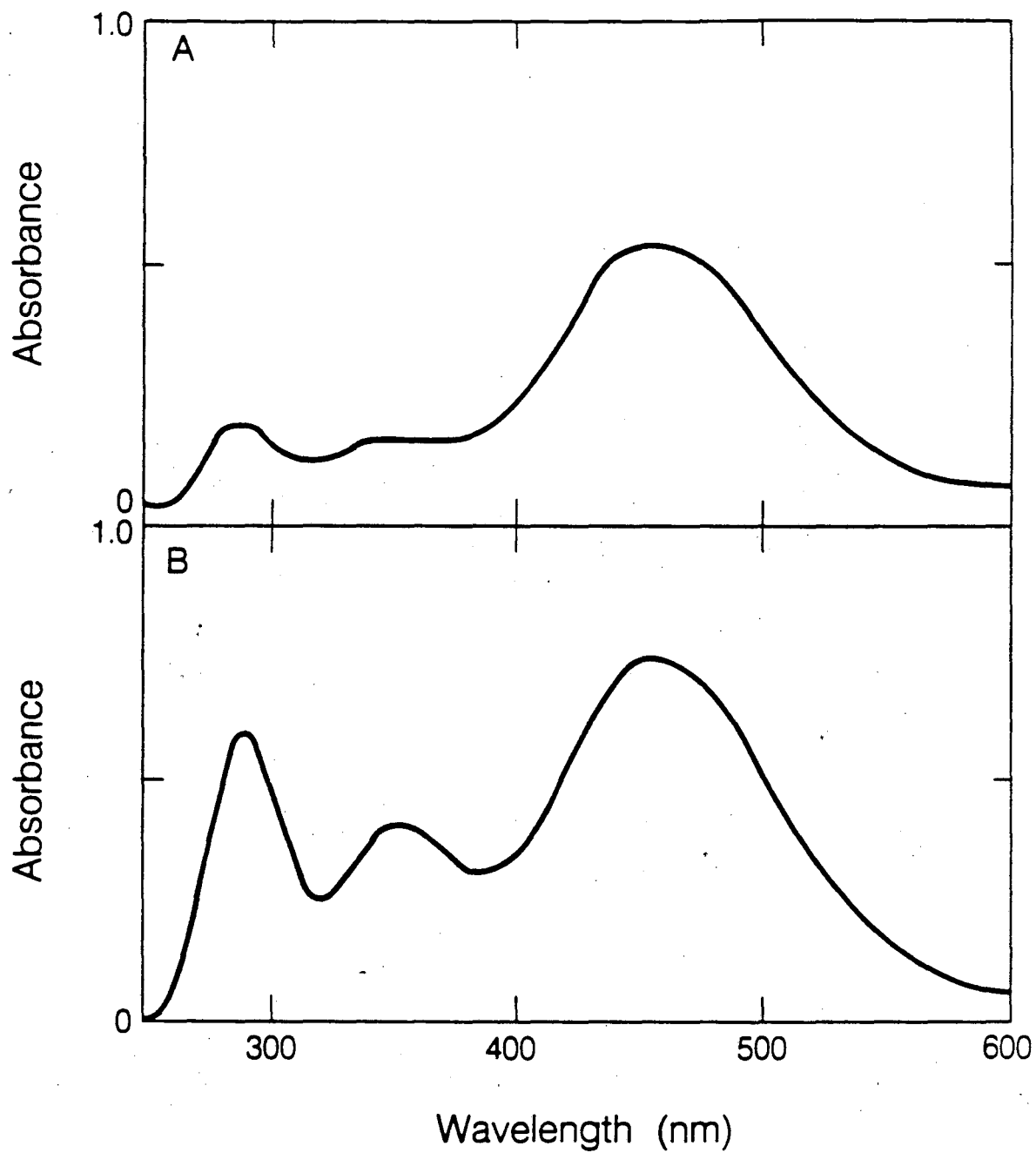
Figure 3.3.5 Spectra of iodine (1.03×10^{-3} F) in pure PC (A) and in 95% PC/5% water (B). The spectra are indistinguishable. Temperature: 25°C.

concentration. Figure 3.3.6A shows the spectrum of a solution of 7.6×10^{-4} F iodine in water (as mixed). Using extinction coefficients reported by Autrey[8], the aqueous solution shows a concentration of 7.45×10^{-4} M iodine and 4.5×10^{-6} M triiodide, or 2% of the original iodine appears as triiodide. The addition of 5% PC (Figure 3.3.6 B) shows a shift from the iodine to the triiodide form. (Note that the initial concentration of iodine is slightly higher.) Assuming the extinction coefficients do not change, 5% of the original iodine has reacted. To gain confidence in these measurements, these experiments were repeated with PC distilled in-house. The observed behavior was the same.

The spectra of solutions of bromine in PC are more sensitive to the water content of PC than iodine solutions. Figure 3.3.7 shows a set of four spectra for 0.038 M bromine solutions in (i) pure PC, (ii) PC + 6% water, (iii) pure water, and (iv) water + 6% PC. Comparison of the first two curves shows that the addition of water to PC/bromine solutions shifts the bromine to the tribromide form. Because the extinction coefficient of tribromide is higher than that of bromine at 462 nm (λ_{\max} for bromine), the bromine absorption appears as a large shoulder. The high stability of tribromide in PC is demonstrated by the addition of 6% PC to an aqueous solution of bromine (curves C and D). An increase in the tribromide peak is clearly observed⁵.

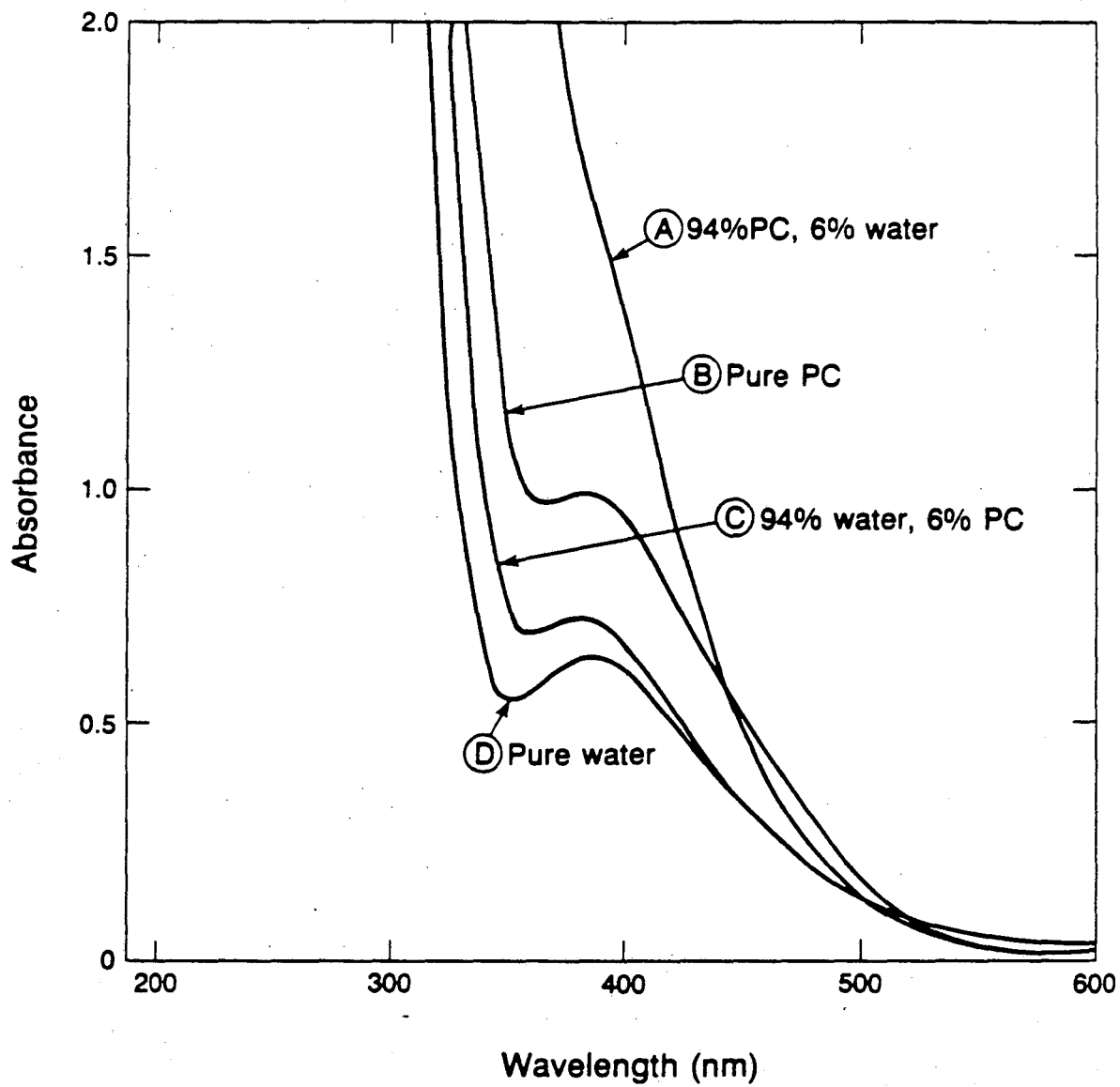
The reason for the higher sensitivity of bromine solutions to the water content of PC, in comparison to iodine solutions, is the higher reactivity of bromine with water. Equilibrium constants for HOX formation in water are 7.2×10^{-9} and 2.0×10^{-13} for bromine and iodine respectively[9].

⁵ The bromine peak also appears to increase because tribromide absorbs at 462 nm.



XBL 849-10814

Figure 3.3.6. Spectra of iodine (7.6×10^{-4} F) in pure water (A), and in 95% water/5% PC (B). Addition of PC increases the triiodide concentration. Temperature: 25°C.



XBL 849-10817

Figure 3.3.7 Spectra of bromine (0.038 F) in pure PC (B), 94% PC/6% water (A), pure water (D), and 94% water/6% PC (C).

3.3.3. Disproportionation Reaction

Extinction Coefficient Determinations

Extinction coefficients for triiodide in PC at 292, 363 and 462 nm were determined from absorption measurements of solutions of iodine and excess KI in PC. Extinction coefficients at 25 °C are reported here; values of the extinction coefficients of iodine and triiodide in PC for 10 to 45 °C, and values of ΔG , ΔS and ΔH for the disproportionation reaction were measured by Johnson and are available elsewhere[10]. Because triiodide absorbs at the λ_{max} for iodine (462 nm), the extinction coefficient of iodine at that wavelength is determined indirectly. The same disproportionation reaction of iodine in PC can be written as,



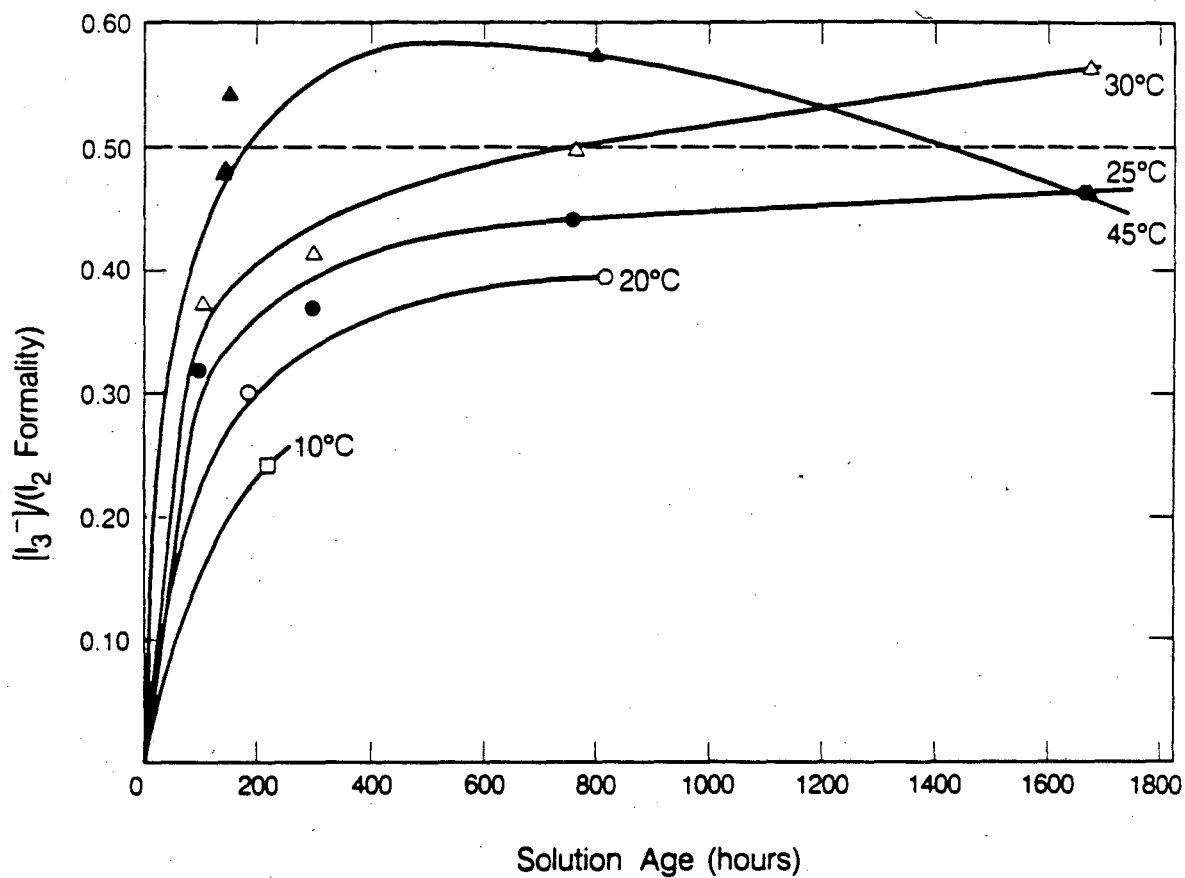
Thus the formation of one mole of triiodide consumes two moles of iodine. The concentration of iodine in solution is calculated by subtracting twice the value of the concentration of triiodide from the formal concentration of iodine. Values of the extinction coefficients of triiodide and iodine are listed in Table 6.7.1.

Mass Balance for Disproportionation Reaction

If reaction (A) represents the only pathway for iodine consumption, the concentration of iodine in solution is related only to the concentration of triiodide in solution. Thus,

$$[I_2] = [I_2]_i - 2[I_3^-] \quad (\text{B})$$

For a completed reaction, the ratio of triiodide to initial iodine concentration, $[I_3^-]/[I_2]_i$, is 0.5. Figure 3.3.8 gives a plot of this ratio as a function of time for several solution temperatures. Based on this argument, at 45 °C the concentration of triiodide is larger than expected after about 200 hours, as the value of the ratio increases to 0.57. After this point, the triiodide concentration slowly declines.



XBL 8410-10908

Figure 3.3.8 Kinetics of iodine disproportionation reaction as a function of temperature. The ratio of triiodide concentration to initial iodine concentration approaches 0.5 for a completed reaction. From reference [10].

The data at lower temperatures show the same behavior but at much lower rates. At 30 °C, no decline is seen. Apparently, the approach to equilibrium is very slow. Values for the ratio which are greater than 0.5 indicate that other reactions are occurring, possibly with impurities in the solution. The decline at long times represents a loss of triiodide and may be a result of a slow decomposition reaction of PC.

3.3.4. Conductivity Experiments

If iodine and bromine disproportionate in PC, the conductivity of the solution as a function of time should reflect the change in the solution composition. To verify the concentration changes observed with UV-Visible spectroscopy, the conductivity of solutions of iodine and bromine in PC were measured.

Experimental

Conductivity measurements were made with a Wayne-Kerr conductivity bridge connected to one of three conductivity cells⁶. The cell constants were determined by measuring the conductivity of aqueous KCl solutions in the concentration range of 10^{-1} to 10^{-3} M and at temperatures between 25 and 35 °C. From published values of the specific conductance of these solutions[11], the cell constants were found to be 1.056, 0.0102, and 0.0806 cm^{-1} . During conductivity measurements, the samples were contained in test tubes which fit into a large heat capacity aluminum block. A temperature controller (Versa-Therm) maintained the temperature to within ± 0.05 °C. All measurements were made at higher than room temperature, 35 °C, to allow accurate temperature control without refrigeration.

Experiments were performed by mixing iodine with PC at 35°C, waiting 15 to 30 minutes for the iodine to dissolve, and then beginning the measurement.

⁶ Two of the cells were manufactured by Yellow Springs, Corp., (nominal cell constants of 1 and 0.1 cm^{-1}) and one cell was made in-house.

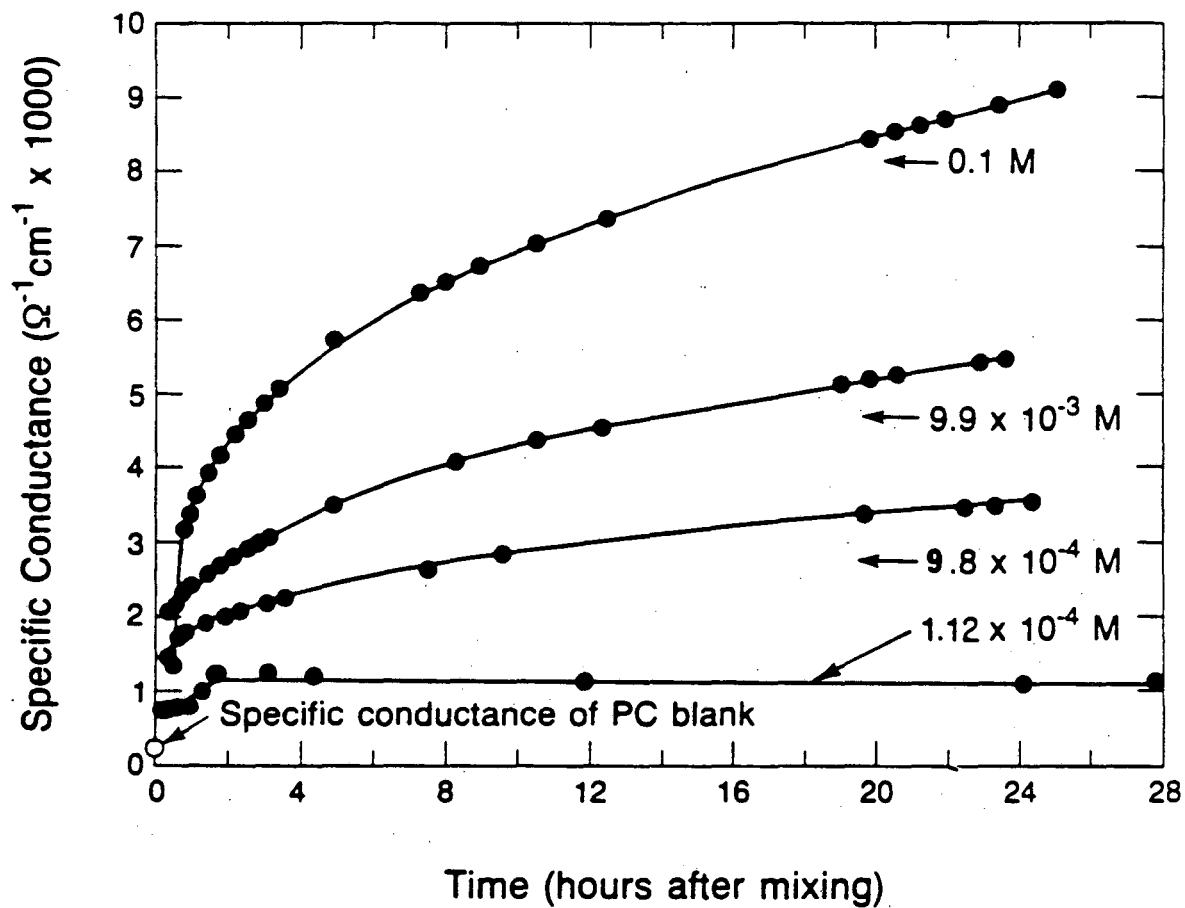
Four iodine solution concentrations were used: 1×10^{-1} M, 9.91×10^{-3} M, 9.82×10^{-4} M and 1.12×10^{-4} M. As a control, the conductivity of a sample containing only PC was monitored concurrently.

Results

The conductivity of solutions of iodine at four different concentrations is given in Figure 3.3.9. The duration of each of the experiments was at least 28 hours. In each case the behavior is similar; the conductivity of the solution rises rapidly in the first two hours, and then continues to slowly increase. The most dilute solution appears to reach a plateau. Two of the solutions were monitored beyond 28 hours. After 98.6 hours, the specific conductance of the 0.1 M solution rose to $5.46 (\mu\text{ohm}/\text{cm})^{-1}$. However, after 45.6 hours the specific conductance of the 1.12×10^{-4} M solution was the same as that obtained after two hours. In all cases, the increase in conductivity of the PC blank was much less than that of the sample solution.

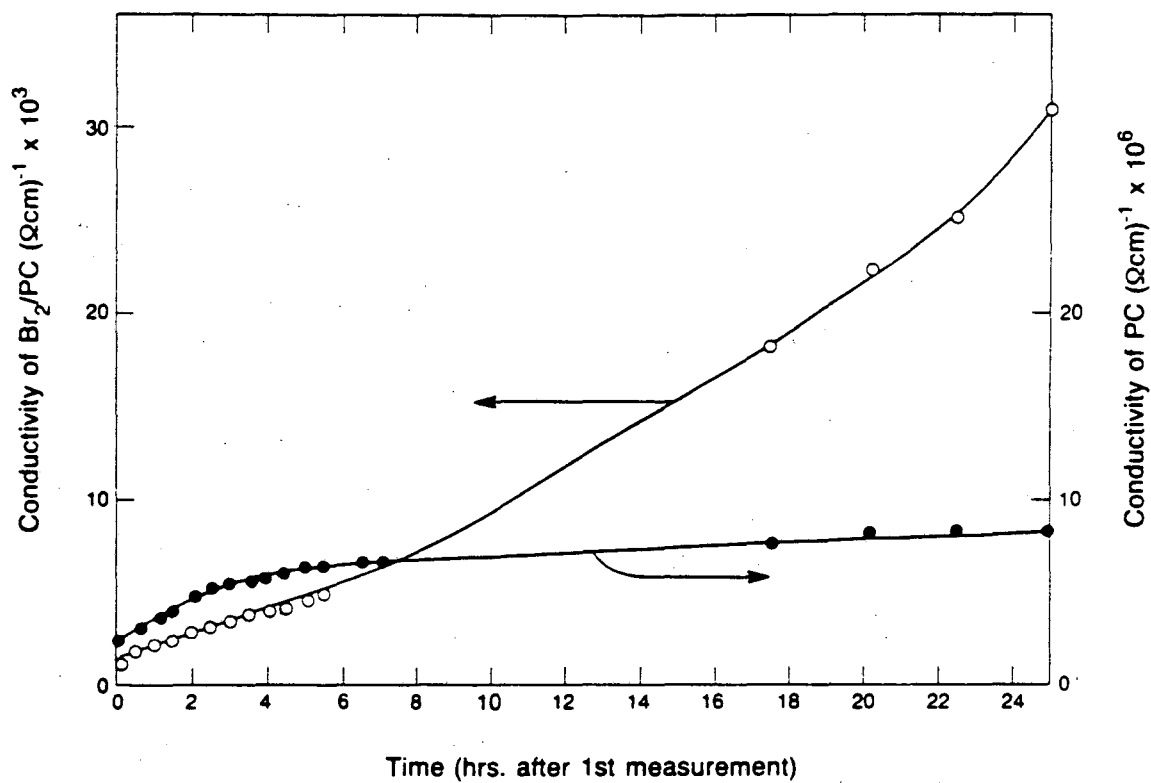
Similar experiments, using bromine in place of iodine, also show an increasing conductivity in time. Figure 3.3.10 demonstrates the specific conductance of a solution of 1.0 M bromine in PC as a function of time. At a high concentration of bromine, the conductivity rises continuously over a 24 hour period.

The conductance behavior of solutions of iodine and bromine in PC in time shows the same shape as the concentration of triiodide or tribromide as a function of time (See, for example, Figure 3.3.8.).



XBL 849-10805

Figure 3.3.9 Conductivity of four solutions of iodine in PC as a function of time. The conductivity of a PC blank is shown as an open circle.



XBL 849-10806

Figure 3.3.10 Conductivity of bromine in PC (1 M) as a function of time (open circles). The conductivity of a PC blank (note scale change) is also given.

3.4. DISCUSSION

From the results of the experiments presented above, it is clear that both iodine and bromine disproportionate in PC to form the trihalide. The equilibrium constant for the iodine disproportionation reaction was determined to be 0.86 at 25 °C [12]; the value for bromine is estimated from our results to be 1.2. Because trichloride is the most stable of the three trihalides (see section 6.2.1) the value of the equilibrium constant for the chlorine reaction is likely to be higher. If a negatively charged ion is formed from a neutral molecule, electroneutrality requires the formation of a positively charged species. What is the nature of this species?

Two possible explanations are offered here. PC is a relatively strong donor solvent and may stabilize a positively charged species by solvation. In this case, the PC carbonyl would be the coordination site. If stable, this species could be detected by NMR (C^{13} NMR would show a chemical shift from the iodine) or Fourier-Transform IR (by changing the C=O stretch at the carbonyl).

Another explanation is that the positively-charged halogen species attacks the PC. The results of the GC study of chlorine in PC are consistent with this idea. Previous explanations of PC decomposition by halogens [13] invoked the ionization of trace water to supply an acidic species which then acts as a decomposition catalyst. Our results indicate that the presence of H^+ may not be necessary to explain the results. Cl^+ is a very strong Lewis acid and could abstract a proton from PC to initiate the decomposition. The production of HCl and glycol in amounts in excess of one percent suggests that PC, not water, is the source of the hydrogen. There is clearly not enough water in the sample to account for the hydrogen in the glycol and HCl detected by the GC.

3.5. CONCLUSIONS

UV-Visible spectrophotometry experiments designed to investigate the stability of PC in the presence of halogens have shown that the stable form of the halogen in PC is the trihalide. This has been carefully studied for the case of iodine, demonstrated for the case of bromine, and inferred for the case of chlorine.

The stability of PC in the presence of the halogens was studied. An investigation of solutions of chlorine in PC using gas chromatography has shown that chlorine attacks even dried, distilled PC. Increasing water content in PC increases the extent of the reaction. The major decomposition products are 1,2 and 1,3 propylene glycol, allyl alcohol, and acetone. Other products were detected but were not identified. Solutions of iodine and PC are stable for several months; only a small fraction (about 5%) of the triiodide is consumed. The behavior of solutions of iodine and PC is relatively insensitive to the water content of the solvent.

The results of these two separate investigations may be related by learning about the nature of the positively charged halogen species formed in the disproportionation reaction. This species may be reactive (acidic) enough to initiate the breakdown reaction by abstracting a proton from PC. FTIR or NMR experiments are suggested to test this hypothesis.

REFERENCES

- [1] H. Law, *Studies on the Electrochemical Behavior of Potassium in Propylene Carbonate*, Ph. D. Thesis, University of California, Berkeley (1979).
- [2] S.M. Yu, P. N. Ross, and C. W. Tobias, *An Investigation of the Degradation of Propylene Carbonate by Chlorine*, LBL Report 10069, (1979).
- [3] R. Jasinski, and S. Kirkland, *Anal Chem.*, **39**, 13, 1663 (1967).
- [4] Leah Zebre, Mass Spectrometry Laboratory, Dept. of Chemistry, personal communication.
- [5] *Sadtler Handbook of UV Spectra* Sadtler Research Laboratories, (1979).
- [6] For bromine spectra, see J. Fritz and G. Wood, *Anal Chem.* **40**, 1, 134, (1968); R. Buckles and J. Mills, *J. Amer. Chem. Soc.* **75**, 552, (1953). For iodine spectra, see A. Autrey and R. Connick, *J. Amer. Chem. Soc.*, **73**, 1842, (1951).
- [7] W. Harris, *Ph. D Dissertation, University of California*, Department of Chemical Engineering, UCRL Report 8381, (1958).
- [8] A. Autrey and R. Connick, *op cit.*
- [9] F. A. Cotton and G. Wilkinson, "*Advanced Inorganic Chemistry*", Third Ed., page 476, J. Wiley & Sons, N.Y. (1972).
- [10] P. Johnson, K. Hanson, C.W. Tobias, *Stability of PC in the Presence of Iodine, Bromine and Chlorine*, LBL Report, to be published.
- [11] *International Critical Tables, Vol. 6*, page 230.
- [12] P. H. Johnson, unpublished results.
- [13] S. M. Yu, and C. W. Tobias, *op cit.*

Chapter IV/ Halide Double Salts in Propylene Carbonate

4.1. INTRODUCTION

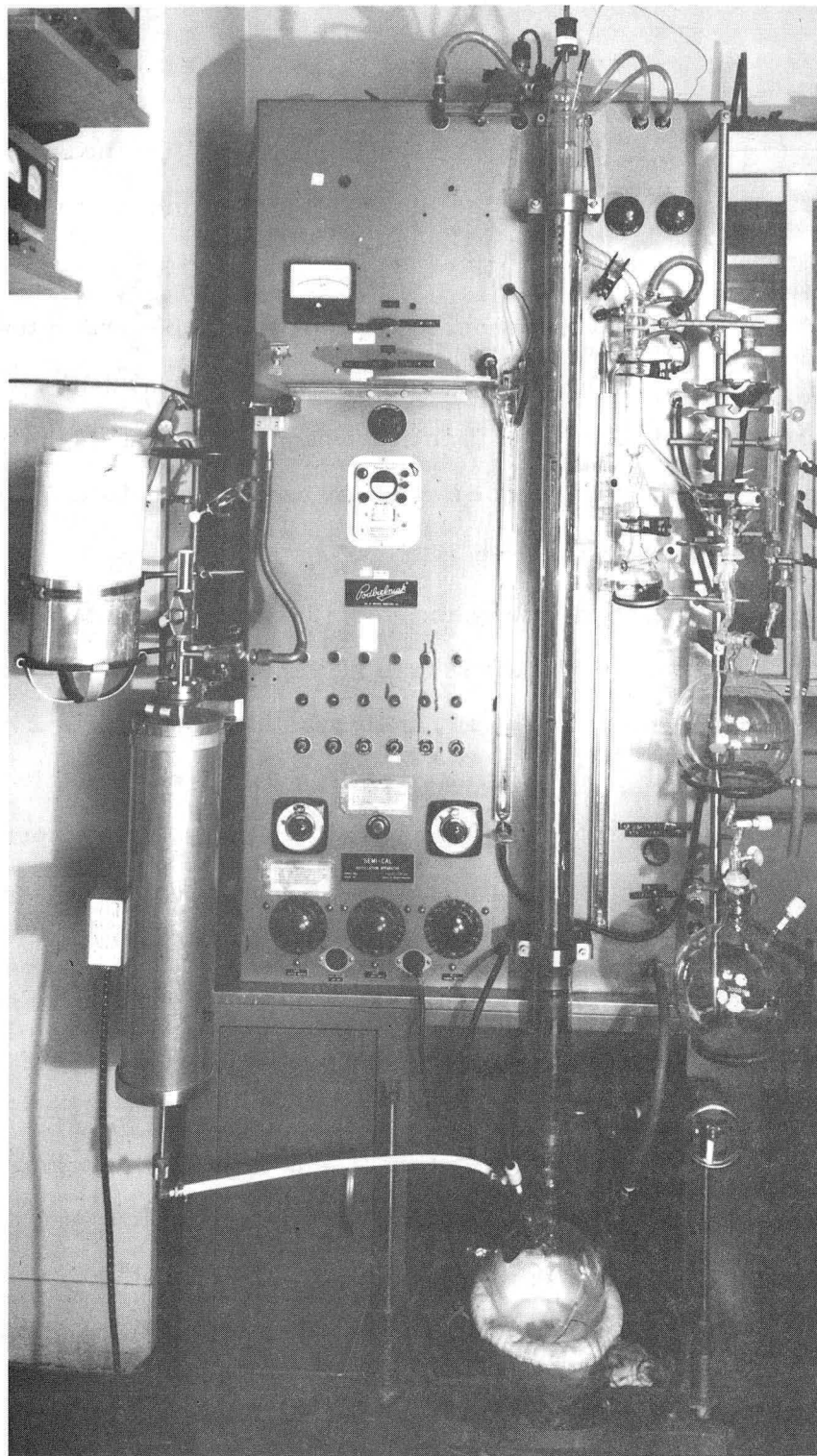
To be considered a practical electrolyte for large scale synthesis application, the solution conductivity should exceed $5 \times 10^{-3}(\Omega\text{cm})^{-1}$ [1]. Thus, a salt which has an equivalent molar conductivity of $20 \text{ cm}^2/(\Omega\text{mol})^{-1}$ (an average value) should be soluble in excess of 0.25 M. The solubility and conductivity of several potassium salts in PC are listed in Table 4.1.1. The most obvious feature of these data is that the solubilities of most salts are much lower than in water. Within the halide series, the trend for solubility is $\text{KI} > \text{KBr} > \text{KCl}$. It is well-known[2] that anions are poorly solvated by PC because of the lack of a center of positive charge in the PC molecule. Therefore, even though PC has a dielectric constant close to that of water (65), the solubilities of many salts are comparable or lower in PC than in many solvents having much lower dielectric constants[3], [4]. As a general rule, salts having large anions are much more soluble in PC. This can be seen in Table 4.1.1 where the solubilities of KPF_6 and KAlCl_4 are soluble in excess of 1 mol/liter. Following the work done in this laboratory on KAlCl_4 [5], the double salts KAlCl_3Br and KAlBr_4 were studied in PC. The results of the synthesis, and the solubility and conductivity experiments are reported in this chapter.

Table 4.1.1 Conductivity of Halide Salts in PC at 25 °C

Salt	Solubility (m)	Conductivity (Conc.) (Ωcm) ⁻¹	Reference
KCl	4×10^{-4}	4×10^{-5} (sat)	[12]
KBr	6×10^{-3}	1.4×10^{-4} (sat)	[12],[12]
KI	2.3×10^{-1}	4.4×10^{-3} (sat)	[14],[12]
LiBr	2.3 3.12 M	4.9×10^{-4} (sat)	[12],[12] [13]
NaBr	8.0×10^{-2}	1.8×10^{-4} (sat)	[12],[12]
KBF ₄	0.012	1.9×10^{-4} (sat)	[12],[12]
KPF ₆	1.5 N	6.8×10^{-3} (0.5N)	[14],[14]
KAlCl ₄	>1 M	1.25×10^{-2} (1 M)	[5],[5]

4.2. EXPERIMENTAL

The synthesis procedure for the double salts was similar to that reported by Law[6] based upon early work by Baud[7], and Kendall[8]. Equimolar amounts (approximately 150 grams) of the aluminum halide and the potassium halide were dried under vacuum, ground to a fine powder, and placed in a pyrex tube inside a polyethylene glovebag under a nitrogen atmosphere. The tube was then connected to a vacuum system, agitated by a vibrator to thoroughly mix the salts, and pumped down to 1 μm Hg vacuum over night. The mixture was then pressurized slightly with helium so that helium was constantly flowing over the top of the tube while the salts were melting. The vacuum system and oven are shown in Figure 4.2.1. The mixtures were heated to approximately 500 °C and kept at this temperature for about two hours. The mixture was cooled very



CBB 830-9677

Figure A1-1 Distillation column and molecular sieve pretreatment column.

slowly to avoid suspending any settled impurities. After the solidification of the salts, the pyrex tube was pumped down to 1 μm Hg and sealed before transferring to the glovebox.

A drawback to this procedure is the possibility of overpressurizing the system when the salt cools. At this time crystals can form at the neck of the tube and create a seal. The stress in the tube can then become high enough to break the glass. This problem can be avoided by being careful to keep the neck of the tube warm and cooling the salt very slowly.

All solutions, conductivity and solubility measurements were made inside the glovebox. Solutions of the salts in PC were made by first chilling the solvent to 0 °C and then slowly adding the finely ground salt to the PC while the solution was being stirred. The temperature of the solution was monitored to avoid solvent breakdown that may result due to a large increase in temperature. All solutions were prepared by weight. The solubility of the salts was measured by stirring PC with an excess of salt for several days (sometimes several weeks), filtering the solution and analyzing for potassium (by atomic absorption) and halide (by titration with silver nitrate¹). The solutions were checked several times to make sure that equilibrium had been reached. The accuracy of the solubility data should be regarded with caution because the solution temperature varied between 20 and 25 °C inside the glovebox. The conductivity was measured with an impedance bridge (Wayne-Kerr Model B224). The conductivity cells and calibration procedure are described in section 5.2.

4.3. RESULTS

The results of the synthesis are summarized in Table 4.3.2, showing the starting compositions, the composition of the products, and the solubility and conductivity of solutions in PC.

¹ Samples were dissolved in dilute aqueous nitric acid solutions. Silver nitrate was added to precipitate the silver halide. Potentiometric endpoint was determined using a silver wire indicator electrode and a saturated calomel reference electrode.

Table 4.3.2 Halide Double Salts			
	$KAlCl_4$	$KAlBr_4$	$KAlCl_3Br$
Starting Composition	$AlCl_3, KCl$	$AlBr_3, KBr$	$AlCl_3, KBr$
Products	$KAlCl_4$	$KAlBr_4$	mixed salt
Description	white	pale purple	3 layers, amber color
Solubility in PC (M)	>1.5	2	2
Conductivity of Saturated Solution (Ωcm^{-1})	$3.4 \pm 0.2 \times 10^{-3}$	$2.7 \pm 0.2 \times 10^{-4}$	$3.3 \pm 0.2 \times 10^{-3}$

$KAlBr_4$

$KAlBr_4$ was produced from a equimolar mixture of KBr and $AlBr_3$ which was heated to $500\text{ }^\circ\text{C}$. The resulting salt had a uniform, large-grained appearance and a very pale purple color. A black oily substance was found in patches on the surface but was not successfully identified. Analysis confirmed a molar ratio of 1/1/4 for potassium, aluminum, and bromide, respectively.

When this salt was dissolved in PC, it dissociated to form a KBr precipitate; $AlBr_3$ remained in solution. The temperature of the solution increased only slightly when the salt was added.

² These salts dissociate in solution as KBr (ppt) and $AlCl_3$ or $AlBr_3$.

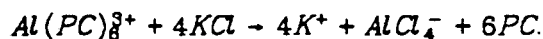
KAlCl₃Br

The salt $KAlCl_3Br$ was prepared from a mixture of KBr and $AlCl_3$ (1.15/1 moles KBr to $AlCl_3$) which was heated to about $350\text{ }^\circ\text{C}$ ³. The resulting salt had a completely different appearance from either $KAlCl_4$ or $KAlBr_4$. While molten (melting point of approximately $140\text{ }^\circ\text{C}$), the solution appeared completely mixed and black in color. Upon cooling, the mixture solidified into three distinct layers. The top layer (about a third of the total) was a dark, large grained salt which was dark amber in color. Analysis gave a molar ratio of 1.05/1/0.97/2.8 for potassium, aluminum, bromide, and chloride, respectively; the expected result for $KAlCl_3Br$. The narrow, middle layer contained a coarse black powder. Potassium, halides, and aluminum were present in a 3.2/1/3.6 molar ratio. Tests for iron, a known contaminant in $AlCl_3$, were negative. The bottom layer (approximately 2/3 of the total) had a finer grain and was much lighter in color. The composition ratio indicated a 1:3 mixture of aluminum chloride and KBr .

This salt showed the same behavior as $KAlBr_4$ in solution. A precipitate of KBr is formed, leaving $AlCl_3$ in solution. Again, the temperature of the solution increased only slightly when the salt was added.

4.4. DISCUSSION

It is surprising that the salts investigated were not stable in PC. In $AlCl_3$ solutions in PC, KCl will dissolve because stable complexes are formed[9],



Very little information is available on the bromo-aluminate salts in nonaqueous solution, although many salts of this type have been studied in the molten state[10], [11]. The reasons for the dissociation have not been explored. It is possible that the bromide ions are simply too large to coordinate four ions to the

³ This salt was briefly exposed to air during the synthesis when a hole blew in the connecting tube.

central aluminum ion. The strength of the PC-aluminum complex may exceed the strength of the Al-Br bond in KAlBr_4 .

Several solutions of KAlBr_4 and KAlCl_3Br yielded 0.31 M solutions of AlBr_3 . It is not known if this value represents the limiting solubility of AlBr_3 in PC because the direct addition of even small amounts of this salt alone to PC caused color changes and evidence of decomposition.

The conductivity of the aluminum bromide salts in PC are about an order of magnitude below the conductivity of aluminum chloride solutions in PC. Again, this reflects the instability of complexes of bromide compared to chloride. Using the data in Table 4.3.2, for a concentration of 0.31 M AlBr_3 in solution, the molar conductivity is $0.8 \text{ cm}^2/\Omega\text{-mol}$. This indicates that aluminum bromide does not ionize to any significant extent in PC. This is consistent with the conductivity data reported by Mary[12] who gives an association constant of 1500 for AlBr_3 in PC.

4.5. CONCLUSIONS

The double salts KAlBr_4 and KAlCl_3Br were synthesized and evaluated as candidate electrolytes in PC. In contrast to the chlorine analog, KAlCl_4 , these salts are not stable in PC. In each case the salt dissociated to form a KBr precipitate, leaving the aluminum halide in solution. Unlike the direct addition of aluminum halides to PC, these solutions were formed with only a small heat of solution. The conductivity of the resulting PC solutions are reported and compared to those of similar salts[13].

REFERENCES

- [1] R. Jasinski, in *Advances in Electrochemistry and Electrochemical Engineering*, Vol. 8, P. Delahay and C.W. Tobias, Editors, Wiley, (1971).
- [2] R. Jasinski, *op cit.*
- [3] M. Jones and W. Gilkerson, *J. Soln. Chem.*, 8, 12, 871 (1979).
- [4] Y. Matsuda and H. Satake, *J. Electrochem. Soc.*, 127, 4, 877 (1980).
- [5] H. Law, *Studies on the Electrochemical Behavior of Potassium in Propylene Carbonate*, Ph.D Thesis, Univ. of California, Dept. of Chem. Eng., LBL Report 9207, (1979).
- [6] H. Law, *op cit.*
- [7] E. Baud, *Ann. Chim. Phys.*, 8, 1, 8 (1904).
- [8] J. Kendall, R. Crittenden, and H. Miller, *J. Amer. Chem. Soc.*, 45, 963, (1923).
- [9] R. Atanasoski, H. Law, and C.W. Tobias *Electrochemical Reduction of Potassium from Potassium Chloride in Propylene Carbonate Electrolyte with Aluminum Anodes*, LBL Report 8505, (1978).
- [10] G. Janz, *Molten Salts Handbook*, Academic Press, page 307, (1967).
- [11] Blander, *Molten Salt Chemistry*, Wiley & Sons, New York, (1964).
- [12] Y. Mary, *Revue de Chemie Minerale*, t. 15, 185, (1978).
- [13] W. S. Harris, "Electrochemical Studies in Cyclic Esters", Ph.D. Dissertation, Univ. of California, Berkeley, California, U.C.R.L -8381, (1958).

Chapter V/ Conductivity of Halide Salts in Propylene Carbonate

5.1. INTRODUCTION

Electrical conductance measurements provide several parameters which are important for engineering design and which can contribute to a fundamental understanding of the solution properties. From the concentration dependence of the equivalent conductance and transference number data, information on single ionic mobilities, λ_0^+ and λ_0^- , can be obtained. The data are useful for estimating the extent of ionic solvation and the size of the solvated species. Conductance data can also be used to estimate the extent of ion-pair formation in solution. In this section, the conductivity literature for propylene carbonate is briefly reviewed with an emphasis on the alkali halides. The results of conductivity experiments designed to estimate the extent of ion-pair formation of KI and KBr in PC are presented. The effect of elemental halogens on the conductivity of salt solutions is discussed. Finally, the effect of solution viscosity on the conductivity is evaluated.

5.2. CONDUCTIVITY OF ALKALI HALIDES

5.2.1. Literature

The generally accepted theory of conductance [1] [2], treats the solvent as a continuum and takes no direct account of solvent properties except for the dielectric constant and the viscosity. The conductance is determined by the mobility of the carrier and the number of carriers. In a given solvent, the mobility of the carrier is related to the size of the solvated ion and the viscosity of the solvent; the number of carriers is related to the extent of association of the salt in solution. It is commonly assumed that ionic salts are completely dissociated in solvents having a dielectric constant greater than about 30. For these dissociated electrolytes, the conductance equation is given by,

$$\Lambda = \Lambda_0 - Sc^{1/2} - Ec \log c + Jc - F\Lambda_0 c. \quad (5.2.1)$$

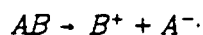
The first four terms describe the theoretical behavior of rigid charged spheres moving in continuum (Debye-Huckel Theory), and the last term is a correction for the solution viscosity. The coefficients depend only on the dielectric constant, the viscosity, temperature, and Λ_0 . In dilute solution, the first two terms are sufficient to describe the results. Thus, in dilute solution, the behavior described by this equation is in agreement with the early observation by Kohlrausch according to which the equivalent conductivity is proportional to the square root of concentration.

If the salt is not completely dissociated in solution, the concentration of ions is less than the formal concentration c , and the conductance is given by,

$$\Lambda = \Lambda_0 - Sc^{1/2}\gamma^{1/2} + Ec\gamma \ln c\gamma + c\gamma F - K_A c\gamma^2 f^2 \Lambda \quad (5.2.2)$$

Here, the association constant, K_A , is the ratio of the equilibrium concentration of undissociated salt to the product of the concentrations of component ions in solution.

For a binary salt in solution, AB, which dissociates to A^+ and B^- according to



K_A is given by,

$$K_A = \frac{1-\gamma}{\gamma^2 c f_{\pm}^2}$$

Here f_{\pm} is the average activity coefficient of the salt, γ is the fraction of the salt in ionic form, and c is the formal concentration of the salt. If the value of K_A is 1.0 and $f_{\pm} = 1$, 38% of a binary salt remains associated in a one molar solution. Unfortunately, data for K_A is not always reported with measurements of Λ_0 .

Despite the relatively high dielectric constant and moderate viscosity of PC, the equivalent conductance of many salts in this solvent is lower than that in a number of solvents having a lower dielectric constant. To illustrate this, conductance parameters for the alkali metal halides and perchlorates in several solvents are listed in Table 5.5.1. The variation of equivalent conductances of a given salt in various solvents can, in part, be rationalized by the degree of specific interaction between the solute and solvent. For example, the equivalent conductance of nearly every salt in Table 5.1.1 declines in the order $\Lambda_0(\text{water}) > \Lambda_0(\text{DMF}) > \Lambda_0(\text{EC}) > \Lambda_0(\text{PC})$. This sequence does not correspond to the order of dielectric constant of the solvent, rather it follows the pattern of the sum of the donor and acceptor numbers. (See Table 5.1.2.) Thus, although this approach is rarely seen in the literature, consideration of the specific interaction between the solute and solvent may be a good indication of the solvent dependence of the limiting equivalent conductance of many salts. To ionize an AB salt, the coulomb interaction of the two ions must be overcome. Specific interaction between the solvent and the ions can decrease this energy barrier. The donor number is a measure of the ability of the solvent to coordinate to a cation. The acceptor number is a measure of the ability of the solvent to coordinate to an anion. Water is a superior ionizing solvent because it has both

a large acceptor number and a large donor number. Thus, it can coordinate both anions and cations. Aprotic solvents have low acceptor numbers so anion solvation is weak although cation solvation may be even stronger than in water. The inability to coordinate anions contributes to the strong tendency to form ion pairs in aprotic solvents. This ion-ion association reduces the number of mobile ions and results in a lower equivalent conductance for salts in aprotic solvents.

	PC (25°C)		EC (40°C)		DMF (25°C)		Water (25°C)	
	Λ_0	K_A	Λ_0	K_A	Λ_0	K_A	Λ_0	K_A
LiCl	27.5 ¹ [b]	557 [c]	30.53 [d]	-	80.1 ¹ [b]	-	115.0 [b]	-
LiBr	26.6 ¹ [b]	19 [c]	33.3 [d]	-	76.7 ¹ [b]	-	116.7 [b]	-
LiI	26.1 [b]	-	33.74 [d]	-	74.81 [b]	-	115.4 [b]	-
NaCl	-	-	36.52 [d]	-	86.5 [b]	-	126.5 [b]	-
NaBr	-	-	39.29 [d]	-	83.1 [b]	-	128.2 [b]	-
NaI	-	-	39.73 [d]	-	81.2 [b]	-	129.9 [b]	-
KCl	32.2 ¹ [b]	-	39.67 [d]	-	88.2 ¹ [b]	-	149.9 [b]	-
KBr	31.3 ¹ [b]	-	42.44 [d]	-	84.8 ¹ [b]	-	151.6 [b]	-
KI	30.8 ¹ [b]	-	42.88 [d]	1.8 [e]	82.9 ¹ [b]	-	150.5 [e]	.69 [e]
LiClO ₄	27.3 [f]	-1.5 [f]	32.85 [g]	-	82.9 ¹ [b]	-	106.0 [b]	-
NaClO ₄	27.9 [f]	-1.2 [f]	38.84 [g]	-	89.3. [b]	-	150.5 [b]	-
KClO ₄	29.6 [f]	0.6 [f]	41.99 [g]	-	91.0. [b]	-	140.9 [b]	-

¹ [a] These values are estimated from summing the values for λ_0^- and λ_0^+ .

² [b] B. G. Cox, in *Annual Report of Progress in Chemistry A*, 70, 249, (1973).

³ [c] L. Mukherjee and D. Boden, *J. Phys. Chem.*, 73, 11, 3985, (1969).

⁴ [d] G. Petrella and A. Sacco, *J. Chem. Soc., Faraday Trans. 1*, 74, 8, 2070, (1978).

⁵ [e] A. D'Aprano, J. Komiyama, and R. Fuoss, *J. Soln. Chem.* 5, 4, 279, (1976).

⁶ [f] M. Jansen and H. Yeager, *J. Phys. Chem.*, 77, 26, 3089, (1973).

⁷ [g] R. Kempa and W.H. Lee, *J. Chem. Soc.*, 1961, 100, (1961).

Table 5.1.2 Physical Properties of Selected Solvents at 25°C				
	PC	EC ^b	DMF	Water
Dielectric Constant	65.1	89	46	78
Viscosity (cp)	2.5	2.54	0.796	1.96
Density (g/ml)	1.2	1.34	0.944	1.10
Donor No.	15.1	16.4	26.6	29.8
Acceptor No.	18	19.3	16	19.3

In PC, the limiting equivalent conductance of a given salt, Λ_0 , is always about a quarter of its value in water. This is generally attributed to the lower viscosity of water (about 40% of the viscosity of PC) and the smaller size of solvated ions in water, but it is also a result of the relatively poor solvation of anions by PC. The alkali metal salts are universally described as completely dissociated in water. In contrast, LiCl and LiBr are found to be associated in PC, with values of K_A of 557 and 19, respectively[3]. No values of the association constant for KBr were found in the literature, but K_A is reported to be 1.8 for KI in ethylene carbonate[4] and "small" in propylene carbonate[5].

Several systematic studies on aprotic solvents[6] [7] have convincingly demonstrated the need to take specific interactions between the solute and solvent into account in the evaluation of conductance properties. For example, D'Aprano et al.[8] studied the conductance of potassium perchlorate and potassium iodide in several mixed solvents. The purpose of this study was to compare

^b The data for ethylene carbonate is given at 40°C.

the ionic association of these salts in pure water and several mixed solvents isodielectric with water. Such solvent mixtures were obtained by adding methanol, acetone, acetonitrile, or sulfolane to ethylene carbonate. From fitting conductance data as a function of concentration, the conductance parameters, Λ_0 (the limiting equivalent conductance), K_A , and α (the solvated ionic diameter), were obtained. The results showed a wide variation of the conductance parameters in the solvents. The values of K_A for both KI and KClO_4 were approximately the same and about 40% larger than the values in water. The results for KI varied depending upon the components of the solvent mixture. Association constants of 1.30 in the EC-TMS mixture and 0.25 in water were found. The conclusion of the study was that salts were more highly associated in the aprotic solvents, but the specific reasons for the difference were not addressed.

Spectroscopic studies of alkali metal salts in PC also show evidence of ion-pair formation for some salts. Using far IR and sodium-23 NMR, Greenberg, Weid, and Popov studied the frequency shifts for LiClO_4 , LiBr, NaI, NaClO_4 , NaBPh_4 , NaBr, and NaSCN in PC[9]. Evidence of ion-pair formation was found for NaBr and NaSCN. An approximate value for the association constant of 36 ± 10 was estimated from the chemical shift data for NaSCN.

Often, conductance data is analyzed assuming that the salt is completely dissociated when this assumption is not valid. This point is discussed by Mukherjee[10] and D'Aprano and Fuoss[11]. Mukherjee points out that plots of the conductance equation (Eq. 5.2.1) versus concentration are not straight lines as expected for completely dissociated electrolytes. Fuoss discusses the fact that negative values of K_A , which are physically meaningless, often result from fitting the conductance equation to data. According to Fuoss, this indicates that the conductivity measurements are not completely reliable indicators of association for values of K_A less than about 1.5.

From this survey, there is evidence in the literature to indicate that the alkali metal salts may be partially associated in propylene carbonate. To advance our understanding of this phenomenon, the conductance of KI and KBr solutions were measured as a function of concentration and as a function of the concentration of a third component, the corresponding halogen.

5.2.2. Experimental

Potassium iodide and bromide salts (Malinckroct, Reagent Grade) were dried under vacuum (less than 1 mm Hg) at temperatures up to 300 °C for several days. All solution preparation and conductivity measurements were done in a glovebox under a helium atmosphere. The glassware for the experiments was cleaned by alcoholic KOH followed by soaking in distilled water for several days and then drying in a vacuum oven. The vials were rinsed with pure PC (prepared as described in chapter 2) before use. The standard solutions were made by slowly adding the powdered salt to dried, distilled PC which had been chilled to 0 °C. The remaining solutions were made by successive dilution; the concentration was later checked by atomic absorption (Perkin-Elmer Model 4000).

The solution conductivity was measured using a ten-range transformer ratio arm bridge (Wayne-Kerr Model B224) at a frequency of 1592 Hz. Temperature control in the glovebox was achieved with a block heater (Scientific Products Model M2025) thermostated at $25 \pm 1.5^\circ\text{C}$. To compensate for small variations in temperature, the conductivity of several solutions was also measured as a function of temperature from 20 to 30 °C. These results were used to correct all values to 25 °C. Conductivity cells were calibrated using aqueous KCl solutions[12].

5.2.3. Results and Discussion

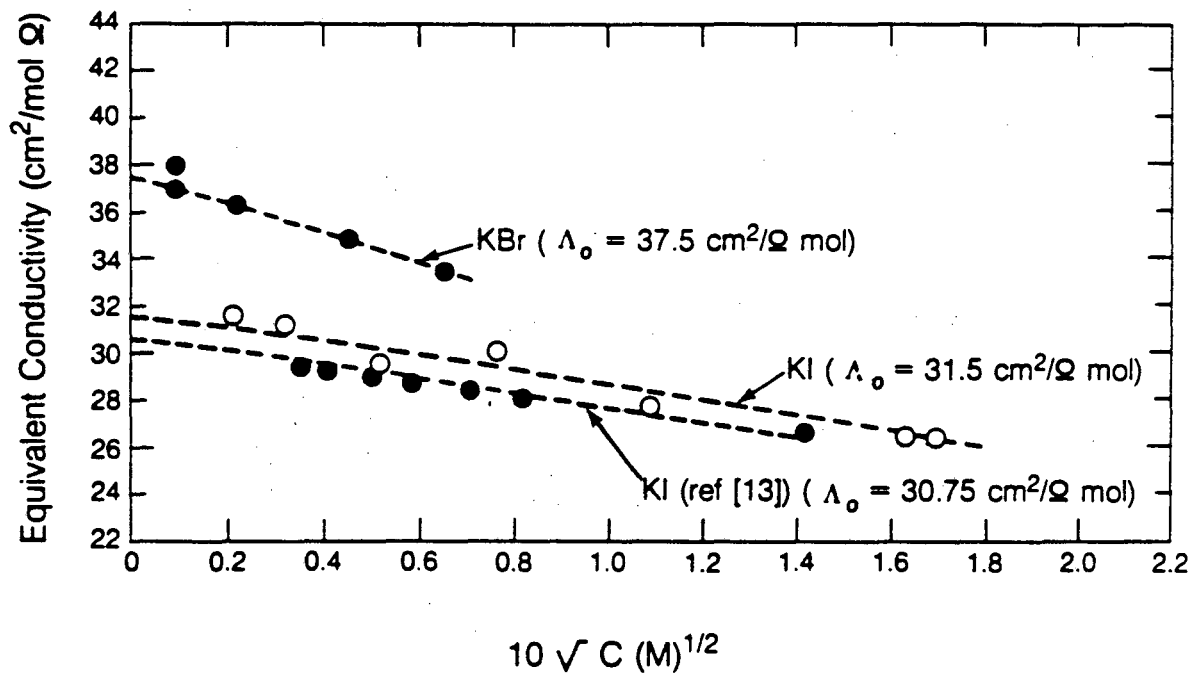
Conductivity of Pure Propylene Carbonate

Propylene carbonate used in this study contained less than 5 ppm water, as measured by GC. (See section 2.3 for details on the purification and characterization of PC.) The conductivity of this solvent was measured in the glovebox using the equipment and glassware described above. The lowest value obtained for the conductivity of PC was $1.7 \pm 0.3 \times 10^{-8} \Omega^{-1} \text{cm}^{-1}$. The results varied slightly with different batches of PC. The measured conductivities were very sensitive to the treatment of the glassware used to contain the sample. The lowest values were obtained in glass vials that were first soaked in dry PC for at least one day. If the glassware was not soaked first, the additional impurities raised the conductivity to as much as $4 \times 10^{-7} \Omega^{-1} \text{cm}^{-1}$. Addition of 470 ppm (0.026 M) water to the $1.7 \times 10^{-8} \Omega^{-1} \text{cm}^{-1}$ PC increased the conductivity slowly (two days) up to $2.4 \times 10^{-7} \Omega^{-1} \text{cm}^{-1}$ but the conductivity remained constant after that point.

Conductivity of KI and KBr in PC

A Kohlrausch plot of the equivalent conductivity of KBr and KI as a function of the square root of concentration is shown in Figure 5.2.1. The equivalent conductance data for solutions less than $1 \times 10^{-4} \text{M}$ yielded anomalous values for Λ_0 which were too high to be physically reasonable. It is believed that this behavior is due to unknown impurities in the solvent or salts. These data have been omitted from Figure 5.2.1. The data for KI plot are well represented by a straight line in the Kohlrausch plot. The intercept gives a value of $31.5 \text{ cm}^2/\Omega \text{mol}$ for Λ_0 , which agrees reasonably well with the value of $30.75 \text{ cm}^2/\Omega \text{mol}$ published by Mukherjee[13]. The slope of the line is also in good agreement with the Mukherjee data.

The data for KBr shows different behavior. Although the Kohlrausch plot is also linear, the derived value of $37.5 \text{ cm}^2/\Omega \text{mol}$ is much higher than the value of $31.3 \text{ cm}^2/\Omega \text{mol}$ estimated from published values of the single ionic mobilities



XBL 8410-4207

Figure 5.2.1 Kolrausch plots for KBr and KI in PC at 25°C. Data from Mukhejee et al. [13] is included for comparison.

of K^+ and Br^- [14]. These mobilities were derived from conductivity measurements of $LiBr$, $KClO_4$ and $n-Bu_4NBr$ under the assumption that $\lambda_o^+ = \lambda_o^-$ for the salt $(i-Am)_4(i-Am)_4B$. Because the equivalent conductance of KI is less than that of KBr , we conclude that KBr is less associated in PC than KI . This is consistent with the donor properties of these halides. Bromide is a better donor than iodide [15], so the interaction between bromide and the solvent is stronger than the interaction between iodide and the solvent. This causes KBr to be less associated than KI .

5.3. CONDUCTIVITIES OF MIXTURES OF HALIDES AND HALOGENS

5.3.1. Experimental

Because of the difficulty of handling bromine and iodine in the glovebox, these experiments were performed outside. The conductivities of these solutions were so much higher than blank experiments (PC only) that any additional impurities introduced from the air did not make a significant contribution. Iodine was added to stock solutions of $0.049\ M$ and $0.099\ M$ KI in PC to obtain the solution compositions listed in Table 5.2.1.

Table 5.2.1 Iodine Concentrations in Two KI Solutions

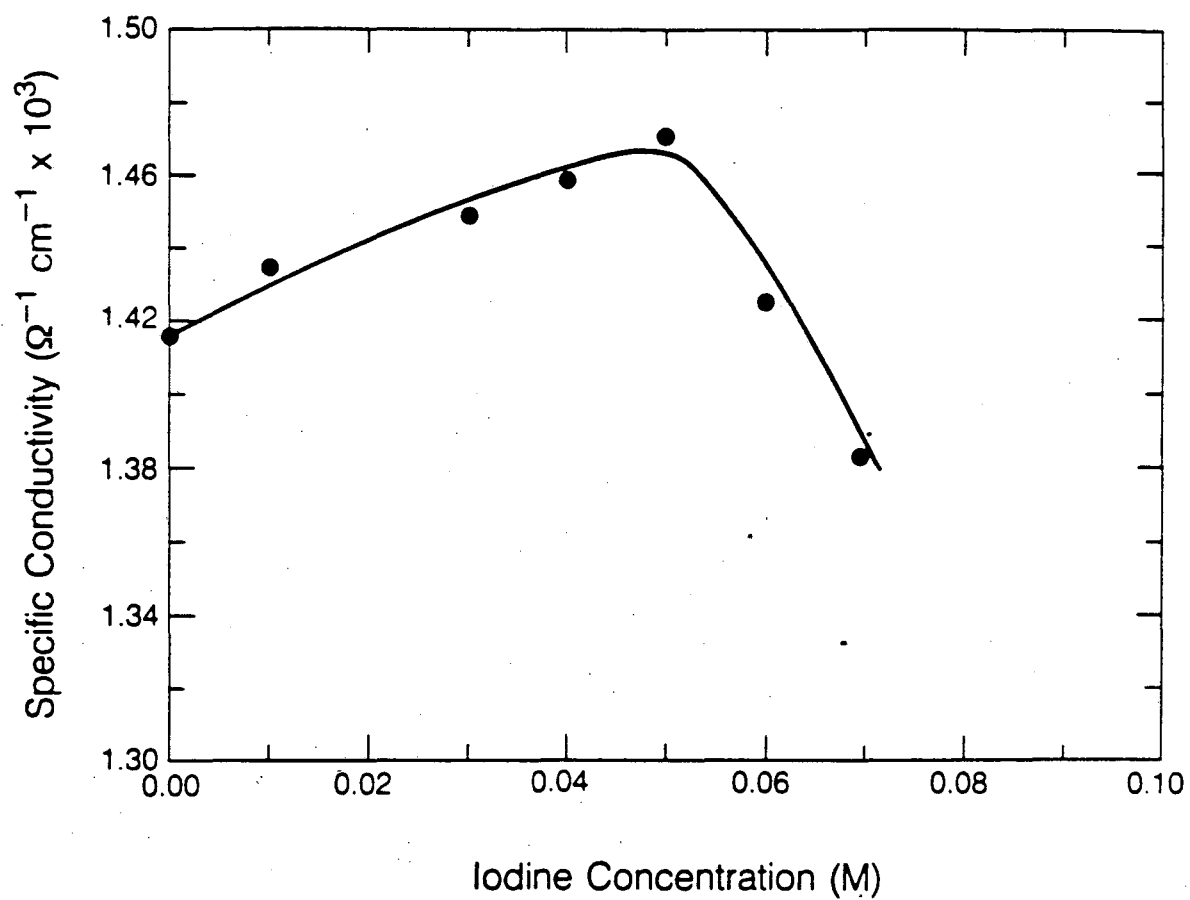
0.049 M KI	0.099 M KI
0.0 M	0.0 M
0.0103 M	0.0401 M
0.0302 M	0.0806 M
0.0399 M	0.0891 M
0.0498 M	0.1010 M
0.0600 M	0.1108 M
0.0700 M	0.1310 M

All measurements were made at higher than room temperature to permit accurate temperature control without refrigeration. Conductivities were measured at 35 °C after the samples had been allowed to equilibrate from 4 to 24 hours. The viscosity of the solutions were measured using an Ostwald capillary viscometer immersed in a 35°C temperature bath.

The bromine experiments were done in a glovebag which had been purged with dry nitrogen. Bromine was added to the bromide solutions using a micropipette.

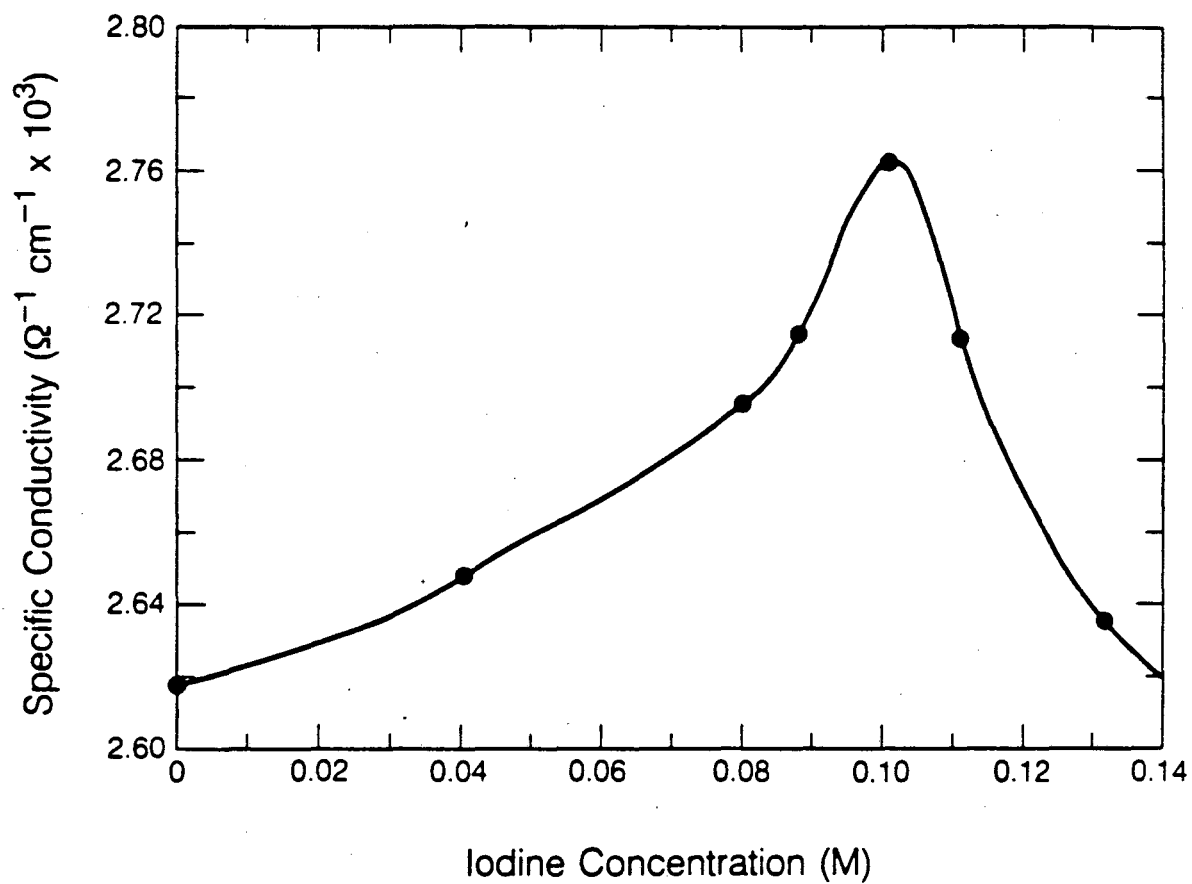
5.3.2. Results and Discussion

The results of the conductivity experiments are presented in Figures 5.3.1 and 5.3.2. The specific conductances of both the 0.05 M and the 0.10 M solutions increased upon the addition on iodine. The conductivity of the 0.05 M solution rose about 3.5%; the conductivity of the 0.1 M solution rose about 5.5%. In each case, the maximum in conductivity occurred when the iodine concentration was



XBL 8410-4208

Figure 5.3.1 Specific conductivity of mixtures of iodide and iodine in PC. KI concentration is constant at 0.05 M. Solution temperature: 35°C.



XBL 8410-10907

Figure 5.3.2 Specific conductivity of mixtures of iodide and iodine in PC. KI concentration is constant at 0.1 M. Solution temperature: 35°C.

equal to the iodide concentration. At higher concentrations of iodine, the conductivity declined.

The viscosity of these solutions at 35 °C, is shown in Figures 5.3.3 A and B. In each case the viscosity was constant, within an experimental error of approximately $\pm 5\%$, for all the concentrations of iodine studied. Thus, changes in the solution viscosity are ruled out as a possible explanation of the rise in conductivity.

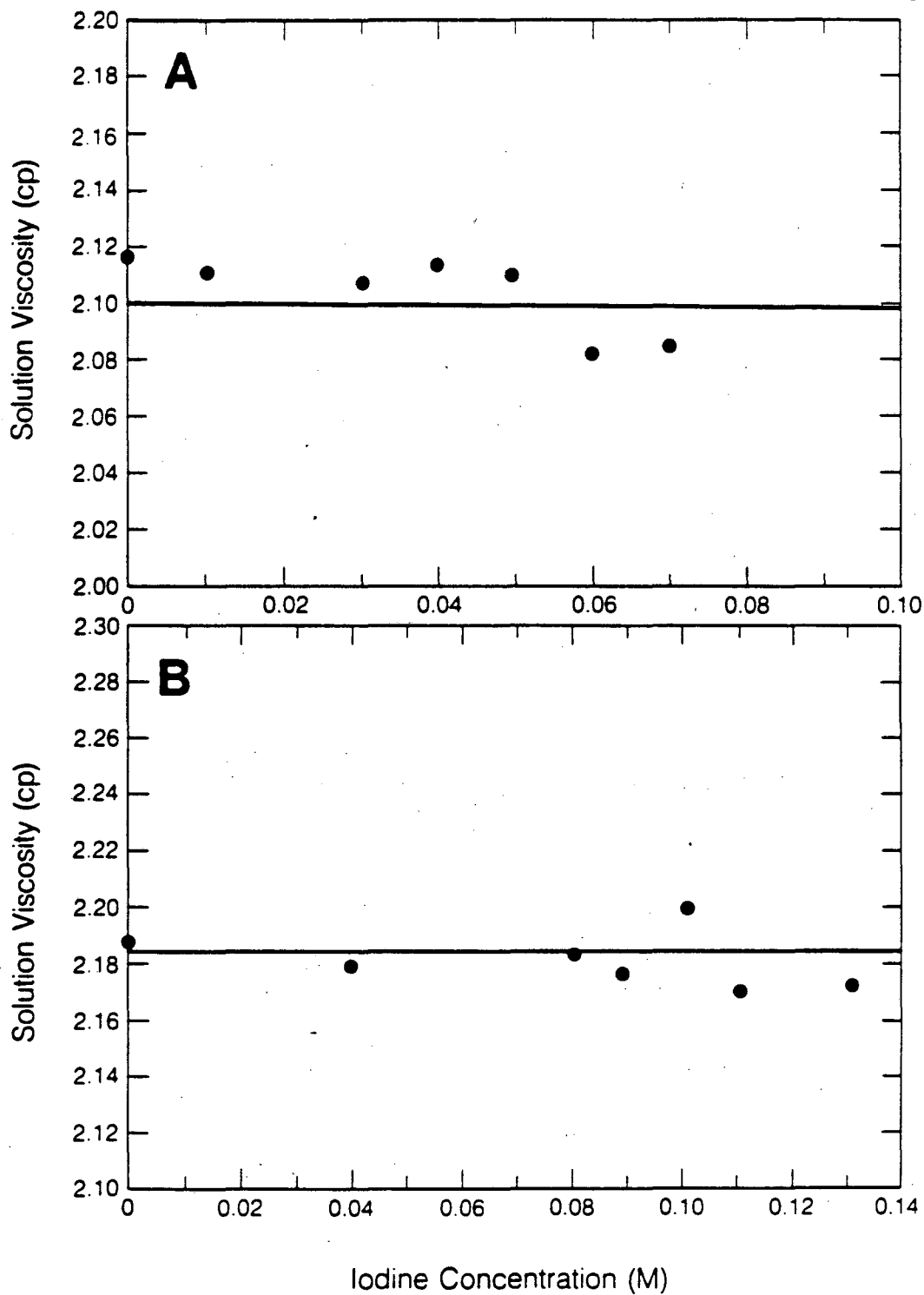
Two explanations for this behavior are possible. If the potassium halide salts are completely dissociated, the behavior of the the conductivity of these solutions simply reflects the increased mobility of the triiodide ion relative to the iodide ion. This explanation is implausible however, because the radius of triiodide is likely to be larger than the radius of the iodide ion⁹. On the other hand, if potassium iodide were not to be completely dissociated in PC, the addition of iodine would shift the equilibrium of the dissociation reaction to the right as iodide is consumed to produce triiodide. The added iodine will be quantitatively converted to triiodide because triiodide is very stable in PC¹⁰. The solvation of triiodide by PC is greater than the solvation of iodide, thus KI_3 will be more dissociated than KI. This increases the number of ionic species in solution. When the total amount of iodide has reacted to triiodide, the conductivity decreases because penta-iodide species begin to be formed¹¹. These large anions should have a lower mobility than triiodide.

The same experiments were performed by adding bromine to bromide solutions. The results, given in Figure 5.3.4, show slightly different behavior than the iodine experiments. No maximum in the conductivity was observed; the specific conductivity rose from $2 \times 10^{-4} \Omega^{-1} \text{cm}^{-1}$ to $30 \times 10^{-4} \Omega^{-1} \text{cm}^{-1}$ when bromine was added to a concentration of 0.7 M. The increase in conductivity may be due to

⁹ Anions are not solvated in PC.

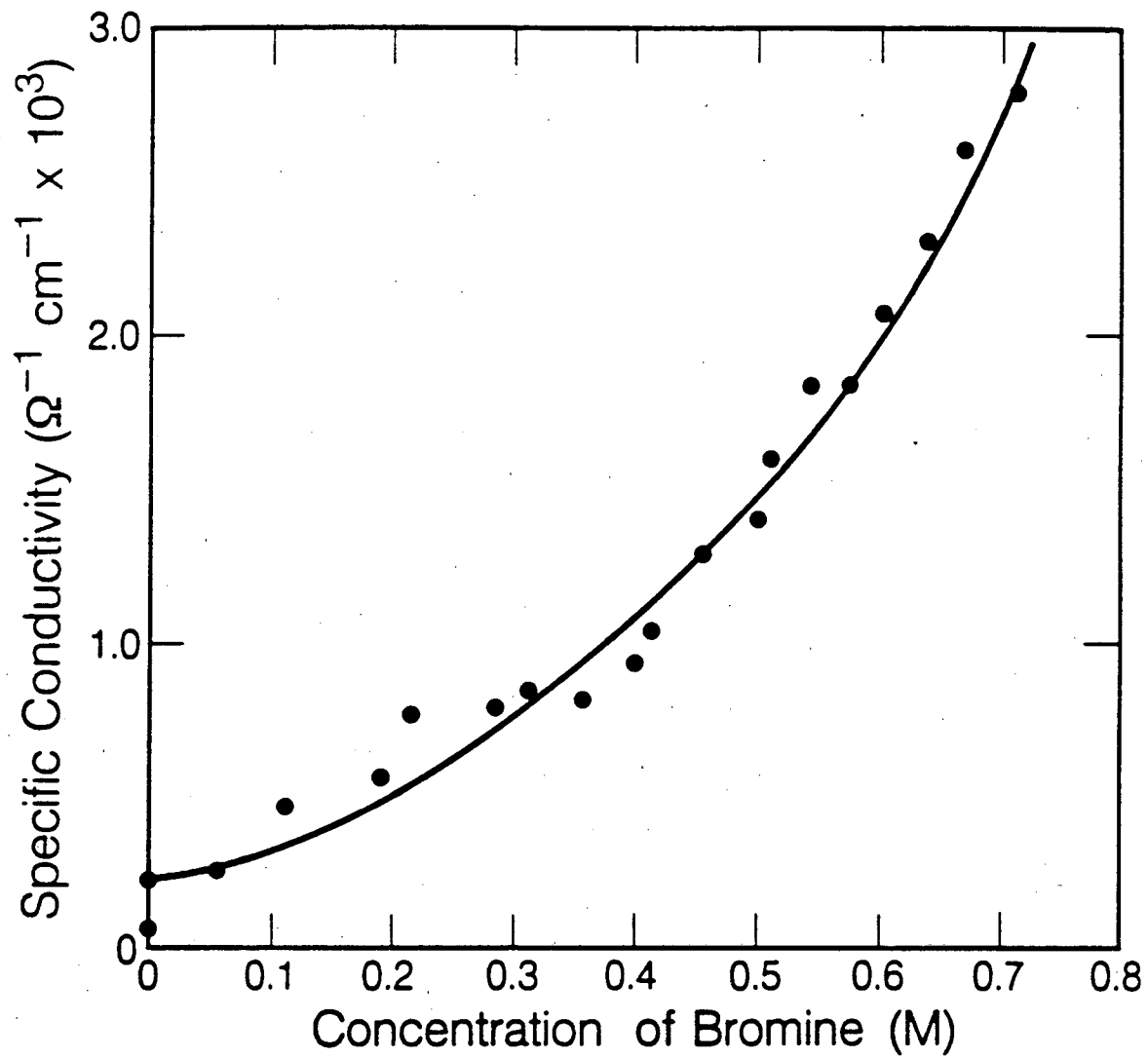
¹⁰ The equilibrium constant for triiodide formation in PC is $10^{7.9}$. (See chapter III.)

¹¹ The equilibrium constant for penta-iodide formation in PC is significant. $pK = 1.9[16]$.



XBL 8410-10904

Figure 5.3.3 Solution viscosity of KI solutions as a function of iodine concentration. Temperature: 35°C. (A) 0.05 M KI, (B) 0.10 M KI.



XBL 849-7973

Figure 5.3.4 Specific conductivity of a saturated KBr solution as a function of bromine concentration. Temperature: 25 °C.

a "Grotthus-type" of conduction mechanism. Although this mechanism is well-established for the conductivity of protons in water, it has generally not been established for other ionic species. According to this mechanism, protons move in aqueous solutions by rapidly hopping from H_3O^+ to H_2O . This leads to unusually high values of the ionic conductivity of protons and OH^- in water. Recently, Rubinstein, Bixon and Gileadi[17] have proposed the same mechanism for the unusually high conductivity of bromide in bromine solutions. They propose that halide ions hop from the trihalide to an adjacent halogen molecule, which could lead to faster ionic transfer.

5.4. CONCLUSIONS

Conductivity experiments designed to determine the extent of ion-pair formation for KI and KBr in PC gave mixed results. In the very dilute range, (concentrations less than $1 \times 10^{-4}\text{M}$), impurities in the solution interfered with the measurement. The results for KI were linear in the higher concentration range, in agreement with theory. However, in contrast to previous studies on halogen salts, we found a higher limiting equivalent conductance for the bromide ion than the iodide ion.

The conductivity of KI and KBr solutions increases if the corresponding halogen is added. Solutions of KI (0.5 M and 0.1 M) show a maximum in conductivity when the concentration of added halogen is equal to the concentration of iodide in solution. A maximum was not observed in KBr solutions. The increasing conductivity is attributed to either the improved mobility of the trihalide ion or possibly a "Grotthus" mechanism of conductivity. In KI solutions, the observed maximum in conductivity may be due to the increased dissociation of the halide salt (KI_3 relative to KI) in halogen solutions.

REFERENCES

- [1] R.M. Fuoss and L. Onsager, *J. Amer. Chem. Soc.*, **61**, 668, (1957).
- [2] R. M. Fuoss, *J. Soln. Chem.* **7**, 10, 771, (1978).
- [3] L. Mukherjee and D. Boden, *J. Phys. Chem.*, **73**, 11, 3965, (1969).
- [4] A. D'Aprano, J. Komiyama, and R. Fuoss, *J. Soln. Chem.*, **5**, 4, 279, (1976).
- [5] L. Mukherjee, D. Boden, and R. Lindauer, *J. Phys. Chem.*, **74**, 9, 1942, (1970).
- [6] D.F. Evans and P. Gardam, *J. Phys. Chem.*, **72**, 3281, (1968)
- [7] F. Accascina, A. D'Aprano, and R. Triolo, *J. Phys. Chem.*, **71**, 3469, (1967).
- [8] A. D'Aprano, I. Donato, and E. Caponetti, *J. Soln. Chem.*, **3**, 5, 371, (1974).
- [9] M. Greenberg, D. Wied, A. Popov, *Spectrochimica Acta*, **29A**, 1923, (1973).
- [10] L. Mukherjee, D. Boden, and R. Lindauer, *op cit.*
- [11] A. D'Aprano, J. Komiyama, and R. Fuoss, *op cit.*
- [12] International Critical Tables, *Vol. 6*, page 230.
- [13] L. Mukherjee, D. Boden, and R. Lindaur, *op cit.*
- [14] B.G Cox, in *Annual Report of Progress in Chemistry, A*, **70**, 249, (1973).
- [15] V. Gutmann, *The Donor-Acceptor Approach to Molecular Interactions*, Plenum Press, New York (1978).
- [16] J. Courtot-Coupez and M. L'Her, *C.R. Acad. Sc. Paris, Serie C*, **266**, 1286, (1968).
- [17] I. Rubinstein, M. Bixon and E. Gileadi, *J. Phys. Chem.*, **84**, 715 (1980).

Chapter VI/ Electrochemical Oxidation of Iodide in Propylene Carbonate: Cyclic Voltammetry Experiments

6.1. INTRODUCTION

The kinetic and thermodynamic properties of the electrochemical oxidation of halides are highly influenced by the properties of the solvent chosen for the process. For example, cyclic voltammetry experiments performed with iodide in a series of solvents including water, methanol, pyridine, acetonitrile, and DMSO showed a 310 mV range in the potential for iodide oxidation and a wide variation in the stability of triiodide[1]. In addition to potential variations, the solvent also influences the kinetics of electrochemical reactions by changing the character of the intermediate or specifically interacting with the product of the reaction. Despite a large effort by workers such as Parker, Gutmann, Popovych and others, methods to predict these properties from single component (solvent and solute) data are not yet accurate enough to be useful. Thus, dependable information about the behavior of an electrochemical couple must still be obtained experimentally. In the following study the chemistry and electrochemistry of the iodide/ triiodide/iodine system in PC is presented.

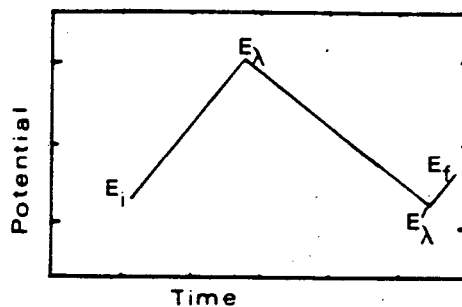
Cyclic voltammetry was the primary technique chosen to study the nature of the electrochemical oxidation of the halides. In addition, potential step experiments were performed to determine the diffusion coefficients and the electroactive area of the electrodes. Spectral electrochemical experiments were also done to independently confirm the chemistry.

The cyclic voltammetry experiment consists of applying a linearly varying potential to the working electrode (relative to the reference potential) and monitoring the resulting current. In this way, the behavior of multiple electroactive species can be followed over a potential range. The only independent parameters of the experiment are the range and rate of the potential sweep. An outline

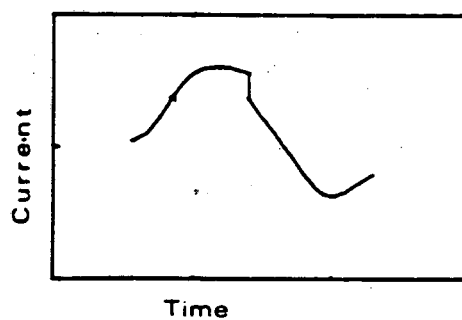
of a typical cyclic voltammetry response for a single reversible oxidation reaction is shown in Figure 6.1.1. Although the experiment is conceptually simple, its interpretation is often complicated by the large number of variables affecting the total current. These include adsorption of the reactant and/or product, double layer charging, kinetic effects, complications due to homogeneous reactions, or unwanted stirring due to natural convection. For this reason, the quality of information available from a cyclic voltammetry experiment depends upon the design of the apparatus and the experimental procedure. The measured parameters in any cyclic voltammetry experiment are the half-wave potential, $E_{1/2}$, for each electrochemical reaction, the peak current at that potential, and the shape of the wave. From the dependence of the peak current on the sweep rate, the number of electrons transferred for an electrode reaction can be determined. In many applications, the number of reactions and the reaction potential are the only results of interest. However, for simple reactions and a well-defined reactor geometry (semi-infinite stagnant solution adjacent to a planar electrode or rotating disc, for example), quantitative information about reaction reversibility, kinetic or transport parameters can be obtained from the shape of the voltammetric curves. The purpose of using cyclic voltammetry to study the electrochemistry of the halogens in propylene carbonate was to characterize the oxidation reaction. Specifically, the questions of interest are:

- i. How many reactions occur?
- ii. What is the stoichiometry of each reaction?
- iii. Are the reactions reversible or are the kinetics slow?
- iv. Is there evidence for solvent decomposition?

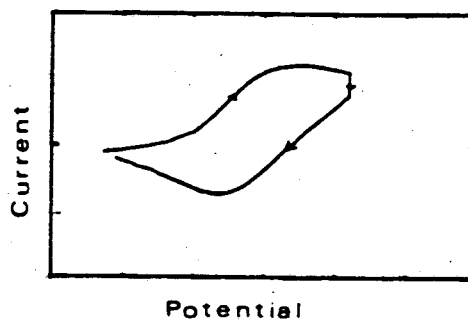
In this chapter the work of previous investigations of halide oxidation in nonaqueous solvents is reviewed and the results of a series of cyclic



a) Applied Potential $[E_i, E_\lambda, E'_\lambda, E_f]$



b) Current



c) Voltammogram

XBL 847-3081

Figure 6.1.1 Cyclic voltammetry. A sawtooth potential is applied to the working electrode (A) and the resulting current (B) is monitored. The results are presented as a voltammogram (C). The applied potential designation, $[E_i, E_\lambda, E'_\lambda, E_f]$, gives the initial, anodic and cathodic switching potentials, and the final potential. Anodic currents are positive.

voltammetry experiments on the halide/halogen couple in propylene carbonate is reported. In addition, a mathematical model is presented which was developed to interpret the voltammograms. Finally, the results of spectral electrochemical experiments are described.

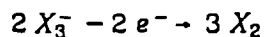
6.2. LITERATURE

6.2.1. Experimental Studies

Since the turn of the century, halide oxidation in aqueous solutions has been exhaustively studied. The equilibrium constant of the triiodide formation, for example, has been measured by distributional methods [2], spectrophotometry [3] [4], solubility [5], conductivity [6], and potentiometry [7]. One author comments that the I^-/I_2 couple "is probably the most extensively studied equilibrium involving a molecule and an ion" [8]. Surveys of the work are available [9] [10], and effort continues to establish the existence and stability of I_5^- and higher atomic chains [11]. By 1956, the chemistry and electrochemistry of the halogen couples in non-aqueous solvents began receiving attention. Literature on this subject generally falls into two categories: either the halogen reactions are studied in detail in a single solvent to investigate the mechanism of the reaction or a single reaction is examined in a series of solvents to study the effect of the solvent on the reaction. In this section a series of papers describing voltammetric studies of halide oxidation in nonaqueous solvents is reviewed. The papers are selected to highlight the effect the solvent on the reactivity of the halogen/halide couple, to review some of the controversies in the literature, and to survey the work done to date in propylene carbonate.

Single Solvent Studies: Acetonitrile

In the final paragraph of their 1957 paper, Kolthoff and Coetzee [12] describe a series of voltammetry experiments in chloride, bromide, and iodide solutions in acetonitrile. They noted that the three halides each gave two anodic waves at a rotating platinum electrode and postulated the following mechanism:



This preliminary work was followed by an extensive study on the voltammetry of the iodine species in acetonitrile reported by Popov and Geske in 1958 [13]. Their observations differed from the earlier work on a major point. Instead of two voltammetric waves, as reported by Kolthoff and Coetzee, they observed four waves. Triiodide formation and subsequent oxidation are assigned to the waves occurring at the low potential (in agreement with the earlier work) and the oxidation of iodine to cationic iodine species is postulated to account for the waves occurring at more positive potentials. Formal potentials and a stability constant for triiodide are presented; these values are compared to other literature values in Table 6.2.1. An attempt to stabilize the I^+ species was made by adding a heterocyclic amine to the solution. They found that increasing the amine concentration increased the height of the positive iodine wave but quantitative evaluation was hampered by the fact that the amines participate in the formation of a film under these highly oxidizing conditions. A third paper entitled "Iodometrie dans l'Acetonitrile" was published by Desbarres in 1961 [14]. Although this is largely an extension of Geske and Popov's work, it includes the effect of water on the electrode potentials and the stability of the triiodide in mixed water-acetonitrile solutions.

Table 6.2.1 Triiodide Stability Constant in Various Solvents		
Solvent	$-\text{pK for } K = \frac{[I_3^-]}{[I^-][I_2]}$	References
AN	7.4 8.6 6.8	Desbarres [14] Nelson & Iwamoto [24] Nakata [26]
DMSO	6.9 6.9	Nakata [26] Parker [25]
DMF	7.0 7.0	Nakata [26] Parker [25]
Water	2.85	Parker [25]
PC	7.9	L'Her [21]

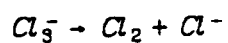
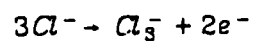
Anhydrous Acetic Acid and Nitromethane

The mechanism of oxidation of bromide and chloride in anhydrous acetic acid was studied by Mastragostino, Casalbore and Valcher [15]. They observed only one anodic wave for both chloride and bromide oxidation. Although the chloride reaction was reversible, the oxidation of bromide was under kinetic control. The authors proposed the following mechanism:

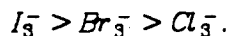
Bromide oxidation:



Chloride oxidation:



From this work they concluded that the order of stability of the tri-halides in acetic acid is



In a later paper the same group studied the oxidation of chloride in nitromethane [16]. Based on the same type of experiments, they arrive at the same mechanism for chloride oxidation as described above. Both these papers are flawed by the reference of all potentials to the "Thalamid electrode #40". This electrode is not characterized or referred to a more conventional reference electrode. Also, only reduced data are given so the conclusions of the authors cannot be checked by examination of peak shapes and background currents.

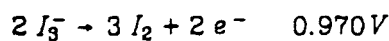
Pyridine

Pyridine, in spite of its odor, is one of the most useful and most studied organic solvents. The polarity of the molecule promotes high solubility of many salts and the aromatic structure stabilizes the molecule and minimizes the availability of solvent protons. Because pyridine is of interest as a solvent for analytical chemistry and as a battery solvent, the electrochemistry of the iodine/iodide couple in pyridine has been thoroughly studied. The use of pyridine as a nonaqueous solvent has been carefully reviewed by Nigretto and Jozefowicz[17].

Halogen solutions in pyridine have received much attention in the literature because strong complexes can form between the solvent and the halogen. As a strong donor solvent (donor number of 33.1), pyridine interacts with iodine to form molecular complexes of the form, PyI_2 [17]. The literature of the complex formation is reviewed in chapter three.

Voltammetric experiments, similar to those done in other solvents, were performed in pyridine to establish the stability of iodine species over a pH range[18]. From this work three distinct couples were characterized in acid

media:



Above pH 5, the iodine begins to disproportionate into triiodide and an unidentified positively charged species, probably the base IOH or its anhydride, I_2O .

Propylene Carbonate

The electrochemistry of the halides in propylene carbonate has received scant attention in the literature. Although several investigations of the stability of triiodide have included PC in the series of solvents considered, there is little information available describing the reactions in detail. From voltammetry experiments, Courtot-Coupez and L'Her [19] observed two waves corresponding to iodide and subsequent triiodide oxidation. From the difference in the half-wave potentials, the stability constant for triiodide formation is determined to be $pK = 7.9$, where pK is defined as,

$$pK_1 = \frac{E_2^0 - E_1^0}{0.087} \quad ; \quad K_1 = \frac{[I_2][I^-]}{[I_3^-]}$$

$$pK_1 = -\log K_1$$

Because a plot of E vs. $\log C$ is not a straight line at high concentrations of iodine, the authors conclude that the penta-iodide complex, I_5^- , is stable in propylene carbonate. This conclusion is reached even though they do not observe a reduction wave for this species. From the deviation from the expected linear behavior of a titration of an iodine solution with iodide, they calculate a stability constant for I_5^- of $pK = 1.9$. Unfortunately, neither the Nernst plot nor the titration data

are presented. Because these experiments were performed using a silver/ silver perchlorate reference electrode, which is known to be unstable in PC in the presence of halogens [20], and because the authors have not recognized the existence of a disproportionation reaction between iodine and PC (see section 3.3) the explanation that a penta-iodide complex exists is not completely convincing.

The stability of triiodide was studied by L'Her, Morin-Bozec, and Courtot-Coupez in a paper on the solvation of anions in mixtures of water and PC [21]. Equilibrium E° values were determined for the iodide/triiodide and triiodide/iodine couples from the analysis of potentiometric titration curves. The potentials are a linear function of $\log [x/(1-x)^3]$ for the titration of iodide solutions with iodine, where x is the amount of titrate added. For the titration of iodine solutions, the potential is a linear function of $\log [(1-x)^3/x^2]$. Values of E° obtained by L'Her et al. are listed in Table 6.2.2.

$E^\circ (I^- / I_3^-)$	-0.292 V
$E^\circ (I_3^- / I_2)$	0.388 V

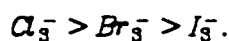
For the difference in E° values, a stability constant of 7.7 l/mole is reported.

Multiple Solvent Studies

The acidity or basicity of halides or halogen species in solution are both strong functions of the solvent properties. For example, triiodide is the most

stable of the tri-halides in water but the least stable in aprotic solvents[22]. Repetitive studies of the same electrode reaction (or reactions) in a variety of solvents is an approach many have taken to evaluate the influence of ionic solvation on reaction thermodynamics. Often, cyclic voltammetry is used for these measurements.

Early work showed a wide variation in tri-halide stability and activity in different solvents. In 1955, Iwamota [23] published a technical note describing the half-wave potentials of halide oxidation from cyclic voltammetry experiments in a series of solvents ranging from protic solvents such as water and ethanol to dipolar aprotic solvents such as acetonitrile and pyridine. He concluded that halide oxidation in aprotic solvents shows two anodic waves while the same reactant in protic solvents exhibits only one wave. In 1964, he followed this work with a paper co-authored with I. Nelson detailing the voltammetric studies of tri-halide stability in nitromethane, acetone, and acetonitrile[24]. As noted above, they found that in contrast to the situation in water, triiodide is the least stable of the tri-halides in these aprotic solvents. The order of stability was reported as:



This order is reversed in water. The reason for the large difference in tri-halide stability is explained by the authors to be a result of the strong hydrogen bonding properties of water. Because aprotic solvents are appreciably less acidic and less basic than water, the halides and halogens have much lower solvation energy in these solutions. Therefore much less energy is required to form the tri-halides and the stability constants are large. Stability constants reported in this paper are also included in Table 6.2.1.

A systematic study of the influence of anion solvation on the chemistry of anions in protic and aprotic solvents was published by Alexander et al.[25]. in

1967. Solvation effects were studied by solubility product measurements of silver, cesium, and potassium salts; and instability constant measurements (the inverse of the stability constant) of silver and halogen complexes in water, methanol, formamide, DMF, DMA, DMSO, acetonitrile, and hexamethylphosphorotriamide (HMPTA). The reported instability constants have been converted to stability constants and are also included in table 6.2.1. In agreement with Iwamoto, their results show that tri-halide ions are much more stable in dipolar aprotic solvents than in protic solvents. According to Parker the stability of the halides observed in water, $I^- > Br^- > Cl^-$, is due to the strong H-bonding solvation of the chloride ion in water, and not due to an intrinsic property such as polarizability. The large stability constant of I_3^- in aprotic solvents is attributed to the high polarizability of the large triiodide ion. This allows it to be more easily solvated by aprotic solvents relative to tribromide and trichloride ions.

In recent work, the polarographic behavior of iodine in a series of aprotic solvents was investigated by Nakata et. al[26]. The solvents included in the study were acetonitrile, benzonitrile, DMA, DMF, PC, DMSO, and HMPTA. In experiments using a dropping mercury electrode, the electrochemistry was dominated by the presence of mercuric iodide which formed at the electrode surface by the the reaction of iodine and mercury. Stability constants for tri-halide formation derived from rotating disc experiments at platinum electrodes are included in Table 6.2.1.

6.2.2. Theoretical Treatments of Cyclic Voltammetry

Since the first demonstration of cyclic voltammetry by Matheson and Nichols [27] in 1938, the theoretical description of the technique has been extensively developed by many investigators. The earliest work described the theory for a reversible electrode reaction and was reported independently by Randles [28] and Sevcik[29] in 1948. By 1953 the theory for irreversible charge

transfer reactions was reported by Delahay [30] and later this work was rederived and extended to quasi-reversible systems by Matsuda and Ayabe [31]. These papers initiated intense activity and by 1965 the theory of the single scan method had been applied to reversible reactions at cylindrical electrodes [32], and at spherical electrodes [33]; deposition reactions [34] and dissolution reactions [35] were examined, as well as systems of consecutive charge transfer reactions [36]. In 1964 Nicholson and Shain [37] published a classic paper on the subject. They reviewed the theoretical work to that date and presented the theory of both single-scan and cyclic voltammetry applied to systems in which preceding, following or cyclic chemical reactions are coupled with reversible or irreversible charge transfer reactions. The following year this work was extended to include the case in which a chemical reaction is coupled between two charge transfer reactions (often called the "ECE mechanism") [38].

A complete discussion of the theory of cyclic voltammetry for the array of reaction mechanisms and kinetic cases is not presented here. Several books cover the subject in detail [39], [40]. Instead I present only the general approach developed by Nicholson and Shain and demonstrate why the existing theory was inadequate to describe the system of electrode reactions proposed for halide oxidation in PC. I will cover only solutions to the problem of reaction at a planar electrode in a stagnant solution and focus on the case of reversible charge transfer.

Reversible Charge Transfer

The solution to the problem of linear sweep voltammetry with reversible charge transfer is a starting point for outlining the general problem. The approach shown here follows the work of Nicholson and Shain. For a single reversible reduction of an oxidized species, O, to a reduced species, R,



the governing equations for a reaction at a planar electrode are described by Fick's second law for both the oxidized and reduced species,

$$\frac{\partial C_R}{\partial t} = D_R \frac{\partial^2 C_R}{\partial x^2} \quad (6.2.1)$$

$$\frac{\partial C_O}{\partial t} = D_O \frac{\partial^2 C_O}{\partial x^2} \quad (6.2.2)$$

where x is the distance from the electrode surface, C_O and C_R are the concentrations of substances O and R , and t is time. These equations apply only under the assumption that the mass transfer in the bulk solution occurs by diffusion only; migration and natural convective effects are neglected. The validity of these assumptions is discussed in section 6.6. Assuming that only O is present at the beginning of the experiment at concentration C_O^* , the initial conditions are

$$C_R(0, x) = 0 \quad (6.2.3)$$

$$C_O(0, x) = C_O^* \quad (6.2.4)$$

We assume that the reaction occurring at the electrode surface has no effect at $x = \infty$, thus:

$$C_R(t, \infty) = 0 \quad (6.2.5)$$

$$C_O(t, \infty) = C_O^* \quad (6.2.6)$$

If the electrochemical reaction is reversible, the kinetics are fast relative to diffusion, and the concentration of the oxidized and reduced species obey the Nernst equation at the electrode surface,

$$\text{for } t > 0, \text{ and } x = 0: \frac{C_O(0, t)}{C_R(0, t)} = \exp\left[\frac{nF}{RT}(E - E^\circ)\right] \quad (6.2.7)$$

Here E is the potential of the electrode relative to a given reference and E° is the formal electrode potential relative to the same reference. Since a linear voltage

ramp is applied to the working electrode, the potential is a function of time. For a single scan,

$$\text{for } 0 < t \leq \lambda \quad E = E_i - bt \quad (6.2.8)$$

$$\text{for } t > \lambda \quad E = E_i - 2b\lambda + bt \quad (6.2.9)$$

where E_i is the initial electrode potential, b is the potential sweep rate, and λ is the time at which the scan is reversed.

The final boundary condition describing the system is the statement of the material balance for reaction A at $x = 0$,

$$D_O \left\{ \frac{\partial C_O}{\partial x} \right\} = -D_R \left\{ \frac{\partial C_R}{\partial x} \right\} \quad (6.2.10)$$

Nicholson and Shain solve the problem by converting the differential equations into integral equations by taking the Laplace transform of equations 6.2.1 - 6.2.4 and solving for the transform of the surface concentrations in terms of the transform of the surface fluxes. These equations are then inverted using the convolution theorem, and the surface concentrations of both species are expressed in the form of an integral.

$$C_O(0,t) = C_O^0 - \frac{1}{\sqrt{\pi D_O}} \int_0^t \frac{f(\tau) d\tau}{\sqrt{t-\tau}} \quad (6.2.11)$$

$$C_R(0,t) = \frac{1}{\sqrt{\pi D_R}} \int_0^t \frac{f(\tau) d\tau}{\sqrt{t-\tau}} \quad (6.2.12)$$

where,

$$f(t) = D_O \left\{ \frac{\partial C_O}{\partial x} \right\}_{x=0} = \frac{i}{nF} \quad (6.2.13)$$

The boundary condition (6.2.7) can now be applied by dividing equation (6.2.11) by equation (6.2.12) and eliminating the concentration terms. The resulting

equation contains a single integral which has the flux of species O at the electrode surface as its solution.

$$\int_0^t \frac{f(\tau) d\tau}{\sqrt{t-\tau}} = \frac{C_0^* \sqrt{\pi D_0}}{1 + \gamma \theta S_\lambda(t)} \quad (6.2.14)$$

where

$$\gamma = \left(\frac{D_0}{D_R} \right)^{\frac{1}{2}} \quad (6.2.15)$$

$$\theta = \exp \left[\left(\frac{nF}{RT} \right) (E_i - E^0) \right] \quad (6.2.16)$$

$$S_\lambda(t) = \begin{cases} e^{-\sigma t} & \text{for } t \leq \lambda \\ e^{-\sigma t - 2\sigma\lambda} & \text{for } t > \lambda \end{cases} \quad (6.2.17)$$

$$\sigma = \frac{nFb}{RT} \quad (6.2.18)$$

Theoretical current-potential curves were obtained by a numerical integration of the integral. The current at a given potential (or time) is expressed as,

$$i = nFC_0^* (\pi D_0 \sigma)^{\frac{1}{2}} \chi(\sigma t) \quad (6.2.19)$$

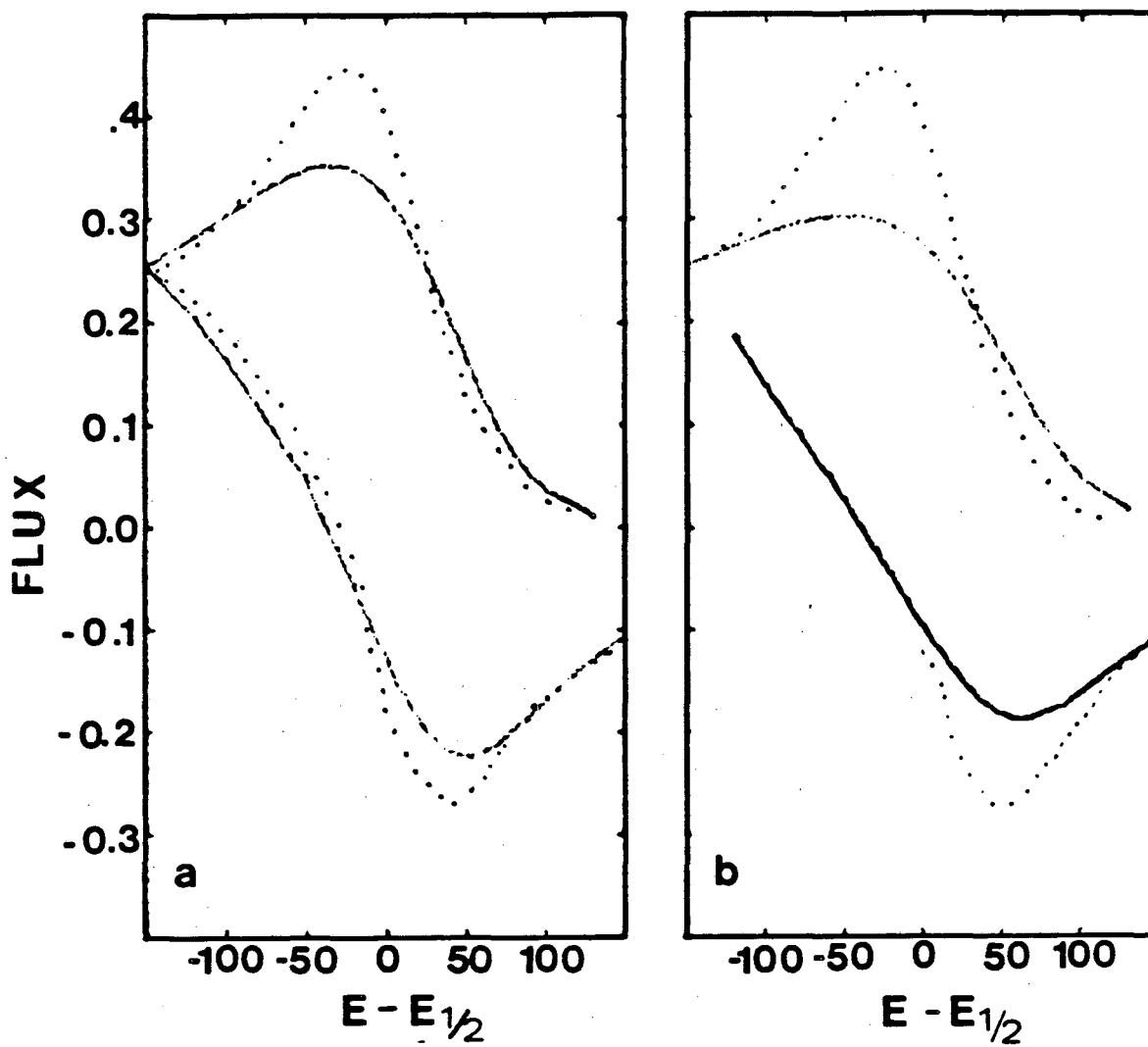
where

$$\sigma t = \left(\frac{nF}{RT} \right) (E_i - E) = \left(\frac{nF}{RT} \right) b t \quad (6.2.20)$$

The value of the dimensionless flux, $\chi(\sigma t)$, is obtained from tables published by Nicholson and Shain and reprinted elsewhere[41].

A graph of the theoretical cyclic voltammogram in dimensionless form is given in Figure 6.2.1 as the dotted lines. The diagnostic criteria for reversible charge transfer are given in terms of the maximum in the current function at a potential relative to the polarographic half-wave potential¹. These values are given in Table 6.2.3.

¹ In this case, $E_{1/2} = E^0 + (RT/nF) \ln(D_R/D_0)^{\frac{1}{2}}$



XBL 848-3339

Figure 6.2.1 The effect of reaction stoichiometry on the shape of the voltammogram. Solid lines show 2:1 (a) and 3:1 (b) stoichiometry. Dotted lines show 1:1 case for comparison.

The extension of this theory to cyclic triangular wave voltammetry follows from the same equations although the peak current and potential now depend upon the switching potential.

Non-Unity Reaction Orders

The application of the theory of Nicholson and Shain to reactions having non-unity reaction orders is not a simple extension. Surface concentrations of the oxidized and reduced species, set by the Nernst equation, are now raised to powers defined by the reaction stoichiometry. This problem was treated by Shuman [42] using the approach of Nicholson and Shain to examine the case of 2:1 and 3:1 reaction stoichiometries. Consider the general case,



In the bulk solution diffusion is still the only form of mass transfer so the governing equations (6.1 and 6.2) remain unchanged. But at the electrode surface the concentrations of O and R are set by their equilibrium values. Therefore the surface boundary condition becomes

$$\frac{\rho_0^{(q-m)} [C_O(0,t)]^m}{[C_R(0,t)]^q} = \exp \left[\frac{nF}{RT} (E - E^0) \right] \quad (6.2.21)$$

The term ρ_0 represents the solvent density and the concentrations are given in units of moles per cc. The initial conditions (equations 6.2.3 and 6.2.4) are the same as those used for the 1:1 stoichiometry model. Therefore the integral equations describing the surface concentrations as a function of time (6.2.11 and 6.2.12) are still valid. But when these are substituted into the Nernst equation, a different integral equation is derived,

$$\left[1 - \frac{1}{C_0^* \sqrt{\pi D_0}} \int_0^t \frac{f(\tau) d\tau}{\sqrt{t-\tau}} \right]^m = \quad (6.2.22)$$

$$(q/m)^q \gamma^q C_0^{(q-m)\theta} S_\lambda(t) \left[\frac{1}{C_0^* \sqrt{\pi D_0}} \int_0^t \frac{f(\tau) d\tau}{\sqrt{t-\tau}} \right]^q$$

Also, the material balance changes to reflect the stoichiometry,

$$q \left[D_0 \frac{\partial C_0}{\partial x} \right] = -m \left[D_R \frac{\partial C_R}{\partial x} \right] = \frac{i}{nF} \quad (6.2.23)$$

Using a numerical technique similar to the one used by Nicholson and Shain, Shuman solved this equation for the cases of a second order reaction ($m = 2$, $q = 1$) and a third order reaction ($m = 3$, $q = 1$). The results are given in the form of a dimensionless current parameter, $\chi(\sigma t)$, for a range of values of $(E - E_{1/2})$, where $E_{1/2}$ is the polarographic half-wave potential² and $\chi(\sigma t)$ is given by equation 6.2.19. A comparison of the cyclic voltammograms for each case is given in Figure 6.2.1. The curves for the second and third order cases are lower and broader than those for the first order case. A comparison of the diagnostic criteria is included in Table 6.2.3.

² Here, $E_{1/2} = E^0 - (RT/nF)[q \ln(\gamma q/m) + (q - m) \ln C_0^*]$
 where $\gamma = (D_0/D_R)^{1/m}$.

Table 6.2.3 Diagnostic Criteria for Single Voltammograms			
	$O + ne^- \rightarrow R$ (Nicholson & Shain [37])	$2O + ne^- \rightarrow R$ (Shuman [42])	$3O + ne^- \rightarrow R$ (Shuman [42])
Peak current $\pi^{1/2} \chi(\sigma t)$	0.4463	0.3533	0.3033
Peak potential $\pi(E_p - E_{1/2})$ (mV)	-28.50	-36.0	-49.8
i_a/i_c	1.0	1.09	1.16

6.3. THEORETICAL MODEL

To simulate the results of the cyclic voltammetry experiments of KI in PC (see section 6.4) a theoretical model was developed in collaboration with M. Matlosz[43]. The distinguishing feature of the voltammogram obtained for a KI solution in well-supported PC (see for example, Figure 6.4.13) is the presence of two electron transfer steps separated by approximately 440 mV. The position of the first peak is weakly dependent on the rate of the potential sweep in contrast to the second peak where the position is independent of the potential sweep rate up to 1 V/sec. The fact that the likely anodic reactions of iodide do not have 1:1 stoichiometries means that the previously published theoretical models for cyclic voltammetry cannot be applied here.

Three possible reaction sequences were considered. The model which showed the best correspondence to the experimental data is listed here as "Case III", but the results of the earlier models (Cases I and II) are included to document different approaches.

In the first case, "Case I", iodide is oxidized to form iodine in the first electron transfer step. Then the electrogenerated iodine diffuses into the solution and reacts with iodide to form triiodide in a *homogeneous* chemical step. At the higher potential, triiodide is oxidized to iodine. All electrochemical steps are assumed to be reversible.

The second mechanism, Case II, is based on the assumption that the formation of triiodide occurs on the electrode surface rather than in the solution. We assumed that this *heterogeneous* chemical step is rate limiting but not potential dependent, and that the second electrochemical reaction is reversible. In contrast, in the third possible mechanism, Case III, the effect of a slow, or rate limiting electrochemical reaction for the first peak is considered but the condition of reversibility for the second reaction is retained. The mathematical description of these cases is summarized in Table 6.3.1 and discussed in detail in this

section. Two different solution techniques were used; finite difference and superposition integrals.

6.3.1. Case I: Homogeneous Formation of Triiodide

Fick's second law is the starting point for the theoretical description of diffusion of the reacting species to and from the electrode. If triiodide is produced by the reaction of iodine and iodide in the solution adjacent to the electrode surface, an additional term is included in the Fick's Law expression to account for the reaction. The governing equations for the three species, iodide, iodine and triiodide are given as,

$$\frac{\partial C_I^-}{\partial t} = D \frac{\partial^2 C_I^-}{\partial x^2} - [k_f C_I^- C_{I_2} - k_b C_{I_3^-}] \quad (6.3.1)$$

$$\frac{\partial C_{I_2}}{\partial t} = D \frac{\partial^2 C_{I_2}}{\partial x^2} - [k_f C_I^- C_{I_2} - k_b C_{I_3^-}] \quad (6.3.2)$$

$$\frac{\partial C_{I_3^-}}{\partial t} = D \frac{\partial^2 C_{I_3^-}}{\partial x^2} + [k_f C_I^- C_{I_2} - k_b C_{I_3^-}] \quad (6.3.3)$$

where

k_f = rate constant for forward chemical reaction

k_b = rate constant for reverse chemical reaction

$$K = \frac{k_f}{k_b} = \frac{1}{\rho_0} \exp\left[\frac{nF}{2RT}(E_2^0 - E_1^0)\right] \quad (6.3.4)$$

We assume that all species have identical diffusion coefficients.

The simplest assumption about the electrode kinetics is that electron transfer is extremely rapid and the reactions are reversible. In this case the condition of chemical equilibrium sets the concentrations of two of the three species at the electrode surface. The boundary conditions at the surface ($x = 0$)

are given by the Nernst equations for each reaction.

$$E = E_1^\circ + \frac{RT}{nF} \ln \frac{\rho_0 C_{I_2}}{C_{I^-}^2} \quad (6.3.5)$$

$$E = E_2^\circ + \frac{RT}{nF} \ln \frac{C_{I_2}^3}{\rho_0 C_{I_3^-}^2} \quad (6.3.6)$$

In addition, by the restriction that there be no accumulation of iodide species at the surface (such as adsorption), a balance on iodine atoms fixes the concentration of iodide.

$$\frac{\partial C_{I^-}}{\partial x} + 2 \frac{\partial C_{I_2}}{\partial x} + 3 \frac{\partial C_{I_3^-}}{\partial x} = 0 \quad (6.3.7)$$

The initial conditions of iodine and triiodide are set to their equilibrium concentrations at the initial potential, E_i , and the initial concentration of iodide is C^* .

The potential is a function of time; for a single anodic sweep,

$$\text{for } 0 < t \leq \lambda \quad E = E_i + bt$$

$$\text{for } t > \lambda \quad E = E_i + 2b\lambda - bt$$

The parameters used in the model are listed in Table 6.3.2. Of this set, E_1° , E_2° , and k_f were fitted from the experimental results. The terms E_i , E_λ , b , and C^* were set by the conditions of the experiment, and the electrode area, A , and the average diffusion coefficient, D , were determined by potential step experiments (see section 6.5).

Table 6.3.2 Parameters for Model		
Symbol	Parameter	Comments
E_i	Initial Potential	Set
E_λ	Reversal Potential	Set
E_1^0	Reversible Potential of Reaction I (I^-/I_2)	Fit
E_2^0	Reversible Potential of Reaction II (I_3^-/I_2)	Fit
b	Sweep Rate	Set
i_{0ref}	Reference Exchange Current Density	Fit
C^0	Initial Concentration of Iodide	Set

Because equations 6.3.1 to 6.3.3 are nonlinear, the problem was solved numerically using a finite difference technique combined with time stepping. The kernel of the program was the "BAND" routine, a program developed by J. Newman[44] to solve coupled linear ordinary differential equations by a generalization of the Thomas Method. Nonlinear equations were solved by iterating a Taylor series expansion about a trial solution. Details of this program are available elsewhere[45].

In this case the solution to the set of differential equations is the concentration of iodide, triiodide, and iodine as a function of the working electrode potential and the distance from the electrode surface. The current is calculated from the gradient of the concentration at the surface. Figure 6.3.1 illustrates the

variation in the concentration distribution of the reacting ion (iodide, in this case) during the course of a single sweep of a cyclic voltammetry experiment for the reaction,



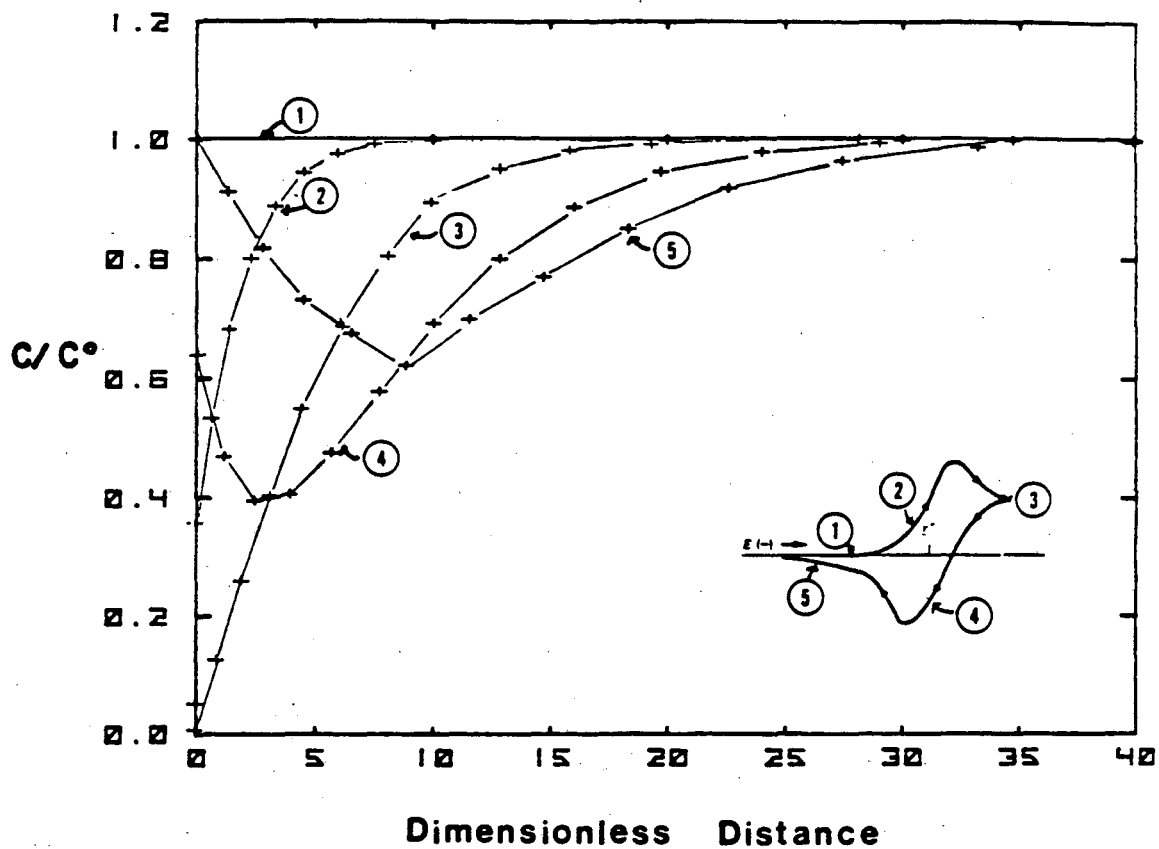
Here the reduced concentration, C/C° , is the fraction of the initial concentration of iodide and the dimensionless distance from the electrode surface is defined by,

$$y = \frac{x}{\sqrt{\frac{DRT}{nFb}}} \quad (6.3.9)$$

The position on the voltammogram corresponding to each curve is shown on the inset figure. Initially, the concentration of the iodide, C° , is uniform throughout the cell (curve 1). As the potential is swept in the anodic direction, the surface concentration of iodide drops (curve 2) until it is effectively zero. At this point the current, limited to the rate of diffusion of the reacting ion to the electrode surface, starts to drop and the boundary layer grows into the solution (curve 3). When the current changes from anodic to cathodic, iodide is produced at the electrode, the concentration rises at the surface, and a minimum appears in the profile (curve 4). Eventually the concentration at the electrode reaches the initial value and the position of the concentration minimum moves away from the electrode.

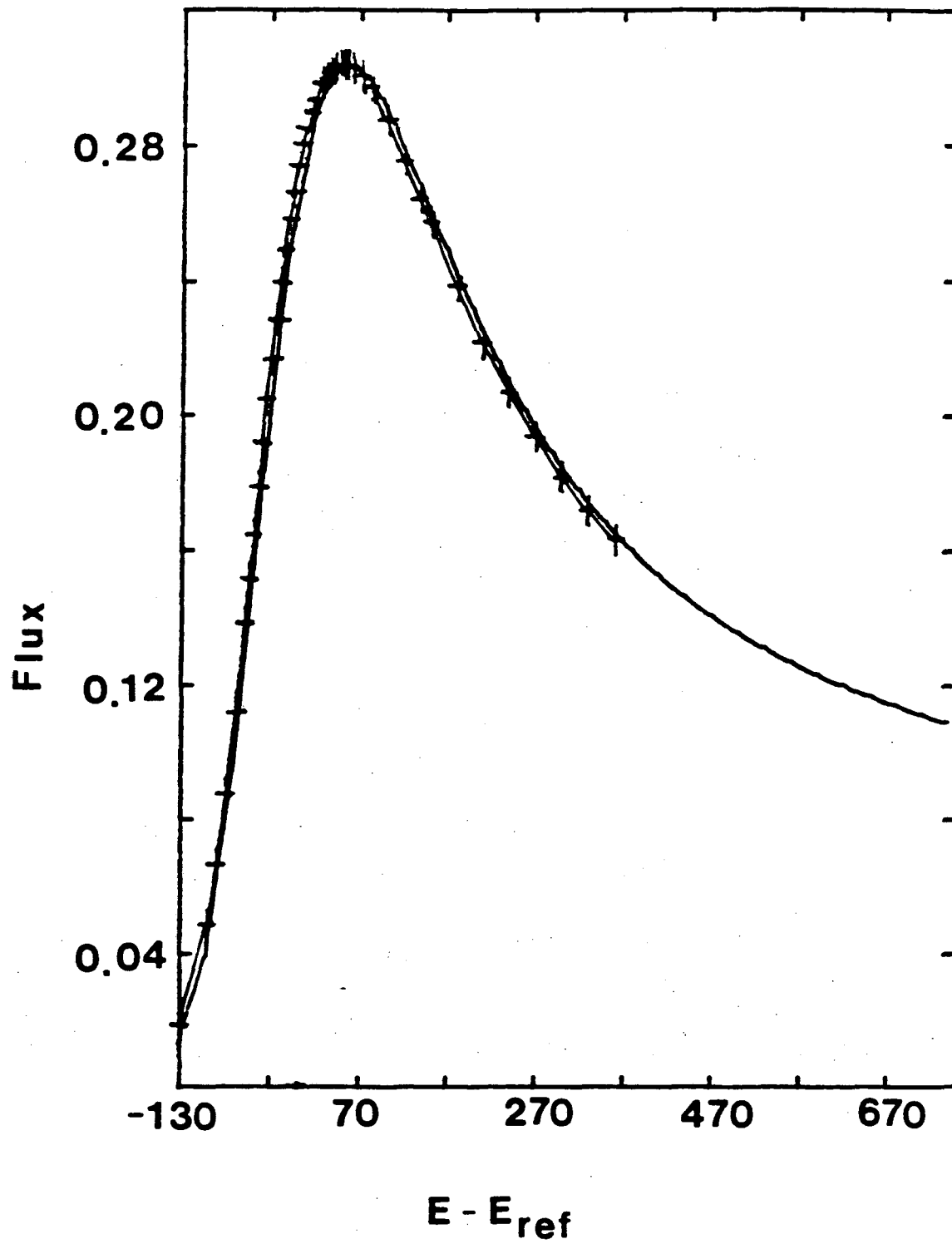
Results

To test the model, the case of 1:1 stoichiometry for a single reaction was solved first and compared to the results of Shuman (see section 6.2.2). The comparison for the anodic sweep, given in Figure 6.3.2, shows that the results are identical.



XBL 847-3078

Figure 6.3.1 Concentration profiles of reactant (A) in a single voltammetry sweep for the reaction $A \rightarrow B + e^-$. The initial concentration is uniform at C° (1). Concentration profiles are shown before (2,3) and after (4,5) the switching potential.



XBL 847-3077

Figure 6.3.2 Comparison of Case I (solid line) to the results of Shuman [42] (cross marks).

Simulations of cyclic voltammograms for two values of k_f are shown in Figure 6.3.3. The results were insensitive to the value of the rate constant for the forward reaction. When the value of k_f is infinity, the simulated voltammogram reflects the fact that iodine cannot exist in the solution phase. Because there is no reactant available for reduction when the potential sweep changes direction, the cathodic peaks are strongly attenuated. These results indicate that the effect of a homogeneous reaction is overshadowed by the restriction of chemical equilibrium at the surface. In the case of a very fast reaction, the shape of the voltammogram is determined by diffusion effects and the surface concentration of the reactants and products. Because the model incorporates reversible behavior for both electrode reactions, the position of the peaks remains unchanged for any value of k_f or sweep rate.

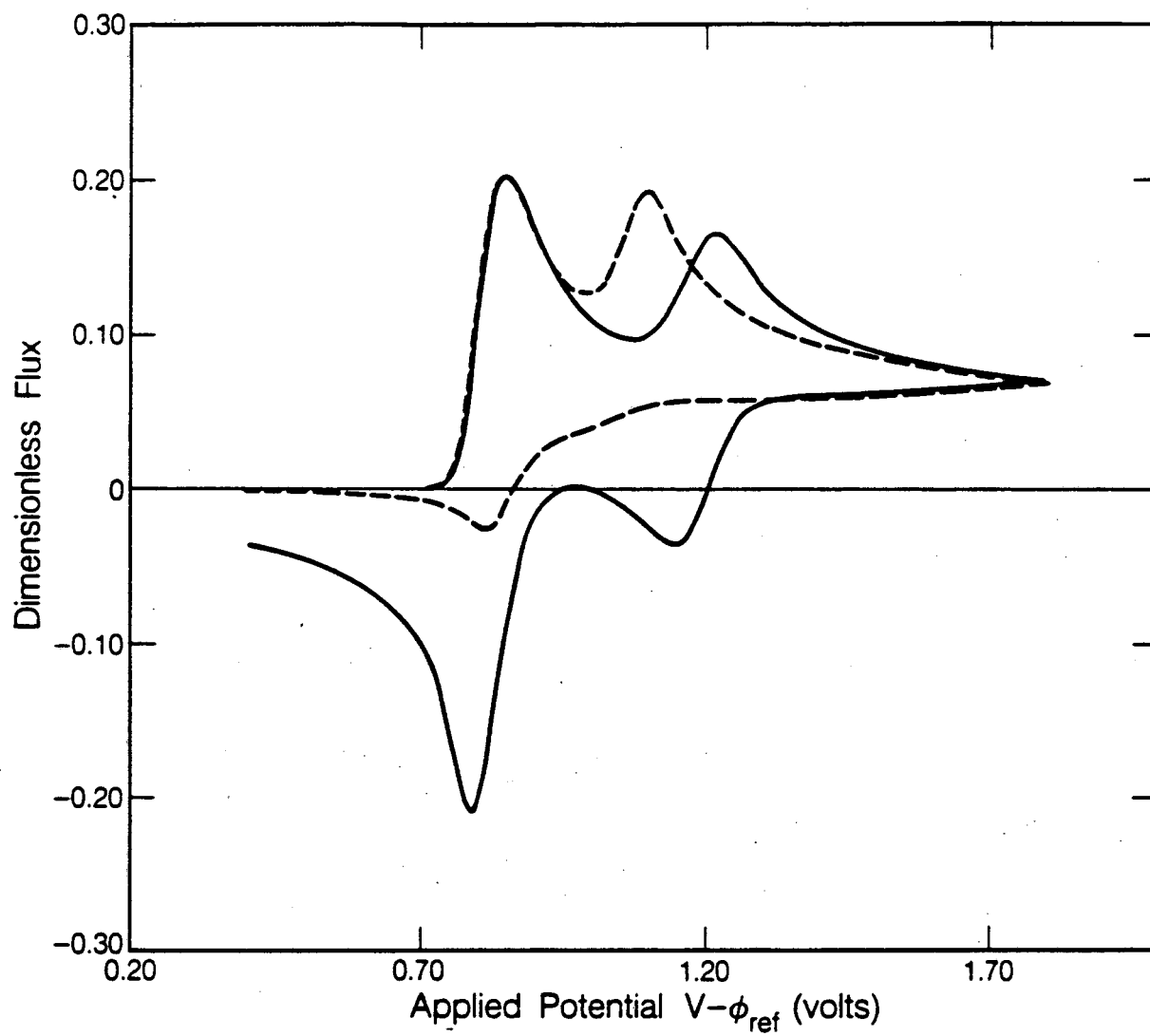
6.3.2. Case II: Heterogeneous Formation of Triiodide

An alternative explanation is that triiodide is formed on the surface of the electrode rather than in the solution. In this case, the chemical reaction can be rate limiting and independent of potential. The governing equations are now unmodified Fick's second law expressions for each species and the boundary conditions at the surface change to reflect the effect of the chemical reaction. The Nernst equation for the first reaction is replaced by a rate equation based on the surface concentrations of the three species.

$$D \frac{\partial C_I}{\partial x} = k_f C_I C_{I_2} - k_b C_{I_3} \quad (6.3.10)$$

Here k_f and k_b represent the rate of the forward and reverse reactions, respectively on the electrode surface³.

³ Note that a Nernst equation for reaction 1 is not included as a boundary condition. This would over-constrain the problem; if both reactions are at equilibrium, the intermediate chemical reaction must be also at equilibrium.



XBL 847-7735

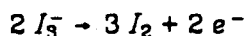
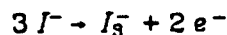
Figure 6.3.3 Simulated voltammogram for Case I. Solid line: $k_f = 0.001$ 1/mol-sec. Dotted line: $k_f = \infty$.

Since the governing equations are linear, the problem was solved using superposition integrals (Duhamel's method[46]) to determine numerically the value of the current at each time step during the potential sweep. (For further details of calculation procedure see reference [43].)

A simulation of a "window opening" experiment (see section 6.4.2) is shown in Figure 6.3.4. Voltammograms for anodic potential scans up to 1.8 V show the change in peak shape and size as a function of switching potential for a forward rate constant of $10^4 \text{ cm}^4/\text{moles} \cdot \text{sec}$. Because the first electrochemical reaction is limited only by the rate of the intermediate chemical reaction, the position of the current peak does not change with sweep rate.

6.3.3. Case III: Slow Electrochemical Formation of Triiodide

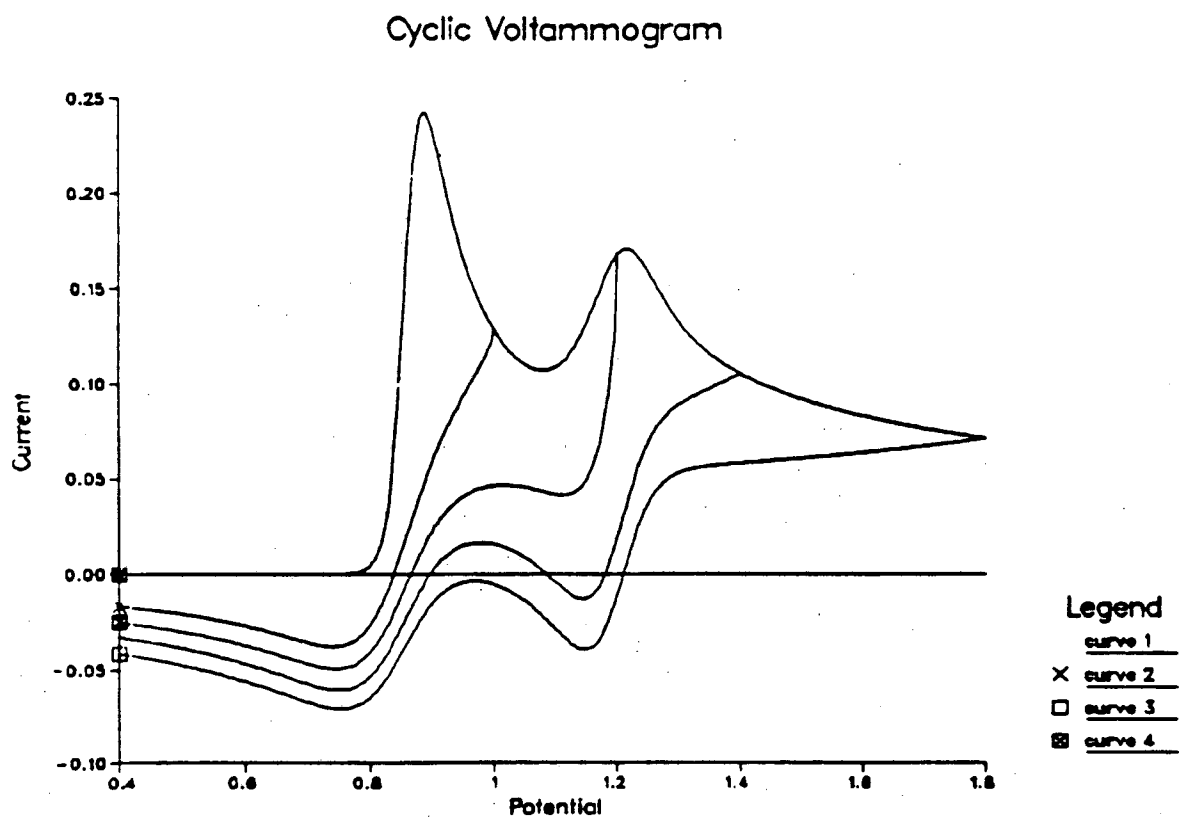
Experimental shifts of peak current for the first electrochemical reaction, either as a function of sweep rate or switching potential, indicate that the charge transfer may be a relatively slow step. When the triiodide is formed directly in a slow *electrochemical* step (no intermediate step), the governing equations do not change but the boundary condition on iodide and triiodide at the surface is replaced by a general Butler-Volmer rate equation. The reaction scheme,



is analyzed here. The surface boundary condition on iodide is given as,

$$D \frac{\partial C_{I^-}}{\partial x} = \frac{3i_{o,ref}}{nF} \left[\left(\frac{C_{I^-}^o}{C^*} \right)^3 \exp\left[\frac{(1-\beta)nFV}{RT} \right] - \left(\frac{C_{I_3^-}}{C^*} \right) \exp\left[\frac{-\beta nRV}{RT} \right] \right] \quad (6.3.11)$$

Here the symmetry factor, β , represents the fraction of the applied potential



XBL 848-3336

Figure 6.3.4 Case II. Simulation of "window opening experiment". Scans have anodic switching potentials of 1.0, 1.2, 2.4, and 1.8 V. Rate constant is 10^4 cm⁴/mol sec.

that promotes the cathodic reaction, $i_{o,ref}$ is the exchange current density at a reference concentration⁴, and V is $(E - E_{ref})$.

The effect of adding a charge transfer resistance for the first reaction reduces the peak currents and shifts the cathodic peak. Figure 6.3.5 illustrates the effect of β on the cyclic voltammogram. As the value of β decreases, the position of the anodic peak moves in the direction of the reversible case while the cathodic peak diminishes in height and shifts away from the reversible potential. The effect of $i_{o,ref}$ on the shape of the voltammogram is demonstrated in Figure 6.3.6. Smaller values of the exchange current shift the peaks away from the equilibrium potential and decrease the peak currents.

⁴ $i_{o,ref}$ is defined at $C_{1-} = C_{1s} = C^*$

Effect of β on Cyclic Voltammogram
 $i_o = 6.5 \times 10^{-5} \text{ A/cm}^2$

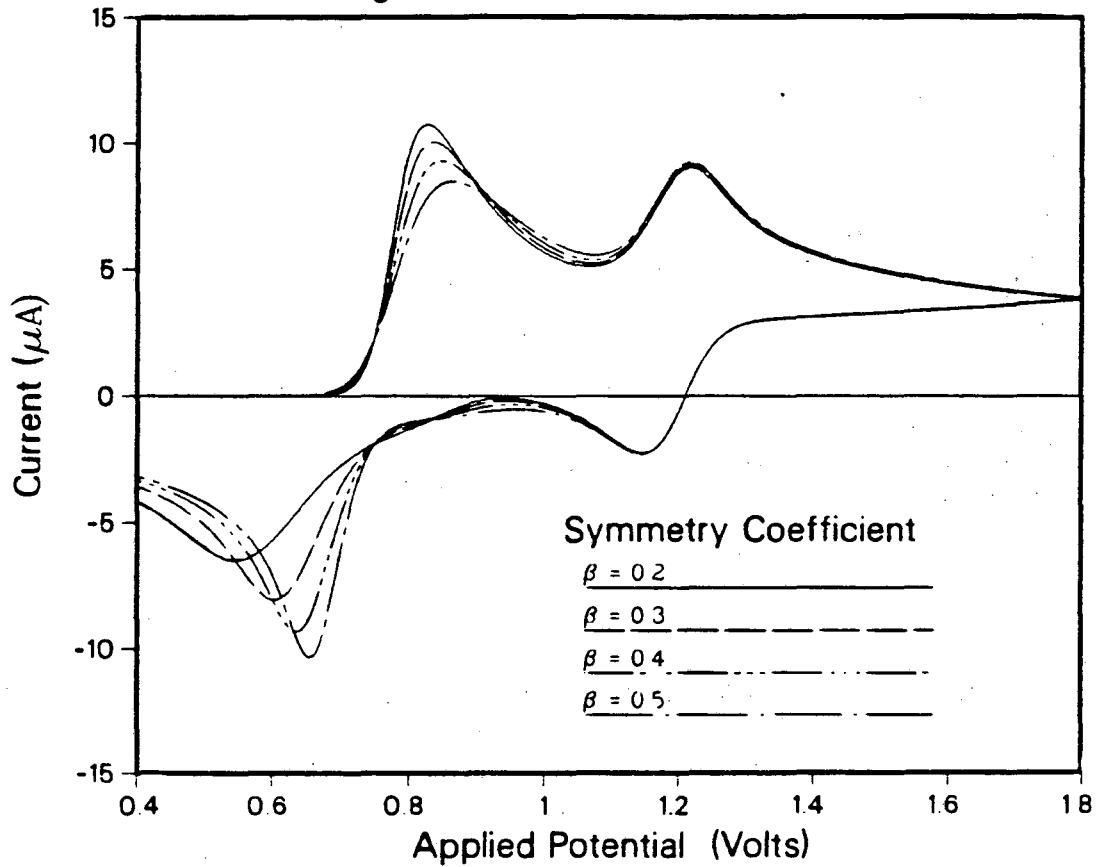


Figure 6.3.5 Case III. Sensitivity of simulation the value of β . The exchange current is constant for each curve.

Effect of i_0 on Cyclic Voltammogram
 $\beta = 0.2$

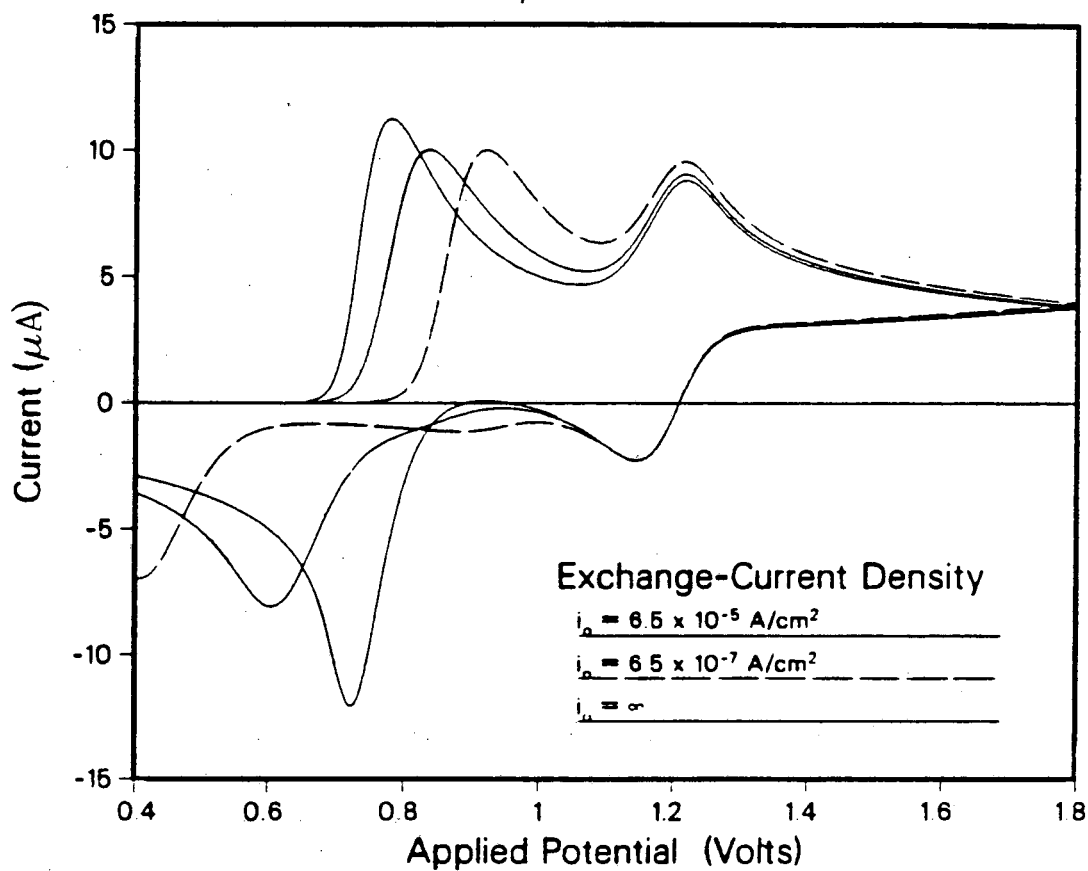


Figure 6.3.6 Case III. Sensitivity of simulation to the value of i_0 . β is constant at 0.2 for each curve.

TABLE 6.3.1		SUMMARY OF MODELS I, II AND III			
CASE NUMBER	REACTION MECHANISM	GOVERNING EQUATIONS	INITIAL CONDITIONS	BOUNDARY CONDITIONS	
				$t > 0, x = 0$	$t > 0, x = \delta$
I	$2I_1^- \rightleftharpoons I_2 + 2e^-$ (reversible) $I_2 + I_1^- \xrightleftharpoons[k_b]{k_f} I_3^-$ (slow rxn in solution) $2I_3^- \rightleftharpoons 3I_2 + 2e^-$ (reversible)	$\frac{\partial C_{I_1^-}}{\partial t} = D \frac{\partial^2 C_{I_1^-}}{\partial x^2} + R_{I_1^-}$ $\frac{\partial C_{I_2}}{\partial t} = D \frac{\partial^2 C_{I_2}}{\partial x^2} + R_{I_2}$ $\frac{\partial C_{I_3^-}}{\partial t} = D \frac{\partial^2 C_{I_3^-}}{\partial x^2} + R_{I_3^-}$	$C_{I_1^-}^0 = C^*$ $E_1 = E_1^0 + \frac{RT}{n_1 F} \ln \left[\frac{(C_{I_2})_0}{(C_{I_1^-})_0^2} \right]$ $E_2 = E_2^0 + \frac{RT}{n_2 F} \ln \left[\frac{(C_{I_2})_0^3}{(C_{I_3^-})_0^2} \right]$	$C_{I_1^-} = C^*$ $C_{I_2} = 0$ $C_{I_3^-} = 0$	$E = E_2^0 + \frac{RT}{nF} \ln \left[\frac{(C_{I_2})_0^3}{C_0 (C_{I_1^-})_0^2} \right]$ $\frac{\partial C_{I_1^-}}{\partial x} + 2 \frac{\partial C_{I_2}}{\partial x} + 3 \frac{\partial C_{I_3^-}}{\partial x} = 0$ $E = E_1^0 + \frac{RT}{nF} \ln \left[\frac{C_0 C_{I_2}}{(C_{I_1^-})} \right]$
II	$2I_1^- \rightleftharpoons I_2 + 2e^-$ $I_2 + I_1^- \xrightleftharpoons[k_b]{k_f} I_3^-$ (Rate limiting rxn on surface) $2I_3^- \rightleftharpoons 3I_2 + 2e^-$ (reversible)	$\frac{\partial C_{I_1^-}}{\partial t} = D \frac{\partial^2 C_{I_1^-}}{\partial x^2}$ $\frac{\partial C_{I_2}}{\partial t} = D \frac{\partial^2 C_{I_2}}{\partial x^2}$ $\frac{\partial C_{I_3^-}}{\partial t} = D \frac{\partial^2 C_{I_3^-}}{\partial x^2}$	Same as I	Same as I	$D \frac{\partial C_{I_1^-}}{\partial x} = (k_f)(I_1^-)C_{I_2} - k_b C_{I_3^-}$ $E = E_2^0 + \frac{RT}{nF} \ln \left[\frac{(C_{I_2})_0^3}{C_0 (C_{I_1^-})_0^2} \right]$ $\frac{\partial C_{I_1^-}}{\partial x} + 2 \frac{\partial C_{I_2}}{\partial x} + 3 \frac{\partial C_{I_3^-}}{\partial x} = 0$
III	$3I_1^- \rightleftharpoons I_3 + 2e^-$ (slow) $2I_3^- \rightleftharpoons 3I_2 + 2e^-$ (reversible)	Same as II	$C_{I_1^-}^0 = C^*$ $E_1 = E_1^0 + \frac{RT}{n_1 F} \ln \left[\frac{(C_{I_3})_0}{(C_{I_1^-})_0^3} \right]$ $E_2 = E_2^0 + \frac{RT}{n_2 F} \ln \left[\frac{(C_{I_2})_0^3}{(C_{I_3^-})_0^2} \right]$	Same as I	$\frac{n_1 F D}{3} \frac{\partial C_{I_1^-}}{\partial x} = I_0 \left(\frac{C_{I_1^-}}{C^*} \right)^3 \exp \left[\frac{(1-B)n_1 F E}{RT} \right]$ $-\left(\frac{C_{I_3^-}}{C^*} \right) \exp \left[\frac{-B n_1 F E}{RT} \right]$ $\frac{\partial C_{I_1^-}}{\partial x} + 2 \frac{\partial C_{I_2}}{\partial x} + 3 \frac{\partial C_{I_3^-}}{\partial x} = 0$ $E = E_2^0 + \frac{RT}{nF} \ln \left[\frac{(C_{I_2})_0^3}{C_0 (C_{I_1^-})_0^2} \right]$

NOTES: (1) $K = \frac{C_{I_3^-}}{C_{I_1^-} C_{I_2}} = \frac{k_f}{k_b} = \frac{k_f'}{k_b}$

(2) $R_{I_3^-} = k_f' [C_{I_1^-}] [C_{I_2}] - k_b [C_{I_3^-}]$
 $R_{I_2} = R_{I_1^-} = -R_{I_3^-}$

(3) $C_0 \equiv$ solvent density (mol/cc)
 $C_1 \equiv$ concentration (mol/cc)

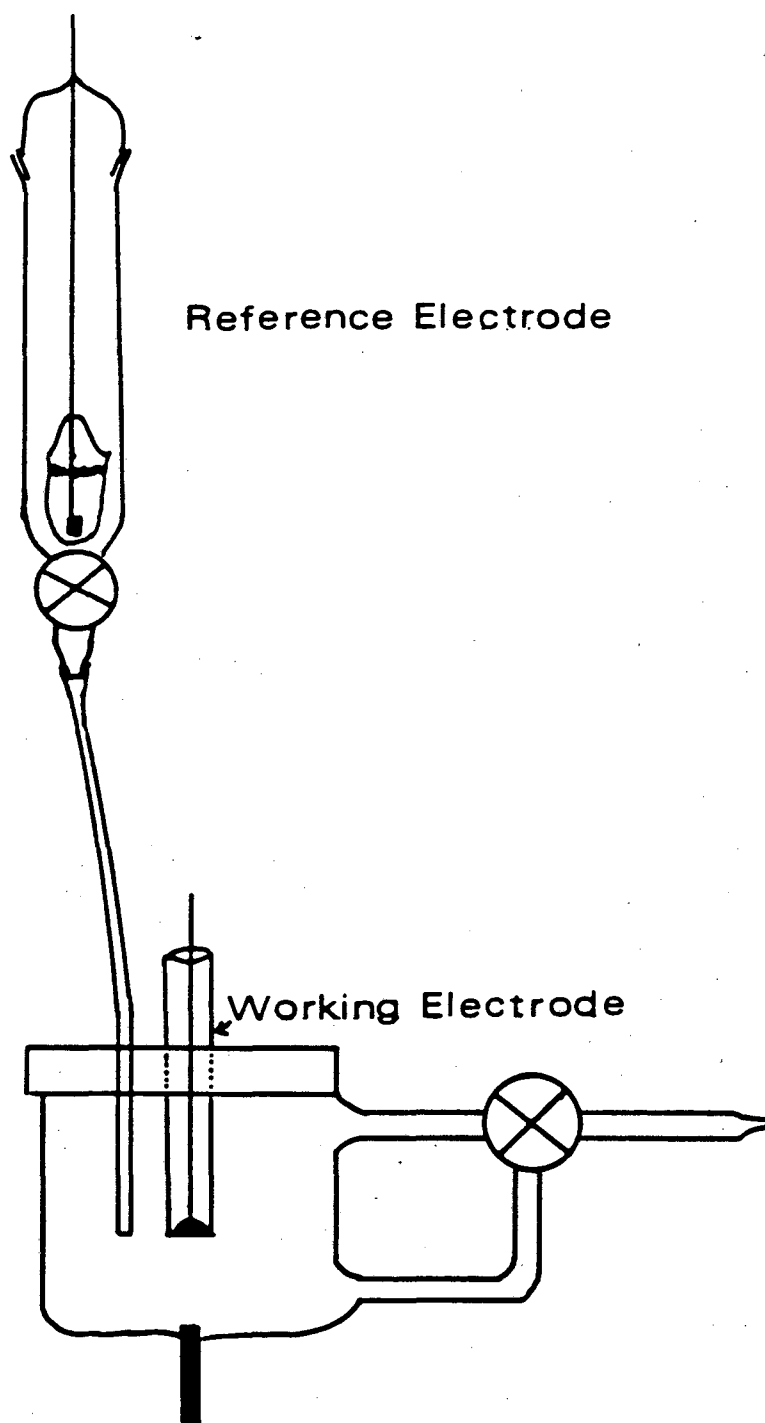
6.4. CYCLIC VOLTAMMETRY EXPERIMENTS

Two different types of cyclic voltammetry experiments were performed to characterize the electrochemical oxidation of the halides in PC. The majority of the work was done using conventional voltammetry experiments. However to independently confirm the chemical reactions postulated from the results of these experiments, spectral electrochemical measurements done simultaneously with cyclic voltammetry experiments were performed to confirm the identity of the species produced at the electrode.

6.4.1. Experimental Methods

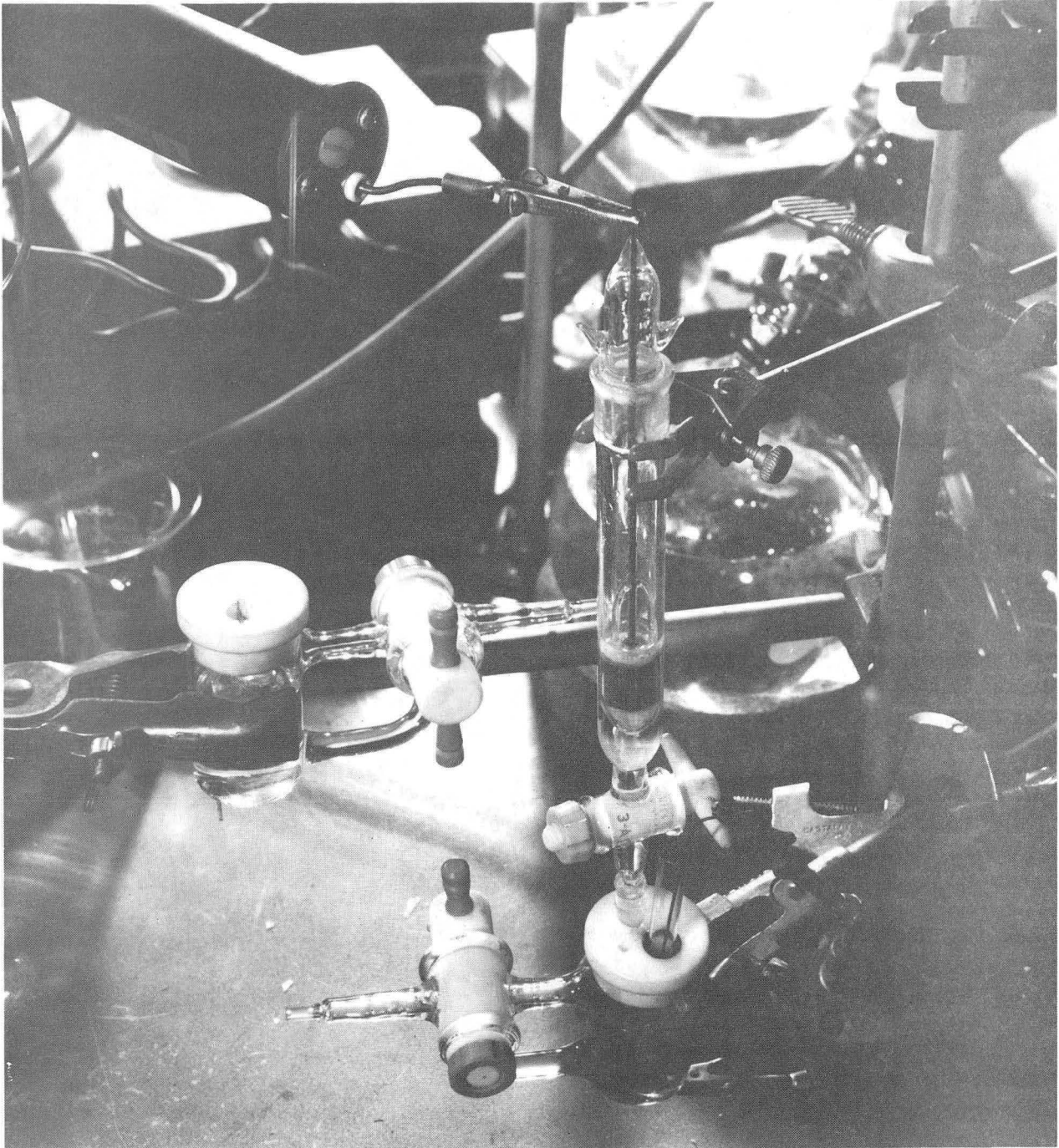
Electrochemical Cell

The design of the electrochemical cells used for the voltammetry experiments was based on a design developed by C. Balfe [47], employing a single compartment glass with a platinum counter electrode embedded in the bottom of the cell. A schematic drawing of the cell is given in Figure 6.4.1, and pictured in Figure 6.4.2. The cell was arranged so that the working electrode was oriented facing downward across from the counter electrode. Five cells were made using the same specifications so that background current measurements or experiments with different solutions could be performed at the same time. Although most of the experiments were done with these cells, early work employed a two-compartment cell pictured in Figure 6.4.3. A platinum foil electrode served as a working electrode, and the counter electrode was a platinum screen. However, the same reference electrode was used. Because the area of the working electrode was about 2 cm², much larger currents (mA range) were obtained in this cell. All experiments were performed in the glovebox under a helium atmosphere.



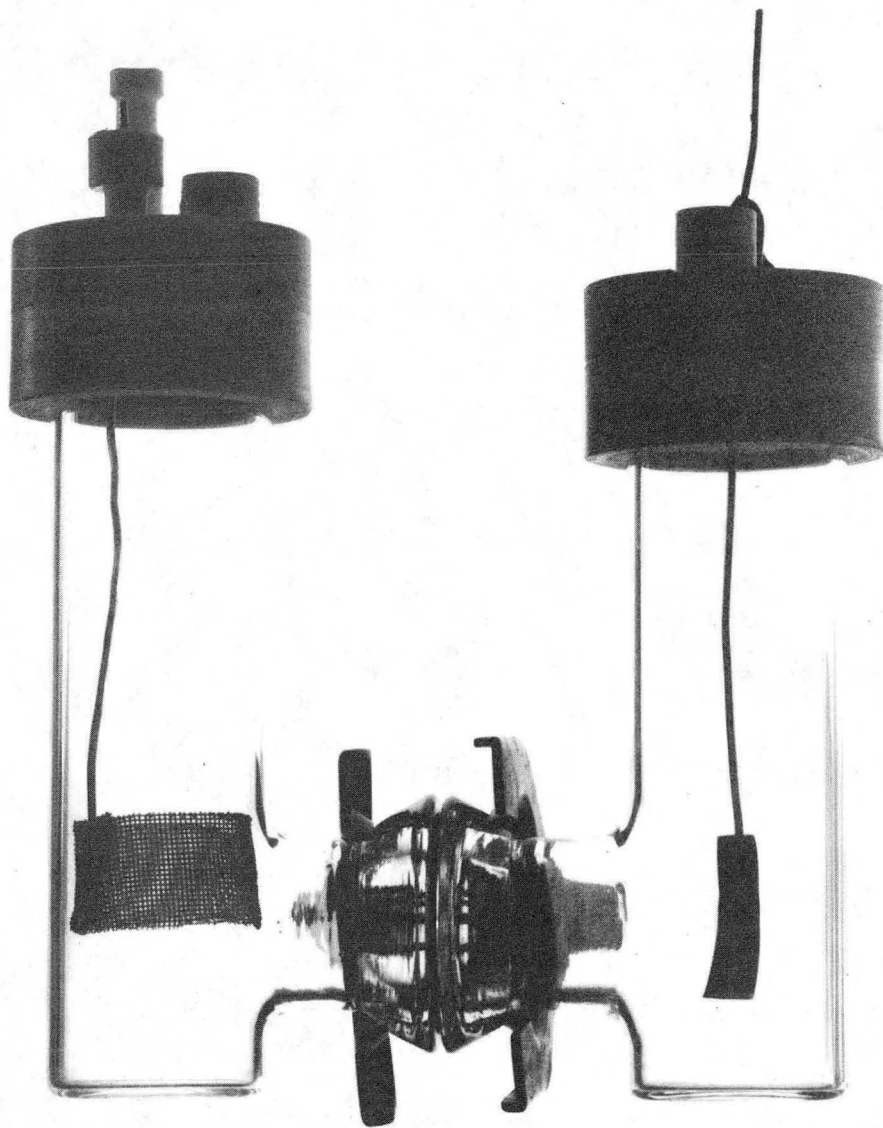
XBL 847-3079

Figure 6.4.1 Schematic drawing of voltammetry cell. A platinum wire is imbedded at the bottom of the cell to serve as a counter electrode.



CBB 830-9685

Figure 6.4.2 Cells and reference electrode in the glovebox.



CBB 830-9687

Figure 6.4.3 Side view of the two-compartment cell.

Before each experiment, the cells were cleaned using the following routine;

- i) soak in alcoholic KOH
- ii) rinse and soak in distilled water
- iii) dry under vacuum at 150 ° C

Reference Electrode

Conventional reference electrodes such as silver/silver halide, calomel, or mercurous halides could not be used in PC solutions because these salts disproportionate to form soluble complexes in PC.[48] For this reason, a thallium amalgam/thallium halide reference was used for all the cyclic voltammetry experiments. The design and construction of this electrode is similar to that described by Baucke and Tobias[49]. The electrodes were constructed by filling glass cups with approximately 2 ml of a saturated thallium amalgam. This exposed about 1 cm² of metal surface area. Thallium wire (Alfa-Ventron, 1/8" wire, 99.999% pure) and triple distilled mercury (Ballards, Quicksilver products, SF) were used to prepare the amalgam inside the glovebox. It was prepared by first "washing" the thallium with dry PC until the surface was shiny and free of surface oxides, and then dissolving the clean wire in a pool of mercury. Using weight measurements, an amalgam containing 16 weight percent thallium was produced. The amalgam was filtered through a pinhole in dry glass fiber filter paper before use.

Thallium iodide and thallium bromide were used as received (ultrapure, Alfa Products) after drying at 150 - 200 ° C under a 1 μ vacuum. After the dry salt was ground to a fine powder inside the glovebox, a small amount was transferred to the surface of the amalgam. When the electrode was tapped, the surface became completely covered with a thin adherent layer of the salt. These electrodes were then immersed in PC solutions containing the supporting electrolyte (usually 0.5 M KAsF₆) and allowed to "age" for several hours to permit the solution to become saturated with the salt. A cup electrode and a reference electrode

chamber are shown in Figure 6.4.4. Electrodes prepared in this way gave reproducible voltages when measured against each other (bias potentials of less than 0.5 mV). The open circuit potential versus a freshly scraped potassium electrode was found to be 2.14V. This potential was stable for several hours.

The reference electrode compartment was connected to the cell by a short length of Teflon tubing (Kontes Glassware). The tip of the tubing was located at the edge of the electrode by Teflon rings. The assembled reference electrode, working electrode and cell is shown in Figure 6.4.5.

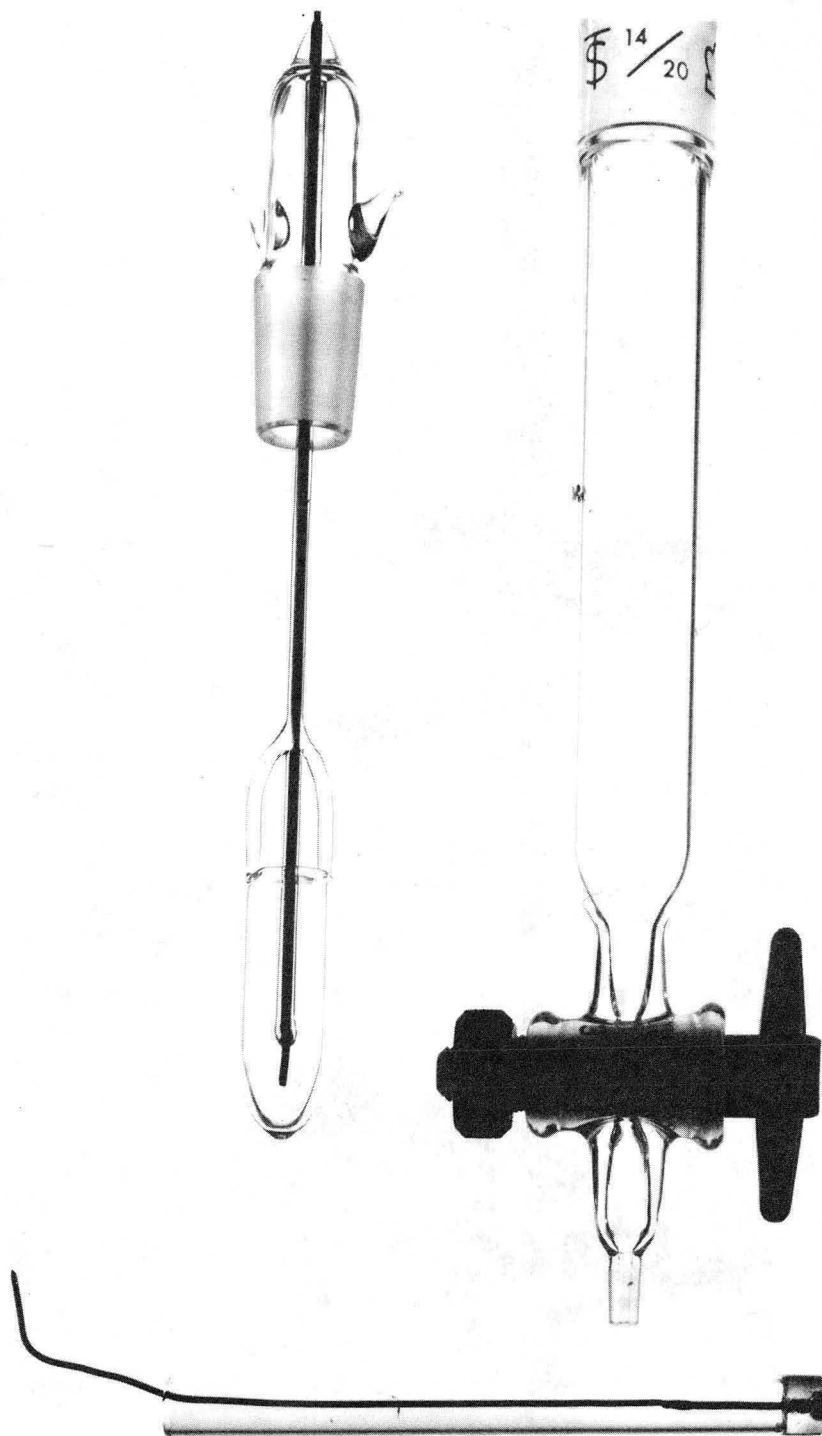
Working Electrode

The working electrode was a planar platinum disc embedded in glass. It was constructed by melting the tip of a platinum wire to form a bead, encasing the bead in uranium glass to form a seal, and cutting the assembly with a diamond wheel to expose a circular cross-section of the platinum. This procedure was suggested by Majda[50].

Electrolyte Preparation

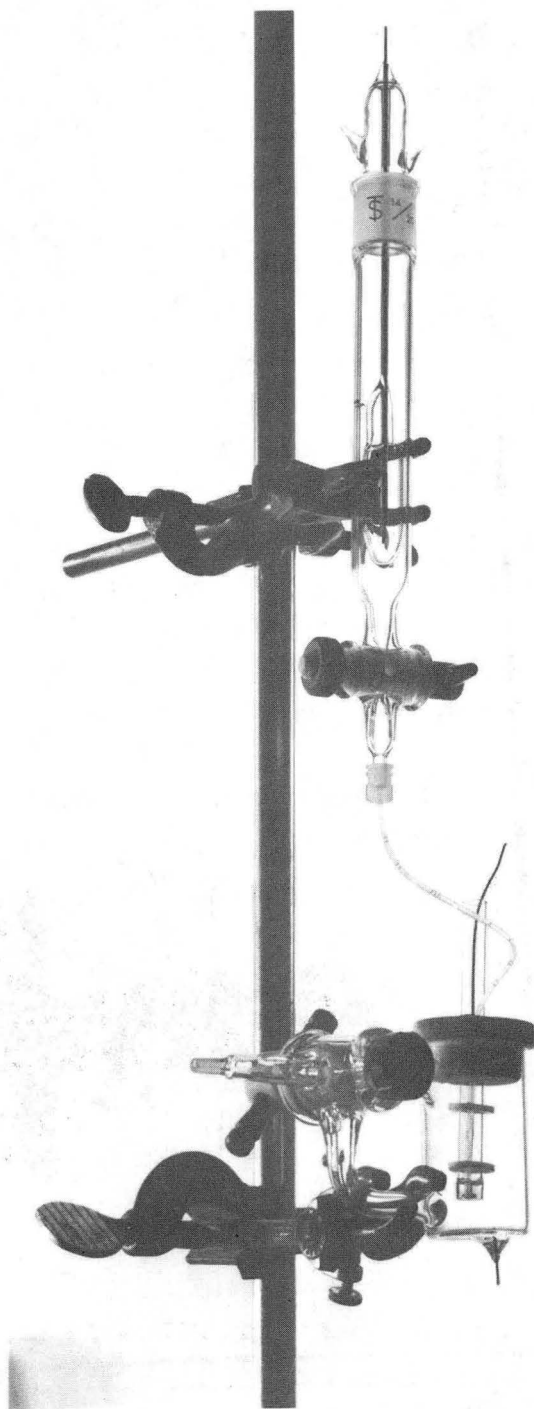
All solutions were made in the glovebox using propylene carbonate purified as described in section 2.2. The salts, KI and KBr (Mallinckrodt Chemicals,) and KAsF_6 (Alfa-Ventron) were analytical reagent grade. The KI was recrystallized from distilled water and all salts were dried under vacuum (approximately 1 $\mu\text{m Hg}$) at high temperature for several days. Solutions were prepared by weight and the concentration was checked by titration with silver nitrate⁵. To avoid heating the PC, concentrated solutions were prepared by first chilling the PC to near 0°C and adding the salt slowly to the solvent while stirring continuously. Solutions prepared in this way were clear and colorless after filtration.

⁵ Titrations were performed by the Microanalytical Laboratory, College of Chemistry, UCB.



CBB 830-9689

Figure 6.4.4 Thallium iodide/thallium amalgam reference electrode and platinum working electrode.



CBB 830-9691

Figure 6.4.5 Fully assembled cell and reference electrode.

KAsF_6 was used as a supporting electrolyte for all voltammetry experiments. The conductivity of this solution is $5 \times 10^{-3}(\text{ohm-cm})^{-1}$ measured as described in section 5.3.

Instrumentation

Electrode potentials were controlled by a potentiostat (Princeton Applied Research, Model 173 Potentiostat and Model 176 Current Follower) driven by a function generator (Princeton Applied Research Model 175). The data were collected with a fast ($1 \mu\text{-sec/point}$) digital oscilloscope (Nicolet Model 4094) for fast sweeps or an XY recorder (HP Model 7046B with a time base) for slow sweeps. The oscilloscope was interfaced to a small desktop computer (HP 9825A) which was connected to peripheral equipment (HP 9885M disc drive, HP 9862A plotter) used to store and plot the data. In this way voltage scans taken at sweep rates up to 20 V/sec were measured. The data acquisition equipment is pictured in Figure 6.4.6.

Software to transfer data from the oscilloscope, store it on floppy disc and plot the data were written for cyclic voltammetry and potential step experiments. These programs are described and listed in Appendix A-2.

6.4.2. Results

Background Voltammetry Scans

The total current at the working electrode can include contributions from undesired sources such as electroactive impurities in the solution or capacitive effects of the double layer. To distinguish the current of the reacting ion from these interferences, cyclic voltammetry scans were carried out with solution containing only the supporting electrolyte salt, KAsF_6 . The scans were taken over the entire voltage range used for the experiments.

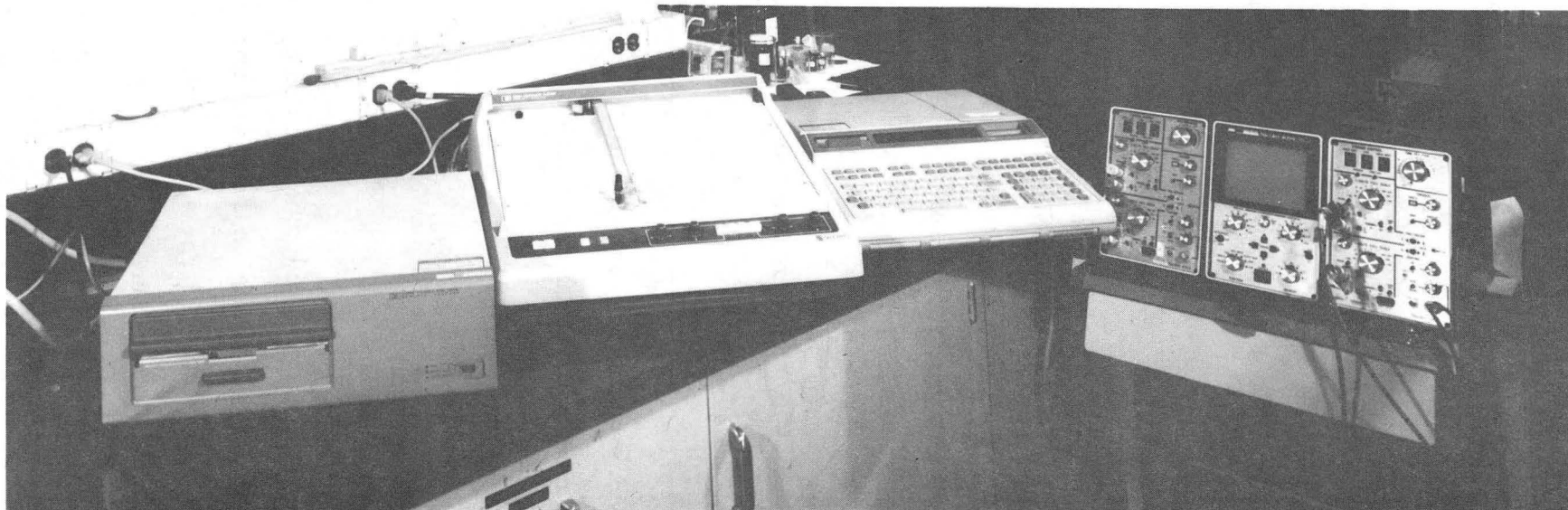


Figure 6.4.6 Voltammetry data acquisition instrumentation. From left to right: disc drive, plotter, computer, oscilloscope.

CBB 830-9679

Background voltammograms for scan rates from 100 mV/sec to 20 V/sec are shown in Figures 6.4.7 and 6.4.8. These scans are largely featureless across the full voltage range and the currents are always at least an order of magnitude lower than those obtained with the electrolytes containing halides.

The fact that the background scans are flat across the full voltage range indicates that the major contribution to the current is double layer charging. The shape of the i - E curves for these background scans can be understood in terms of a simplified model of the solution-electrolyte interface. (See, for example, Bard[51].) A cell consisting of an ideally polarizable electrode and a reversible reference electrode is approximated by an electrical circuit consisting of a resistor and a capacitor, such as the one shown in Figure 6.4.9a. The terms, R_s and C_d , represent the solution resistance and the double layer capacitance at the ideally polarizable working electrode. The response of this simple circuit to a linearly ramped (triangular wave) applied potential at a sweep rate b , is shown in Figure 6.4.9b. This current is given for the forward scan (time from E_i to E_λ) as,

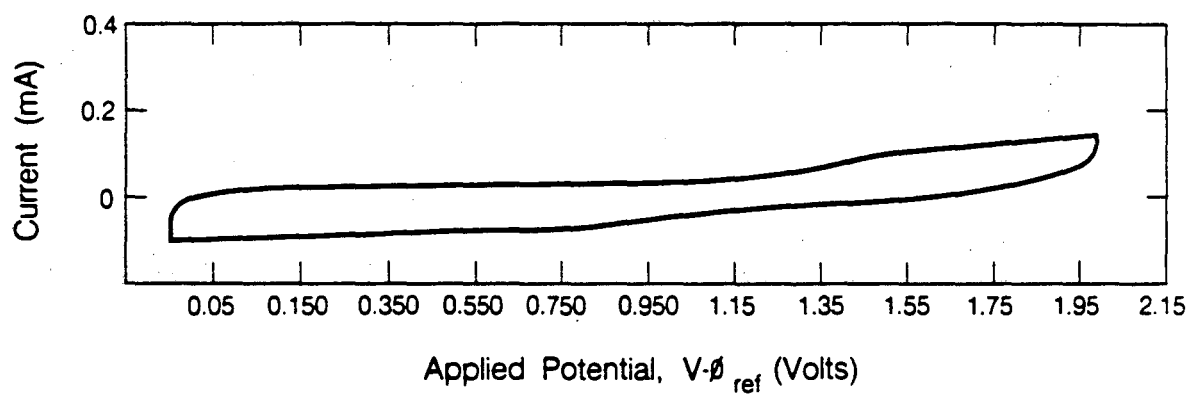
$$i = b C_d + \left[\left(\frac{E_i}{R_s} - b C_d \right) \exp \frac{-t}{R_s C_d} \right] \quad (6.4.1)$$

where the first term is the steady state solution and the second term describes the initial transient. At long times the solution reduces to,

$$i_{ss} = b C_d \quad (6.4.2)$$

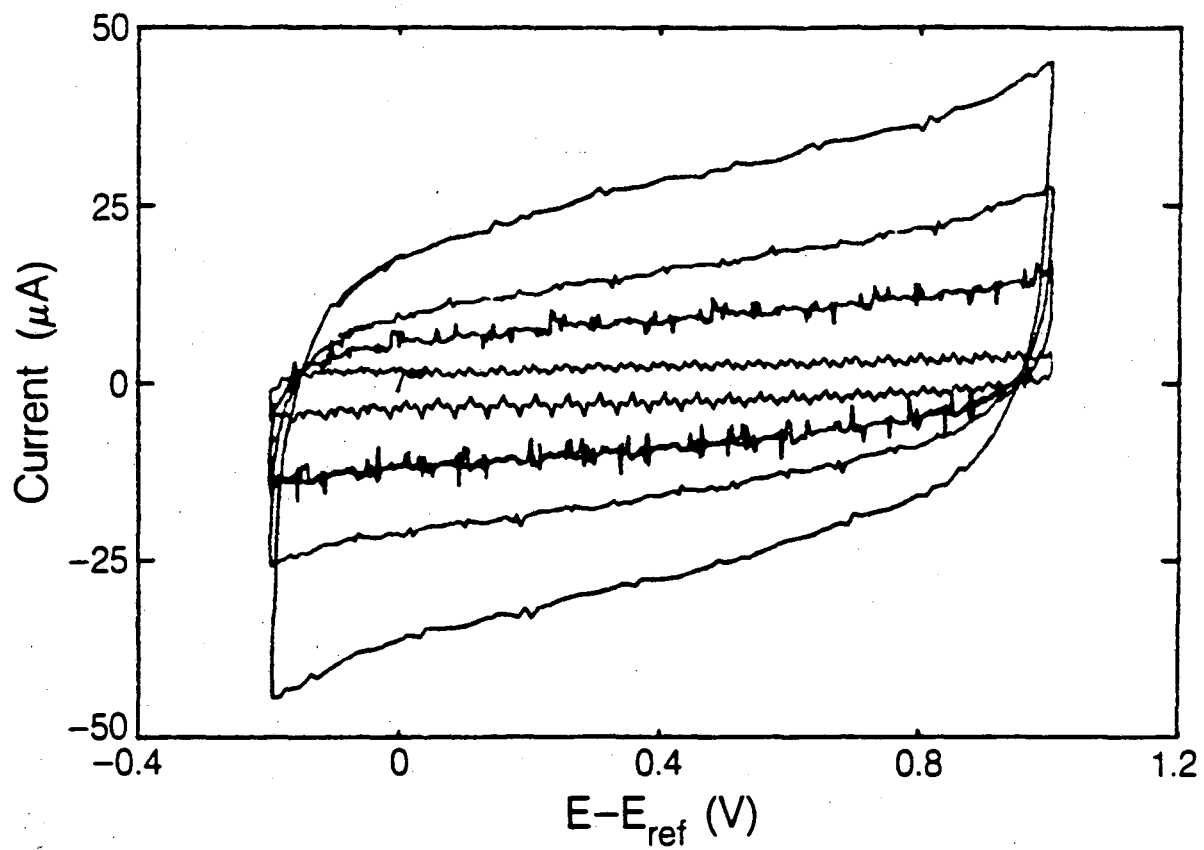
Thus, the slope from a plot of i_{ss} vs. b gives an approximate value for the electrode capacitance.

A plot of the average steady state current as a function of the sweep rate for the background scans shown above is given in Figure 6.4.10. From the slope of the line, the value of the electrode capacitance was found to be $26 \mu\text{F}/\text{cm}^2$. This is approximately the same value of the differential capacitance of a 0.5 M NaF



XBL 849-10811

Figure 6.4.7 Background scan for 0.5 M KAsF_6 solution. Sweep rate: 100 mV/sec.



XBL 847-7738

Figure 6.4.8 Background sweep at high sweep rates. Curves for 20, 10, 5, and 1 V/sec. Electrolyte: 0.5 M KAsF_6 .

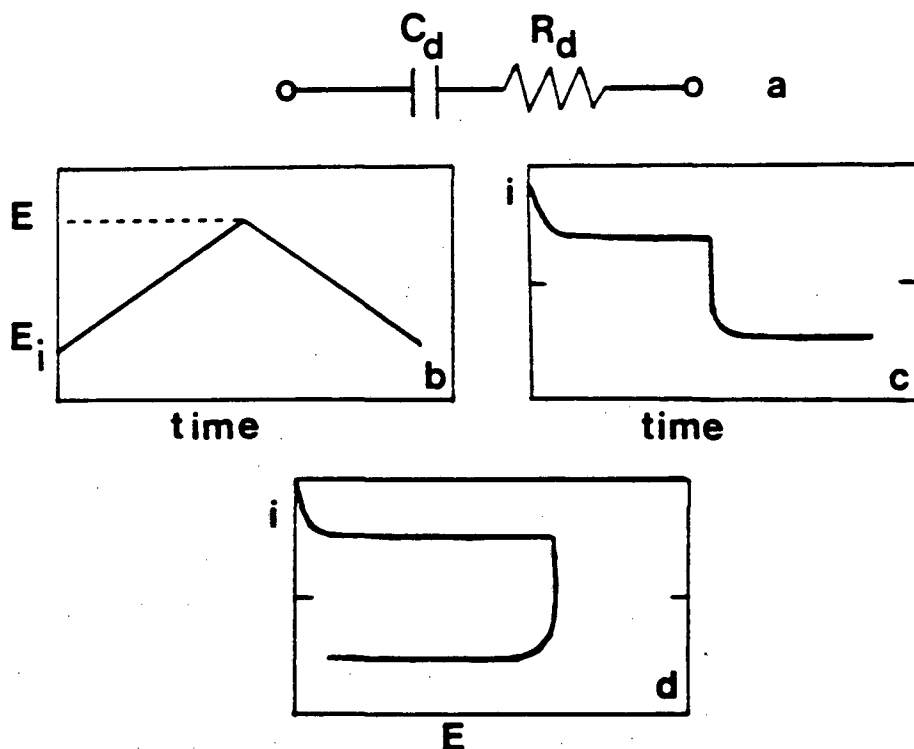


Figure 6.4.9 Simplified model of the solution-electrolyte interface. The response of the circuit (a) to an applied potential (b) is shown in (c) and (d).

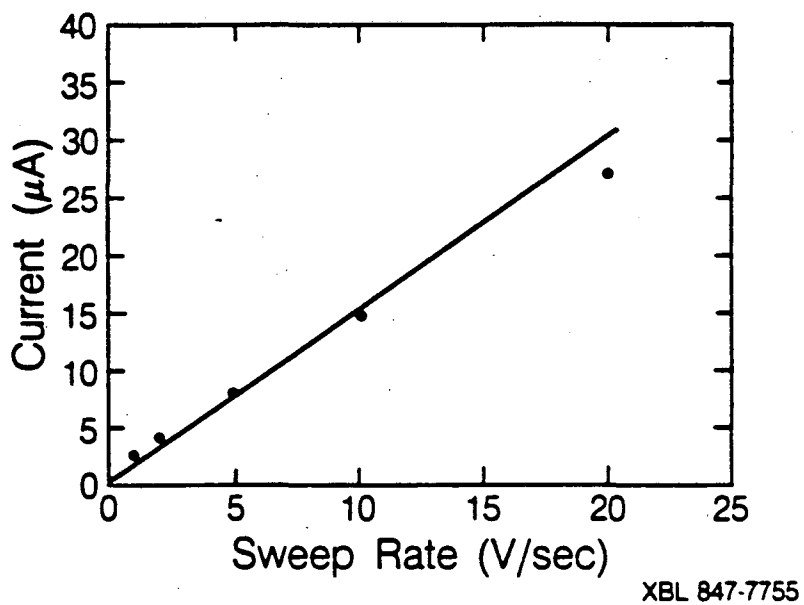


Figure 6.4.10 Dependence of average steady current in background scans of the potential sweep rate.

(aqueous)/mercury interface.[52]

Once a value for C_d is known, the time necessary to charge the double layer for a potential step can be estimated. For the circuit given above, the behavior of the current resulting from a potential step of magnitude, E , is

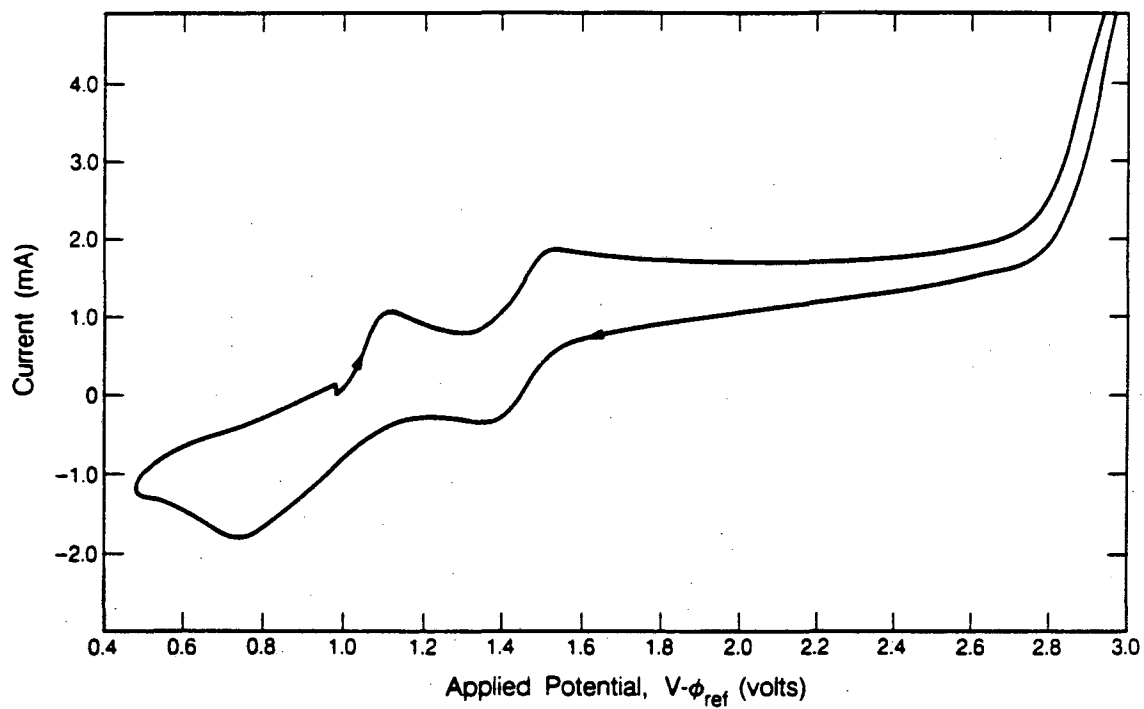
$$i = \frac{E}{R_s} \exp \frac{-t}{\tau} \quad (6.4.3)$$

where $\tau = R_s C_d$. Thus the current for charging the double layer drops to 37% of its initial value at $t = \tau$, and to 5% of the starting value at $t = 3\tau$. For a solution resistance of 1 ohm, and an electrode capacitance of $26 \mu\text{F}/\text{cm}^2$, the double layer is 95% charged in $26 \mu\text{sec}$.

Decomposition Potential of KAsF_6 Solutions

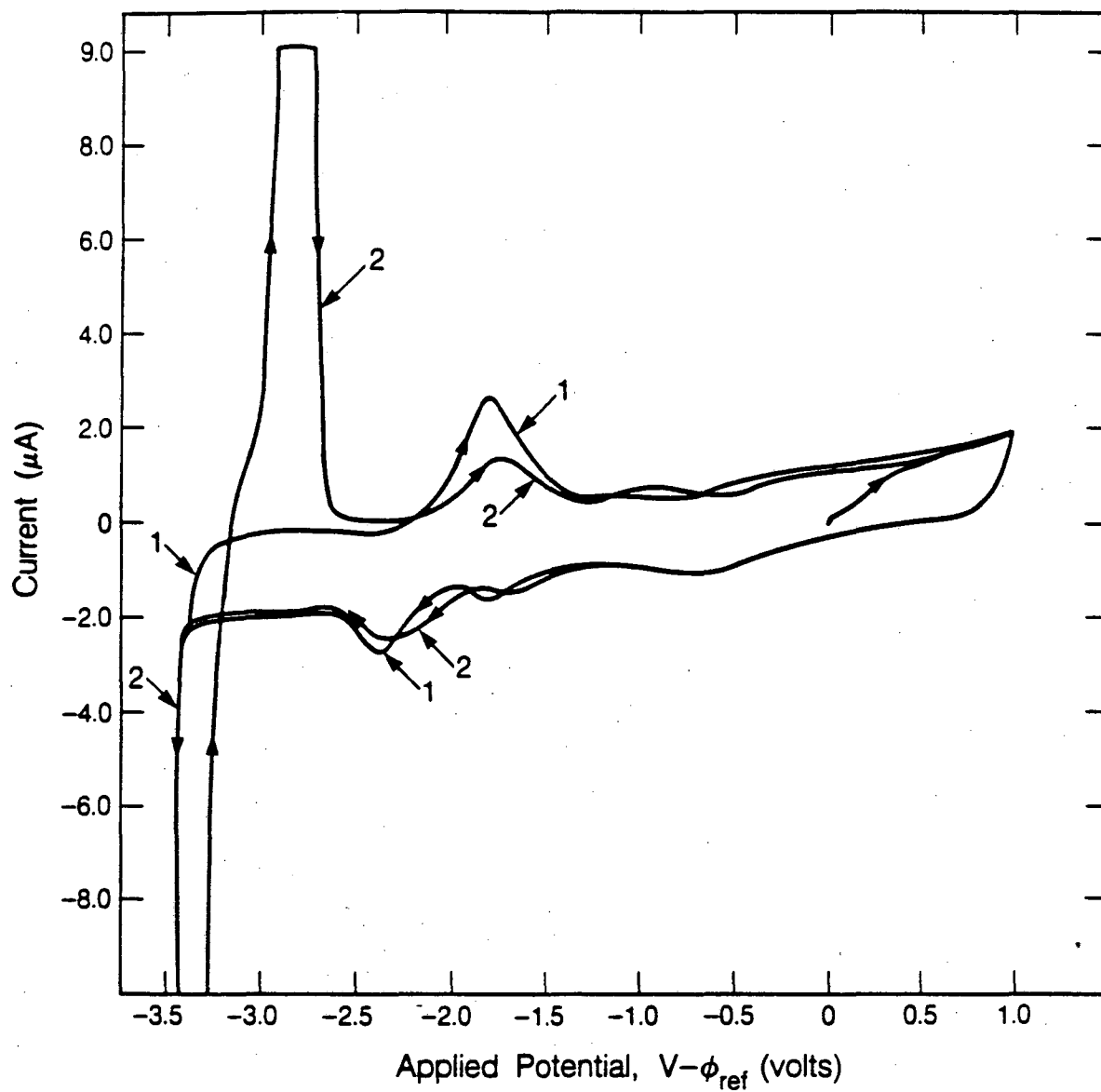
The anodic decomposition potential for a 0.5 M solution of KAsF_6 in PC was determined by cycling sequentially to progressively more anodic potentials. The anodic breakdown of 0.5 M KAsF_6 solution (2×10^{-3} M KI) can be seen in Figure 6.4.11. The large anodic wave at 2.9 V is probably due to oxidation of the solvent. The fact that there is no accompanying cathodic wave for this reaction indicates that electroactive products are not formed.

Potassium deposition is the limiting reaction for a cathodic sweep in the same solution. The thermodynamic potential for potassium deposition versus a thallium/thallium iodide reference electrode is -2.16 V. Experiments using a potassium working electrode and a thallium/thallium iodide reference electrode gave an open circuit potential of -2.18 V (± 10 mV). However, the potential for deposition of bulk potassium is a function of the amount of impurities in the solution. Figure 6.4.12 shows the voltammetry wave for the reduction and oxidation of potassium in a relatively wet (~ 40 ppm water) solution. In this case the wave corresponding to bulk potassium deposition is shifted to -3.45 V, reflecting the difficulty of plating potassium onto a hydroxide covered surface.



XBL 847-7205

Figure 6.4.11 Anodic decomposition of KAsF_6 solution in PC. Concentration is 0.5 M.



XBL 847-7204

Figure 6.4.12 Cyclic voltammogram showing potassium deposition and dissolution. Solution: 0.5 M KAsF_6 .

The accompanying anodic wave overlaps the cathodic trace which probably indicates that a surface film is formed on the deposited potassium which slightly increases the overpotential for potassium dissolution.

Window Opening Experiments

The oxidation of iodide in propylene carbonate is illustrated in Figure 6.4.13. A sequence of voltammetry scans, taken by cycling each scan to progressively more anodic potentials, traces out the important features of the iodide electrochemistry in PC. The most interesting observation from these results is that two electrochemical reactions occur. Anodic and cathodic peaks are present for both reactions. The peaks are denoted I and II, as shown on the figure, and the primes indicate the cathodic peak. The anodic peaks are separated by 440 mV, and are independent of the switching potential, but the cathodic peak separation depends upon the history of the potential scan.

Sweep Rate Behavior

Additional information can be obtained from the change in peak potential and current as the sweep rate increases. If the electrode reaction proceeds at a rate faster than the transport of the reactant to the electrode surface, the peak potential is determined only by the thermodynamic potential and is independent of sweep rate. Kinetic limitations are indicated if the peak potential shifts with increasing sweep rate. For reversible reactions, the peak current is a linear function of the square root of the sweep rate. In addition, the width of the peak is fixed for reversible reactions. The behavior of the cyclic voltammogram as a function of sweep rate was investigated for scan rates up to 1 V/sec across the full potential range. The first peak was examined in detail at sweep rates up to 20 V/sec.

CYCLIC VOLTAMMETRY
OF KI IN

PROPYLENE CARBONATE

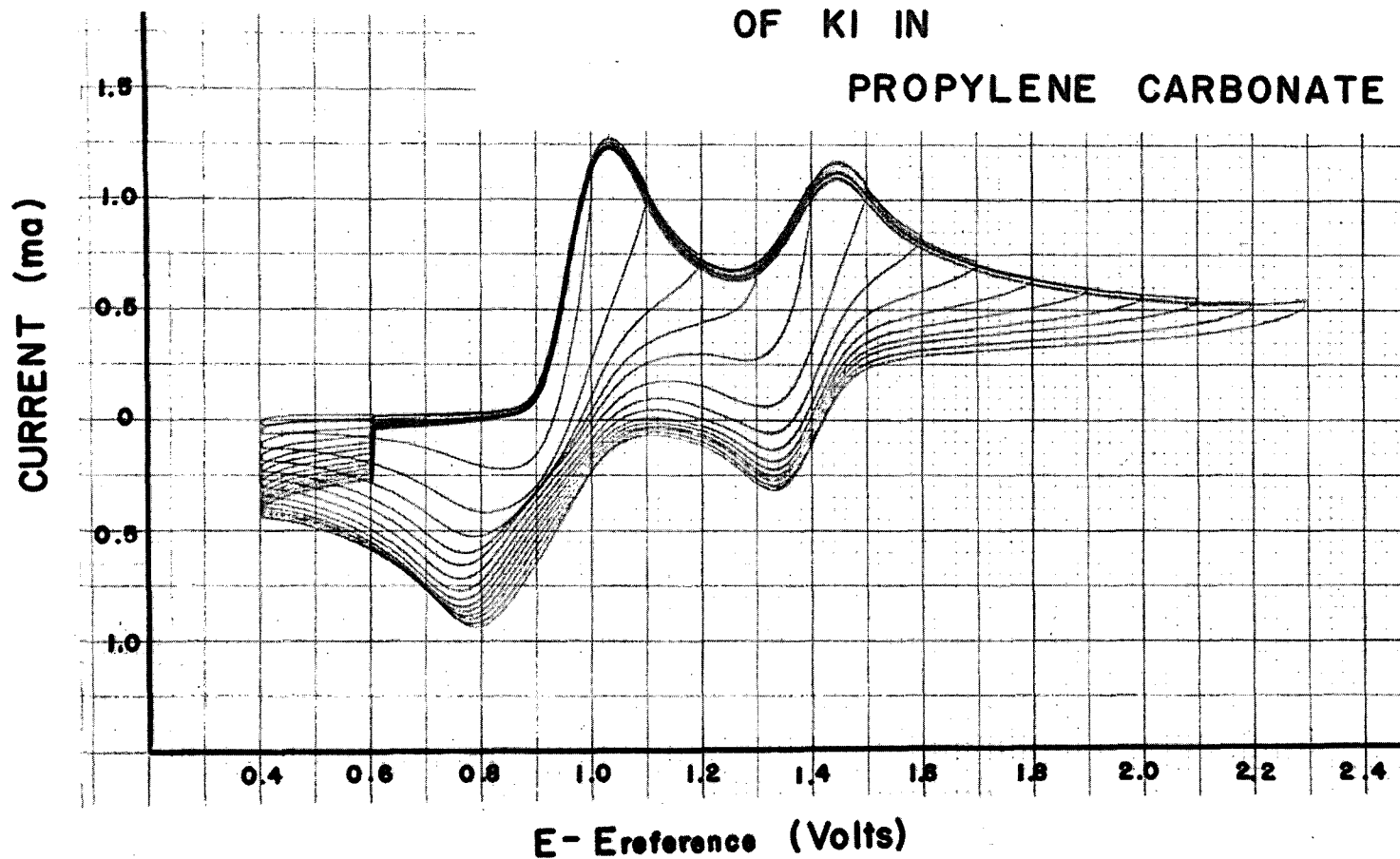


Figure 6.4.13 Window opening experiment for KI (0.004 M) in supported (0.5 M KAsF_6) PC solution. Initial scan is [0.6 V/1.0 V/0.4 V/0.6 V]. The anodic switching potential of each succeeding scan is 100 mV more anodic. Data are taken with the two-compartment cell.

CBB 830-9576

Figures 6.4.14 and 6.4.15 illustrate the effect of sweep rate on the shape of the cyclic voltammogram. Sweep rates from 10 to 1000 mV/sec are shown. These data were taken with the two compartment cell, and the solution concentration was 4.0×10^{-3} M KI and 0.5 M KAsF_6 in PC. Brief observation reveals that the position of the first peak (peak I) is shifted slightly, and peak I' is significantly offset as the sweep rate is increased. In contrast, the position of the peaks for the second electrochemical reaction are relatively independent of sweep rate in this range. The peak shift is plotted as a function of sweep rate in Figure 6.4.16 for all four peaks. These figures confirm the observation: peak I' shifts by 130 mV between sweep rates of 10 to 500 mV/sec whereas the shift for peaks II and II' is only 30 mV.

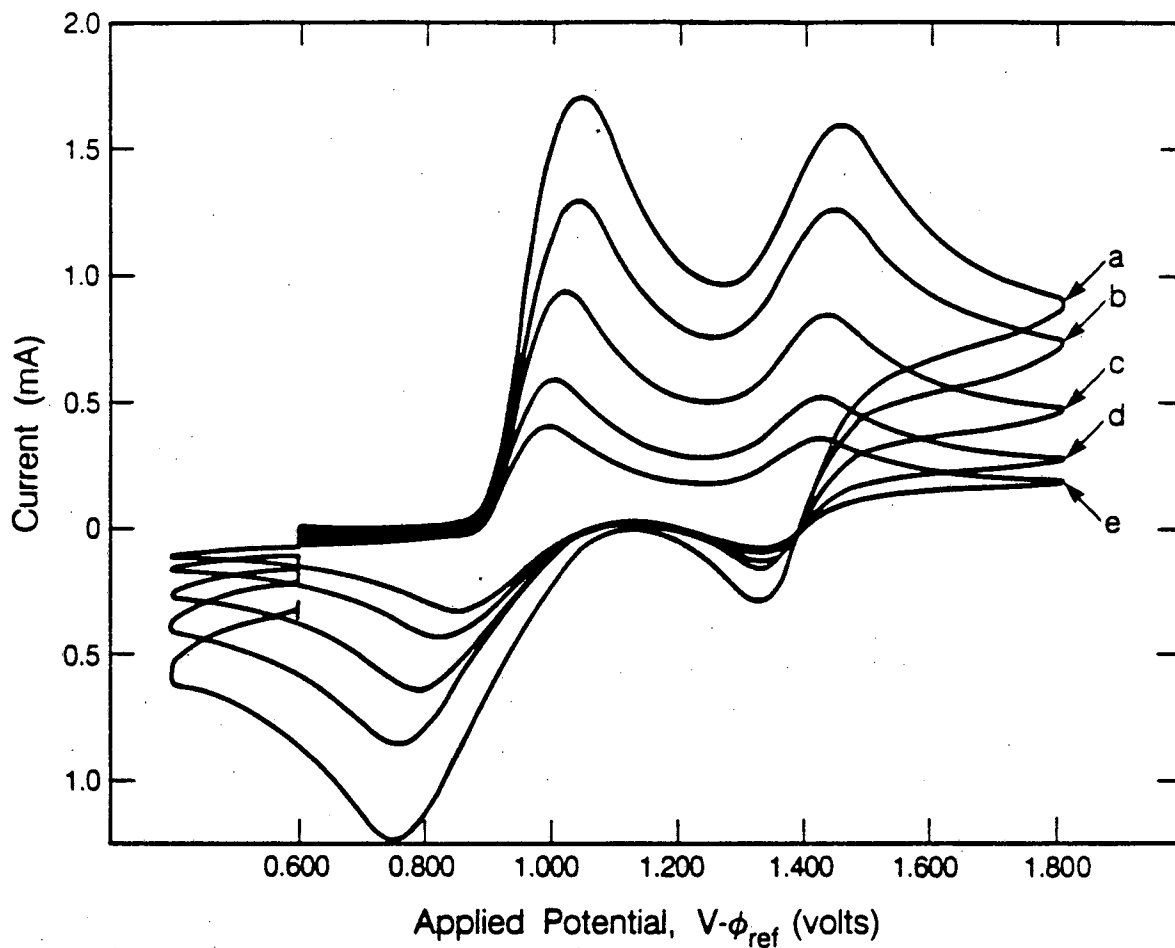
The theory of reversible reactions (section 6.2.2) describes the dependence of the current on the sweep rate. The value of the current is determined by the area of the electrode, the reaction stoichiometry, and the diffusion coefficient. From Shuman's work (see section 6.2.2),

$$i_p = nFAC^* \left[\frac{\pi D_o n F}{RT} \right]^{1/2} \chi(\sigma t) b^{1/2}. \quad (6.4.4)$$

Thus,

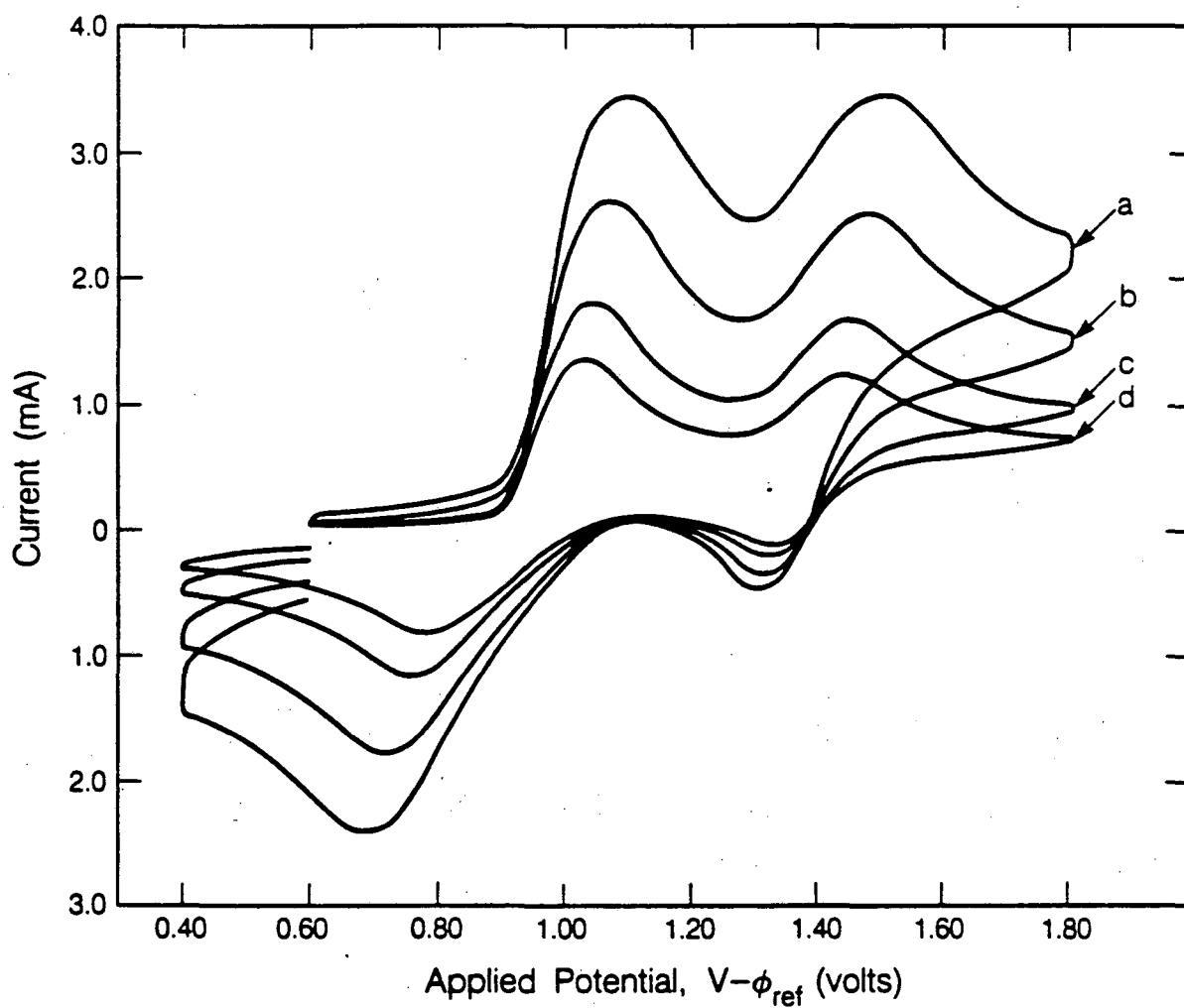
$$i_p = \text{constant} \times b^{1/2}. \quad (6.4.5)$$

The variation of peak current with the square root of the sweep rate is shown in Figure 6.4.17 a-d. The results for peaks II and II' must be regarded as qualitative. Because the total current in this potential region includes a contribution from the previous reaction, the baseline for peak II is estimated by extrapolating the tail of peak I, assuming that the current declines with the square root of time. The same problem of determining a baseline exists for peak II'. Here the baseline was determined by extending the baseline obtained just after the potential switches direction. A semi-empirical procedure for determining these baseline currents is outlined by Nicholson[53] and these guidelines were followed. In view



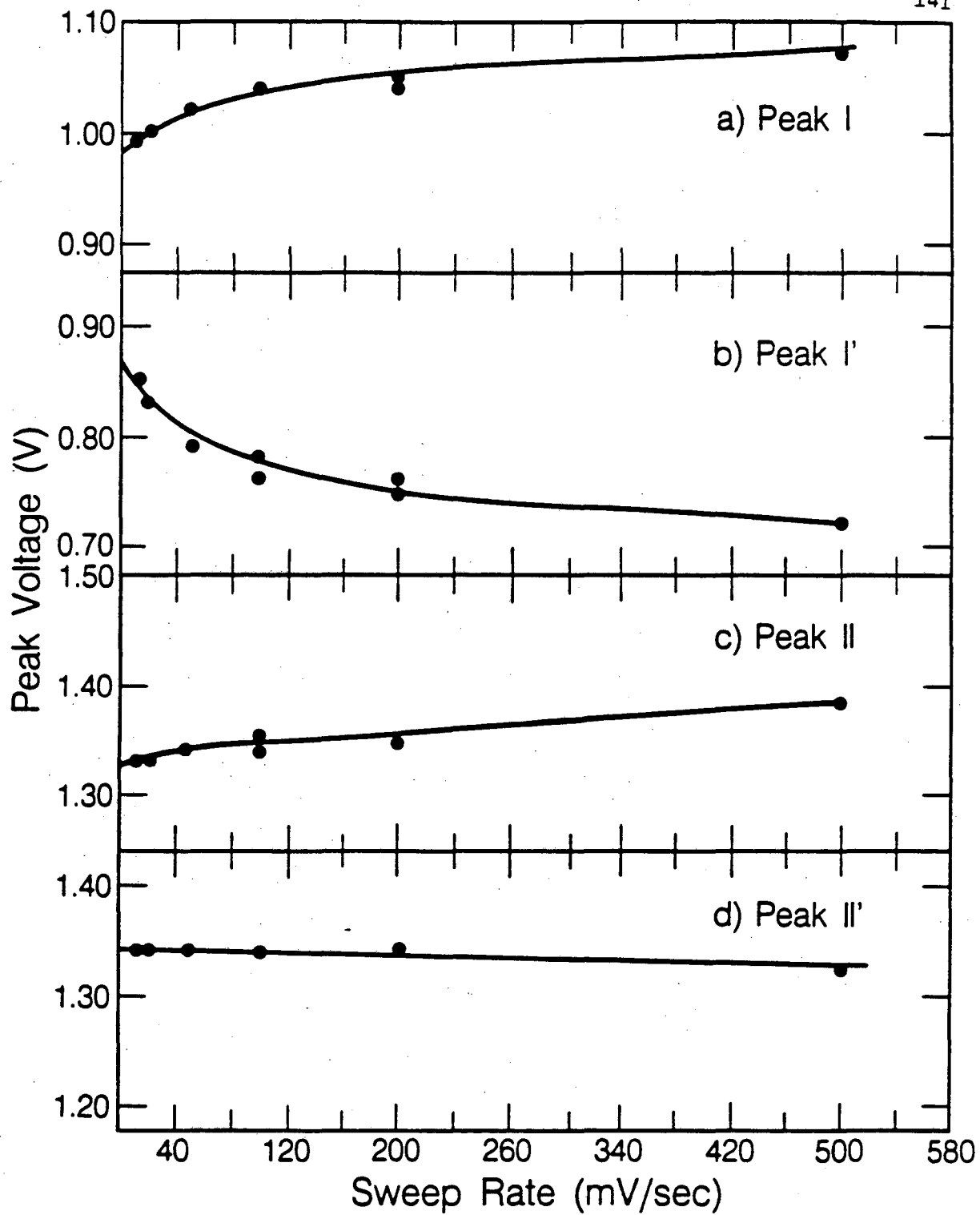
XBL 847-7202

Figure 6.4.14 Effect of sweep rate. Scan is [0.6 V/1.8V/0.4 V/0.6 V].
(a) 200 mV/sec, (b) 100 mV/sec, (c) 50 mV/sec, (d) 20 mV/sec, and
(e) 10 mV/sec. Solution: 0.004 M KI, 0.5 M $KAsF_6$.



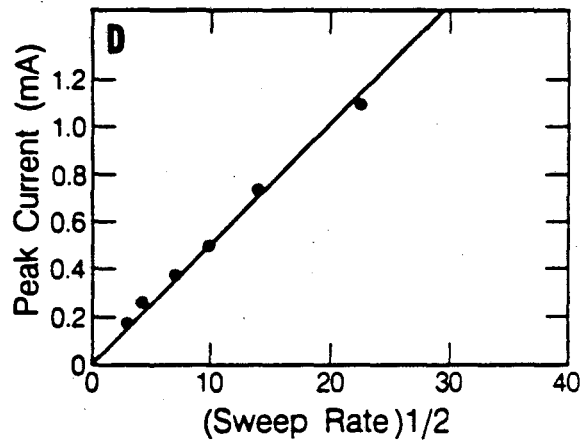
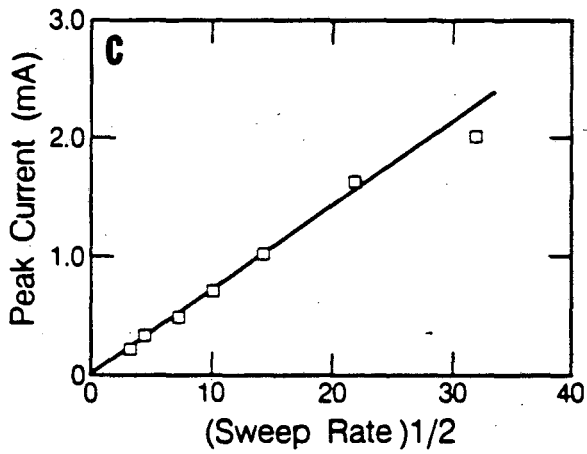
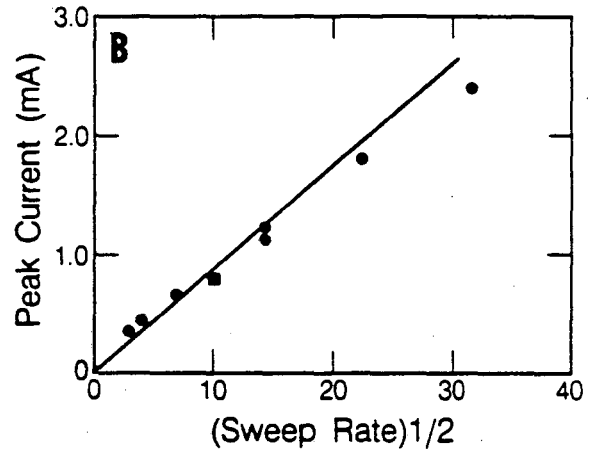
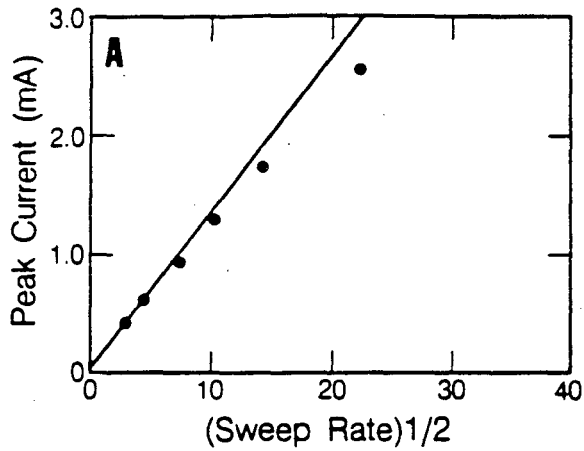
XBL 847-7203

Figure 6.4.15 Effect of Sweep rate. Scan is [0.6 V/1.8 V/0.4 V/0.6 V].
(a) 1000 mV/sec, (b) 500 mV/sec, (c) 200 mV/sec (d) 100 mV/sec.
Solution: 0.004 M KI, 0.5 M KAsF₆.



XBL 847-7740

Figure 6.4.16 Shift of peaks as a function of sweep rate. (Data from Figures 6.4.14 and 6.4.15).



XBL 847-7741

Figure 6.4.17 Dependence of peak current on square root of sweep rate.
 (A) Peak I, slope: $0.12 \text{ ma-sec}^{1/2}/\text{mV}^{1/2}$, (B) Peak I', slope: 0.08,
 (C) Peak II, slope: 0.06, (D) Peak II', slope 0.06.

of these built-in inaccuracies the results for peaks II and II' are surprisingly linear (regression coefficients of 0.9921 and 0.9979, respectively). The theory is based upon the initial condition of a uniform concentration of the reactant; a condition which is almost certainly not met for triiodide at 1.2 V or for iodine at the reversal potential--especially at high sweep rates. Apparently, the first and second peaks are sufficiently separated to approximate this condition. By sweeping about 150 mV past the second peak, the concentration of iodine in the boundary layer becomes relatively uniform. Although one would expect identical slopes for these two curves, they differ by about 14%. The results for the anodic and cathodic peaks for the first reaction (peaks I and I') are very different. Here the slopes vary by an order of magnitude, indicating that the anodic reaction probably proceeds via a different mechanism than the cathodic reaction.

The width of the peak is also an indication of reversibility. Figure 6.4.18 shows how the width of peak I varies with sweep rate. The value at the intercept is 52 mV; from theory, Shuman predicts a value of 52.25 mV for a 3:1 stoichiometry.

Peak I

A series of voltammetric experiments were performed to focus on the electrochemistry of the first peak. Figures 6.4.19, 6.4.20, and 6.4.21 show scans showing the change in the voltammogram of the first peak for sweep rates ranging from 1 mV/sec to 20 V/sec. These data were taken with the single compartment cell using the oscilloscope to collect data. The change in peak current as a function of sweep rate is shown in Figure 6.4.22. In the upper curve the range between 1 mV/sec and 500 mV/sec is shown; the linear range extends to about 200 mV/sec. From the slope of the curve, a diffusion coefficient of 2.0×10^{-6} cm²/sec can be estimated⁶.

⁶ This number was calculated from equation 6.4.4 using a value of 0.0571 cm² for the area of the electrode (see section 6.5).

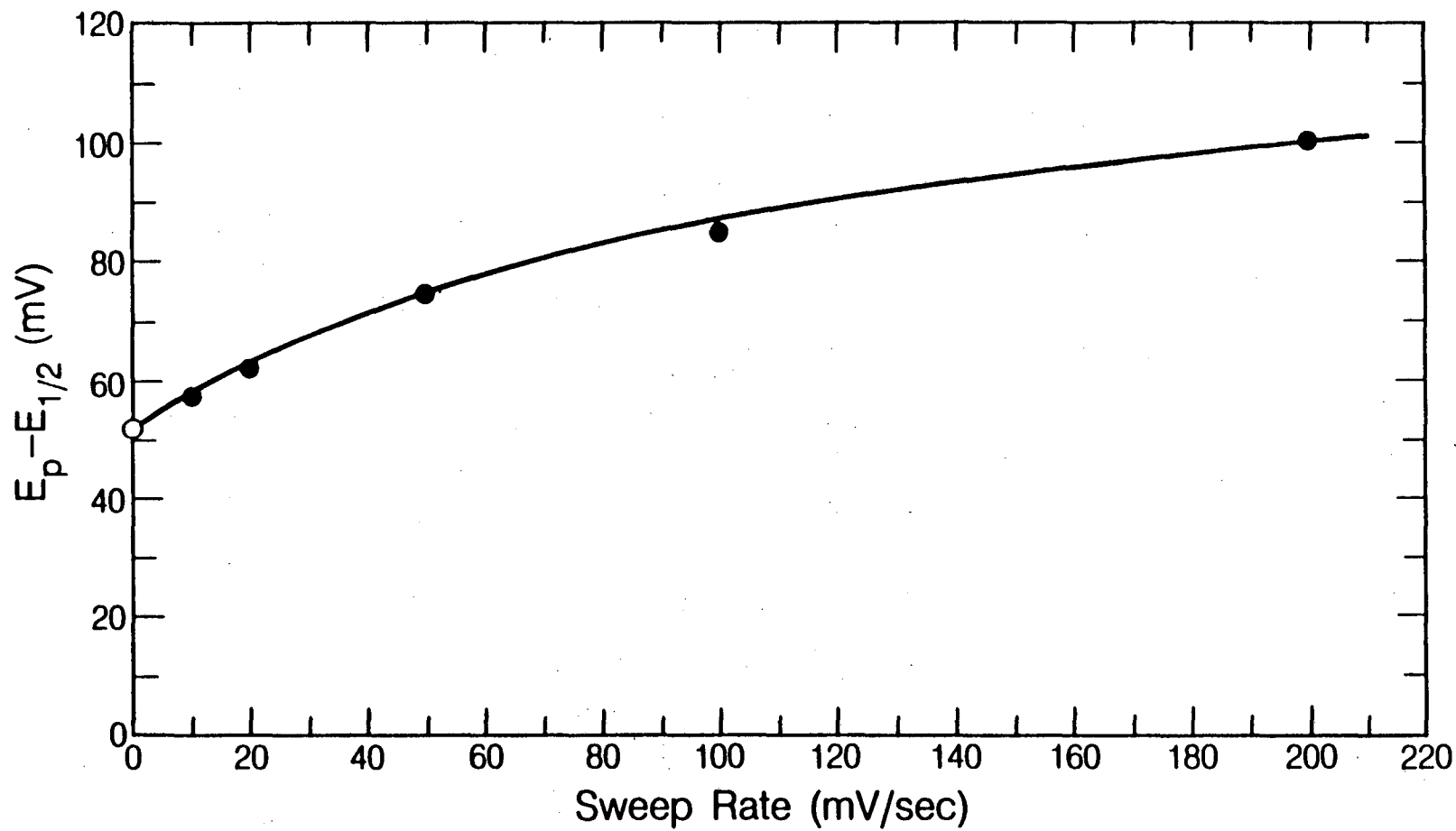
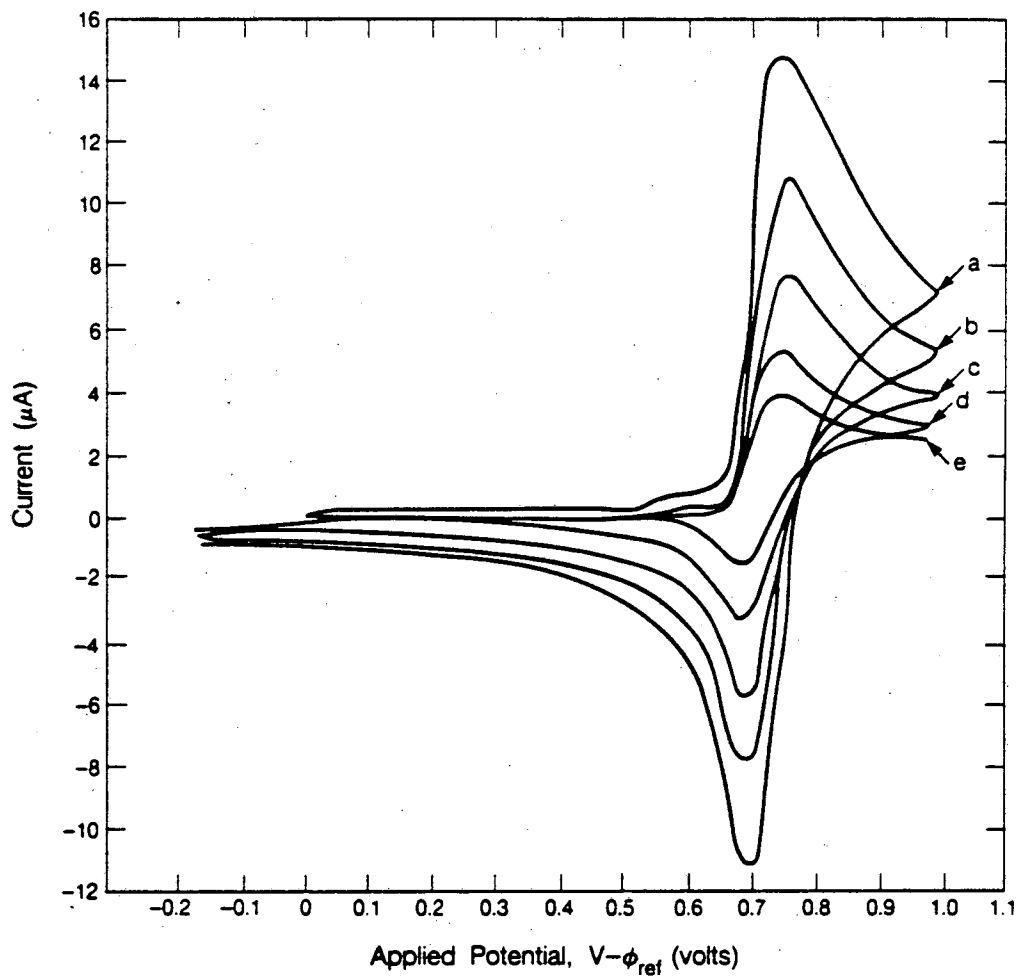


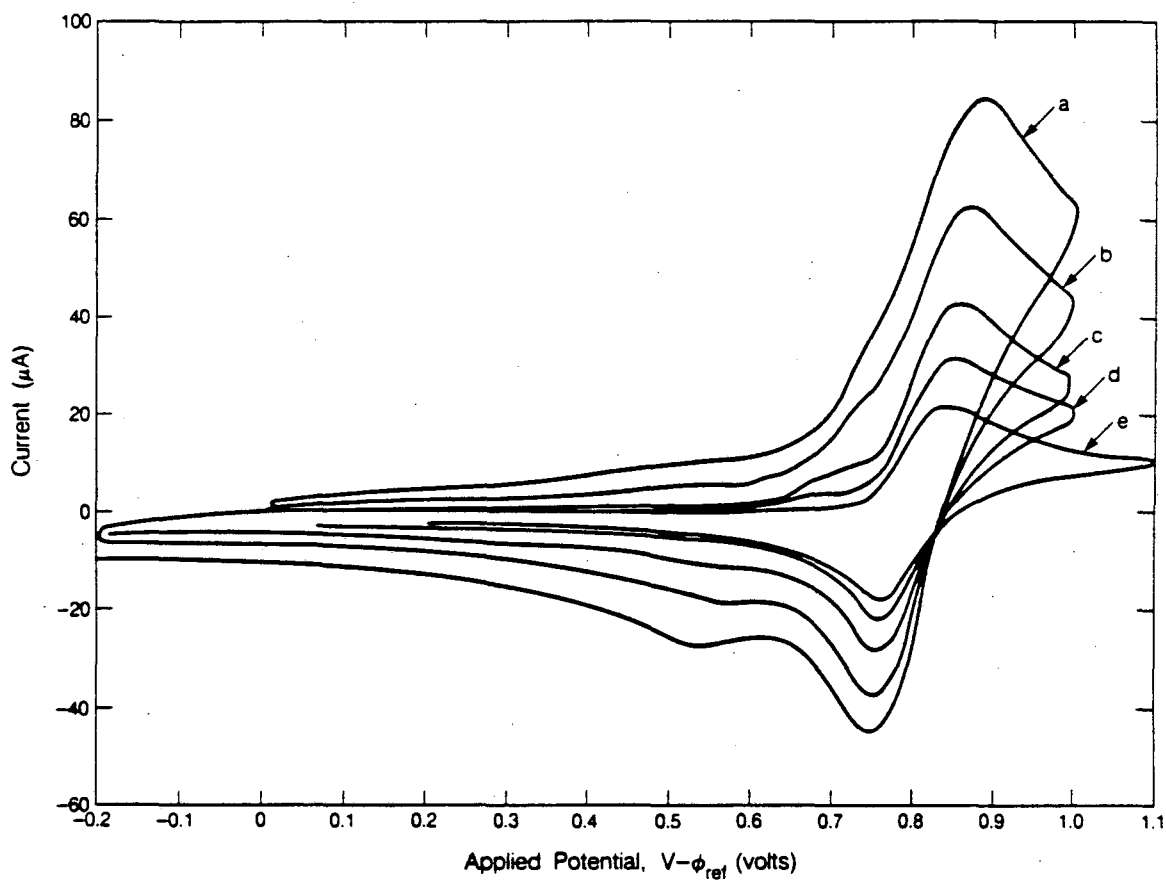
Figure 6.4.18 Change of peak width for peak I with sweep rate.
Data from Figures 6.4.14 and 6.4.15.

XBL 847-7736



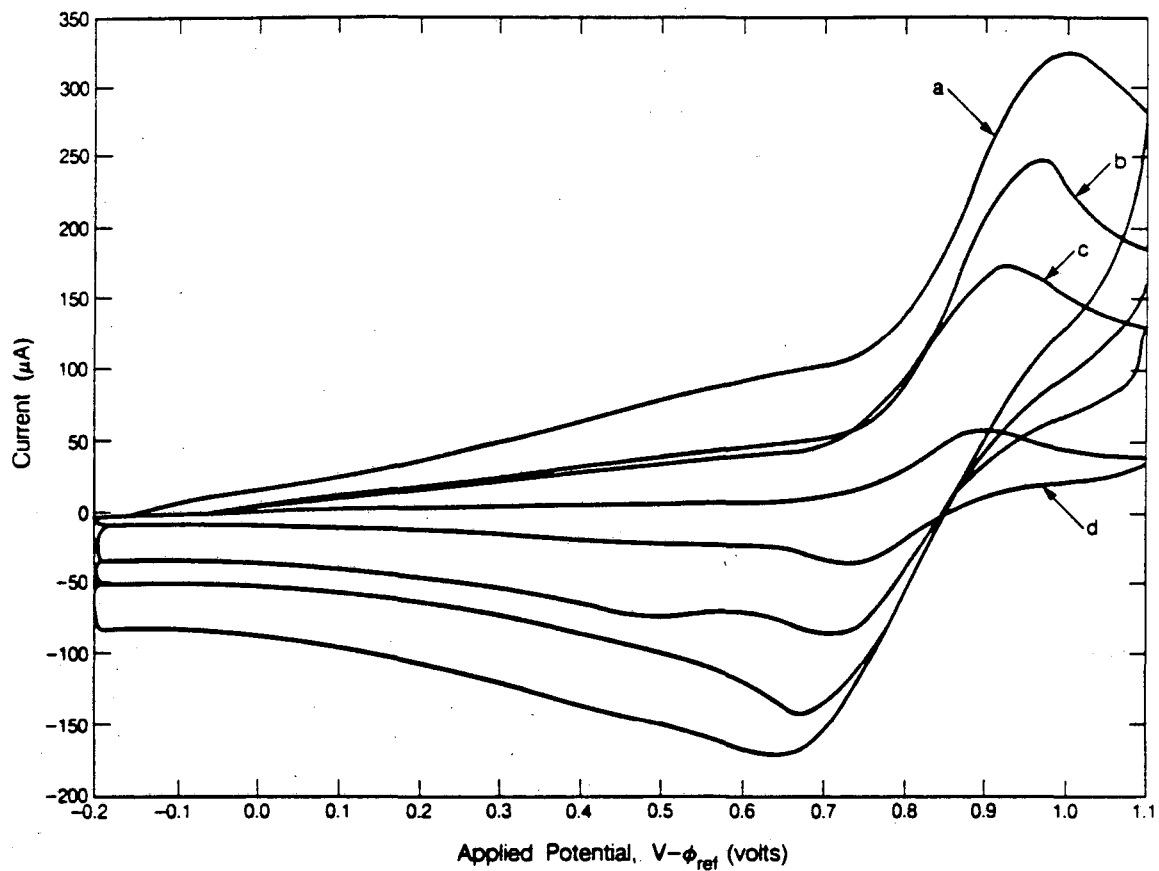
XBL 846-7164

Figure 6.4.19 Sensitivity of Peak I with sweep rate. (a) 20 mV/sec, (b) 10 mV/sec, (c) 5 mV/sec, (d) 2 mV/sec, (e) 1 mV/sec. Solution: 0.005 M KI, 0.5 M KAsF_6 .



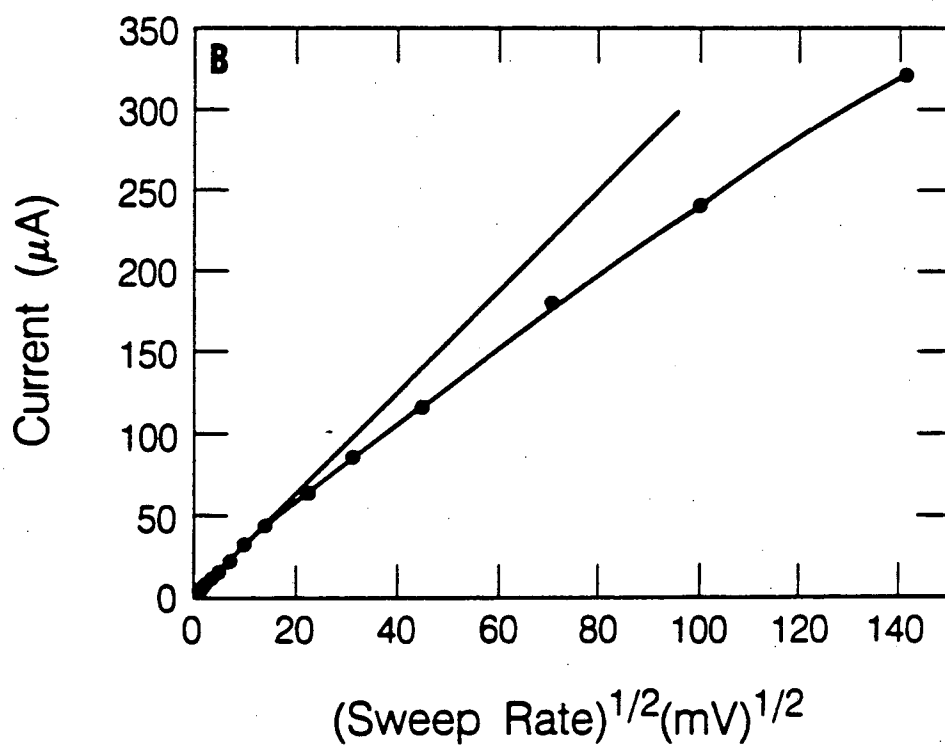
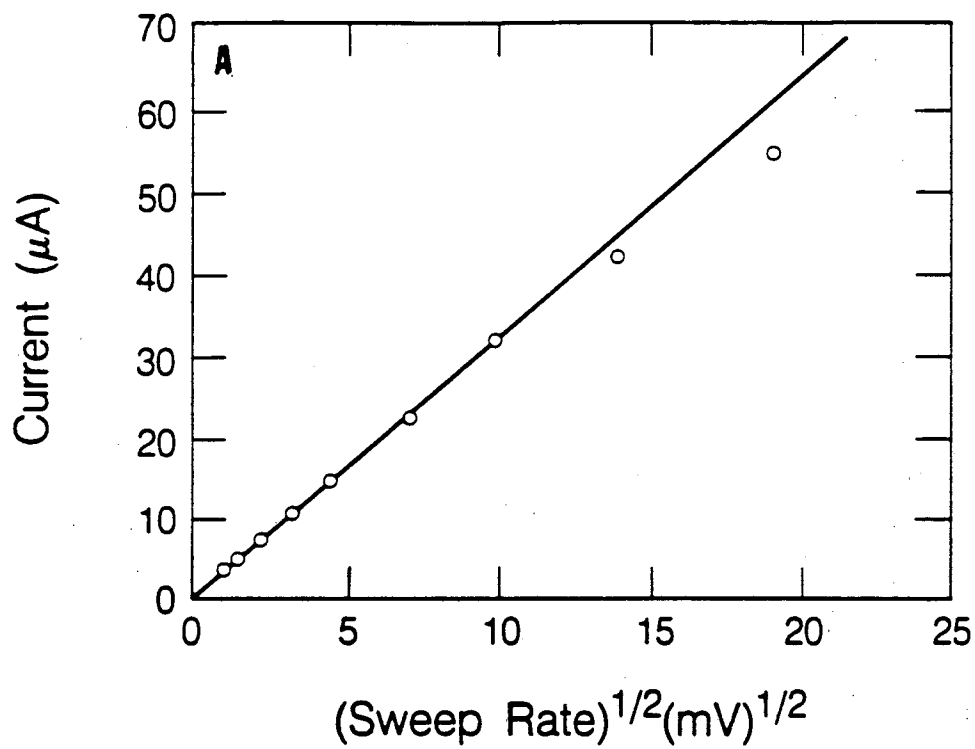
XBL 846-7163

Figure 6.4.20 Sensitivity of Peak I with sweep rate. (a) 1000 mV/sec, (b) 500 mV/sec, (c) 200 mV/sec, (d) 100 mV/sec, (e) 50 mV/sec.



XBL 846-7165

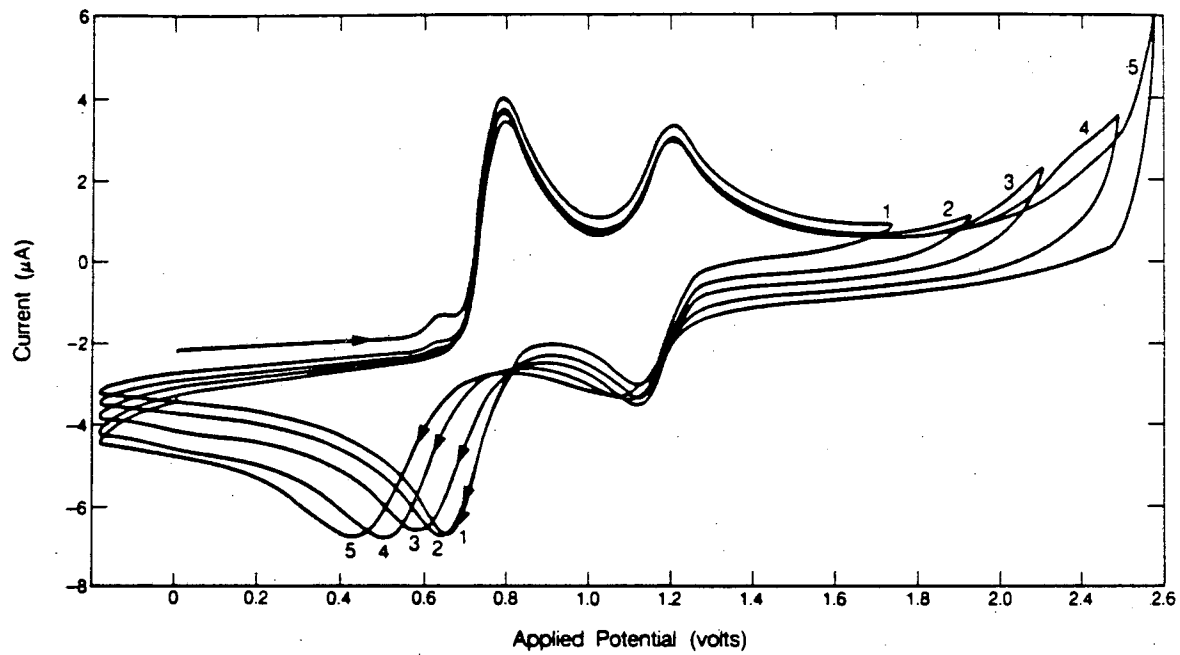
Figure 6.4.21 Sensitivity of Peak I with sweep rate. (a) 20 V/sec, (b) 10 V/sec, (c) 5 V/sec, (d) 2 V/sec.



XBL 849-10807

Figure 6.4.22 Change in peak current for Peak I as a function of the square root of sweep rate. (A) Slow sweep rates. Range is 1 mV/sec to 500 mV/sec. (B) Range is 1 mV/sec to 20 V/sec.

The irreversibility of the first peak is related to the state of the electrode surface. Figure 6.4.23 illustrates the shift of this peak with the reversal potential. The peak appears in the same position at switching potentials of 1.7 and 1.9 V, but when the potential sweep reverses at 2.1 V or greater, the position of the cathodic peak moves in the cathodic direction.



XBL 846-7166

Figure 6.4.23 Effect of switching potential on position of Peak I'.
Solution: 4.3×10^{-3} M KI, 0.5 M KAsF_6 .

6.5. PARAMETERS FOR MODEL

Potential step experiments were used to determine the area of the electrode and the diffusion coefficient of iodide in PC. The mathematical description of the current response to a potential step at a planar electrode in a stagnant solution is the Cottrell equation. Under the assumption that a single electrode reaction occurs ($R \rightarrow O + ne^-$), and that the potential step is sufficiently positive to assure that the surface concentration of R is zero, the current as a function of time is given by [54],

$$i(t) = \frac{nFAD_R^{1/2}C_R^0}{3\pi^{1/2}t^{1/2}} \quad (6.5.1)$$

This relationship was used in two different ways in this work. To determine the electrode area, potential step experiments were done in aqueous electrolyte using the Fe^{+2}/Fe^{+3} couple which has a known diffusion coefficient. To determine the diffusion coefficient of I^- in PC, potential step experiments were done in iodide solutions in PC.

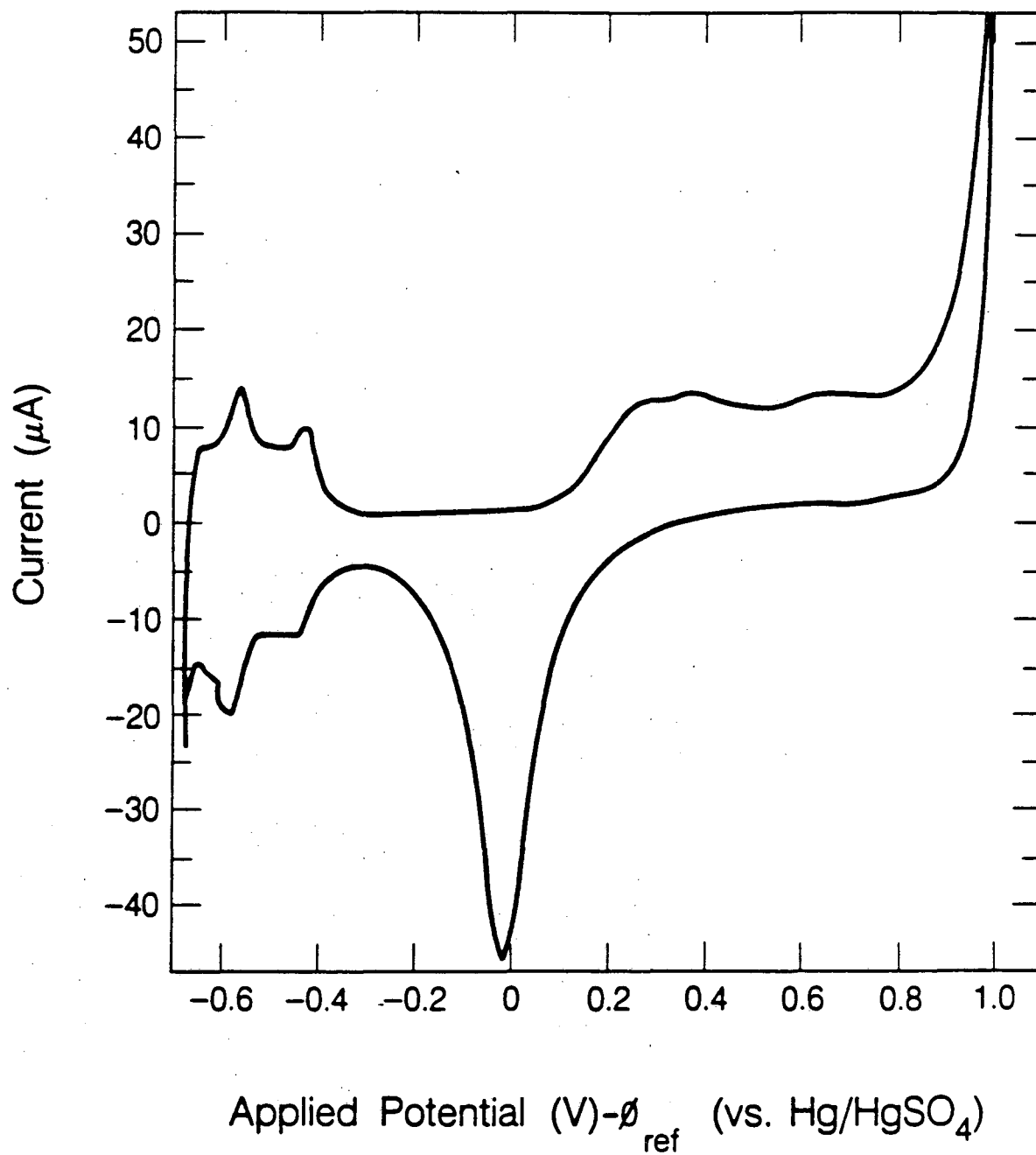
Determination of Working Electrode Area

Three different values for the area of the working electrode were measured. The smallest possible area is the projected area. This was measured by photographing the electrode through the aperture of a light microscope. Under 10X magnification, the electrode appears slightly oval; the projected area was determined from the lengths of the major and minor axes to be 0.0571 cm^2 .

In contrast to the projected area, the largest value of electrode area for an electrochemical experiment is the area available for adsorption. This value was determined by using the same electrode to perform a series of cyclic voltammetry experiments in $0.5 \text{ M H}_2\text{SO}_4$. The electrode was pre-treated by the method described earlier, but an additional step of soaking for 30 minutes in nitric acid was included. Because these were aqueous experiments, the electrode was not

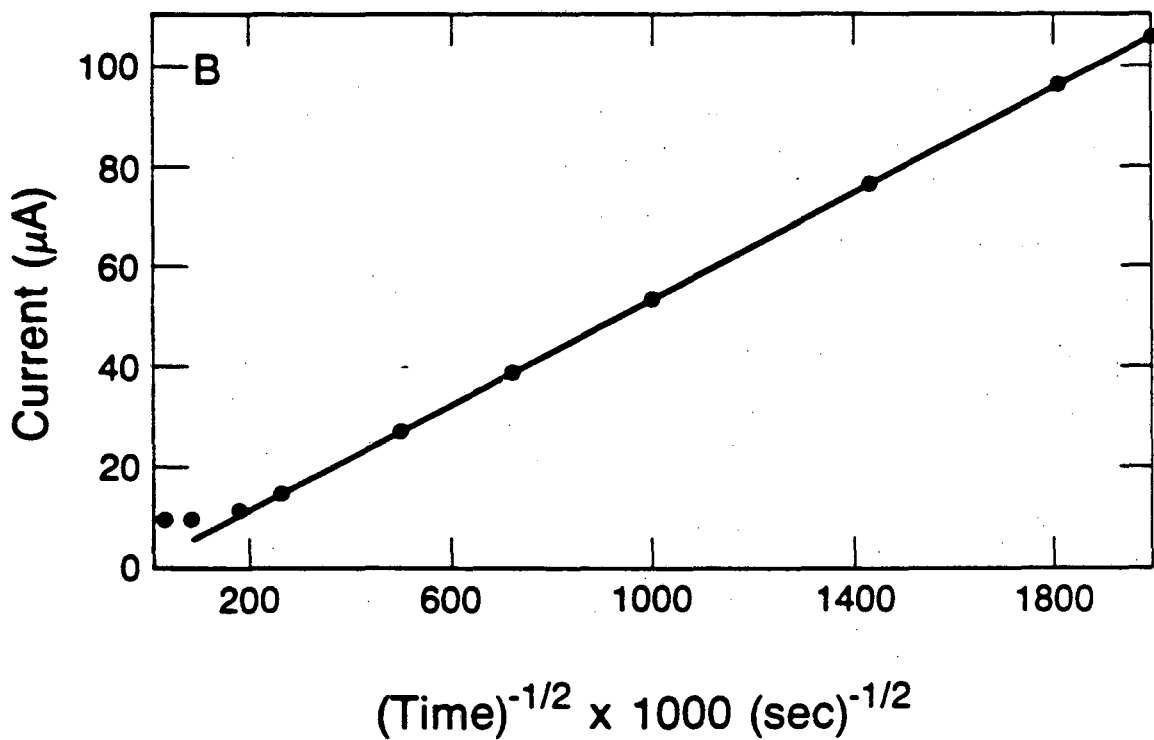
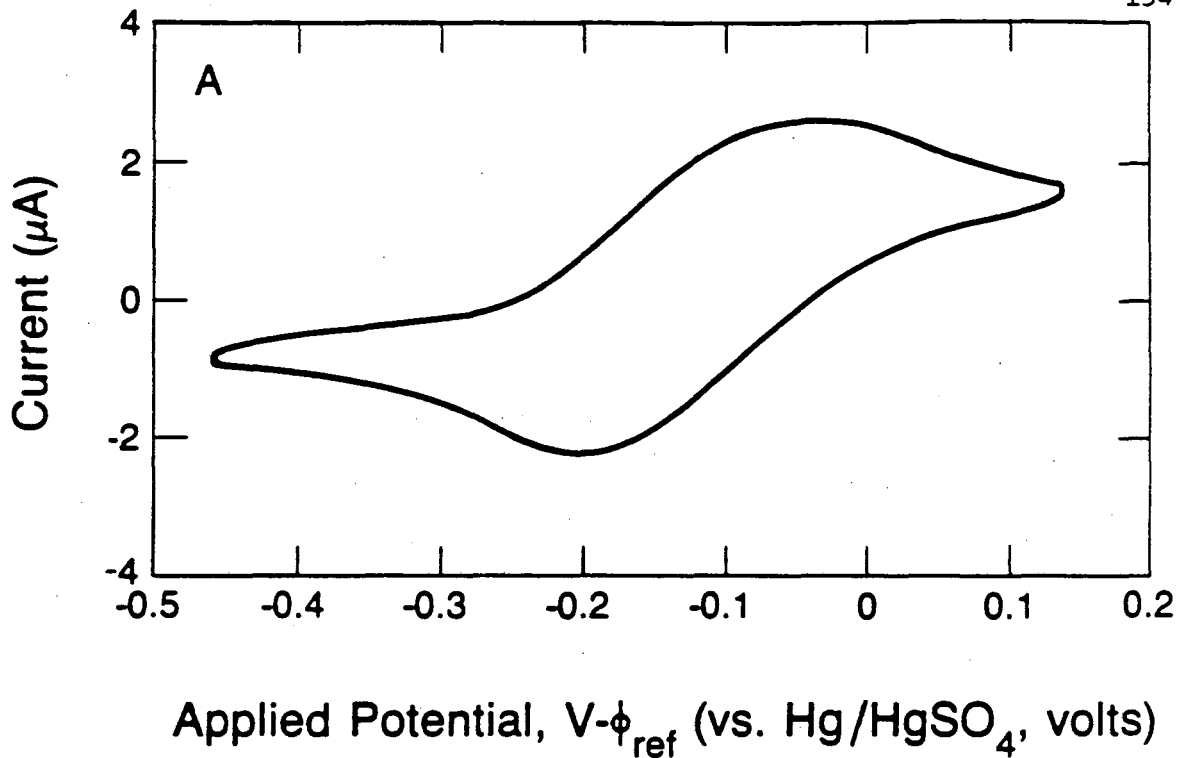
dried, but used after repeated rinsing with distilled water. Before each experiment the electrode was cleaned as suggested by Gileadi et. al.[55]. This consists of several steps. First, the electrode is abraded with powdered alumina (0.3μ) for about one minute on a polishing wheel. After rinsing with distilled water, the electrode is electrochemically pre-treated in $0.5 \text{ M H}_2\text{SO}_4$. The potential (controlled versus a Hg/HgSO_4 reference electrode) is set to $+1.8 \text{ V}$ (vs. RHE) for 10 seconds to oxidize impurities. It is then held at $+1.2 \text{ V}$ for 30 seconds to remove oxygen formed at the higher potential, and switched to $+0.05 \text{ V}$ for 30 seconds to reduce surface oxides formed in the last step. This procedure is repeated several times. Figure 6.5.1 shows the voltammogram obtained after the pre-treatment. The area of the electrode available for adsorption was determined by integrating the charge passed between -0.68 V and -0.4 V (vs. Hg/HgSO_4). Assuming that the hydrogen charge corresponds to a monolayer, and that $200 \mu\text{C}$ corresponds to a square cm on polycrystalline platinum[56], the area is estimated to be 0.117 cm^2 .

The third measurement of electrode area was made by potential step experiments. This corresponds to the projected geometric area for electrochemical reaction and is the value used in the voltammetry simulations. The experimental cell and electronics are those used in the cyclic voltammetry experiments. Software to collect and reduce the data for the potential step experiments is given in Appendix A-2. The experiment is illustrated in Figure 6.5.2. The oxidation wave of a 5 mM solution of $\text{K}_4\text{Fe}(\text{CN})_6$ appears at 0.80 V (vs. Hg/HgSO_4 reference) as shown in Figure 6.5.2 a. A Cottrell plot for potential steps between -0.46 V and 1.4 V is given in Figure 6.5.2 b. From the slope of the line, and a diffusion coefficient of $0.739 \times 10^{-5} \text{ cm}^2/\text{sec}$ [57], the area of the electrode is calculated to be 0.071 cm^2 . This value falls between the adsorption surface area and the projected area.



XBL 849-4047

Figure 6.5.1 Voltammogram of platinum electrode in 0.5 M H₂SO₄ (aq) after pretreatment. Potential is referenced to Hg/HgSO₄.



XBL 849-10810

Figure 6.5.2 Potential step measurement to determine electrode area. (A) Voltammogram of $K_4Fe(CN)_6$ (0.005 M, aq). Potential is referenced to Hg/HgSO₄ electrode. (B) Cottrell plot for potential steps between -0.46 V and 1.4 V.

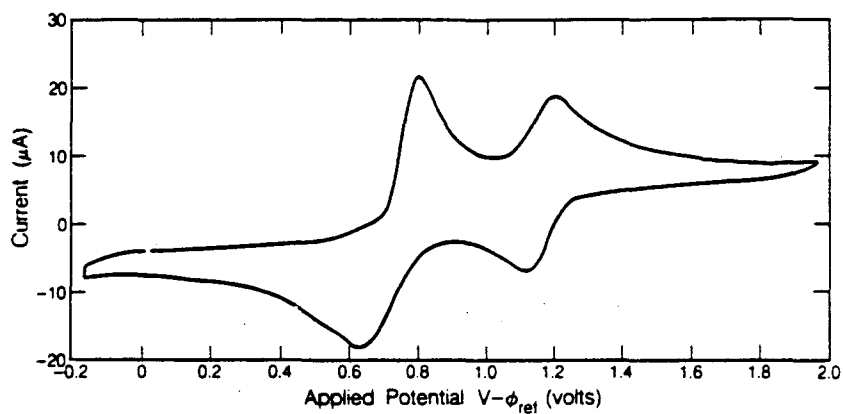
Determination of Diffusion Coefficient of Iodide

Using the same electrode and cell, potential step experiments were done in a series of solutions of iodide in PC. The experiment is illustrated in Figure 6.5.3. The voltammogram in Figure 6.5.3 a shows the position of the two peaks for a solution of 6.7 mM KI in a supported (0.5 M KAsF₆) PC solution at a sweep rate of 100 mV/sec. The current transient for potential steps from 0.0 to 1.0 V for various time scales is shown in Figure 6.5.3 b. From these curves, the current as a function of the inverse square root of time is plotted, as shown in Figure 6.5.3 c. Because the stoichiometry of this reaction is 3:1, for a given current the flux at the electrode is three times that for a 1:1 reaction. Accordingly,

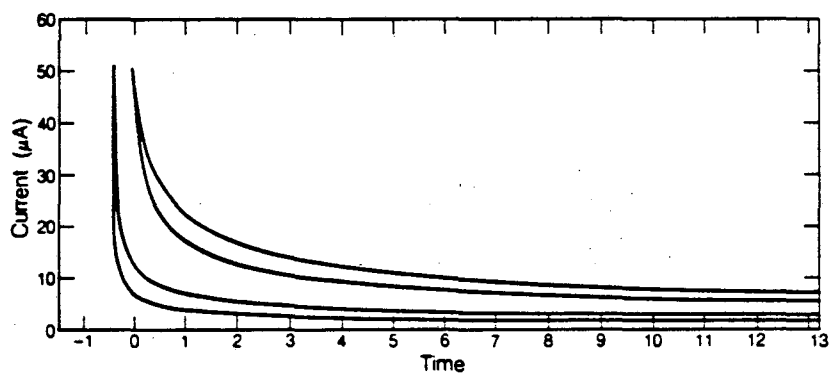
$$\text{slope} = \frac{nFAD_R^{3/2}C_R^*}{3\pi^{1/2}}$$

Using the superficial area of 0.0571 cm², the diffusion coefficient of iodide is found to be 4.0 × 10⁻⁶ cm²/sec.

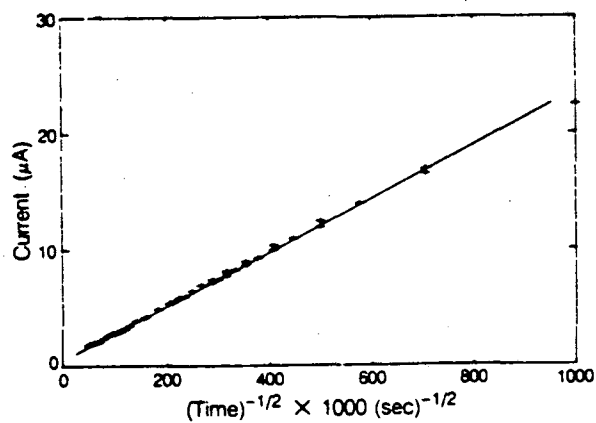
Relatively few studies of diffusion of electrolytes in nonaqueous solvents have been reported. (In Janz and Tomkins' two-volume, 2000-page compendium of nonaqueous data[58], five pages are devoted to diffusion studies.) Thus, it is difficult to assess the validity of this measurement. Popovych and Tomkins[59] report diffusion coefficients for iodide and triiodide in DMSO and two different aqueous solutions. These values are listed in Table 6.5.1. Included in the table are diffusion coefficients reported by Nakanishi and Furusawa [60] for iodine in THF and 1,4 dioxane and for KI reported by Janz and Tomkins[61]. As a general rule, the product of the viscosity and the diffusion coefficient is approximately constant for a given solute. Obviously, this does not account for specific interactions such as hydrogen bonding or for the variation in the donor/acceptor properties of the solvents. These "reduced diffusion coefficients" are given in the last column in Table 6.5.1. All values for iodide fall between 2.2 and 4.5 × 10⁻¹⁰ dynes/deg. An average value is 3.2 × 10⁻¹⁰ dynes/deg which is approximately



(A) Voltammogram for 0.0067 M KI, 0.5 M KAsF_6 in PC. Scan rate: 100 mv/sec



(B) Current transient for potential steps from 0.0 to 1.0 V. Various time scales are shown.



(C) Cottrell Plot.

XBL 847-7737A

Figure 6.5.3 Potential step measurement to determine the diffusion coefficient of iodide in PC.

the value in formamide. Assuming that this constant is valid for PC solutions, the "calculated" diffusion coefficient for iodide in PC is $3.9 \times 10^{-6} \text{cm}^2/\text{sec}$. This compares favorably with the measured value of $4 \times 10^{-6} \text{cm}^2/\text{sec}$. It is also interesting to note that the ratio of the diffusion coefficients of iodide to triiodide (approximately 2:1) is the same in DMSO, aqueous KI, and aqueous sulfuric acid solutions. If we assume that the same ratio holds in PC, the diffusion coefficient of triiodide in PC is approximately $2.0 \times 10^{-6} \text{cm}^2/\text{sec}$.

Table 6.5.1 Diffusion Coefficients of Iodide, Triiodide, and Iodine

Solute	Solvent (Donor No. ⁷)	η_0 (cp)	D ($10^6 \text{cm}^2/\text{sec}$)	Ref.	$\frac{D\eta}{T}$ (10^{10}dynes/deg)
Iodine	THF (20)	0.48	0.235	[59]	3.8
Iodine	1,4 Dioxane 3.8 (14.8)	1.19	9.6	[59]	-
Triiodide	DMSO (.8M KClO_4) (30)	1.96	3.7	[60]	2.4
Triiodide	Water (1.0 N H_2SO_4)	-	4.2	[60]	-
Triiodide	Water (0.1 M KI)	-	11.3	[60]	-
Iodide	DMSO (.8 M KClO_4) (30)	1.96	6.9	[60]	4.5
Iodide	FA (24)	3.03	3.0	[59]	3.3
Iodide	NMF (26.3)	1.65	4.7	[59]	2.6
Iodide	DMF (27.8)	0.796	8.3	[59]	2.2
Iodide	1 N H_2SO_4 (aq)	-	8.1	[60]	-
Iodide	1.5 M KI (aq)	-	22.0	[60]	-
Iodide	PC (15.1)	2.5	4.0	This work	3.4

⁷ All values for solvent donor numbers are from Gutmann[82].

6.6. COMPARISON OF MODEL AND EXPERIMENT

A mathematical model for an experiment is useful because it provides a test of our understanding of the underlying physical processes which govern the results of the experiment. For example, if only one electrochemical reaction occurs in a cyclic voltammetry experiment, correlations available in the literature for peak width, half-wave potential, and peak current can help provide an understanding of the electrochemistry. However, even for a relatively simple problem such as the cyclic voltammetry of iodide in PC, it is very difficult to justify the shape of the curve without a detailed understanding of the surface concentrations of the three species involved.

In this section, simulated voltammograms based upon the models of the electrode processes presented in section 6.3 are compared to experimental results taken at a sweep rate of 100 mV/sec. From these comparisons, a number of conclusions are drawn about the mechanism of the overall reaction, the rate of the electrochemical steps, the accuracy of the independent parameters, and the value of the dependent fitting parameters. A stronger test of the model is to try to predict the shape of the voltammogram at higher sweep rates using the fitting parameters determined at 100 mV/sec. The results are described below. The physical models are summarized in Table 6.3.1.

Model I

The case of reaction of iodine to triiodide in the solution adjacent to the electrode was considered first. Figure 6.6.1A shows the results of an experiment at a sweep rate of 100 mv/sec compared to the simulation. The rate constant for the chemical reaction used in the simulation is given as 1×10^{-2} l/mol-sec and values for E_1° and E_2° were taken from the literature [63]. Three major discrepancies exist between the model and the experiment. These include: (i) the peak separation is incorrect, (ii) the current at the end of the anodic scan is too low

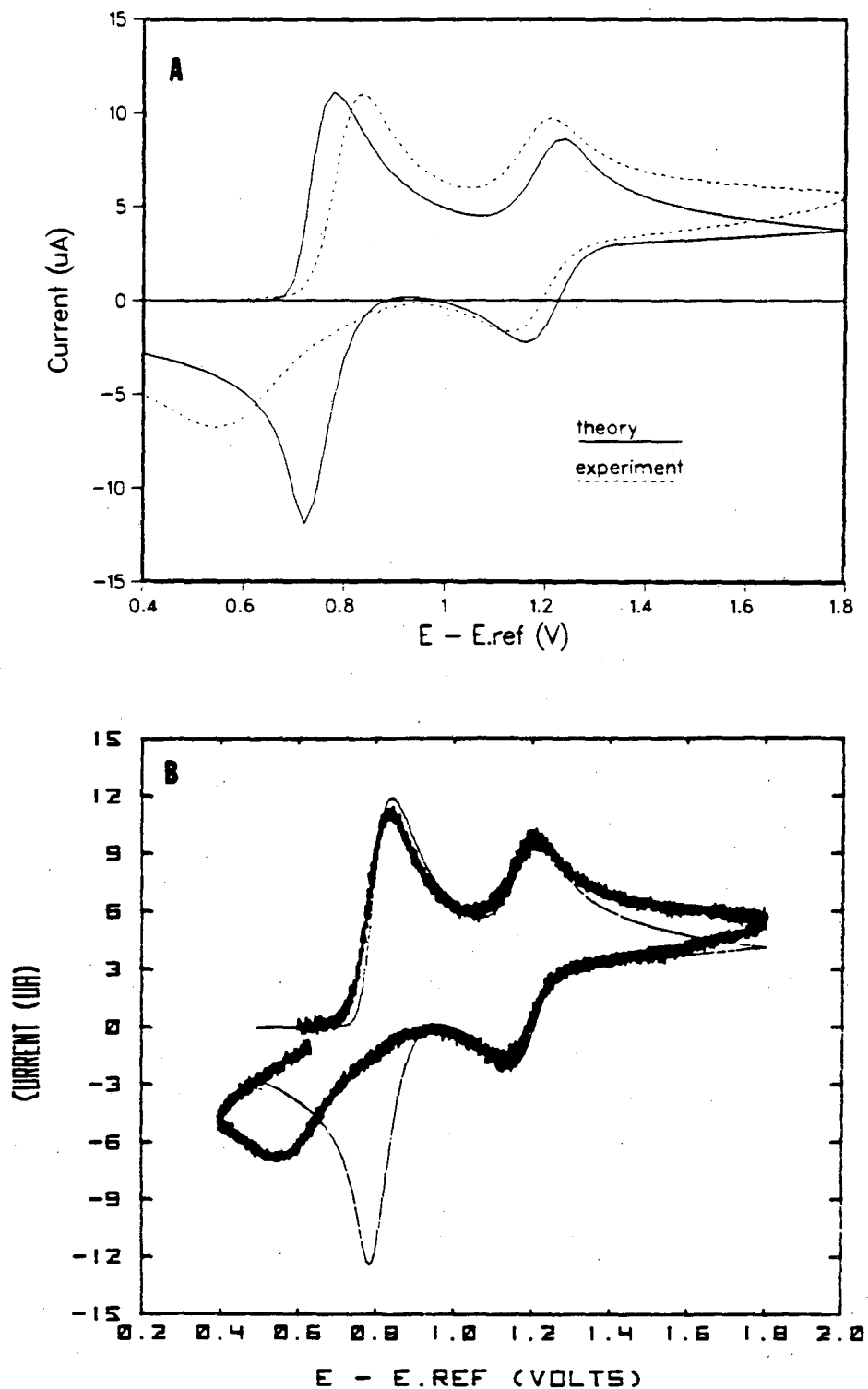


Figure 6.6.1 (A) Comparison of cyclic voltammetry simulation (Case I) to experiment. Electrolyte: 0.004 M KI, 0.5 M KAsF₆. 100 mV/sec. Rate constant: 0.01 l/mol-sec. $E_1^{\circ} = 800$ mV, $E_2^{\circ} = 1265$ mV. (B) Same simulation with $E_1^{\circ} = 865$ mV, $E_2^{\circ} = 1265$ mV.

in the simulation, and (iii) the model incorrectly predicts the behavior of peak I', the reduction of triiodide to iodide. Figure 6.6.1b shows essentially the same voltammograms, except that the values of E_1^0 and E_2^0 were adjusted to fit the curve. In this way we obtain values of 865 mV and 1265 mV for E_1^0 and E_2^0 respectively. The failure of the model to describe peak I' indicates that either the rate of the electrochemical reduction of iodine to iodide is slow, or that the preceding chemical reaction, the dissociation of triiodide to iodide and iodine, is slow. The latter case is explored as model II.

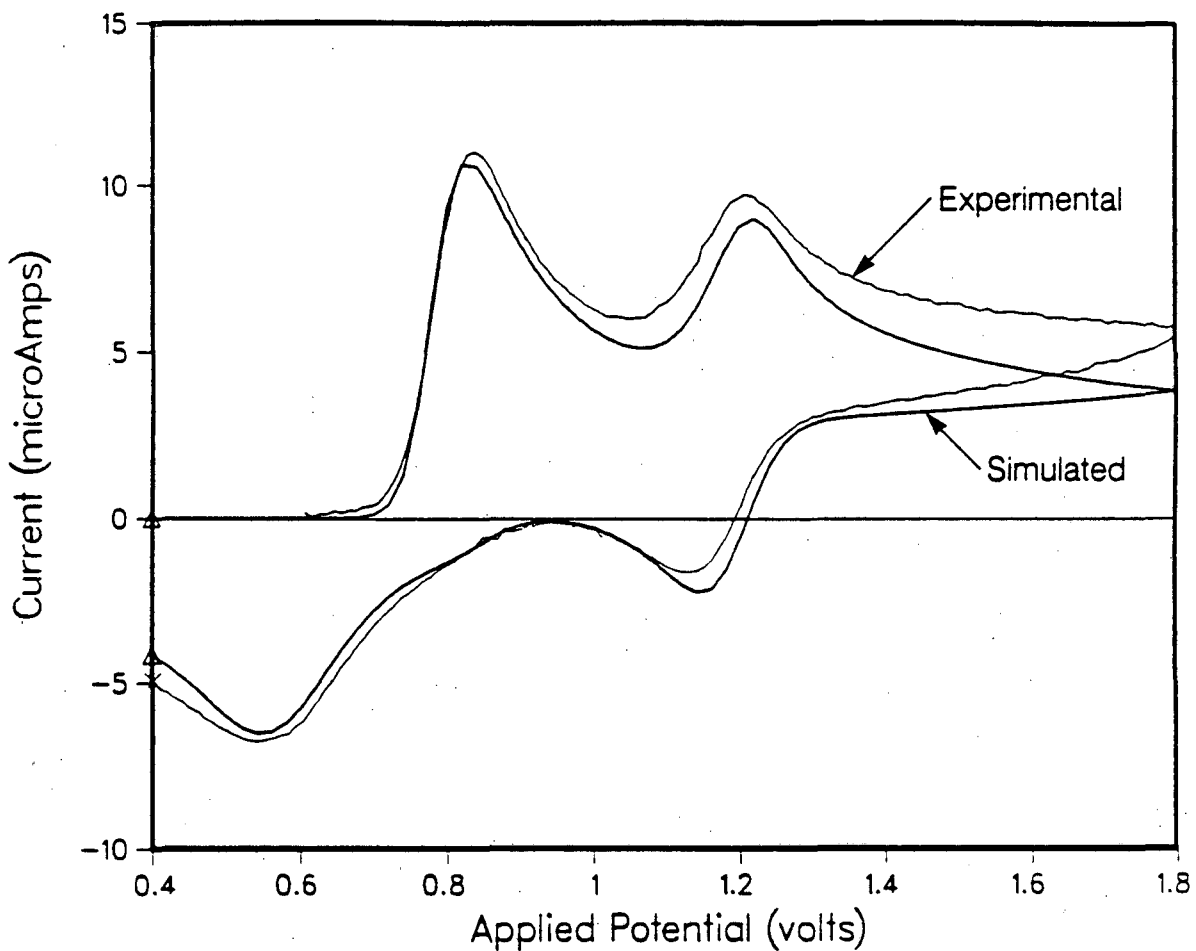
Model II

In section 6.3.2, the simulation of a voltammogram based upon a rate limiting chemical reaction on the electrode surface was shown. A single fitting parameter, k_f , controls both the rate of the chemical reaction and the rate of the first electrochemical reaction. The rate constant k_f provides a fitting parameter which changes the height of the peak I', but because we still assume that the electrochemical reaction is reversible, the position of the peak does not change with sweep rate.

Model III

The best fit of model III and the experimental data is shown in Figure 6.6.2. The parameters used in the model are listed in the figure caption. The most serious error appears near the end of the anodic sweep. This discrepancy is due to unsubtracted background currents from the supporting electrolyte solution (see figure 6.4.8) which are high in this potential region.

The parameters given in Figure 6.6.2 are not necessarily a unique set. The fit shown here was made by considering the precision with which each of the parameters is known. Good estimates of the iodide diffusion coefficient, the area of the electrode, the solution concentration, and the equilibrium potential values



XBL 847-7739

Figure 6.6.2 Best fit of model III and experiment. The experiment is described in Figure 6.6.1. Simulation parameters: $E_1^\circ = 0.60$ V, $E_2^\circ = 1.265$ V, $C^* = 2.5 \times 10^{-6}$ mols/cm³, area = 0.0571 cm², all diffusion coefficients are 2×10^{-6} cm²/sec, sweep rate is 100 mV/sec, $i_0 = 6.5 \times 10^{-5}$ A/cm², $\beta = 0.2$.

for the two reactions were made from experiments or from reported literature values. However, small changes in these values (within experimental error) allowed us to fit the curve much more closely. The parameters β and i_0 are truly unknowns. (The sensitivity of the model to the last two parameters is shown in Figures 6.3.6 and 6.3.7.) Small changes in a single parameter such as the diffusion coefficient induces changes throughout the voltammogram. Thus, to obtain a quantitative understanding of the sensitivity to all of these parameters, a multi-variable regression analysis should be conducted. However, because the model includes several simplifying assumptions, (migration and convection effects are neglected, for example), the work is probably not warranted.

Another assumption in the model is the equality of all diffusion coefficients. It can be seen in Figure 6.6.2 that this is not a severe restriction. As noted in section 6.5, the diffusion coefficient of iodide is probably twice the diffusion coefficient of triiodide.

Simulated Sweep Rate Behavior

Figures 6.6.3 and 6.6.4 show the model simulation of the experiments given in figures 6.4.14 and 6.4.15. An additional term was included in the model to account for the higher ohmic drop associated with experiments done in the two-compartment cell. However, because the experiment was done in a different cell than the cell used to obtain data for fitting the model parameters, the simulation does not track the experimental curves exactly. In spite of this drawback, the model qualitatively describes the the shape of the voltammograms including the cathodic shift of peak I'.

In conclusion, by comparing the experimental cyclic voltammograms to computer-generated simulations, we find that the data are fit best by a model which is based on the assumption that reaction I follows Butler-Volmer electrochemical kinetics and that reaction II is reversible.

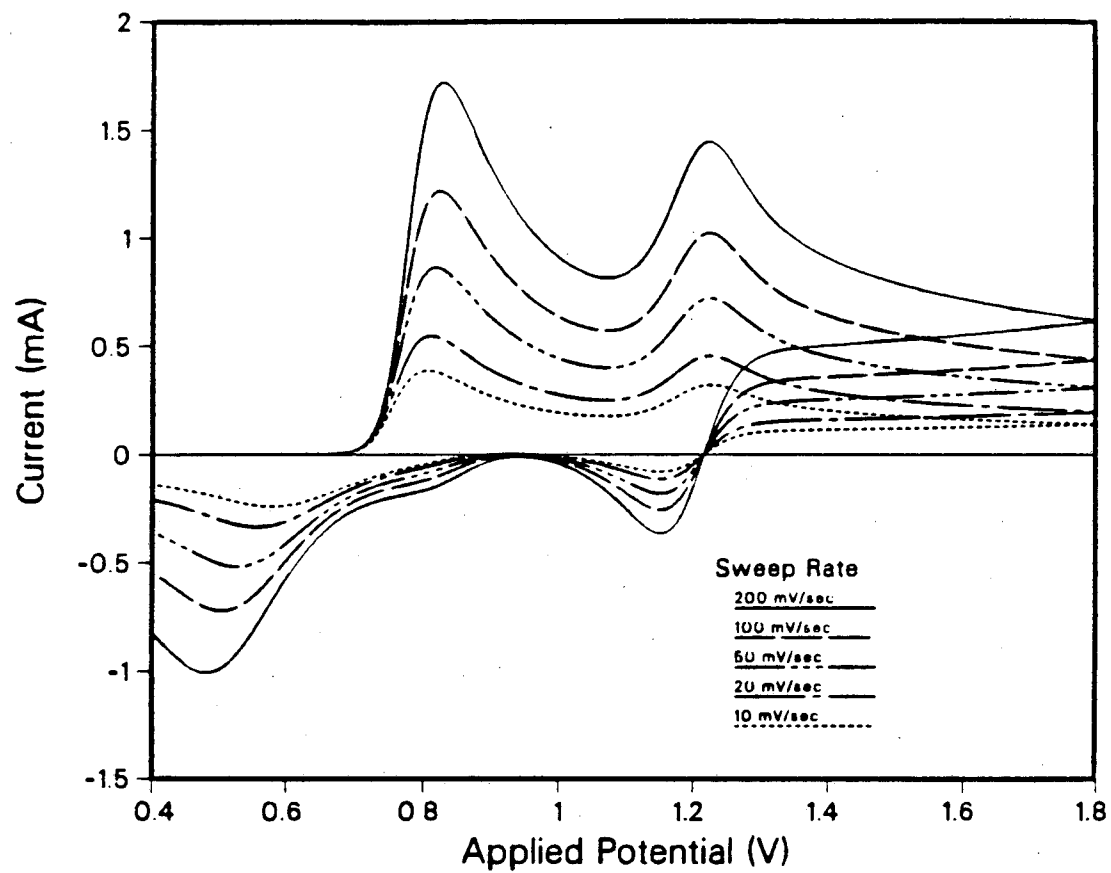


Figure 6.6.3 Simulation of Figure 6.4.14 and 6.4.15 using model III. Parameters are given in Figure 6.6.2.

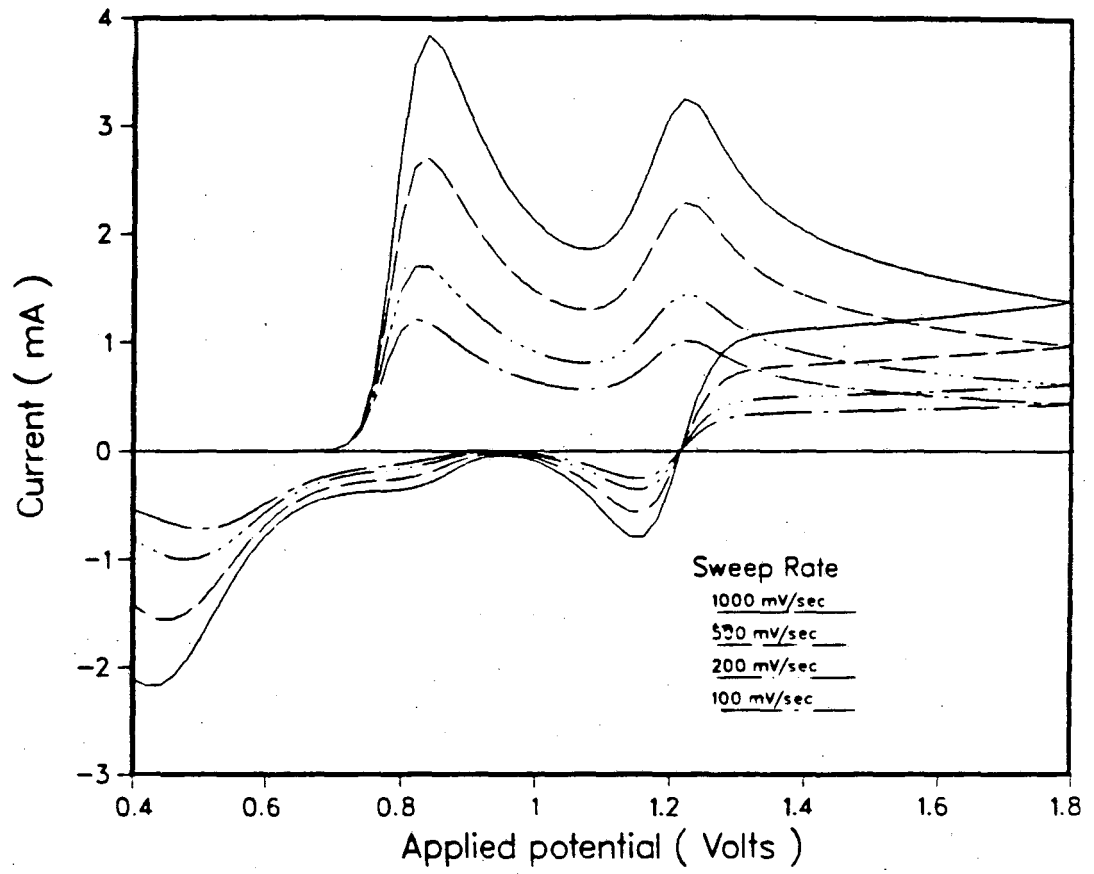


Figure 6.6.4 Simulation of Figures 6.4.14 and 6.4.15 using model III. Parameters are given in Figure 6.6.2.

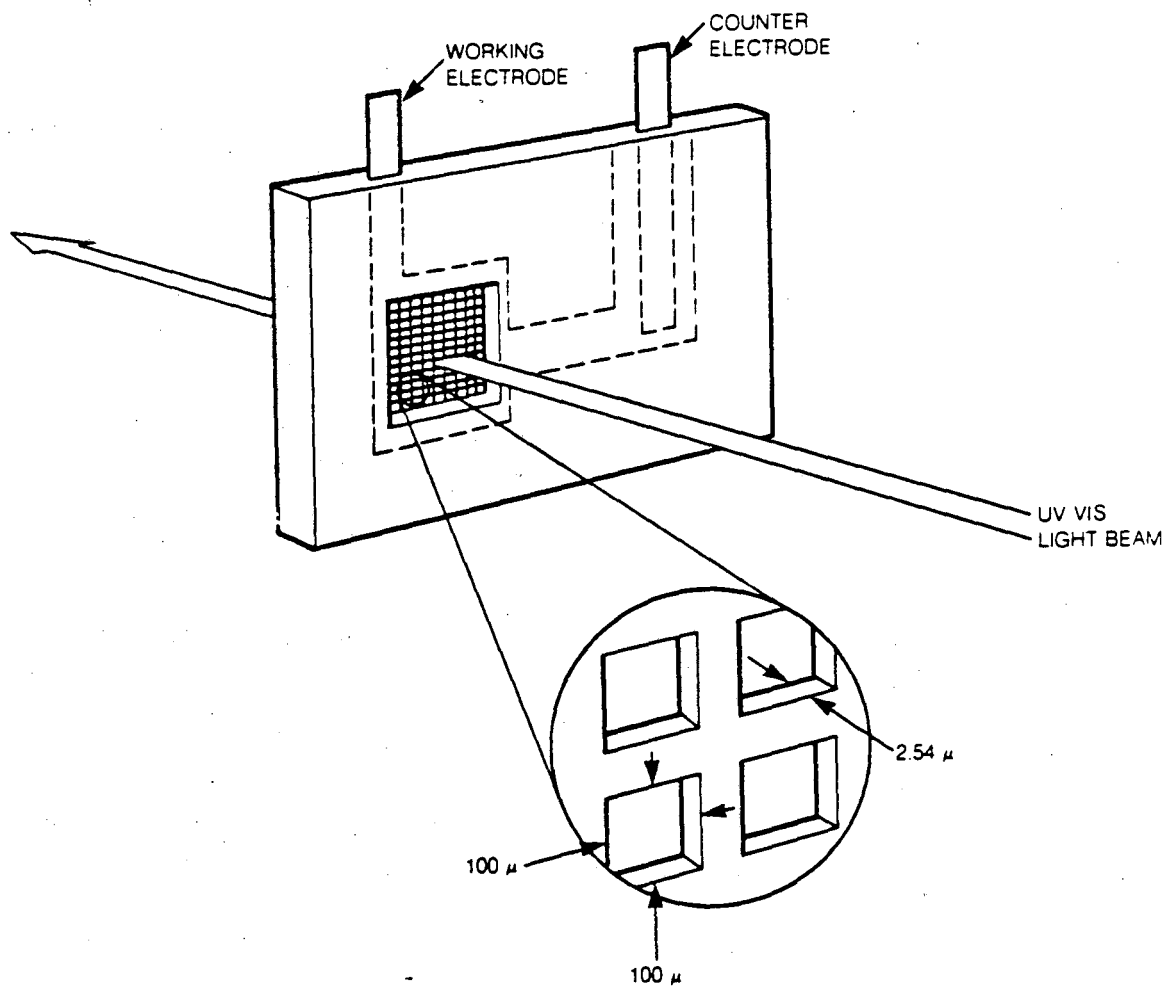
6.7. SPECTRAL ELECTROCHEMICAL EXPERIMENTS

In conventional cyclic voltammetry experiments, the identity of the reaction products is inferred from the position of the half-wave potential, the number of electrons transferred, and the stoichiometry of the reaction. If the reaction products or reactants are active in the UV-visible range, spectral electrochemical techniques can be used to track the course of reaction and directly identify the products. In this case an optically transparent, thin-layer electrode placed in the beam of a fast scanning spectrophotometer is used to provide spectral information about the electrochemical products as a function of applied potential. Thus, the electrode reaction is monitored simultaneously via the electrode current (as in a normal cyclic voltammetry experiment) and by the UV-visible spectra. The goal of this set of experiments is to qualitatively confirm the reaction mechanism of the oxidation of iodide in PC that was derived from the cyclic voltammetry experiments.

The technique was developed by by Hawkridge [64], and others [65] to combine the advantages of thin layer electrochemistry (such as quantitative conversion of reactants to products) with the benefit of an in-situ detection technique.

Thin-layer electrochemistry is performed in cells in which the reactant is confined to a thin layer at the surface of the electrode. Several reviews of this technique have been published [66], [67]. Because the goal of these experiments was solely to identify the reaction products, this technique was not used to its full capability.

A schematic drawing of the experiment is given in Figure 6.7.1. The counter and reference electrodes are located on the side of the working electrode. Light from the spectrophotometer is transmitted through the optically transparent working electrode to the detector. The potential at the working electrode is ramped in a sawtooth wave at a rate of 1 mV/sec. A single spectral scan is completed in one second, so the electrode potential changes by only one mV in the



XBL 845-8936

Figure 6.7.1 Schematic drawing of electrochemical cell containing optically-transparent, thin-layer electrode. The dimensions of the gold mesh electrode are shown.

time interval of one scan. Thus, each scan is essentially a "snap shot" of the solution absorbance at a given potential.

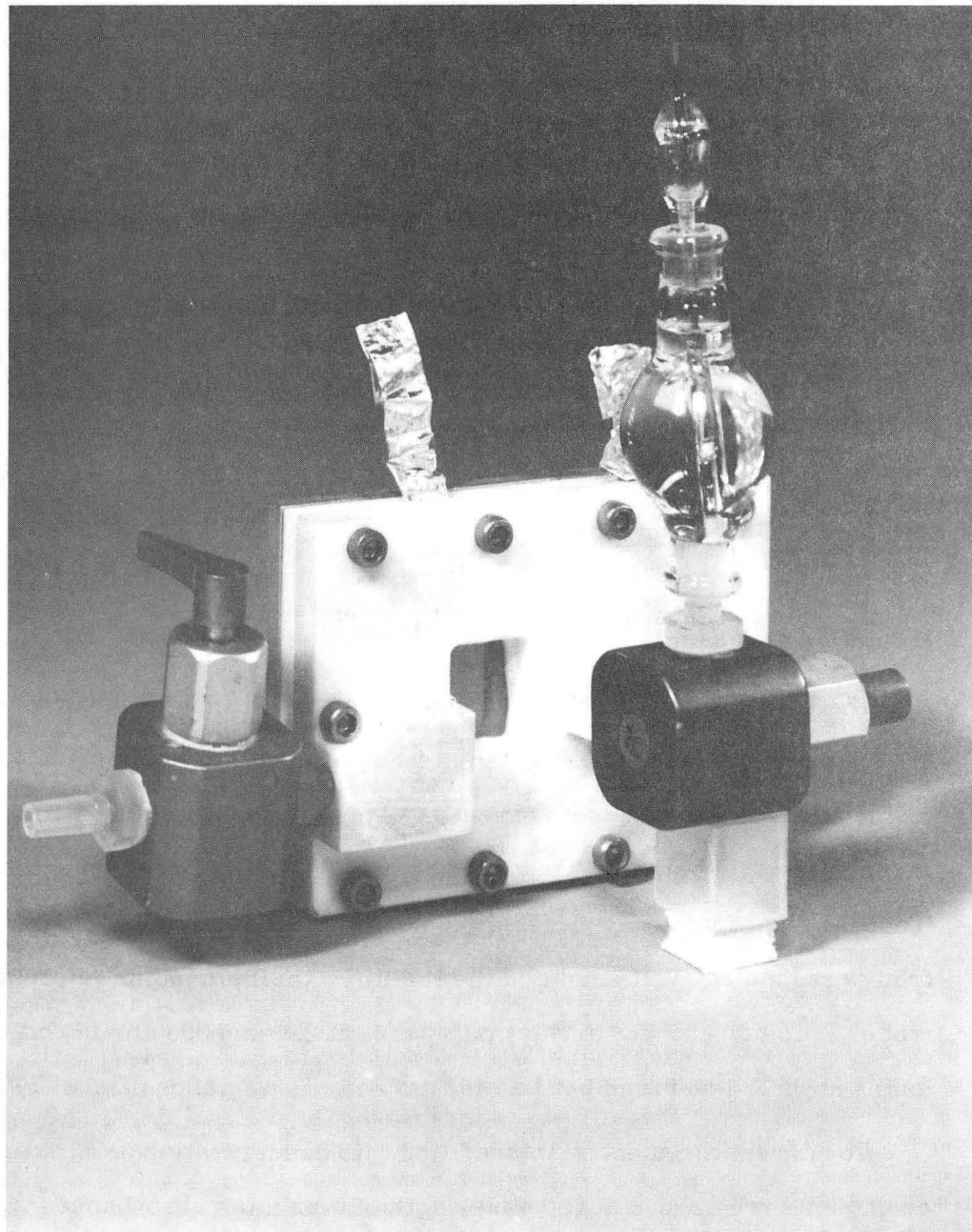
6.7.1. Experimental Methods

Cell Design

The spectral electrochemical cell was developed for experiments performed by Carol Balfe to study the electrochemistry of manganese porphyrins in acetonitrile. Details of the cell design, materials of construction, cell preparation etc. are available in her thesis.[68] The cell is pictured in Figure 6.7.2. The working electrode is a fine (200 lines/inch, 0.1 mm thick, 78% transmission) electroformed gold mesh (Buckbee-Mears Co., St. Paul, Minn.). The counter-electrode is a strip of platinum foil, located adjacent to the working electrode chamber. The reference electrode is the same couple used the cyclic voltammetry experiments: thallium amalgam/thallium iodide.

Experimental Procedure

The cell is filled in the glovebox as follows: The amalgam is first injected into a thin fritted tube and the entire assembly is fitted into a glass bulb which is separated from the working electrode chamber by a Hamilton valve. Solution is introduced into the cell using a glass pipette to fill the cell and the reference chamber with electrolyte. The cell volume is about 30 μ l. Before the cell is removed from the glovebox, a fine platinum wire into the amalgam is inserted into the reference electrode chamber, and it is sealed by closing the Hamilton valves. The wire is held in a ground glass stopper which was sealed with vacuum grease. No problems from contamination were noted during the experiments.



CBB 841-608

Figure 6.7.2 Experimental cell. Reference electrode is contained in the bulb.

The cell was calibrated using Methyl Red Dye in an acidic propylene carbonate solution[69]. From these measurements, the path length for the gold minigrid electrode is 0.007 cm.

The electrochemical instrumentation was the same as that described in section 6.4.1. A Hewlett-Packard Model HP 8450 UV/visible spectrophotometer interfaced to an XY plotter (HP model 7225B) and a flexible disc drive (HP model 82901M) was used to measure, record and store spectra. A Data Precision model 3500 digital volt-ohm meter was used to monitor the potential between the reference and working electrode.

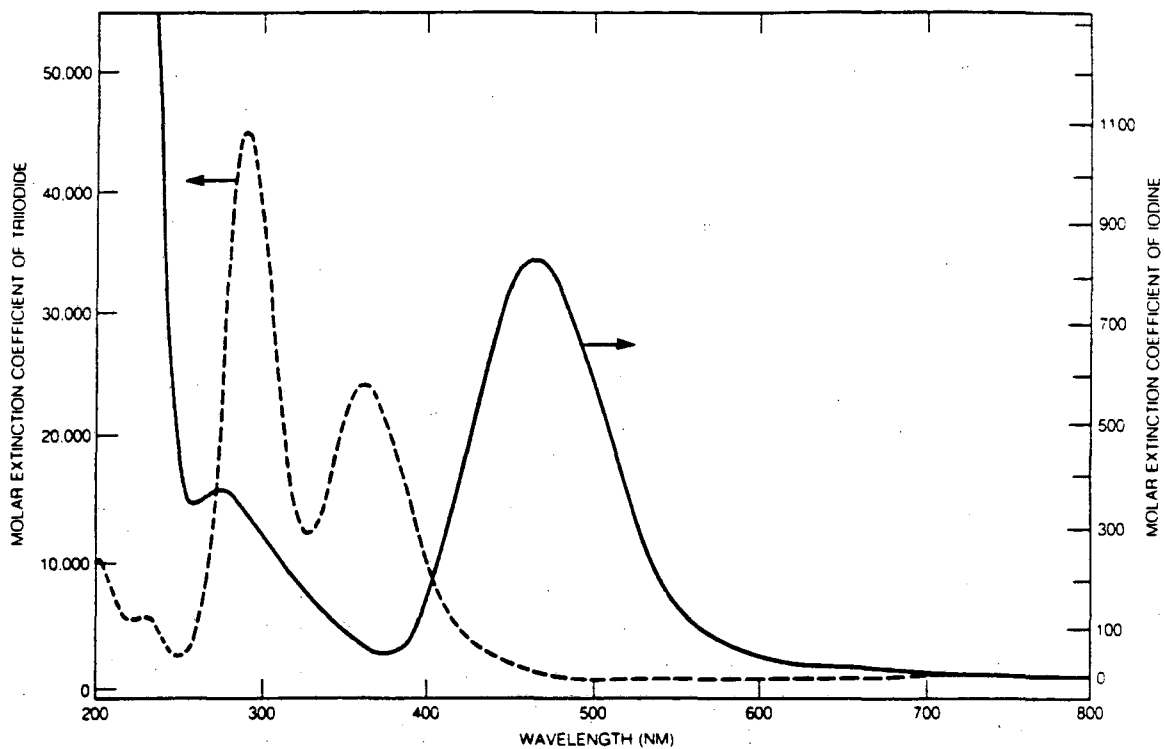
Extinction Coefficients

The UV-visible absorption of triiodide and iodine in PC is shown in Figure 6.7.3. The triiodide spectrum is taken from a solution of equimolar 2×10^{-4} F iodine and KI in PC. The iodine spectrum is for a solution of 0.15 F iodine in PC, taken in the thin layer cell described above. To eliminate any triiodide formed from the disproportionation reaction of iodine (see section 3.3) the working electrode was held at 1 volt anodic of the thallium/thallium iodide reference electrode. Triiodide absorbs in two sharp peaks at 292 and 363 nm. In contrast, iodine absorbs in a broad band at 462 nm and has a smaller band at 290 nm.

To convert the spectral information into concentration data, extinction coefficients are needed at the wavelength of maximum absorbance (λ_{\max} for each species. This information, along with the path length of the cell specifies the concentration as a function of absorbance according to Beer's Law,

$$\text{Absorbance} = \epsilon l C$$

where ϵ is the extinction coefficient, "C" is the concentration, and "l" refers to the path length of the cell. The extinction coefficient information was compiled in connection with the study of PC stability in the presence of iodine (Johnson[70]) and the details are presented elsewhere.



XBL 845-8938

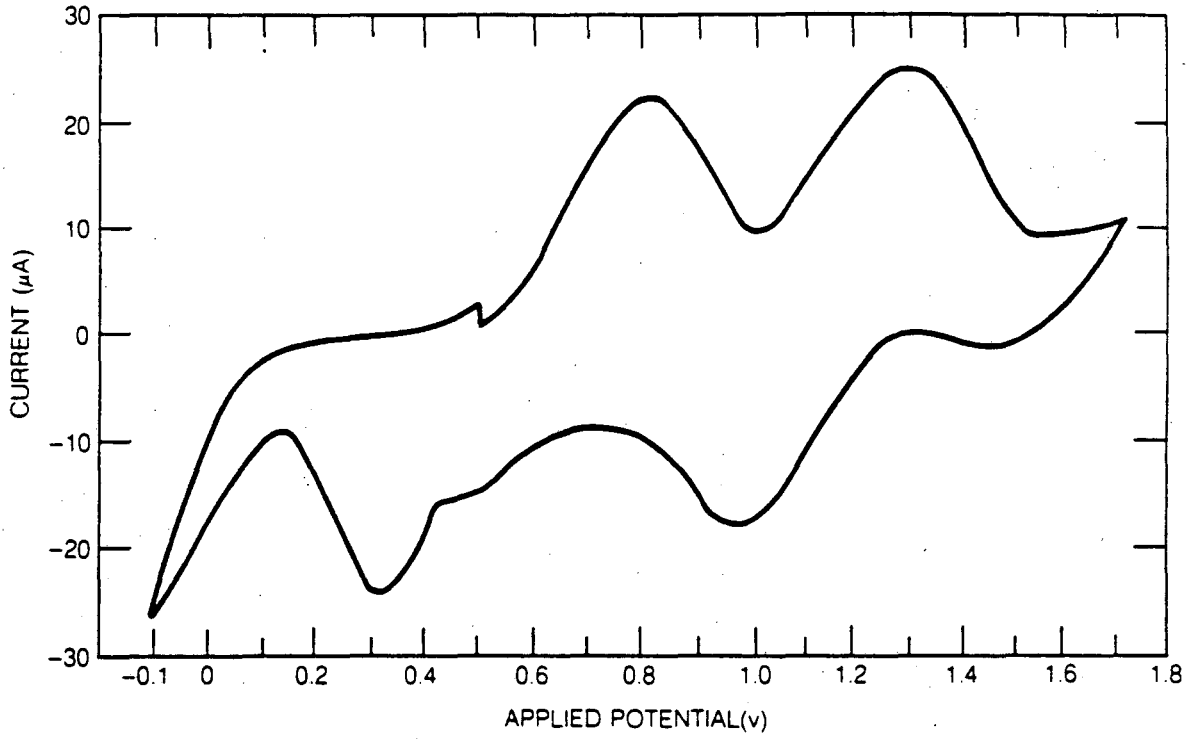
Figure 6.7.3 UV-visible absorption spectra of triiodide and iodine in PC. Triiodide solution: equimolar (2×10^{-4} M) iodide and iodine. Iodine solution: 0.15 M. From reference [69].

A compilation of extinction coefficients from Johnson is presented in Table 6.7.1. Triiodide absorbs very strongly in the visible range, with extinction coefficients of 24,000 and 44,000 at 363 nm and 292 nm, respectively. For example, at 292 nm concentrations as low as 5×10^{-6} M triiodide can be detected in a 1.0 cm cuvette. In contrast, because the extinction coefficients of iodine are low, this technique is relatively insensitive to iodine concentration.

Table 6.7.1 λ_{\max} and Extinction Coefficients for Iodine and Triiodide in Propylene Carbonate at 25° C		
Molecule	ϵ , l/mole-cm	λ_{\max} , nm
Iodine	837 (462 nm) 59 (363 nm) 315 (293 nm)	462
Triiodide	1053 (462 nm) 24091 (363 nm) 44881 (293 nm)	363, 293

6.7.2. Results

Figure 6.7.4 shows the cyclic voltammetry scan for the oxidation of 6.7×10^{-3} M KI and 0.5 M KAsF_6 in PC at 1 mV/sec. The potential sweep is initiated at 0.5 V (approximately open circuit potential), switches from anodic to cathodic at 1.7 V, and switches from cathodic to anodic at -0.1 V. Despite the fact that the cell geometry is completely different, the shape of the voltammogram is qualitatively the same as the corresponding conventional CV experiment reported in section 6.4. The shape of the cathodic voltammogram is altered by spurious background reactions probably due to reduction of gold compounds formed



XBL 845-8939

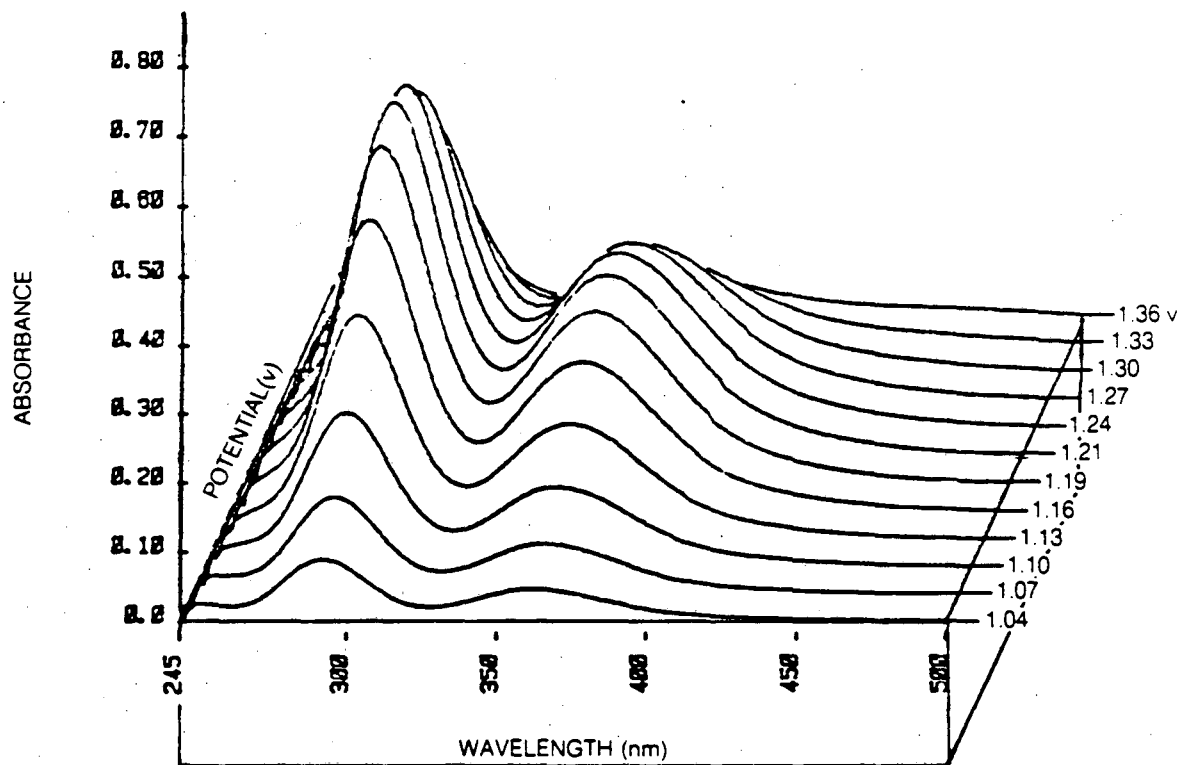
Figure 6.7.4 Voltammetry scan of iodide solution (6.7×10^{-3} M KI, 0.5 M KAsF_6 in PC) taken in thin cell.

by reaction with iodine. The presence of these side reactions suggests that a platinum electrode would be a preferable electrode material for quantitative studies. However, since the goal of this experiment is to qualitatively confirm the chemical species present as a function of potential, these side reactions do not interfere.

The results of the experiment are presented in the form of a series of spectral scans taken at 30 second (or 30 mV) intervals throughout the potential sweep. The first sweep, taken at open circuit, was stored and automatically subtracted from all subsequent scans. The results are most clearly demonstrated in a three dimensional plot of absorbance as a function of wavelength and potential. Contour lines on Figure 6.7.5 show the appearance and disappearance of triiodide during the anodic sweep from 1.04 V to 1.33 V.

A complete set of spectra for the entire voltammetric sweep is given in Figures 6.7.6 to 6.7.14. Figure 6.7.6 shows the first portion of the anodic sweep. Except for a negative peak which corresponds to the disappearance of iodide (at 230 nm), little activity is observed until the potential reaches almost 1 V. From 1.03 to 1.34 V the triiodide absorbance increases monotonically with each scan, showing a maximum at 1.24 V. From this point to the end of the anodic sweep the triiodide absorbance decreases, as shown in Figures 6.7.7 and 6.7.8. This behavior is consistent with the oxidation of triiodide to iodine in this potential range.

The behavior of the iodine as a function of potential can be seen using a more sensitive absorbance scale. Figures 6.7.8 and 6.7.9 show the development of the iodine peak from a shoulder of the triiodide peak at 1.37 V to a single large broad peak at 1.7 V, corresponding to the conversion of triiodide to iodine. Unfortunately, the extinction coefficient of triiodide at 462 nm is of the same order of magnitude as that of iodine so the iodine variation is not directly apparent. To follow the change in concentration of iodine, the absorbance due



XBL 845-8949

Figure 6.7.5 UV-visible spectra from 1.04 V to 1.36 V. Anodic sweep.

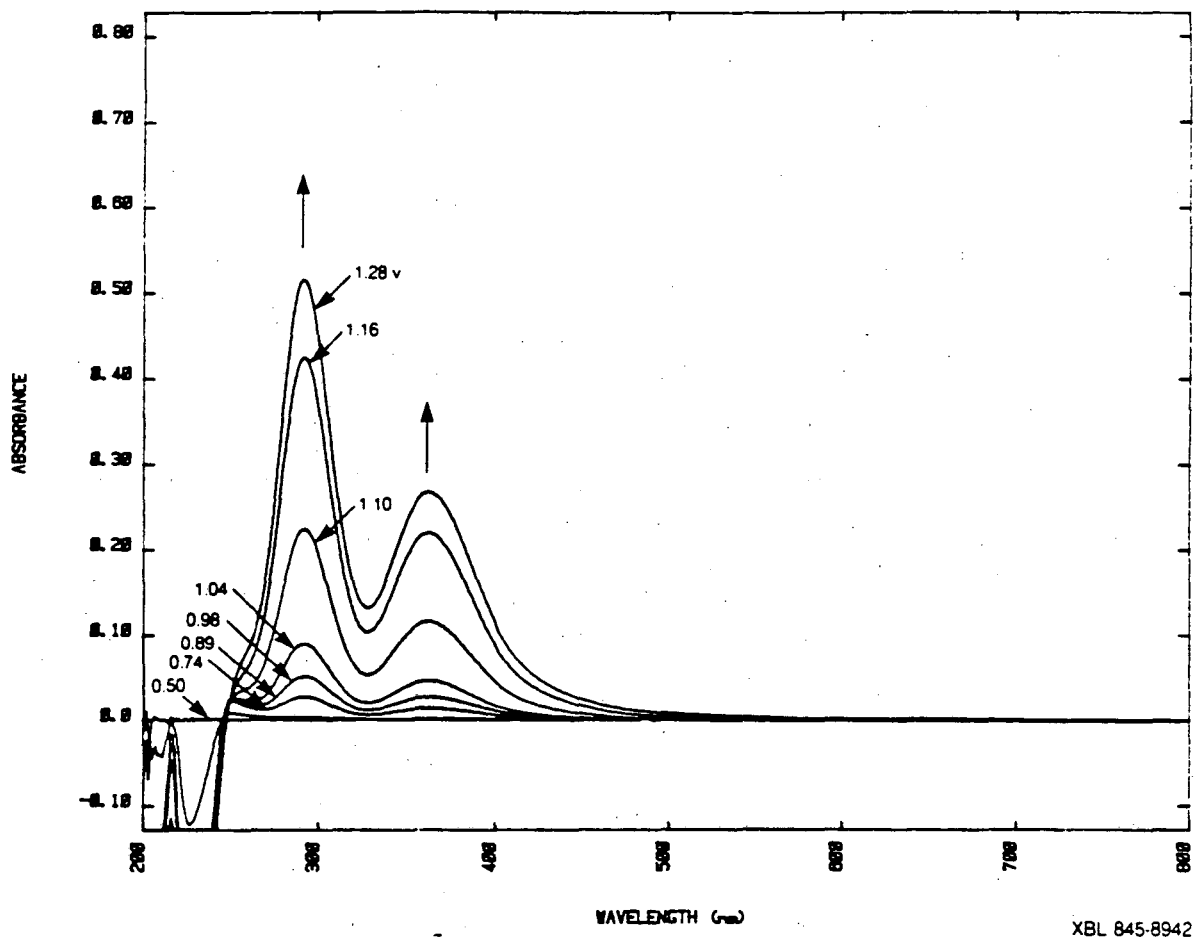


Figure 6.7.6 UV-visible spectra from 0.5 V to 1.28 V. Anodic sweep.

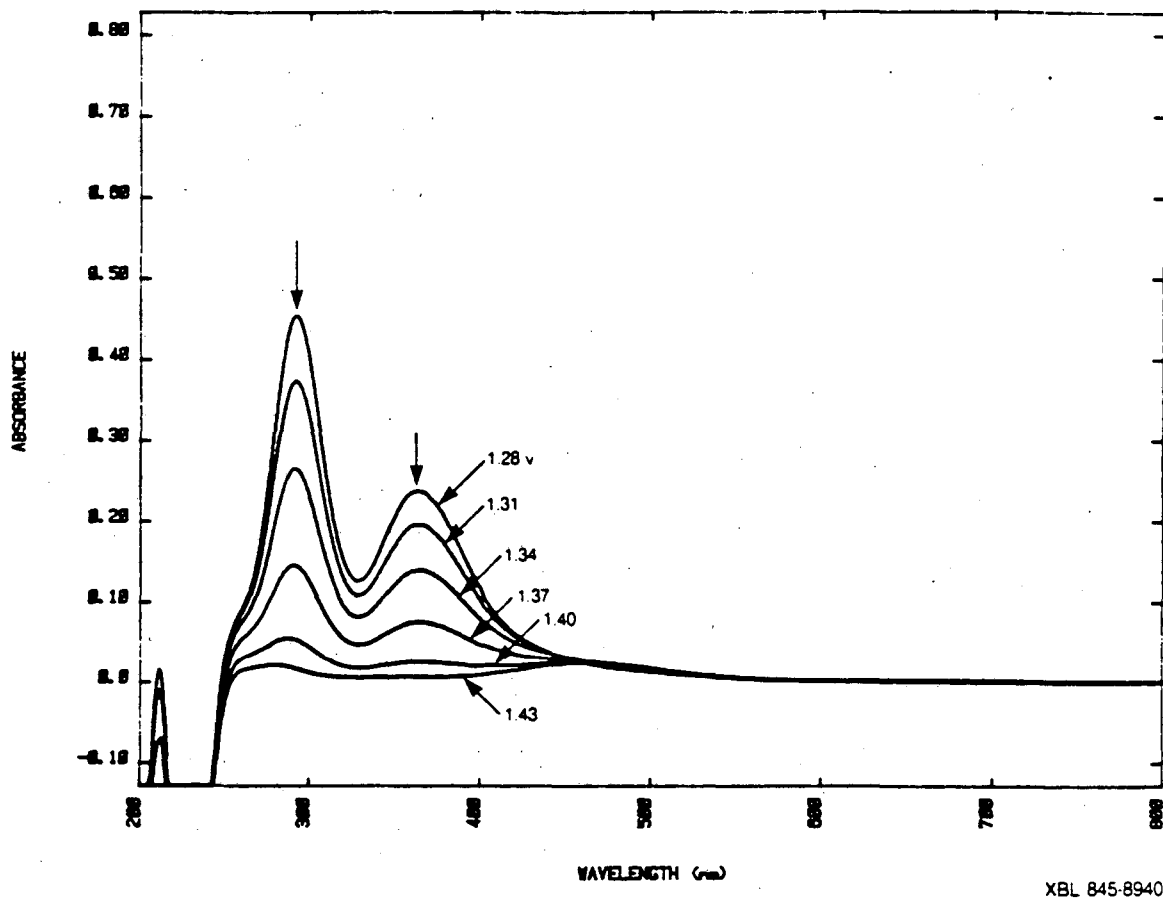


Figure 6.7.7 UV-visible spectra from 1.28 to 1.43 V. Anodic sweep.

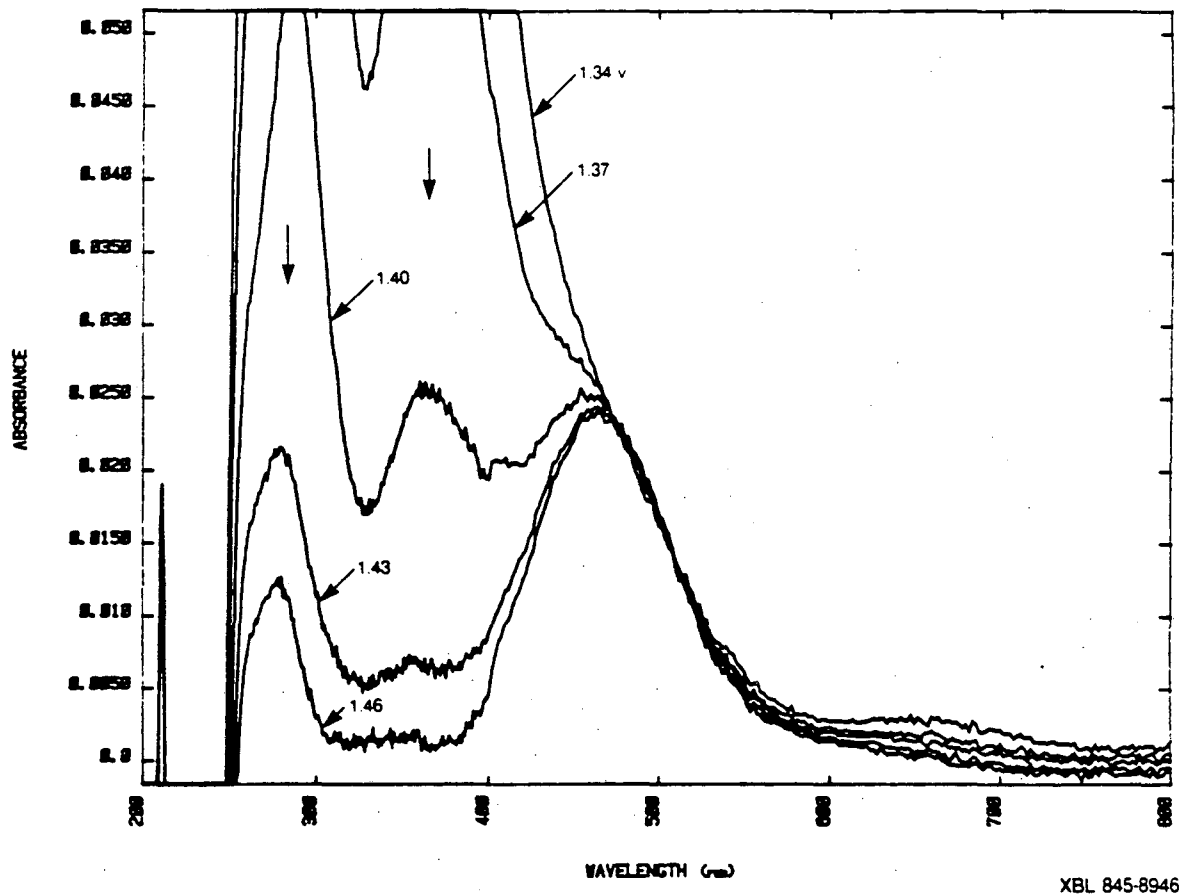


Figure 6.7.8 UV-visible spectra from 1.34 to 1.46 V. Anodic sweep.

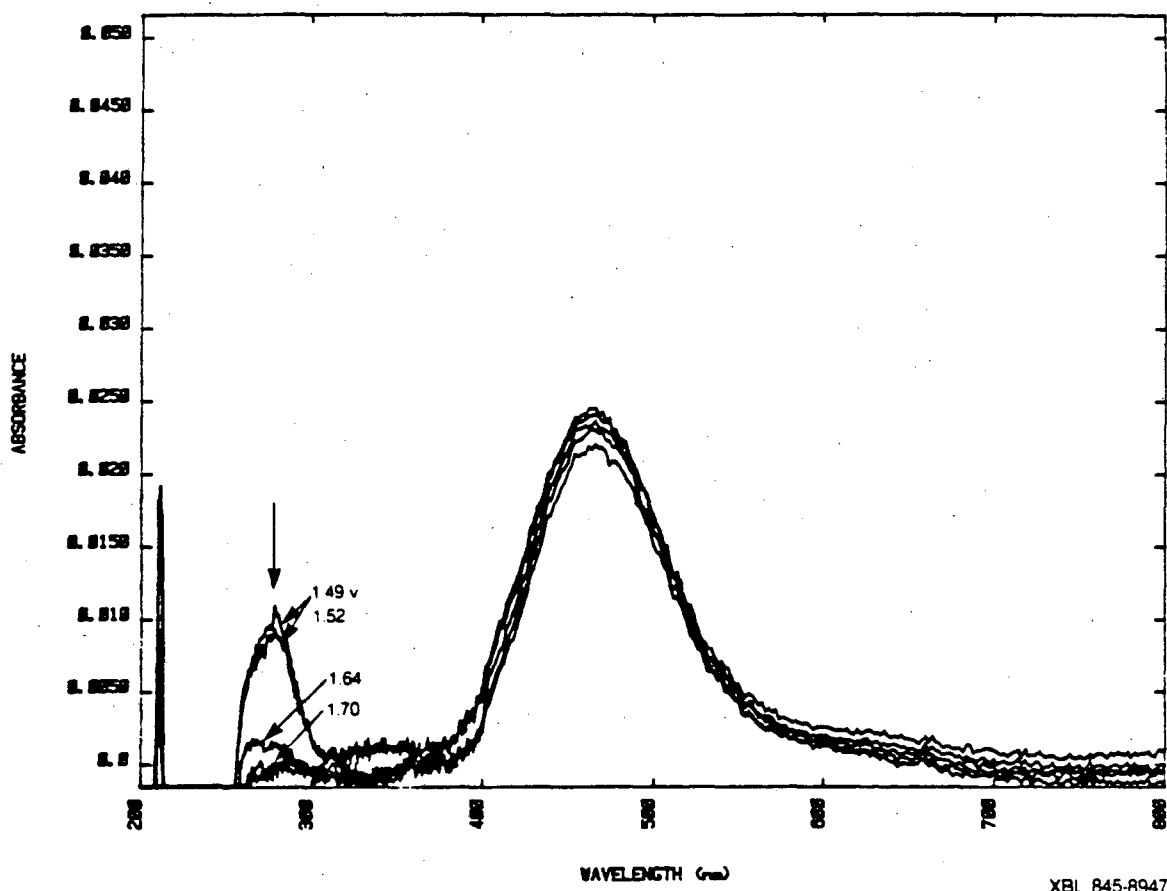


Figure 6.7.9 UV-visible spectra from 1.49 to 1.70 V. Anodic sweep.

to triiodide must be subtracted.

The reverse of the anodic scan is observed for the cathodic sweep. In Figures 6.7.10 and 6.7.11 the triiodide concentration increases for the portion of the voltage sweep between 1.46 and 0.89 V. Then as the triiodide is reduced to form iodide, from 0.86 V to 0.26 V, the triiodide peaks successively decrease (see Figure 6.7.12 and 6.7.13) until only absorbances characteristic of iodide appear at the end of the sweep (Figure 6.7.14).

The information presented above is summarized in Figure 6.7.15 in a plot of the fractional conversion iodide to triiodide and iodine as a function of time (or potential) throughout a single sweep of the cyclic voltammetry experiment. The fractional conversion is defined as the concentration of the iodine species divided by the concentration for 100% conversion to that species. Thus,

$$\text{Fractional Conversion of } I_3^- = \frac{[C_{I_3^-}]}{3[C^*]}$$

$$\text{Fractional Conversion of } I_2 = \frac{[C_{I_2}]}{2[C^*]}$$

where C^* is the initial concentration of iodide. The concentration of iodine is calculated by subtracting the contribution of triiodide at 462 nm. This figure illustrates the concentration changes during the course of the reaction as triiodide is first formed from the oxidation of iodide, then oxidized to produce iodine. When the potential sweep reverses, the iodine is reduced back to triiodide which is, in turn, reduced to iodide. The slight dip in iodine concentration at 1.7 V is probably due to the corrosion of the gold electrode by iodine.

In conclusion, the use of simultaneous cyclic voltammetry and UV-visible spectroscopy has been demonstrated for the iodide/triiodide/iodine system in propylene carbonate. The results of these spectral electrochemical experiments clearly confirm the chemical reaction mechanism postulated from the cyclic voltammetry experiments described in section 6.4.2.

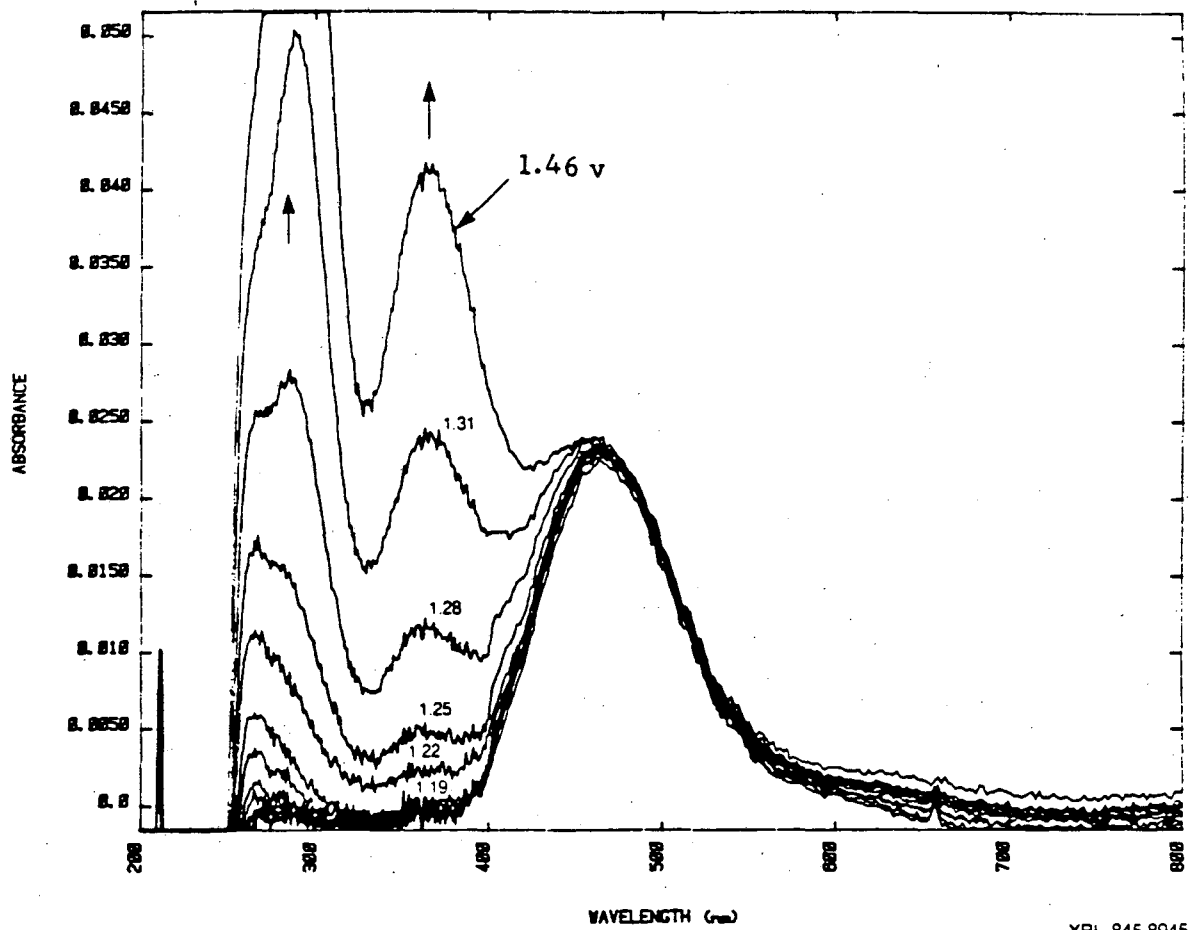


Figure 6.7.10 UV-visible spectra from 1.46 to 1.19 V. Cathodic sweep.

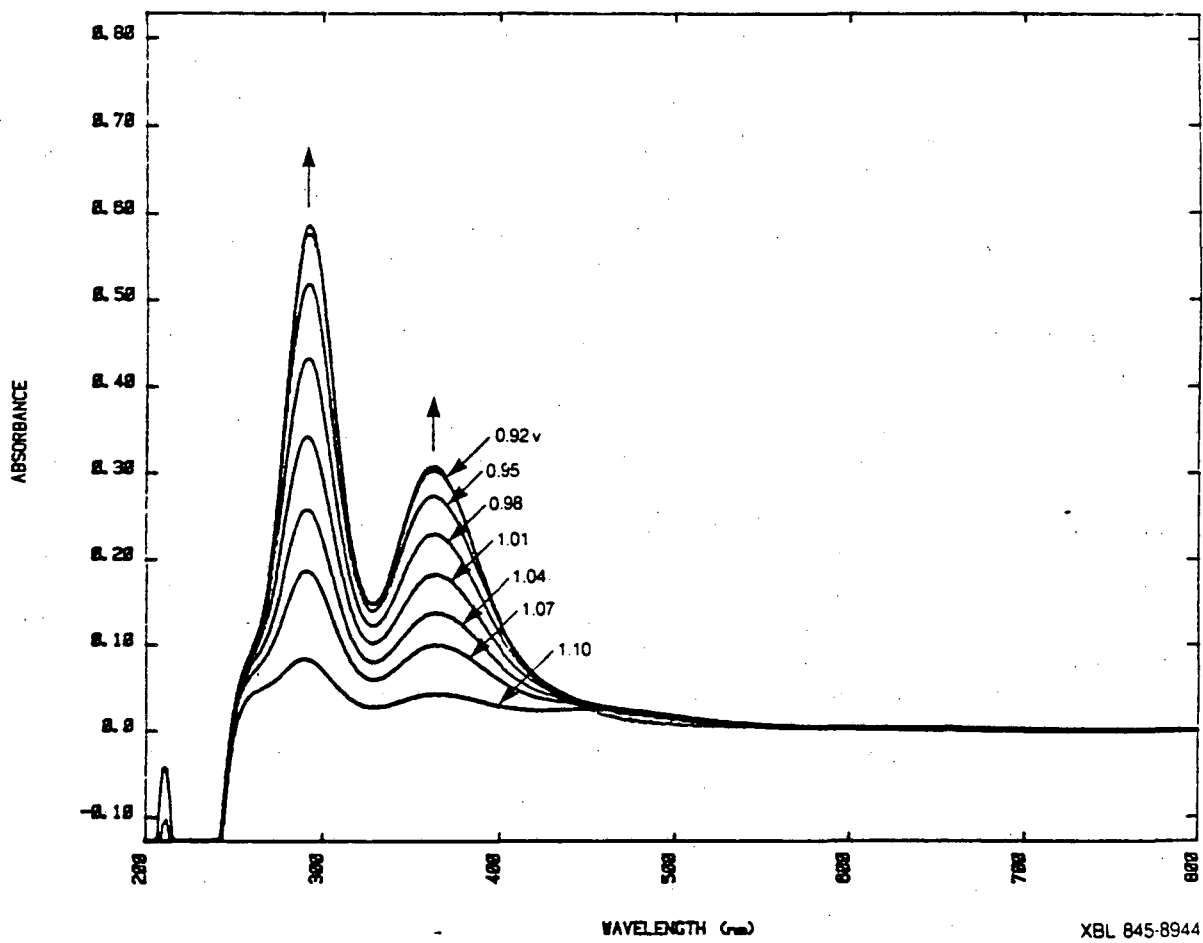


Figure 6.7.11 UV-visible spectra from 1.10 to 0.92 V. Cathodic sweep.

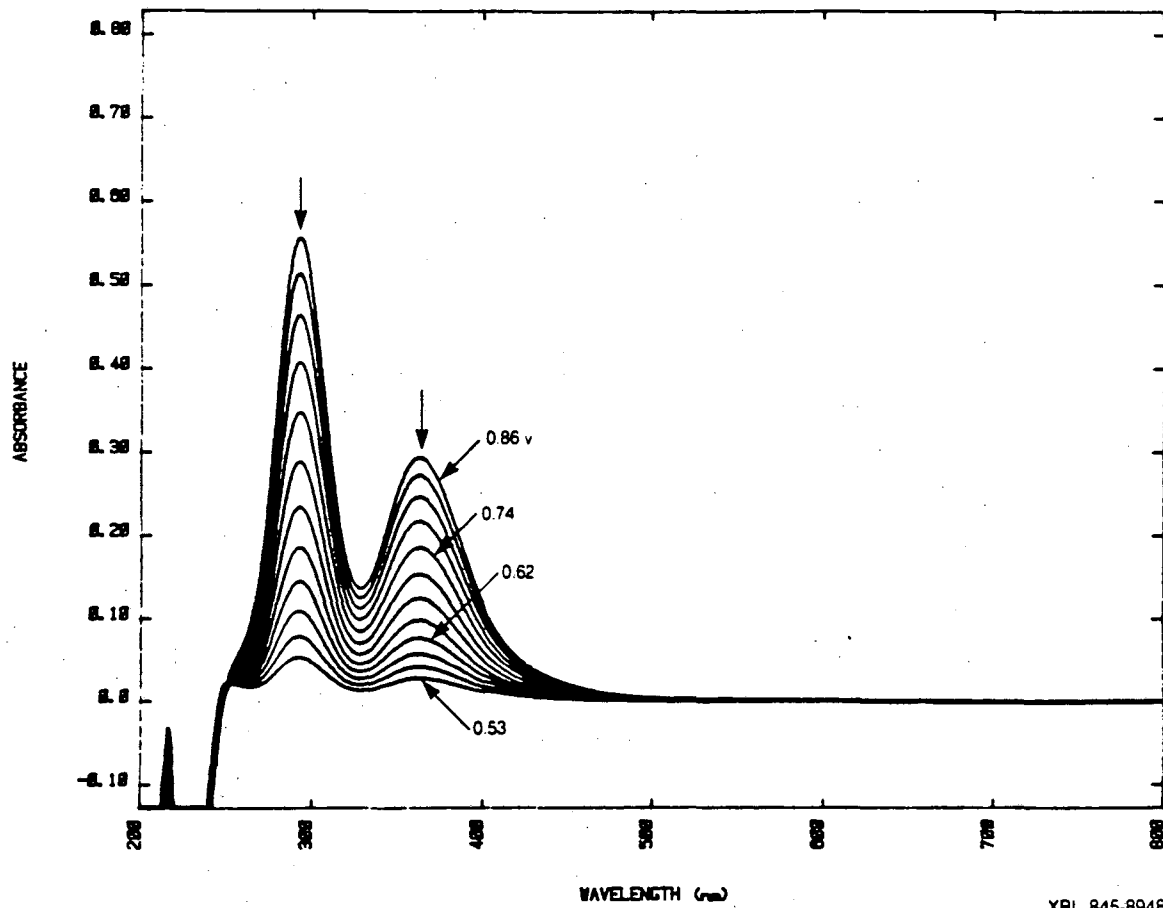


Figure 6.7.12 UV-visible spectra from 0.86 to 0.53 V. Cathodic sweep.

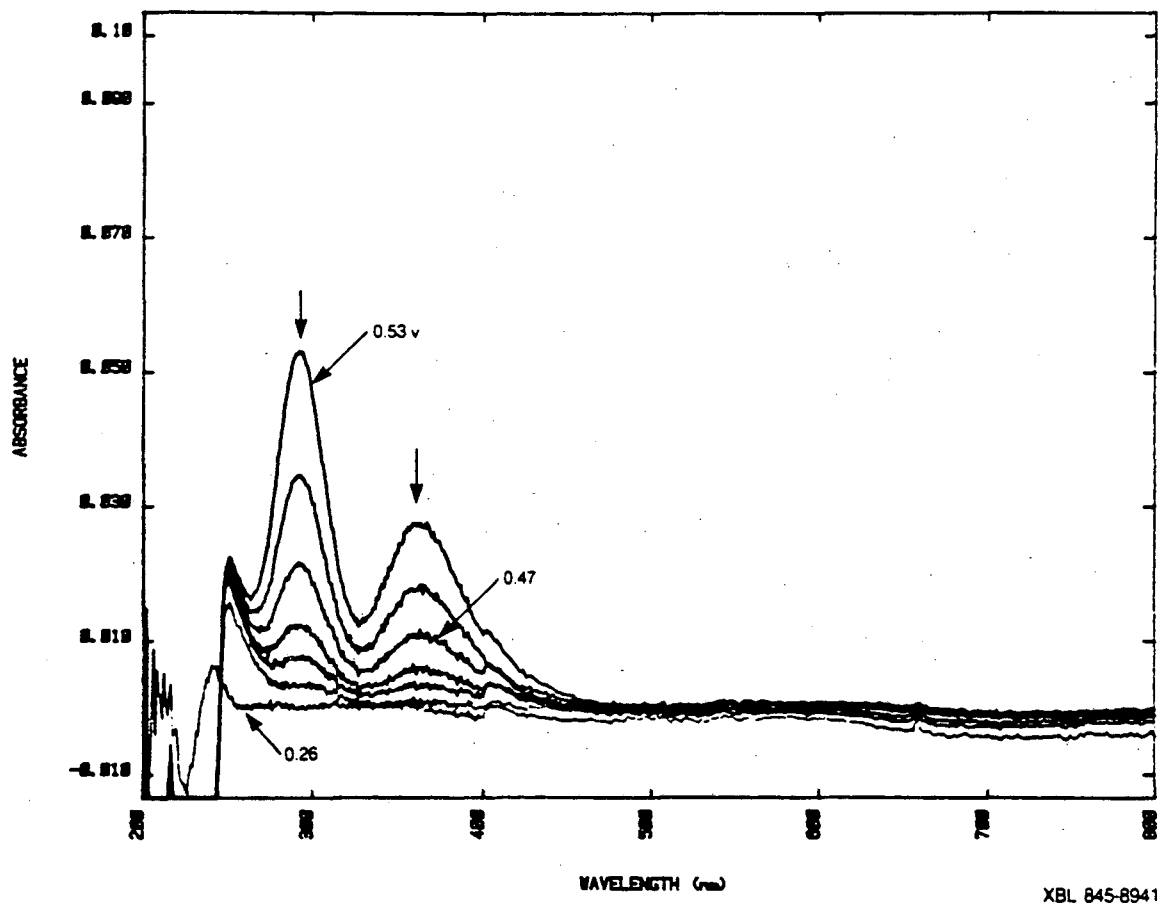


Figure 6.7.13 UV-visible spectra from 0.53 to 0.26 V. Cathodic sweep.

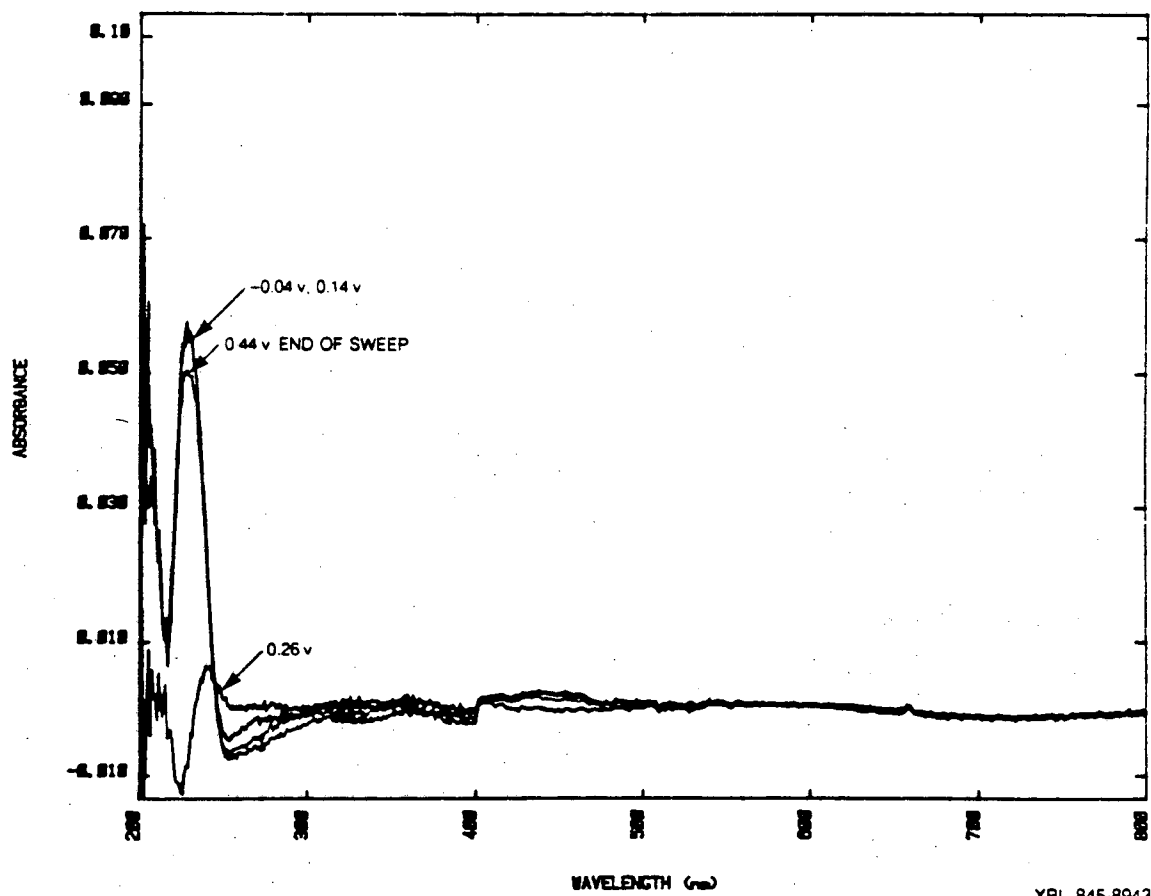
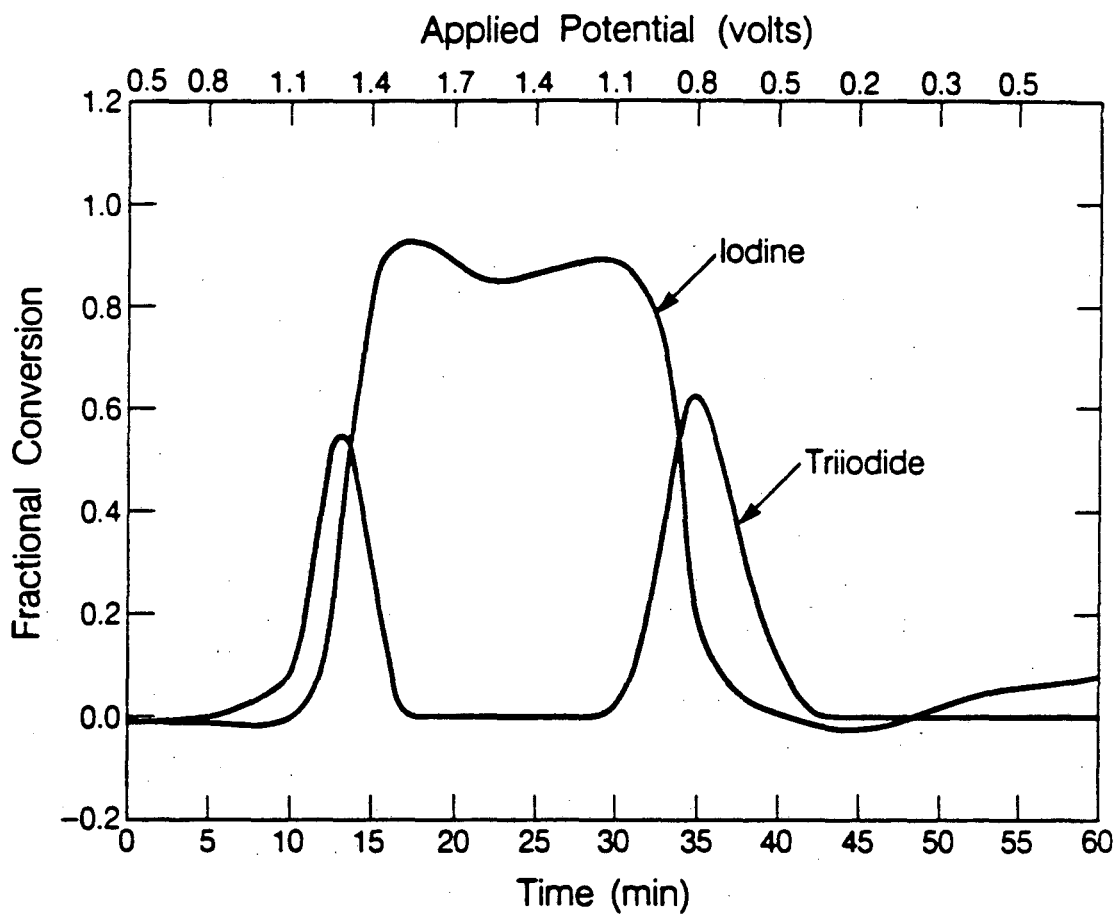


Figure 6.7.14 UV-visible spectra from 0.26 to -0.04 V. Cathodic sweep.
UV-visible spectra from -0.04 to 0.44 V. Anodic sweep.



XBL 846-7162

Figure 6.7.15 Fractional conversion of iodide to triiodide and iodine during a single voltammetry scan. Data are from Figures 6.7.6 to 6.7.14.

6.8. DISCUSSION

The results of the cyclic voltammetry experiments indicate that the first oxidation peak (peak I) is irreversible and the second peak (peak II) is reversible. It is interesting to consider the reasons for these conclusions and to attempt to rationalize the values of the parameters derived in terms of a physical understanding of the process. Consider the two peaks representing the iodide/triiodide redox pair. From fitting the simulated voltammograms to the experimental data, we obtain values of 0.2 and $6.5 \times 10^{-5} \text{A/cm}^2$ for β and $i_{o,ref}$ respectively. Obviously the oxidation of iodide to triiodide involves the formation of two covalent bonds between three atoms. This is a relatively complicated process and yet it occurs rapidly (relative to diffusion) on the electrode surface at sweep rates exceeding 200 mV/sec. Similarly, the reduction of triiodide to three iodide ions must involve breaking two I-I bonds. Since β represents the fraction of the surface overpotential that promotes the cathodic reaction, this process is evidently much more difficult. The fact that a single Butler-Volmer kinetic expression can successfully be used to model both the oxidation and reduction peaks indicates that the rate determining step is probably the same for the forward and reverse reaction.

From literature on the electrochemistry of iodide oxidation on platinum and from consideration of the solvation states of the three species involved, a physical picture of the reaction sequence begins to emerge. Literature studies clearly show that the surface of platinum is covered with an adsorbed layer of iodine and triiodide. Using the technique of thin layer chronopotentiometry, Hubbard, Osteryoung and Anson [71] have shown that about 2×10^{-9} moles/cm² of iodide ion or iodine are adsorbed onto platinum. This adsorbed layer is not electroactive; *i.e.*, it cannot be detected by reduction or oxidation near the reversible iodide/iodine potential. An additional 1×10^{-9} moles per square cm of iodine, but not iodide, are adsorbed in an electroactive state. This adsorbed layer is the

likely reason for the disparity in forward and reverse reaction rates for this peak. In the anodic direction, the reactant and products are strongly adsorbed to the platinum surface and charge transfer is not impeded. In the cathodic direction, the triiodide has to be reduced at an iodine covered surface. Therefore, the large cathodic overpotential may be a measure of the additional energy required to overcome the adsorption energy of iodine, $\Delta G_{\text{adsorption}}$.

The effect of adsorption on the location of a voltammetry wave is analogous to the effect of complex formation of the reactant or product. Examples of this kind are well-known in the polarographic literature. Bard and Faulkner[72] show the effect of complexation of a metal ion, for example. In this case the complexation stabilizes the oxidized form of the ion which raises the free energy for reduction. The stronger the complex, the larger is the shift away from the free metal potential.

In view of the complexity of the reaction system, cyclic voltammetry experiments are only a beginning step to understanding the details of the kinetics. Rotating ring-disc experiments to detect triiodide at the ring, or pulse techniques are more controlled experiments which could provide a greater insight into the reaction mechanism.

6.9. CONCLUSIONS

In summary, the electrochemical behavior of the iodide/triiodide/iodine system was investigated in propylene carbonate using the technique of cyclic voltammetry. We found that iodide is oxidized in two electrochemical steps; triiodide is formed first and then the oxidation proceeds to iodine. A mathematical model was developed to describe the kinetics of the two electrochemical steps and the transport of the three species involved. Simulated voltammograms based upon this model correctly predict the experimental results up to sweep rates of 200 mV/sec. Spectral electrochemical experiments confirm the proposed mechanism.

REFERENCES

- [1] R. Iwamoto *Anal Chem* 31, 955, (1959).
- [2] E. Rengevich, and E. Shilov, *Ukr. Khim. Zh.*, 28, 1080 (1962).
- [3] A. D. Awtry, and R. E. Connick, *J. Amer. Chem. Soc.*, 73, 1842, (1951).
- [4] G. Daniele, *Gazz. Chim. Ital.*, 90, 1068, (1960).
- [5] R. W. Ramette, and R. W. Sandford, *J. Amer. Chem. Soc.*, 77, 5001, (1965).
- [6] W. C. Bray, and C. M. MacKay, *ibid*, 32, 914, (1910).
- [7] J. D. Burger and H. A. Liebhafsky, *Anal. Chem.*, 45, 800, (1973).
- [8] A. Haddock, M. Steidemann, and M. Readnour, *Synth. React. Inorg. Met.-Org. Chem.*, 9 (1) 39, (1979).
- [9] R. W. Ramette, *op. cit.*
- [10] E. C. Toren and C. P. Driscoll, *Anal. Chem.*, 38, 692, (1966).
- [11] W. C. Bray et. al. *op. cit.*
- [12] I. M. Kolthoff, J. F. Coetzee, *J. Amer. Chem. Soc.*, 79, 1852, (1957).
- [13] A. Popov, and D. Geske, *J. Amer. Chem. Soc.*, 80, 1340, (1958).
- [14] J. Desbarres, *Soc. Chim. 5th Serie, Memoirs*, (1961).
- [15] M. Mastragostino, G. Casalbore, and S. Valcher, *Electroanal. Chem. Interfac. Electrochem.*, 44, 37, (1973).
- [16] M. Mostragastino, G. Casalbore and S. Valcher, *Electroanal. & Interfac. Electrochem.*, 48, 419, (1973).
- [17] J. M. Nigretto, and M. Jozefowicz, in *The Chemistry of Nonaqueous Solvents*, vol VA ed. J.J. Lagoqski, Academic Press, Inc. NY, NY, 1978.
- [18] J. M. Nigretto, and M. Jozefowicz, *Electrochim. Acta*. 19, 809, (1974).
- [19] J. Courtot and M. L'Her, *C.R.Acad.Sc.Paris 266 Serie C* 1286, (1968).
- [20] R. Jasinski, in "Advances in Electrochemistry and Electrochemical

- Engineering", P. Delahay and C. W. Tobias, ed, Vol. 8, p. 289, Wiley-Interscience, (1971).
- [21] M. L'Her, D. Morin-Bozec and J. Courtot-Coupez, *Electroanal. Chem. and Interfacial Electrochem.*, 61, 99, (1975).
- [22] R. Iwamoto, *Anal. Chem.*, 31, 5, 955 (1959).
- [23] R. Iwamota *Anal. Chem.*, *op. cit.*
- [24] I. Nelson and R. Iwamoto, *J. Electroanal. Chem.*, 7, 218, (1964).
- [25] Alexander, Ko, Mac, and Parker, *J. Amer. Chem. Soc.*, 89, 15, 3703 (1967).
- [26] R. Nakata, S. Okazaki, and T. Fujinaga, *J. Electroanal. Chem.*, 125, 413, (1981).
- [27] L. A. Matheson, N. Nichols, *Trans. Electrochem. Soc.*, 73, 193 (1938).
- [28] J. E. Randles, *Trans. Faraday Soc.*, 44, 327 (1948).
- [29] A. Sevcik, *Collection Czechoslov. Chem. Commun.*, 13 193 (1938).
- [30] P. Delahay, *J. Am. Chem. Soc.* 75 1190 (1953).
- [31] H. Matsuda, and Y. Ayabe, *Z. Elektrochem.*, 59 494 (1955).
- [32] W. H. Reinmuth, *Anal. Chem.* 33, 185, (1960).
- [33] R. P. Frankenthal and I. Shain *J. Am. Chem. Soc.*, 78, 862, (1963).
- [34] T. Berzins and P. Delahay, *J. Am. Chem. Soc.*, 75, 555, (1953).
- [35] M. Nicholson, *J. Am. Chem. Soc.* 79, 7 (1957).
- [36] Y. P. Gokhshtein, in *Advances in Polarography*, I.S. Longmuir, ed., Vol II, p465, Pergamon Press, New York, 1960.
- [37] R. Nicholson and I. Shain, *Anal. Chem.* 36, 4, (1964).
- [38] R. Nicholson and I. Shain, *Anal Chem.* 37, 178, (1965).
- [39] A.J. Bard and L. R. Faulkner, "Electrochemical Methods", J. Wiley and Sons, Inc., N.Y. (1980).
- [40] Z. Galus, "Fundamentals of Electrochemical Analysis", J. Wiley & Sons,

London, (1976).

[41] A. J. Bard and L. R. Faulkner, *op. cit.* page 218.

[42] M. S. Shuman *Anal. Chem.* 41 (1) 142 (1969).

[43] M. Matlosz, *Ph.D Thesis*, University of California-Berkeley, Department of Chemical Engineering, (1985).

[44] J. Newman, *Ind. Eng. Chem. Fundamentals*, 7, 514, (1968).

[45] M. Matlosz, *op. cit.*

[46] A. Acrivos and P. Chambre, *Ind. Eng. Chem.*, 49, 1125, (1957).

[47] C. Balfe, *Ph.D Thesis, Department of Chemistry*, University of California, (1984).

[48] R. Jasinski, *op. cit.*

[49] F. G. Baucke and C. W. Tobias, *J. Electrochem. Soc.* 116, 1 (1969).

[50] M. Majda, Dept. of Chemistry, Univ. of California, Berkeley, California, personal communication.

[51] A. J. Bard and L. R. Faulkner, *op. cit.*, p. 10 -13.

[52] J. O'M. Bockris and A. K. N. Reddy, *Modern Electrochemistry*, vol. 2, Plenum Press, N.Y., (1977). p. 733.

[53] R. Nicholson, *Anal. Chem.*, 38, 1406 (1966).

[54] see Bard and Faulkner, *op. cit.*, page 142 for derivation.

[55] E. Gileadi, E. Kirowa-Eisner, and J. Penciner *Interfacial Electrochemistry*, Addison-Wesley Publishing Co., 1975. Page 311, 312.

[56] P.N. Ross Jr., Lawrence Berkeley Laboratory, Materials and Molecular Research, personal communication.

[57] J. S. Newman, *Electrochemical Systems*, Prentice Hall, Inc. Englewood Cliffs, N.J. (1973).

- [58] G. J. Janz and R. P. Tomkins, *Nonaqueous Electrolytes Handbook*, Vol I & II, Academic Press, (1972).
- [59] O. Popovych and R. Tomkins, *Nonaqueous Solution Chemistry*, J. Wiley and Sons, (1981) page 307.
- [60] K. Nakanishi and Y. Furusawa, *J. Chem & Eng. Data*, 23, 2, (1978).
- [61] G. J. Janz and R. P. Tomkins, *op. cit.* page 906 vol I.
- [62] V. Gutmann, "The Donor-Acceptor Approach to Molecular Interactions", Plenum Press, N.Y. (1978).
- [63] M. L'Her, D. Morin-Bozec, and J. Courtot-Coupez, *op cit.*
- [64] F. M. Hawkrige, and E. F. Bowden, *J. Electroanal. Chem.* 125, 367, (1981).
- [65] R. W. Murray, W. R. Heineman, and G. W. O'Dom, *Anal. Chem.*, 39, 1666, (1967).
- [66] A. T. Hubbard, and F. C. Anson, *Electroanal Chem.* 4, 129 (1971).
- [67] A. T. Hubbard, *CRC Critical Review Anal. Chem.*, 3, 201, (1973).
- [68] C. Balfe, "Electrochemistry and Spectroelectrochemical Studies of Some Coordination Compounds in High Oxidation States", PhD Thesis, LBL-17269, January 1984.
- [69] P. Johnson, K. Hanson, C.W. Tobias, *Stability of Propylene Carbonate in the Presence of Iodine, Bromine and Chlorine*, LBL Report to be published (1984).
- [70] P. Johnson, *Unpublished work.*
- [71] A. Hubbard, R. Osteryoung and F. Anson, *Anal. Chem.*, 38, 6, 892, (1966).
- [72] A. J. Bard and L. R. Faulkner, *op cit.* page 163-164.

Chapter I/ Conclusions

The feasibility of the electrochemical production of chlorine, bromine, and iodine in propylene carbonate has been studied. Uv-visible spectroscopy experiments of iodine and bromine have shown that the stable form of the halogen in PC is the trihalide. Iodine and bromine disproportionate to form the trihalide and probably a positively charged halide species. The equilibrium constant for the disproportionation of iodine was determined to be 0.85. Solutions of chlorine in PC are not stable. Even dried, distilled PC containing less than 7 ppm water is attacked by chlorine to form 1,2 and 1,3 propylene glycol as major decomposition products. The extent of the reaction is increased by water in the solution.

The conductance behavior of KI and KBr in PC was studied. Kolraush plots for both salts were linear in the high concentration range but trace impurities in the solution interfered with the measurement at concentration less than 10^{-4} M. The conductivity of solutions of KI and KBr increases if the corresponding halogen is added. Solutions of 0.05 M and 0.1 M KI reached a maximum in conductivity when the concentrations of the iodide and iodine were equal. A maximum was not observed for KBr solutions.

Cyclic voltammetry experiments of KI in supported PC solutions demonstrated that iodide is oxidized in two electrochemical steps; triiodide formed in the first step is oxidized to iodine at the higher potential. A mathematical model based upon the transport of the three species and the kinetics of the electron transfer reaction was developed to simulate the voltammograms. Spectral electrochemical experiments provided an independent confirmation of the proposed mechanism.

Appendix 1 / Distillation Manual

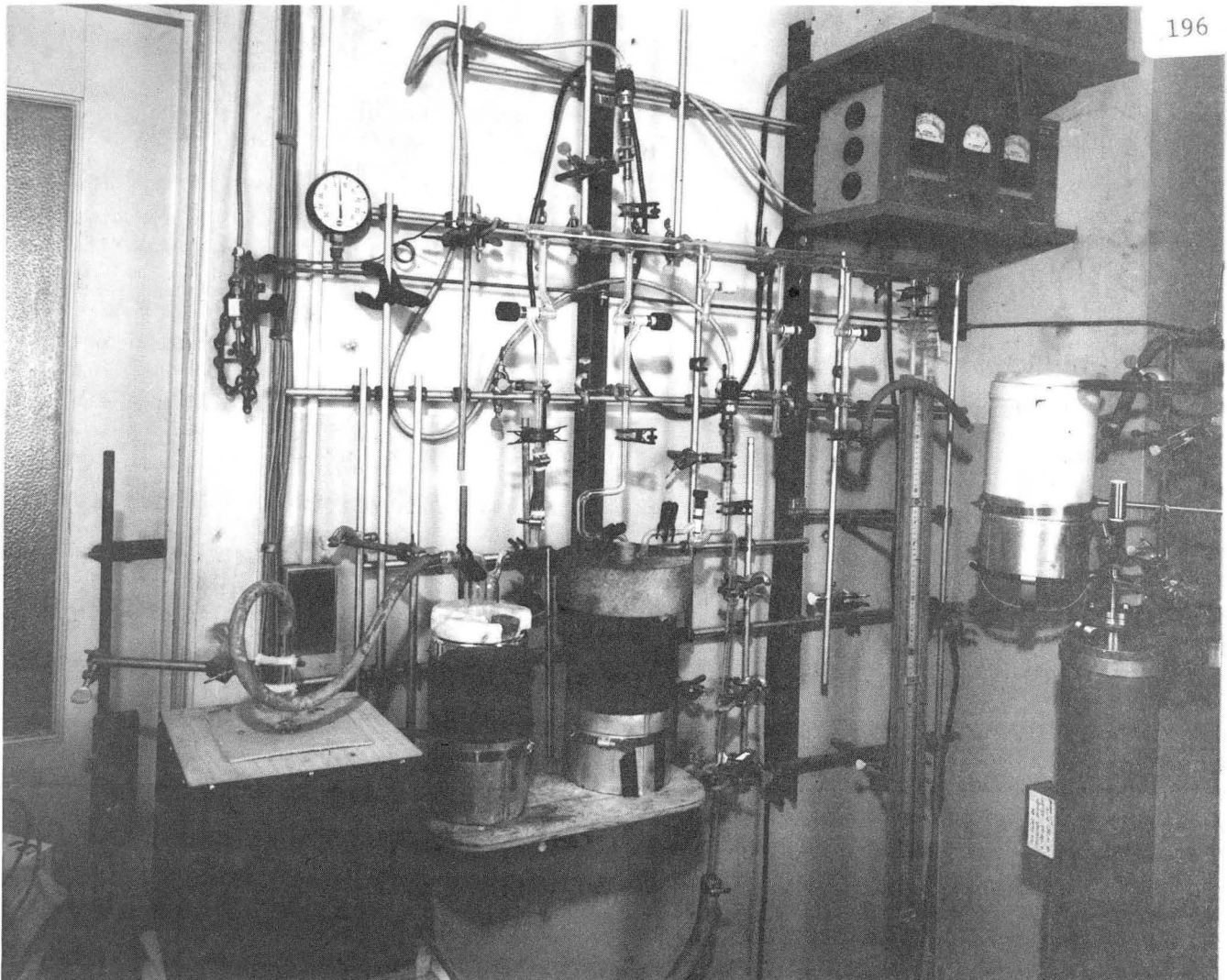
INTRODUCTION

The present method of distillation of propylene carbonate involves three steps. First the "as received" PC is passed over molecular sieves and alumina to remove water and other low molecular weight impurities. This first step removes most of the impurities-pale yellow PC from Jefferson Chemical becomes clear after passing through this column. Secondly, dry helium is bubbled through the PC overnight to remove the very volatile components and to saturate the column. The final step is distillation under vacuum while a stream of dry helium is bubbled through the PC in the distillation flask. The purpose of this paper is to outline the procedure so that the process can be easily reproduced.

APPARATUS

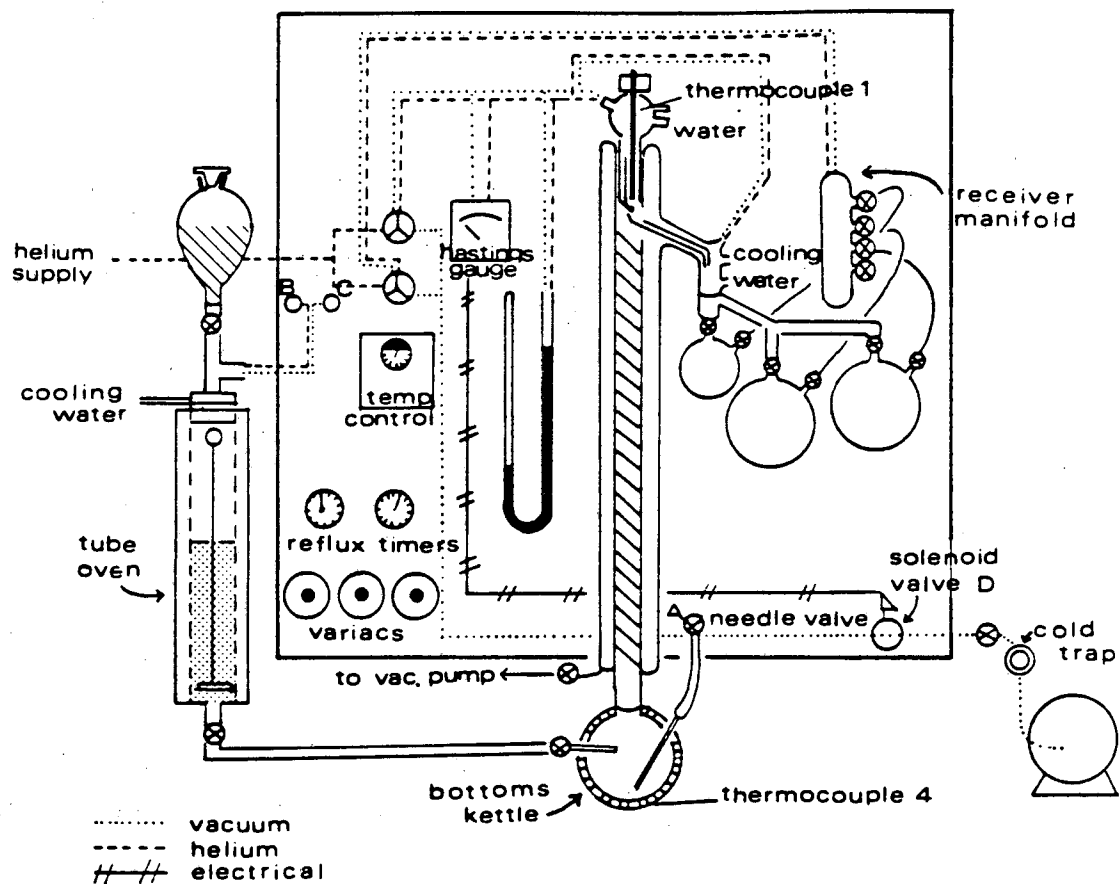
The distillation column is pictured in Figure A1-1 and a drawing of the entire system is given in Figure A1-2. The receiver design has been altered many times and can easily be altered again. The column design is for batch (Rayleigh) distillation, but the bottoms kettle holds only about two liters so we have occasionally re-filled it during a run. The vertical metal cylinder to the left of the column is a "tube oven" designed to heat its core of molecular sieves and alumina under vacuum. The PC is passed through this column before admission to the bottoms kettle. We think that most of the water is removed by the molecular sieves rather than by distillation. Studies done by GC show that the amount of time the PC is exposed to the sieves is very important. Therefore the PC passes through three stages of dry sieves before distillation.

The present receiver design is shown in Figure A1-3. The first cut is taken off separately in the small flask. The middle cut is usually the best and is separated from the last cut by using two flasks instead of one large one. An important



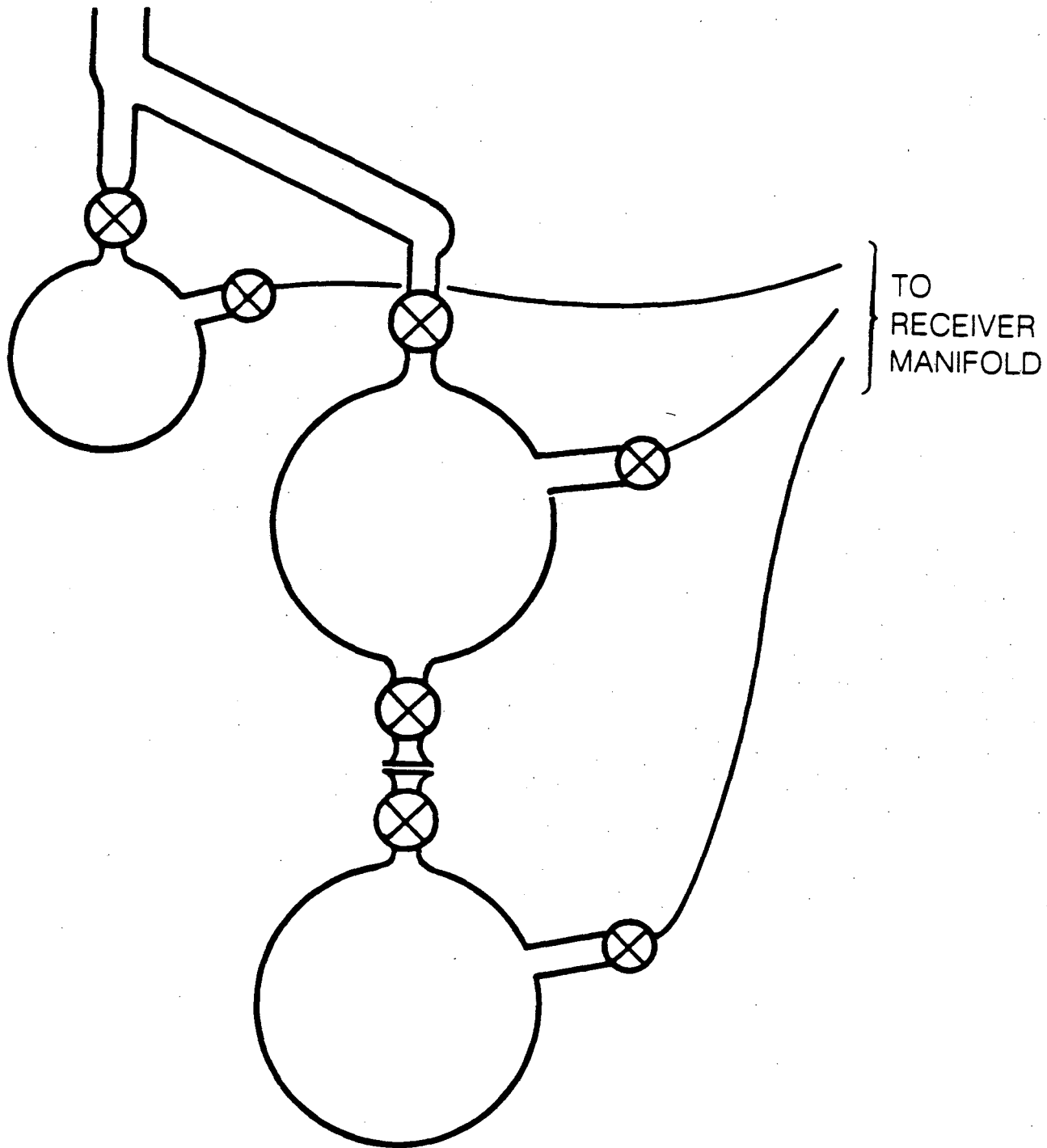
CBB 830-9681

Figure 4.2.1 Vacuum system and oven



XBL 847-3080

Figure A1-2 Distillation column schematic.



XBL 845-8937

Figure A1-3 Alternative design for distillation receiver.

consideration in the design of the receiver arrangement is size relative to the glove box port. The entire assembly must be transferred to the glove box so the bottles are not opened until they are under helium. The present system just barely fits into the port for the new glove box. Alternative receiver designs have been used. Figure A1-3 shows a "tiered" arrangement of receiver flasks designed so that when the center compartment is full, it is drained all at once into the lower flask. This "washes" the center flask with clean PC to eliminate any residue that may be left on the glassware.

It is important to have a good understanding of the helium network in the lab before starting to use facilities in the distillation room. Helium from the inert gas purification system is connected to the main helium manifold that is located above the doorway to the purification system (grey manifold). From here it is routed to the gloveboxes and to the distillation room. The helium valves to the pressure/vacuum manifold and the distillation column are located on the right side of the door to the hallway in the distillation room.

GLASSWARE PREPARATION:

Because the breakdown of PC is catalyzed by both acid and base, it is very important that the glassware is as clean and dry as possible. The procedure we follow is outlined below.

- i) All grease joints are cleaned with hexane.
- ii) If the glass is dusty, it is washed with detergent.
- iii) Soak overnight in alcoholic KOH.
- iv) Rinse with distilled water the chromic acid cleaning solution or aqua regia.
- v) Soak in distilled water for several hours.

- vi) Dry in very clean vacuum oven overnight.

Conductivity measurements have indicated that this procedure still leaves a residual film on the surface which can be leached into the solution. Probably the most effective step is to rinse the glass with the first PC that is distilled without ever opening up the column. This is one reason why the first cut is discarded. The column is put together with viton o-rings and screw-type clamps to make everything vacuum tight. Most grease connections have been eliminated but whenever the column design gets changed or repaired, an effort should be made to totally convert to o-ring fittings.

TEFLON AND O-RING PREPARATION:

Cleaning teflon and o-rings is difficult because they cannot be heated to high temperatures to dry. Literature articles on cyclic voltammetry of platinum suggest that the best method is to soak teflon in ultra pure water for months, constantly changing the water, to leach out impurities. We are primarily interested in removing water so we cleaned the teflon and o-rings as follows:

- i) Clean with acetone and soak in pure acetone for several hours.
- ii) Wash with absolute methanol to desorb the acetone.
- iii) Place in vacuum oven at about 70 °C overnight or longer.

COLUMN PREPARATION:

The clean and dry receiver assembly is assembled as shown in Figure one. Use viton o-rings (marked with two strips) and screw-type clamps. Check the connections by pulling a vacuum on the entire column and all receivers. When everything is tight, it can be pumped down below one micron. Sometimes a small coating of vacuum grease is needed on the o-ring fittings. After a good vacuum is achieved, purge the system several times with helium. Continue to pump on the

column until the distillation is finished. Be especially careful to never let the cold traps get dry.

MOLECULAR SIEVE PREPARATION:

Linde 13X molecular sieves are pretreated by heating in a furnace to about 500°C under a stream of argon (8 to 12 cfh). The furnace and pan for heating are in the solvent room. One consideration is that a heat gun or another furnace should not be operated while this furnace is on because a circuit breaker will blow. Even when two vacuum pumps are on, a heat gun should be connected outside the room.

TUBE OVEN, MOLECULAR SIEVE-ALUMINA PREPARATION

The column is resting on the tube oven and is removed by disconnecting the teflon connection at the bottom and lifting it out. First the old sieves and alumina (Woelm Basic, ICN, Cleveland, Ohio) are cleaned out by tapping the column to dislodge the contents. The column has a false bottom connected to a rod which extends to the top. This is used to completely empty the column. It is cleaned by rinsing with distilled water, then hexane, then reagent grade acetone. It is dried with a heat gun until very hot and then repacked. The first layer is dry glass wool, then about 300 cc of alumina, then 300 cc of molecular sieves, and finally another layer of glass wool. Be careful to put in sufficient glass wool to prevent the alumina from sifting into the distillation column. Carefully clean up any alumina that gets spilled into the o-ring groove so that the o-ring will make a good seal. The top is bolted down so that the cooling water connections are correctly aligned. This column is pretreated by first pulling a vacuum to about 1 micron Hg from the vac-line manifold. Evacuation must be done very slowly to avoid mixing up the sieves and alumina in the tube. The procedure we follow is first bring the vacuum to the needle valve marked (C) on the drawing. Then turn

that valve very slowly until it moves the vacuum gauge for the manifold, then back off a quarter turn. Wait until it rises to about 200 microns and open it a quarter turn again. Repeat this procedure about 5 times to open up to full vacuum. Also be careful when filling with helium. To pressurize the molecular sieve column first pressurize the manifold, turn the helium off, then open the valve slowly. Repeat this procedure until the manometer indicates atmospheric pressure. After the cooling water that runs around the o-ring is turned on, the sieves are heated under vacuum. The column oven is connected to a variac located below the oven and slowly heated to about 400°C. Never plug the tube oven directly into the wall outlet. (The variac was set to 70 for about 1.5 to 2 hours, then reset to 55 to maintain the temperature at about 400 °C). Before using the column, it is back-filled with helium to atmospheric pressure.

DISTILLATION PRETREATMENT

The process of purification of PC can begin once the molecular sieve column is prepared and the distillation column is pumped down. First 500 ml of molecular sieves are added to a bottle of Burdick and Jackson PC that has been pre-chilled. The absorption of water by the sieves is exothermic so we cool the PC by placing the bottles in an ice (sometimes dry ice) bath for two hours first. Then dry molecular are added to chilled PC. The sieves are added to the PC instead of pouring PC over the sieves to prevent the PC from heating too much. (The Burdick and Jackson PC starts with about 75-100 ppm of water. This is enough water to heat a gallon of PC up to 100°C or more). The absorption of water by the sieves is slow. The bottled sieves and PC are removed from the ice bath after an hour and left to "incubate" for about 8 hours.

The separatory funnel is installed above the tube furnace and supported by a ring stand. A layer of dry glass wool is laid on the bottom to filter out the sieves. The pretreated sieves are dumped on top of the glass wool, the funnel is

capped, and brought to less than 10 micron vacuum through the valve marked (C) on Figure A-1. (The ball valve to the tube oven should be closed.) These valves connect the oven to the glass pressure/vacuum manifold on the east side of the room. There is a place for a cold trap just above the tube oven. The vacuum gauges for this system are located on the east wall. When a good vacuum is achieved, bring the system up to atmosphere with helium (also through the manifold), but be careful not to blow off the cap. We leave the the PC in the sepratory funnel for at least four hours. Then the valve to distillation column flask is opened slowly and the PC is drawn into the column bottom.

Once the bottom flask is filled and the column is under vacuum, helium is bubbled through the solution overnight. Start with a full cylinder of helium and adjust the regulator pressure down to about seven pounds. To open the line to the column, open the main valve just to the right of the door to the hallway. The pressure will indicate on the gauge near the door. (The other valve opens the manifold to helium.) The helium is introduced to the bottoms kettle through a glass pipette. The rate of bubbling is controlled by the needle valve marked (A) in Figure A-1. This valve is tricky to operate-it takes several turns to open it enough to let any helium pass and then it surges out. The bubbling rate should be slow-about six bubbles a minute or slow enough to keep the column pressure at 2 mm Hg (Hasting gauge).

DISTILLATION

To start the distillation of PC, connect the heater mantle to the outlet marked "heater #2" on the panel. Decrease the helium flow rate so that the column pressure is about 1.5 to 1.8 mm Hg. Then insulate the top of the bottoms kettle with cloth rags and aluminum foil. (A covering heater mantle should be built for this flask, but the cloth and foil suffices.) Set the rheostat to 30 and then monitor the temperature until it reaches about 70°C, reset to 40 and the tem-

perature of the bottoms should go up to 150°C. The bottoms temperature will reach 150°C fairly quickly (2 hours if heated slowly), but it takes several more hours for the hot vapor to travel up the column. The time it takes is determined both by the helium flow rate which sets the vacuum on the column. After the bottoms kettle temperature reaches 150°C, it seems to help to run the helium flow rate up (so the column pressure goes to about 3 mm Hg) for a short time. When the head temperature starts to rise above ambient, it will increase very quickly. When this happens, turn on the cooling water at the nozzle just to the right of the still on the west side of the room. Set the flow of water high enough so that it flows continuously. In the past we have had problems with this flow cutting off and allowing the head temperature to get too hot. A log of past distillations is kept in a blue notebook marked "distillation workbook". Check there to get an idea of the time it takes to start distilling and the head temperatures and column pressure settings we have used in the past.

When the head temperature reaches 55 or 60°C, start collecting distillate by opening the needle valve in the top of the column by starting the timers to control the reflux ratio. The timer on the left controls the length of time that the needle is open, allowing the distillate to flow into the receiver. The timer on the right sets the time that the needle is down. We set the first timer for 5 seconds and the second for 20 seconds.

When the level in the bottoms kettle has dropped to about one third or one fourth of the original volume, the distillation is finished. (Sometimes the last fraction is collected in a separate receiver to check the purity.) Turn the timer and heater off, close all valves to the receiver flasks, and remove the insulation around the bottoms kettle. Turn the helium off at the needle valve leading to the bottoms kettle. This leaves the helium on to the still so that all receivers can be brought up to atmospheric pressure before they are transferred to the glovebox. The connections between the receiver flasks and the still must also be at atmo-

pheric pressure or the glassware will break when you try to break the seal. When this is finished, turn the helium off to the still using the valve near the door to the hallway in the still room. Do not pump the receiver flasks down to full vacuum (160 microamps) in the glovebox port or the o-ring seal will open. Generally, we pump down to about 75 microamps, backfill with helium, and then repeat this cycle several times.

Appendix 2/Computer Programs for HP9825

Oscilloscope Program: Data Transfer for Cyclic Voltammetry

The HPL program used to transfer cyclic voltammetry data from the Nicolet oscilloscope to the Hewlett-Packard HP9825 computer is given below. The program is organized into three sections: transfer of the data from the oscilloscope to the computer, storage of the data on a floppy disc, and plotting the data in any one of several optional formats. These formats include current as a function of time (CT), applied voltage as a function of time (VT), and current as a function of applied voltage (CV). In addition, if the data is plotted in the form of current as a function of time, an optional integration routine is included to calculate the total charge passed in any time interval.

The program is outlined in the flow chart given in Figure A2-1. The numbers referenced at each step are program line numbers. A list of the dimensioned and undimensioned variables is given in Table A2-1. The required format for the data transfer and the listing of error codes are explained in the *Nicolet Oscilloscope Manual*. The program listing is given as Figure A2-2.

Table A2-1/ OSCILLOSCOPE PROGRAM VARIABLES			
Dimensioned Variables		Undimensioned Variables	
B\$ [485]	W output	A	No. of waveforms
V [32]	Conversion info	E	Errors
H\$ [32,55]	N output	N & D	Transfer code variables
CS [80]	Expt. comments	I	Iteration number
DS [31760]	Scope data	M	Waveform No. to plot
RS [6]	File name	B	Dummy waveform no.
QS [5]	Question	T	Time
Z\$ [3,2]	Plot select	r1	V Norm
S [6]	Plot parameters	r2	H Norm
H [2]	No. of digits	r3	V Zero
G [2]	X,Y Label	r4	H Zero
A\$ [6,50]		r5	H Zero
A\$ [1]	Title	r6	No. of data points
A\$ [2]	X Caption	r7	Norm Step
A\$ [3]	Y Caption		Dummy variables in plot routine
A\$ [4]	Line 1	N,L,V,R	
A\$ [5]	Line 2	O,K,Q	
A\$ [6]	Line 3	P,J,U	
S [6]	Plot parameters		
S [1]	X-Min		
S [2]	X-Max		
S [3]	Y-Min		
S [4]	Y-Max		
S [5]	X-Tic		
S [6]	Y-Tic	r11	V Norm for CV plot
		r13	V Zero CV plot

Figure A2-1

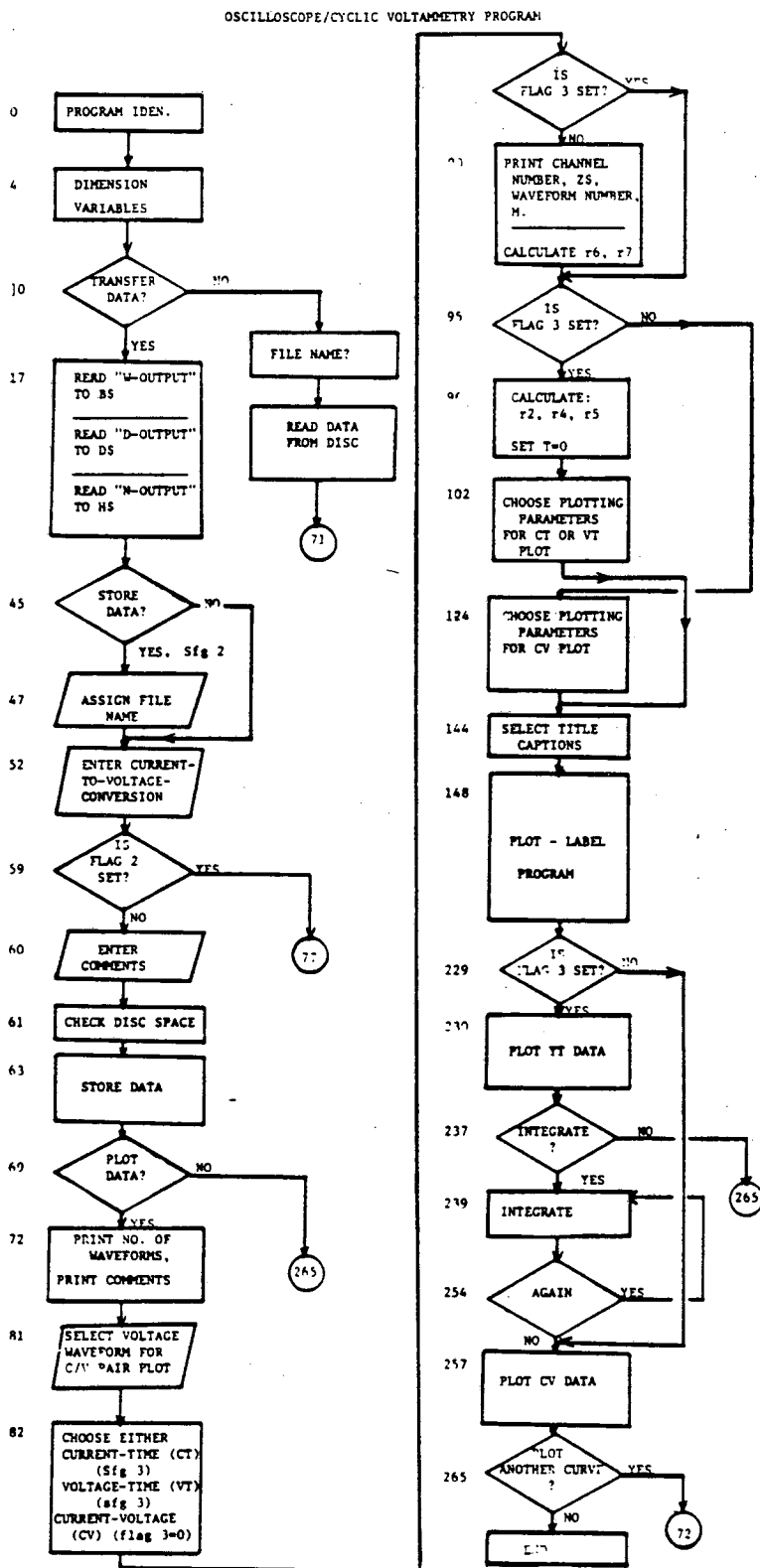


Figure A2-2

```

0: dsp "4094
  OSCILLOSCOPE
  PROGRAM"
1: wait 2000
2: dsp "RECORDS,
  PLOTS AND INTE
  GRATES DATA"
3: wait 2000
4: dim S[6],H[2]
  ,A#[6,80],G[2],
  Z#[2],E[6]
5: cf# 1,2,3
6: dim B#[485],
  V[32],H#[32,
  55],C#[80],D#[3
  1760]
7: dim R#[6]
8: dim Q#[5]
9: buf "data",
  D#,3
10: ent "IS DATA
  TO BE TRANSFER
  RED ?",Q#
11: if cap(Q#)="
  YES";sto 17
12: ent "WHAT
  IS THE FILE
  NAME?",R#
13: asen R#,1
14: sread 1,B#,
  V[*],H#,C#,D#
15: prt "RUN
  NUMBER ",R#
16: sto 71
17: dsp "IN ORDE
  R TO EXCHANGE
  DATA"
18: wait 2000
19: dsp "PRESS
  CONTINUE"
20: stp
21: fxd 0
22: wrt 727,"W"
23: red 727,E
24: if E#0;dsp
  "ERROR # ",E,"
  IN W";stp
25: red 727,B#
26: val(B#[1,
  2])>A
27: val(B#[3+A#
  15,4+A#15])>E
28: if E#0;dsp
  "ERROR # ",E,"
  IN W OUTPUT";
  stp
29: wrt 727,"D,
  4,0,0,15872,1"
30: red 727,E
31: if E#0;dsp
  "ERROR # ",E,"
  IN D";stp
32: tfr 727,"dat
  a",31744
33: red 727,E
34: if E#0;dsp
  "ERROR # ",E,"
  IN D OUTPUT";
  stp
35: for I=1 to A
36: wrt 727,"N,
  ",B#[(I-1)*15+
  11,(I-1)*15+12]
37: red 727,E
38: if E#0;dsp
  "ERROR # ",E,"
  IN N";stp
39: red 727,H#[I
  1
  40: val(H#[I,53,
  54])>E
41: if E#0;dsp
  "ERROR # ",E,"
  IN N OUTPUT";
  stp
42: next I
43: dsp "DATA
  HAS BEEN TRANSF
  ERRED"
44: wait 2000
45: ent "IS DATA
  TO BE STORED
  ?",Q#
46: if cap(Q#)#
  "YES";sfa 2;sto
  52
47: ent "WHAT
  IS 6 CHARACTER
  FILE NAME?",R#
48: if len(R#)=6
  ;jmp 4
49: dsp "FILE
  NAME IMPROPER
  LENGTH";wait
  2000
50: dsp "PRESS
  CONTINUE TO
  RESET";stp
51: jmp -4
52: for I=1 to A
53: dsp "WAVEFOR
  M # ".I
54: wait 2000
55: dsp "CURRENT
  -TO-VOLTAGE
  CONVERSION"
56: wait 2000
57: ent "IN uA/
  VOLT FOR WAVEFO
  RM",V[I]
58: next I
59: if fl#2=1;
  sto 77
60: ent "COMMENT
  S: ",C#
61: ent "DO YOU
  WANT TO CHECK
  DISK SPACE",Q#
62: if cap(Q#)="
  YES";cat 0
63: dsp "PRESS
  CONTINUE TO
  STORE";stp
64: open R#,150
65: asen R#,1
66: sprt 1,B#,
  V[*],H#,C#,D#,
  "end"
67: dsp "DATA
  IS RECORDED"
68: wait 2000
69: ent "IS THE
  DATA TO BE PLOT
  TED ?",Q#
70: if cap(Q#)#
  "YES";sto 267
71: spc
72: val(B#[1,
  2])>A
73: prt "COMMENT
  S:"
74: spc
75: prt C#
76: cf# 3
77: prt "THERE
  IS (ARE) ".A,"
  WAVEFORMS"
78: wait 2000
79: flt 5
80: if A=1;1>M;
  jmp 3
81: ent "VOLTAGE
  WAVEFORM # TO
  BE PLOTTED",B
82: if B>A;dsp
  "NOT A VALID
  #";wait 2000;
  jmp -1

```

Figure A2-2 - continued

```

83: ert "CURRENT
    TIME PLOT?"
    ,Q$
84: if cap(Q$)="
    YES";B+A/2+M;
    "CT"+Z$;sfs 3;
    sto 93
85: ert "VOLTAGE
    VS TIME PLOT?"
    ,Q$
86: if cap(Q$)="
    YES";E-M;"VT"+Z
    $;sfs 3;sto 93
87: dsp "FOR A
    CURRENT VS VOLT
    AGE PLOT";B+A/
    2+M
88: wait 2000
89: dsp "PRESS
    CONTINUE";"CV"+
    Z$;sto
90: val(B#[15+
    (M-1)*15,15+(M-
    1)*15])>r21
91: prt Z$;"Chan
    nel no.,">r21
92: prt "wavefor
    m no.,">M
93: val(B#[15+15*
    (M-1),10+15*(M-
    1)])>r6
94: val(B#[13+
    15*(M-1),14+15*
    (M-1)])>r7
95: if fl=3=0;
    sto 124
96: val(H#[M,14,
    18])>10*val(H#[
    M,20,22])>r2
97: val(H#[M,23,
    34])>r4
98: val(H#[M,35,
    40])>r5
99: ert "DO YOU
    WANT T=0 AT
    TRIGGER TIME";
    Q$
100: if cap(Q$)="
    YES";r4*65536+
    r5+T;Jmp 2
101: 0+T
102: ert "IS
    AXIS TO BE PLOT
    TED?";Q$
103: if cap(Q$)#
    "YES";sto 228
104: (r6-1-T)*
    r2>S[2]
125: -T+r2>S[1]
106: prt "T-MAX="
    ",S[2]","SEC"
107: src
108: prt "T-MIN="
    ",S[1]","SEC"
109: src
110: ert "WHAT
    IS T-TIC?";S[5]
111: ert "# OF
    DIGITS AFTER X-
    DECIMAL?";G[1]
112: "TIME (SEC)
    ">A#[2]
113: val(H#[M,5,
    9])>10*val(H#[M
    ,11,13])>r1
114: val(H#[M,
    23,28])>r3
115: prt "YMAX="
    ",(32000-r3)*r1*
    V[M]","VOLTS(OR
    mA)"
116: ert "YMAX
    IN VOLTS(OR
    MILLIAMPS)",
    S[4]
117: prt "YMIN="
    ",(-32000-r3)*
    r1*V[M]","VOLTS(
    OR mA)"
118: ert "YMIN
    IN VOLTS(OR
    MILLIAMPS)",
    S[3]
119: ert "WHAT
    IS Y-TIC?";S[6]
120: ert "NO. OF
    DIGITS AFTER
    Y-DECIMAL?";
    G[2]
121: if cap(Z$)="
    CT";"CURRENT
    (uA)">A#[3];
    Jmp 2
122: "E-E.REF
    (VOLTS)">A#[3]
123: sto 144
124: B+A/2+M
125: val(H#[M,5,
    9])>10*val(H#[M
    ,11,13])>r1
126: val(H#[M,
    23,28])>r3
127: prt "C-MAX="
    ",(32000-r3)*
    r1*V[M]","uA"
128: ert "C-MAX"
    ",S[4]
129: prt "C-MIN="
    ",(-32000-r3)*
    r1*V[M]","uA"
130: ert "C-MIN"
    ",S[3]
131: ert "WHAT
    IS C-TIC?";S[6]
132: ert "NO.
    OF DIGITS AFTER
    Y-DECIMAL?";
    G[2]
133: "CURRENT
    (uA)">A#[3]
134: B+M
135: val(H#[M,5,
    9])>10*val(H#[M
    ,11,13])>r1
136: val(H#[M,
    23,28])>r3
137: prt "V-MAX="
    ",(32000-r13)*
    r11*V[M]","VOLTS"
138: ert "V-MAX"
    ",S[2]
139: prt "V-MIN="
    ",(-32000-r13)*
    r11*V[M]","VOLTS"
140: ert "V-MIN"
    ",S[1]
141: ert "WHAT
    IS V-TIC?";S[5]
142: ert "NO. OF
    DIGITS AFTER X-
    DECIMAL?";G[1]
143: "E-E.REF (VOLT
    S)">A#[2]
144: ert "TITLE?"
    ",A#[1]
145: R#>A#[4];",
    WAVEFORM ">A#[4
    ,7,17];fxd 0;
    str(M)+A#[4,18]
146: C#>A#[5]
147: ert "LINE
    3 CAPTION?";
    A#[6]
148: "PLOT LABEL
    PROGRAM";
149: fxd G[1]
150: S[2]-(7/
    5)(S[2]-S[1])+
    .2(S[2]-S[1])+L
151: S[2]+.2(S[2]
    ]-S[1])+N
152: S[4]-(8.5/
    7)(S[4]-S[3])-
    .05(S[4]-S[3])-
    0

```

Figure A2-2 - continued

```

153: S[4]+(1/
7)(S[4]-S[3])-
.05(S[4]-S[3])+
P
154: scl L,N:0,P
155: pen
156: plt S[1],
S[3],-2
157: (1/16/4.5)(
S[2]-S[1])+H[1]
158: (1/16/7)(S[
4]-S[3])+H[2]
159: int((S[2]-
S[1])/S[5])+Q
160: int((S[4]-
S[3])/S[6])+R
161: for I=1 to
0
162: islt S[5],
0,0
163: islt 0,H[2]
,0
164: islt 0,-
H[2],0
165: next I
166: plt S[2],
S[3],0
167: for I=1 to
R
168: islt 0,S[6]
,0
169: islt -H[1],
0,0
170: islt H[1],
0,0
171: next I
172: plt S[2],
S[4],-1
173: plt S[1],
S[3],-2
174: for I=1 to
R
175: islt 0,S[6]
,0
176: islt H[1],
0,0
177: islt -H[1],
0,0
178: next I
179: plt S[1],
S[4],0
180: for I=1 to
0
181: islt S[5],
0,0
182: islt 0,-
H[2],0
183: islt 0,H[2]
,0
184: next I
185: plt S[2],
S[4],-1
186: csiz 1.5,2,
1.357,0
187: for I=0 to
0
188: S[1]+I*S[5]
+U
189: -(len(str(U
))/2+.3)+V
190: plt U,S[3],
0
191: cplt V,-
1.25
192: lbl U
193: next I
194: fxd G[2]
195: for I=0 to
R
196: S[3]+I*S[6]
+U
197: -(len(str(U
))+1)+V
198: plt S[1],U,
0
199: cplt V,-.3
200: lbl U
201: next I
202: csiz 1.5,2,
1.357,0
203: for I=4 to
6
204: 6-I+J
205: plt L,0,0
206: cplt 0,J
207: lbl A#[I]
208: next I
209: csiz 1.75,
2,1.357,0
210: -(len(A#[2]
)/2+.3)+V
211: (S[2]-S[1])
/2+S[1]+U
212: plt U,S[3],
0
213: cplt V,-3
214: lbl A#[2]
215: des
216: csiz 1.75,
2,1.357,90
217: -(len(A#[3]
)/2+.3)+V
218: (S[4]-S[3])
/2+S[3]+U
219: plt L,U,0
220: cplt V,-1
221: lbl A#[3]
222: csiz 2,2,
1.357,0
223: -(len(A#[1]
)/2+.3)+V
224: (S[2]-S[1])
/2+S[1]+U
225: plt U,P,0
226: cplt V,-1
227: lbl A#[1]
228: des "T0
PLOT DATA, PRES
S CONTINUE";
stp
229: if fl=0;
sto 257
230: for J=M to
15872-A+M by r7
231: (J-M)/r7+K
232: (K-T)*r2+X
233: (itf(D#[2+
J-1,2*J])-r3)*
r1+V[M]+Y
234: plt X,Y,-2
235: next J
236: pen
237: ent "DO
YOU WANT TO
INTEGRATE?",0#
238: if cos(Q#)#
"YES";sto 265
239: ent "TIME
INTEGRATION
START(SEC)?",
E[1]
240: ent "TIME
INTEGRATION
STOP?(SEC)",
E[2]
241: r2+E[4]
242: r7(E[1]/r2+
T)+M+G
243: r7(E[2]/r2+
T)+M+H
244: (itf(D#[2+
G-1,2*G])-r3)*
r1+V[M]+A
245: (itf(D#[2+
H-1,2*H])-r3)*
r1+V[M]+B
246: A+E+F;sfa 5
247: for J=G+4
to H-4 by r7
248: if fl=1;
(itf(D#[2+J-1,
2*J])-r3)*r1+
V[M]+Y;4Y+F+F;
cfa 5;Jme 2
249: if fl=0;
(itf(D#[2+J-1,
2*J])-r3)*r1+
V[M]+Z;2*Z+F+F;
sfa 5
250: next J

```

Figure A2-2 - continued

```
251: F*E[4]/3000
    +E[5]
252: flt 4
253: prt "TOTAL
    AREA FROM",E[1]
    ,"TO",E[2],"EQU
    ALS",E[5],"COUL
    OMBS"
254: ent "INTEGR
    ATE AGAIN?",0#
255: if cap(0#)=
    "YES";sto 239
256: sto 265
257: B+A/2+M
258: for J=M to
    15872-A+M by r7
259: (itf(0#(2*
    J-1,2*J))-r3)*
    r1*V[M]+Y
260: (itf(0#(2*
    (J-A/2)-1,2*(J-
    A/2)))-r13)*
    r11*V[M-A/2]+X
261: if J=15872-
    A+M;plt X,Y,-2
262: if J#15872-
    A+M;plt X,Y
263: next J
264: Ren
265: ent "PLOT
    ANOTHER CURVE?"
    ,0#
266: if cap(0#)=
    "YES";sto 72
267: sto iend
*22753
```

Data Transfer from HP9825 to ADM Terminal

The HPL program to transfer data (or string variables) from an HP9825 file to the ADM terminal is given in Figure A2-3. In order to effect this transfer, it is necessary to procure a device which can translate data received on a GPIB (IEEE) bus (parallel transfer from the HP9825) to data in a form which can be transmitted on a RS232 bus (serial transfer to the terminal). The device we used was a serial transfer module (TNW model 2000) on loan from the UCB electronics shop.¹

The device code for this instrument is "switch selectable" and was set as '04' when we used it. The designation of the GPIB interface from the HP is '7', so the HPL statement to send data is "wrt 704,".

The program is outlined as follows:

Dimension variables, string variables, and data buffer	lines 4 - 9
Read data from floppy disc	lines 12 - 14
Change V[*] parameters as needed	lines 24 -29
Select voltage/current combination to transfer by choosing voltage waveform number	line 32
set parameters for voltage and current waveforms	lines 33 - 43
Convert data file to full decimal and store as X,Y pair. Write each pair to device 704.	lines 45 - 51

¹ Note that a "Null Modem Cable" (cable to switch the #2 and #3 pins) is also necessary to use this device with the ADM terminal.

Figure A2-3

```

0: dsp "4094 TO
  DEVICE 704 TRANSFER PROGRAM"
1: wait 2000
2: dsp "SENDS SCOPE DATA TO
  IEEE BUS"
3: wait 2000
4: dim S[6],H[2],A[6,80],G[2],
  Z[2],E[6]
5: cfe 1,2,3
6: dim B[485],V[32],H[32,55],C[80],D[31760]
7: dim R[6]
8: dim Q[5]
9: buf "data",D[3]
10: ent "DATA FROM DISC?",Q[5]
11: if cap(Q[5])# "YES"; goto 17
12: ent "WHAT IS THE FILE NAME?",R[5]
13: asgn R[5],1
14: sread 1,B[5],V[*],H[5],C[5],D[5]
15: prt "RUN NUMBER ",R[5]
16: spc
17: val(B[5],2)→A
18: prt "COMMENT S:"
19: spc
20: prt C[5]
21: wrt 704,C[5],R[5]
22: prt "THERE IS(ARE) ",A," WAVEFORMS"
23: wait 2000
24: ent "CHANGE V[*] PARAMETERS?",Q[5]
25: if cap(Q[5])# "YES"; jmp 5
26: for I=1 to A
27: ent "V[I]=?",J
28: J→V[I]
29: next I
30: flt 5
31: if A=1;1→M
32: ent "VOLTAGE WAVEFORM TO BE TRANSFERRED",B
33: "SET PARAMETERS FOR VOLTAGE",X":
34: B→M
35: val(H[M,5,9])*10↑val(H[M,11,13])+r11
36: val(H[M,23,28])+r13
37: prt "V-MAX=", (32000-r13)*r11*V[M],"VOLTS"
38: "SET PARAMETERS FOR CURRENT",Y":
39: B+A/2→M
40: val(B[13+15*(M-1),14+15*(M-1)])→r7
41: val(H[M,5,9])*10↑val(H[M,11,13])+r1
42: val(H[M,23,28])+r3
43: prt "C-MAX=", (32000-r3)*r1*V[M],"uA"
44: B+A/2→M
45: fxd 4
46: for J=M to 15872-A+M by r7
47: (itf(D[2*J-1,2*J])-r3)*r1*V[M]→Y
48: (itf(D[2*J-A/2-1,2*(J-A/2)])-r13)*r11*V[M-A/2]→X
49: if J=15872-A+M; wrt 704,X,Y
50: if J#15872-A+M; wrt 704,X,Y
51: next J
52: ent "SEND ANOTHER CURVE?",Q[5]
53: if cap(Q[5])# "YES"; goto 22
54: stop iend
+11856

```

Potential Step Program

The software to collect and plot data from potential step experiments is listed below as Figure A2-4. The structure of the program is essentially the same as the oscilloscope program. The only change is that the plotting routine includes a plot of current as a function of the inverse square root of time between any two time intervals.

Figure A2-4

```

0: dsp "4094
  POTENTIAL STEP
  PROGRAM"
1: wait 2000
2: dsp "RECORDS,
  PLOTS AND INTE
  GRATES DATA"
3: wait 2000
4: dim S[6],H[2]
  ,A#[6,80],G[2],
  Z#[2],E[6],C[12]
]
5: cfe 1,2,3
6: dim B#[485],
  V[32],H#[32,
  55],C#[80],D#[3
  1760]
7: dim R#[6]
8: dim Q#[5]
9: buf "data",
  D#,3
10: ent "IS DATA
  TO BE TRANSFER
  RED ?",Q#
11: if cap(Q#)="
  YES";sto 17
12: ent "WHAT
  IS THE FILE
  NAME?",R#
13: asen R#,1
14: spre 1,8#,
  V[*],H#,C#,D#
15: prt "RUN
  NUMBER ",R#
16: sto 71
17: dsp "IN ORDE
  R TO EXCHANGE
  DATA"
18: wait 2000
19: dsp "PRESS
  CONTINUE"
20: sto
21: fxd 0
22: wrt 727,"W"
23: red 727,E
24: if E#0;dsp
  "ERROR # ",E,"
  IN W";sto
25: red 727,B#
26: val(B#[1,
  2])→A
27: val(B#[3+A+
  15,4+A+15])→E
28: if E#0;dsp
  "ERROR # ",E,"
  IN W OUTPUT";
  sto
29: wrt 727,"D,
  4,0,0,15872,1"
30: red 727,E
31: if E#0;dsp
  "ERROR # ",E,"
  IN D";sto
32: tfr 727,"dat
  a",31744
33: red 727,E
34: if E#0;dsp
  "ERROR # ",E,"
  IN D OUTPUT";
  sto
35: for I=1 to A
36: wrt 727,"N,
  ",B#[[(I-1)*15+
  11,(I-1)*15+12]
37: red 727,E
38: if E#0;dsp
  "ERROR # ",E,"
  IN N";sto
39: red 727,H#[I
  ]
40: val(H#[I,53,
  54])→E
41: if E#0;dsp
  "ERROR # ",E,"
  IN N OUTPUT";
  sto
42: next I
43: dsp "DATA
  HAS BEEN TRANSF
  ERED"
44: wait 2000
45: ent "IS DATA
  TO BE STORED
  ?",Q#
46: if cap(Q#)="
  YES";sfe 2;sto
  52
47: ent "WHAT
  IS 6 CHARACTER
  FILE NAME?",R#
48: if len(R#)=6
  ;jmp 4
49: dsp "FILE
  NAME IMPROPER
  LENGTH";wait
  2000
50: dsp "PRESS
  CONTINUE TO
  RESET";sto
51: jmp -4
52: for I=1 to A
53: dsp "WAVEFOR
  M # ",I
54: wait 2000
55: dsp "CURRENT
  -TO-VOLTAGE
  CONVERSION"
56: wait 2000
57: ent "IN uA/
  VOLT FOR WAVEFO
  RM",V[I]
58: next I
59: if fls2=1;
  sto 77
60: ent "COMMENT
  S : ",C#
61: ent "DO YOU
  WANT TO CHECK
  DISK SPACE",Q#
62: if cap(Q#)="
  YES";cat 0
63: dsp "PRESS
  CONTINUE TO
  STORE";sto
64: open R#,150
65: asen R#,1
66: sprt 1,8#,
  V[*],H#,C#,D#,
  "end"
67: dsp "DATA
  IS RECORDED"
68: wait 2000
69: ent "IS THE
  DATA TO BE PLOT
  TED ?",Q#
70: if cap(Q#)="
  YES";sto 287
71: spc
72: val(B#[1,
  2])→A
73: prt "COMMENT
  S:"
74: spc
75: prt C#
76: cfe 3
77: prt "THERE
  IS(ARE) ",A,"
  WAVEFORMS"
78: wait 2000
79: flt 5
80: if A=1;1→M;
  jmp 3
81: ent "VOLTAGE
  WAVEFORM # TO
  BE PLOTTED",B
82: if B>A;dsp
  "NOT A VALID
  #";wait 2000;
  jmp -1

```

Figure A2-4 - continued

```

83: ent "CURRENT
VS TIME PLOT?"
,Q#
84: if cap(Q#)="
YES";B+A/2+M;
"CT"→Z#;afa 3;
eto 92
85: ent "VOLTAGE
VS TIME PLOT?"
,Q#
86: if cap(Q#)="
YES";B+M;"VT"→Z
#;afa 3;eto S1
87: dsp "FOR A
CURRENT VS 1/
r(TIME) PLOT";
B+A/2+M
88: wait 1000
89: dsp "PRESS
CONTINUE";sta
90: val(B#[15+
(M-1)÷15,15+(M-
1)÷15])→r21
91: prt Z#,"Chan
nel no.";r21
92: prt "wavefor
m no.";M
93: val(B#[5+15+
(M-1),10+15*(M-
1)])→r6
94: val(B#[13+
15*(M-1),14+15*
(M-1)])→r7
95: val(H#[M,14,
18])÷10↑val(H#[
M,20,22])→r2
96: val(H#[M,29,
34])→r4
97: val(H#[M,35,
40])→r5
98: if fl93=0;
eto 124
99: ent "DO YOU
WANT T=0 AT
TRIGGER TIME";
Q#
100: if cap(Q#)=
"YES";r4÷65536+
r5→T;jmp 2
101: 0→T
102: ent "IS
AXIS TO BE PLOT
TED?";Q#
103: if cap(Q#)#
"YES";eto 227
104: (r6-1-T)*
r2→S[2]
105: -T*r2-S[1]
106: prt "T-MAX=
",S[2],"SEC"
107: spc
108: prt "T-MIN=
",S[1],"SEC"
109: spc
110: ent "WHAT
IS T-TIC?";S[5]
111: ent "# OF
DIGITS AFTER X-
DECIMAL?";G[1]
112: "TIME (SEC)
"→A#[2]
113: val(H#[M,5,
9])÷10↑val(H#[M
,11,13])→r1
114: val(H#[M,
23,28])→r3
115: prt "YMAX="
,(32000-r3)*r1+
V[M],"VOLTS(OR
uA)"
116: ent "YMAX
IN VOLTS(OR
MICROAMPS)";
S[4]
117: prt "YMIN="
,(-32000-r3)*
r1+V[M],"VOLTS(
OR uA)"
118: ent "YMIN
IN VOLTS(OR
MICROAMPS)";
S[3]
119: ent "WHAT
IS Y-TIC?";S[6]
120: ent "NO.
OF DIGITS AFTER
Y-DECIMAL?";
G[2]
121: if cap(Z#)=
"CT";"CURRENT
(uA)"→A#[3];
jmp 2
122: "E - E.REF
(VOLTS)"→A#[3]
123: eto 143
124: B+A/2+M
125: val(H#[M,5,
9])÷10↑val(H#[M
,11,13])→r1
126: val(H#[M,
23,28])→r3
127: prt "C-MAX="
,(32000-r3)*
r1+V[M],"uA"
128: ent "C-MAX?
",S[4]
129: prt "C-MIN="
,(-32000-r3)+
r1+V[M],"uA"
130: ent "C-MIN?
",S[3]
131: ent "WHAT
IS C-TIC?";S[6]
132: ent "NO.
OF DIGITS AFTER
Y-DECIMAL?";
G[2]
133: "(CURRENT)
(uA)"→A#[3]
134: prt "1/RT
MIN=";1/r((r6-
(T+1))*r2),"SEC
↑-1/2"
135: ent "1/RT
MIN?";S[1]
136: spc
137: prt "1/RT
MAX=";1/r((-T+
1)*r2),"SEC ↑-
1/2"
138: ent "1/RT
MAX?";S[2]
139: spc
140: ent "WHAT
IS 1/RT TIC?";
S[5]
141: ent "# OF
DIGITS AFTER X-
DECIMAL?";G[1]
142: "1/r(TIME);
(1/r(SEC))"→A#
[2]
143: ent "TITLE?
",A#[1]
144: R#→A#[4];";
WAVEFORM "→A#[4
,7,17];fxd 0;
str(M)→A#[4,18]
145: C#→A#[5]
146: ent "LINE
3 CAPTION?";
A#[6]
147: "PLOT LABEL
PROGRAM";
148: fxd G[1]
149: S[2]-(7/
5)(S[2]-S[1])+
.2(S[2]-S[1])+L
150: S[2]+.2(S[2
]-S[1])→N
151: S[4]-(8.5/
7)(S[4]-S[3])-
.05(S[4]-S[3])+
0
152: S[4]+(1/
7)(S[4]-S[3])-
.05(S[4]-S[3])+
P
153: scl L,N,0,F
154: pen
155: plt S[1],
S[3],-2

```

Figure A2-4 - continued

```

156: (1/16/4.5)(
  S[2]-S[1])+H[1]
157: (1/16/7)(S[
  4]-S[3])+H[2]
158: int((S[2]-
  S[1])/S[5])+0
159: int((S[4]-
  S[3])/S[6])+R
160: for I=1 to
  0
161: ielt S[5],
  0,0
162: ielt 0,H[2]
  ,0
163: ielt 0,-
  H[2],0
164: next I
165: plt S[2],
  S[3],0
166: for I=1 to
  R
167: ielt 0,S[6]
  ,0
168: ielt -H[1],
  0,0
169: ielt H[1],
  0,0
170: next I
171: plt S[2],
  S[4],-1
172: plt S[1],
  S[3],-2
173: for I=1 to
  R
174: ielt 0,S[6]
  ,0
175: ielt H[1],
  0,0
176: ielt -H[1],
  0,0
177: next I
178: plt S[1],
  S[4],0
179: for I=1 to
  0
180: ielt S[5],
  0,0
181: ielt 0,-
  H[2],0
182: ielt 0,H[2]
  ,0
183: next I
184: plt S[2],
  S[4],-1
185: csiz 1.5,2,
  1.357,0
186: for I=0 to
  0
187: S[1]+I*S[5]
  +U
188: -(len(str(U
  ))/2+.3)+V
189: plt U,S[3],
  0
190: cplt V,-
  1.25
191: lbl U
192: next I
193: fxd G[2]
194: for I=0 to
  R
195: S[3]+I*S[6]
  +U
196: -(len(str(U
  ))+1)+V
197: plt S[1],U,
  0
198: cplt V,-.3
199: lbl U
200: next I
201: csiz 1.5,2,
  1.357,0
202: for I=4 to
  6
203: 6-I+J
204: plt L,0,0
205: cplt 0,J
206: lbl A#[I]
207: next I
208: csiz 1.75,
  2,1.357,0
209: -(len(A#[2]
  )/2+.3)+V
210: (S[2]-S[1])
  /2+S[1]+U
211: plt U,S[3],
  0
212: cplt V,-3
213: lbl A#[2]
214: def
215: csiz 1.75,
  2,1.357,90
216: -(len(A#[3]
  )/2+.3)+V
217: (S[4]-S[3])
  /2+S[3]+U
218: plt L,U,0
219: cplt V,-1
220: lbl A#[3]
221: csiz 2,2,
  1.357,0
222: -(len(A#[1]
  )/2+.3)+V
223: (S[2]-S[1])
  /2+S[1]+U
224: plt U,P,0
225: cplt V,-1
226: lbl A#[1]
227: dsr "TO
  PLOT DATA, PRES
  S CONTINUE";
  str
228: if fl#3=0;
  goto 256
229: for J=M to
  15872-A+M by r7
230: (J-M)/r7+K
231: (K-T)*r2+X
232: (itf(D#[2+
  J-1,2*J])-r3)*
  r1*V[M]+Y
233: plt X,Y,-2
234: next J
235: pen
236: ent "DO
  YOU WANT TO
  INTEGRATE?",0#
237: if cap(0#)#
  "YES";goto 284
238: ent "TIME -
  INTEGRATION
  START(SEC)",
  E[1]
239: ent "TIME
  INTEGRATION
  STOP(SEC)",
  E[2]
240: r2+E[4]
241: r7(E[1]/r2+
  T)+M+G
242: r7(E[2]/r2+
  T)+M+H
243: (itf(D#[2+
  G-1,2*G])-r3)*
  r1*V[M]+A
244: (itf(D#[2+
  H-1,2*H])-r3)*
  r1*V[M]+B
245: A+B+F;sf# 5
246: for J=G+4
  to H-4 by r7
247: if fl#5=1;
  (itf(D#[2+J-1,
  2*J])-r3)*r1*
  V[M]+Y;4Y+F+F;
  c# 5;jmp 2
248: if fl#5=0;
  (itf(D#[2+J-1,
  2*J])-r3)*r1*
  V[M]+Z;2*Z+F+F;
  sf# 5
249: next J
250: F+E[4]/3000
  +E[5]
251: flt 4
252: prt "TOTAL
  AREA FROM",E[1]
  ,"TO",E[2];"EQU
  ALS",E[5];"COUL
  OMBES"

```

Figure A2-4 - continued

```

253: ent "INTEGR
ATE AGAIN?",Q$
254: if cap(Q$)=
"YES";eto 238
255: eto 264
256: B+A/2+M
257: for J=M to
15872-A+M by r7
258: (J-M)/r7+K
259: 1/r((K-T+
1)*r2)+X
260: (itf(Q$[2+
J-1,2+J])-r3)*
r1+V[M]+Y
261: if J=15872-
A+M;plt X,Y,-2
262: if J#15872-
A+M;plt X,Y
263: next J
264: pen
265: ent "CALCUL
ATE SLOPE?",Q$
266: if cap(Q$)#
"YES";eto 282
267: enr "MIN
X",C[1],"MAX
X",C[2]
268: for J=M to
15872-A+M by r7
269: (J-M)/r7+K;
1/r((K-T+1)*
r2)+X
270: (itf(Q$[2+
J-1,2+J])-r3)*
r1+V[M]+Y
271: if X>C[1]
and X<C[2];C[3]
+X+C[3];C[4]+
Y+C[4];C[5]+
XX+C[5]
272: if X>C[1]
and X<C[2];C[6]
+YY+C[6];C[7]+
XY+C[7];C[8]+
1+C[8]
273: next J
274: flt 3
275: C[7]-C[3]+
C[4]/C[8]+C[9]
276: C[9]/(C[5]-
C[3]*C[3]/C[8])
+C[10]
277: C[4]/C[8]-
C[10]+C[3]/C[8]
+C[11]
278: C[9]*C[10]/
(C[6]-C[4]*C[4]
/C[8])+C[12]
279: prt "SLOPE
=",C[10],"INTER
CEPT =",C[11],
"COEF OF DETERM
=",C[12]
280: prt "NO.
OF POINTS=";
C[8]
281: ent "CALCUL
ATE ANOTHER
SLOPE?",Q$
282: if cap(Q$)#
"YES";jmp 2
283: for J=1 to
8;0+C[J];next
J;eto 267
284: ent "PLOT
ANOTHER CURVE?"
,Q$
285: if cap(Q$)=
"YES";eto 72
286: ent "CALCUL
ATE SLOPE?",Q$
287: sto iend
+7911

```

This report was done with support from the Department of Energy. Any conclusions or opinions expressed in this report represent solely those of the author(s) and not necessarily those of The Regents of the University of California, the Lawrence Berkeley Laboratory or the Department of Energy.

Reference to a company or product name does not imply approval or recommendation of the product by the University of California or the U.S. Department of Energy to the exclusion of others that may be suitable.

TECHNICAL INFORMATION DEPARTMENT
LAWRENCE BERKELEY LABORATORY
UNIVERSITY OF CALIFORNIA
BERKELEY, CALIFORNIA 94720